Editors: Mateja Jemec Auflič, Matjaž Mikoš, Timotej Verbovšek

Advances in Landslide Research

Proceedings of the 3rd Regional Symposium on Landslides in the Adriatic Balkan Region

11-13 October 2017, Ljubljana, Slovenia

ICL
ICL ADRIATIC-BALKAN NETWORK
GeoZS Geološki zavod Slovenije
Univerza v Ljubljani

Editors: Mateja Jemec Auflič, Matjaž Mikoš, Timotej Verbovšek

Advances in Landslide Research

Proceedings of the 3rd Regional Symposium on Landslides in the Adriatic Balkan Region

11-13 October 2017, Ljubljana, Slovenia

Geological Survey of Slovenia
September, 2018

Advances in Landslide Research

Proceedings of the 3rd Regional Symposium on Landslides in the Adriatic Balkan Region
11-13 October 2017, Ljubljana, Slovenia

Electronic edition

Editors

Mateja Jemec Auflič, Geological Survey of Slovenia
Matjaž Mikoš, University of Ljubljana, Faculty of Civil and Geodetic Engineering
Timotej Verbovšek, University of Ljubljana, Faculty of Natural Sciences and Engineering

International Scientific Committe

Citation:

The publication should be cited in the bibliography using doi number as follows:
Jemec Auflič M., Mikoš M., Verbovšek T. (eds.): Advances in Landslide Research. Proceedings of the 3rd Regional Symposium on Landslides in the Adriatic Balkan Region, 11-13 October 2017, Ljubljana. Geological Survey of Slovenia, 2018.
doi: https://doi.org/10.5474/9789616498593

Published by: © Geological Survey of Slovenia, Ljubljana, 2018
Graphic Design: Staška Čertalič
Cover photo: Erazem Dolžan (Stogovce landslide)
Web page: http://www.geo-zs.si/ReSyLAB2017/
Printed by: Solos d.o.o., realizacija grafičnih idej
Print run: 120 copies

Kataložni zapis o publikaciji (CIP) pripravili v
Narodni in univerzitetni knjižnici v Ljubljani
COBISS.SI-ID=296216832
ISBN 978-961-6498-59-3 (pdf)

Preface

The Regional Symposium on Landslides in the Adriatic-Balkan Region (ReSyLAB) is a bi-annual event, organized by the Adriatic-Balkan Network of the International Consortium on Landslides, Kyoto, Japan (ICL, http://icl.iplhq.org/). The 3rd ReSyLAB in Ljubljana 2017 followed two previous successful symposia in Zagreb, Croatia (1st ReSyLAB 2013) and Belgrade, Serbia (2nd ReSyLAB 2015). A regional symposium aims specifically to strengthen the cooperation of the ICL members in the region and generally among the network of stakeholders involved in landslide research and landslide risk reduction. The next, 4th ReSyLAB is scheduled for October 2019 and is to be held in Sarajevo, Bosnia and Hercegovina.

The main objective of the 3rd ReSyLAB symposium (http://www.geo-zs.si/ReSyLAB2017/) was to provide a stimulating forum for geoscientists, engineers, professionals, and decision-makers concerned with landslide hazards and risks as well as their impact on society-in the Adriatic-Balkan Region as well as worldwide. Following the ISDR-ICL Sendai Partnerships 2015–2025 for the Global Promotion of Understanding and Reducing Landslide Disaster Risk and the 2017 Ljubljana Declaration on Landslide Risk Reduction, the 3rd ReSyLAB symposium explored possible ways of enhancing cooperation between the landslide science community and the diverse range of stakeholders both in the Adriatic-Balkan Region and around the world. Many landslides exist in the region, triggered mainly by short but intensive or by less intense but prolonged rainfall, and have caused substantial material damage and human casualties. The fact is that landslide damages cannot be entirely avoided, but with adequate spatial planning based on landslide risk zones, we can minimize these damages and prevent large negative impacts on society. In the following years, the ICL ABN will look forward to joint projects that tackle and contribute to landslide research improvement and to put expertise, knowledge and experiences into practice.

This book “Advances in Landslide Research” is a collection of twenty five peer-reviewed papers prepared by authors from seven countries (Austria, Croatia, Italy, Macedonia, Serbia, Slovenia, and Spain) in the context of the 3rd ReSyLAB topics: mapping, investigating, monitoring, analysis, and mitigation of landslides, as well as case studies on innovative landslide analysis techniques and landslide risk mitigation solutions. Recent developments in landslide research and new-advanced technologies for landslide monitoring are presented.

We would like to thank all of the authors of the submitted research papers and the numerous reviewers that peer reviewed the papers. We appreciate all the help we have received from the members of the International Scientific Committee and all of those individuals that expressed their support throughout the organization process. Finally, we would like to thank all of the sponsors who made the organization of this symposium possible.

Mateja Jemec Auflič

Matjaž Mikoš

Timotej Verbovšek

Contents

Combined interpretation of optical and SAR data for landslide mapping

Daniel Hölbling[(1)], Barbara Friedl[(1)], Jirathana Dittrich[(1)], Francesca Cigna[(2)], Gro Birkefeldt Møller Pedersen[(3)]

1) Department of Geoinformatics - Z_GIS, University of Salzburg, Schillerstraße 30, 5020 Salzburg, Austria, daniel.hoelbling@sbg.ac.at

2) Scientific Research Unit, Italian Space Agency (ASI), Rome, Italy

3) Institute of Earth Sciences, University of Iceland, Askja, Reykjavik, Iceland

Abstract In this study we present three case studies addressing the combination of optical and synthetic aperture radar (SAR) data in integrated landslide mapping by making use of an object-based image analysis (OBIA) framework. For the first test site, located in northern Italy, SPOT-5 imagery was used together with a digital elevation model (DEM) to map landslides with OBIA. Deformation rates were derived using Persistent Scatterer Interferometry (PSI) processing of ERS-1/2, ENVISAT and RADARSAT-1 data. The combined interpretation of landslide boundaries detected through OBIA with PSI-derived surface displacements facilitated the updating of the pre-existing landslide maps. The second example comprises the investigation of typhoon-triggered landslides and debris flows in southern Taiwan. Through the integration of multispectral information (SPOT-5), SAR intensity values (TerraSAR-X) and DEM derivatives in an OBIA environment, landslides could be examined more efficiently than relying on single data sources only. The multiple data analysis was especially useful for delineating single, large-scale landslides. Finally, a third case study was performed in south-east Iceland. We investigated how SAR coherence information and optical imagery could be synergistically used to assist in mapping landslides in glacio-volcanic landscapes.

Keywords landslides, remote sensing, optical satellite imagery, synthetic aperture radar (SAR), object-based image analysis (OBIA)

Introduction

The wide range of Earth Observation (EO) data from different optical and synthetic aperture radar (SAR) sensors and the increasing temporal and spatial resolution offer new opportunities to derive valuable landslide information. Optical satellite images have largely been employed, in combination with morphological properties derived from digital elevation models (DEMs), to map event-triggered landslides; traditionally using visual interpretation and manual digitization, and more recently by employing semi-automated image analysis methods, either pixel-based or object-based (Scaioni et al. 2014). Since recent landslides usually appear brighter than their immediate surroundings due to the exposure of bare ground, it is mainly the spectral properties of optical images that are used for purposes of landslide recognition. Multi-temporal SAR interferometry and advanced techniques such as Persistent Scatterer Interferometry (PSI) (Ferretti et al. 2001) and Small Baseline Subset (SB or SBAS) (Berardino et al. 2002) have primarily been used for identifying slow-moving landslides and for quantifying movement rates. Semi-automated approaches that integrate both data sources to produce added value by making use of the specific characteristics of each data source are still rare. Landslide mapping using object-based image analysis (OBIA) based solely on SAR data presents a challenge, and has only been tested in a few studies (e.g. Friedl and Hölbling 2015; Plank et al. 2015). The combination of post-event optical and SAR data for detecting and delineating event-based landslides using OBIA seems more promising, since the properties of both data sources can be exploited (e.g. Friedl et al. 2012). Plank et al. (2016), for example, presented a semi-automatic change detection approach based on pre-event high-resolution (HR) Landsat 8 and Sentinel-2 optical imagery and very high-resolution (VHR) polarimetric SAR (PolSAR) data from TerraSAR-X acquired shortly after the landslide-triggering event. Moreover, coherence information derived from a complex SAR image pair can be used as a measure of the stability of the interferometric phase or as a tool for image classification (Hanssen 2001). Since the interferometric correlation is destroyed by erosional and depositional processes that disturb the scattering surface, the extent of disturbance can be identified (Smith 2002). However, there is a lack of object-based methods that can be used for the investigation of landslide activity derived from an integrated analysis of coherence information and other remote sensing data.

The advantages of SAR sensors over optical sensors are their ability to acquire data during both day and night and their ability to penetrate clouds. This can be beneficial for rapid mapping of event landslides that are triggered by intense or prolonged rainfall. Limited access to optical imagery might be compensated to some extent

through the use of SAR intensity data in such cases.

We present three case studies from different regions that combine optical satellite imagery and SAR data to produce an integrated interpretation and mapping of landslides focussing on analyses within an OBIA framework.

Materials and Methods

Study areas

Case study I: Mont de la Saxe, northern Italy

Study area I, the Mont de la Saxe area, is located in the Aosta Valley, in north-western Italy near the Mont Blanc massif, and covers approximately 70 km². Courmayeur and Entréves represent the major villages in the area. The Dora Baltea River originates here as the confluence of the Dora di Ferret and Dora di Vèny streams. The mountainous study area is characterized by steep terrain, with altitudes ranging from approximately 1,100 m to over 4,000m above sea level. Due to the high relief energy and the steep slopes, slope instability is widespread in the area. The northern face of Mont de la Saxe is affected by the Bois de Plan Cereux landslide, which constitutes an active portion of a large, deep-seated gravitational slope deformation (DSGSD) affecting the whole of the Mont de la Saxe ridge (Hölbling et al. 2012; Crosta et al. 2014). It poses a high risk to nearby villages as well as to the infrastructure in the valley. The southern-facing slope of the Mont de la Saxe ridge is characterized by the presence of complex and planar/rotational slides.

Case study II: Xiaolin, southern Taiwan

Study area II is situated in southern Taiwan, more precisely in the Kaoping watershed around the former Xiaolin village. In Taiwan, the strong uplift rate and the associated seismicity lead to a topography that is characterised by small drainage basins, highly-fractured rocks, high relief and steep stream gradients (Liu et al. 2009). The island of Taiwan is located in the tropical and subtropical climate zones. During the summer season, especially from July to October, Taiwan is affected by tropical cyclones, also called typhoons. These particular climatic and geologic settings render Taiwan extremely susceptible to rainfall- and earthquake-induced mass movements, with shallow landslides and debris flows occurring most frequently. The study site covers an area of approximately 30.5 km² and is characterized by mountainous terrain with steep slopes and dense forest as the main land cover type. The area gained widespread attention on 9 August 2009, when Typhoon Morakot brought torrential rains to Taiwan and as a result triggered numerous landslides. The Xiaolin landslide and the subsequent dam breach-flooding event wiped out an entire village, inflicting 465 casualties (Wu et al. 2013) and causing severe infrastructure damage.

Case study III: Öræfajökull, south-eastern Iceland

Case study III focuses on a test site located in southern Iceland, an area south-east of the Öræfajökull massif. The Öræfajökull area is exposed to dynamic landscape changes caused by natural processes and geomorphological hazards such as slow and rapid mass movements, soil erosion and floods. The interaction of tectonic, volcanic, glacial and extreme weather processes causes progressive changes in land surface morphology. The area is influenced by the retreat of the Vatnajökull glacier, the largest and most voluminous glacier in Iceland, which causes significant isostatic uplift (Auriac 2014). This uplift, coupled with the steep relief, the large amount of unconsolidated debris, glacial erosion, permafrost thaw and high precipitation make the Öræfajökull area highly susceptible to slope instability, resulting in numerous landslides and debris flows (e.g. Saemundsson et al. 2011).

Remote sensing data and pre-processing

Different optical satellite images and SAR data were used for each study area (Tab. 1).

A pan-sharpened SPOT-5 image with 2.5 m spatial resolution together with a DEM (20 m) and its derived products (slope, aspect, curvature and plan curvature) served as the basis for object-based landslide mapping in the study area in Italy. Based on the optical image the NDVI (Normalized Difference Vegetation Index) and the MSAVI (Modified Soil-Adjusted Vegetation Index) were calculated. SAR data, which was used to estimate slow-moving landslides, encompassed ERS-1/2, ENVISAT ASAR (Advanced SAR) and RADARSAT-1 scenes acquired in ascending and descending mode.

Table 1 Overview of the optical and SAR remote sensing data for each study area. Data sets were selected based on the availability of cloud-free, post-event optical data and near-term SAR archive data.

Data type	Study area I (Italy)		Study area II (Taiwan)		Study area III (Iceland)	
	Sensor	Acquisition date	Sensor	Acquisition date	Sensor	Acquisition date
Optical image	SPOT-5	05/05/2005	SPOT-5	20/03/2011	RapidEye	12/09/2012
SAR data	ERS-1/2 ENVISAT ASAR RADARSAT-1	1992–2000 2004–2009 2006–2009	TerraSAR-X SpotLight	09/08/2011	TerraSAR-X StripMap (L1b, SSC Complex product)	26/07/2012 17/08/2012

For the case study in Taiwan a pan-sharpened SPOT-5 image (2.5 m resolution) was used together with a TerraSAR-X SpotLight scene acquired in descending pass configuration and single polarization (HH). Additionally, a DEM (5 m) derived through photogrammetric analysis of aerial images (acquired in 2004/2005) was used as ancillary data. Based on the optical image the NDVI and a brightness layer were calculated. TerraSAR-X data has been speckle filtered and terrain corrected and a radiometric normalization has been applied. Finally, various DEM derivatives were calculated (e.g. slope, curvature, flow accumulation).

For the Iceland case study an optical RapidEye image with 5 m spatial resolution, a LiDAR derived DEM (2m) and two TerraSAR-X StripMap scenes acquired in ascending pass mode and single polarization (HH) served as the basis for analysis. Data pre-processing incorporated calculation of the NDVI and a brightness layer from the optical image and generation of the DEM derivative slope. In order to obtain coherence estimates, the two available complex SAR images were first co-registered. Then the coherence magnitude (0 to 1) of the pixels of interest was computed based on the moving window (10 x 10 by default) principle. The coherence value of 0 (zero) indicates that the radar echoes between two acquisitions are totally de-correlated, while the value of 1 (one) represents completely coherent signals. Finally, the coherence image was geometrically corrected using the ArcticDEM available at 5 m spatial resolution (https://www.pgc.umn.edu/data/arcticdem). The radar data processing was carried out using the Sentinel Application Platform (SNAP) software (ESA).

Combined interpretation of optical and SAR data

OBIA and PSI interpretation for integrated landslide mapping

For the Mont de la Saxe test site in northern Italy, the SPOT-5 image was used together with the DEM and its derived products to semi-automatically map landslides with OBIA using the eCognition (Trimble Geospatial) software. We distinguished the two classes – *flow-like landslides* and *other landslide types* (falls, topples, slides and spreads) – following the kinematic-based classification of Cruden and Varnes (1996). Image objects that served as basic units for the knowledge-based classification were created by using the multi-resolution segmentation algorithm. Mainly the NDVI and the MSAVI were used to differentiate landslides from their surroundings (i.e. vegetated areas) in the first classification step. In order to refine this preliminary classification several additional spectral, spatial and contextual image object properties were used, e.g. the maximum spectral difference within image-objects, length/width ratio, compactness and maximum change in elevation within an object. The slope gradient together with aspect, curvature and plan curvature was used not only to better detect landslide areas, but also to differentiate between the two landslide classes. Further details about the OBIA mapping workflow can be found in Hölbling et al. (2012).

To quantify the deformation rates of the unstable areas identified through OBIA we used the PSI technique and ascending and descending ERS-1/2, ENVISAT and RADARSAT-1 data stacks. This technique allowed the detection of slow, point-based movements that were then interpreted in combination with the polygon-based OBIA landslide delineations. This was done by interpolating the Line of Sight (LOS) velocity resulting from SAR data analysis while considering the landslide boundaries derived from the optical data. Consequently, we were able to produce results with higher information content than we were using only a single data source.

Object-based landslide detection by integrating optical, DEM and SAR intensity data

For the Taiwanese case study the main objective was to develop a semi-automated landslide detection and classification approach that is capable of identifying *shallow landslides*, *debris flows* and, through the accumulation of debris, indirectly affected areas (*main river beds filled with debris*) in an OBIA domain. The approach is implemented using the eCognition software and based on the combined use of optical imagery (SPOT-5), SAR data (TerraSAR-X Spotlight) and a DEM including its derived products, i.e. slope, flow accumulation, curvature. Multiresolution segmentation was employed in order to extract homogeneous image objects forming the basis for subsequent classification. Since land cover changes, which are caused by fresh failures, are best represented in terms of the NDVI, as live green vegetation is missing (e.g. Barlow et al. 2003; Martha et al. 2010), the NDVI was applied as a key criterion in the identification of landslide candidates. Yet several false positives were assigned to the landslide candidate class owing to their similar spectral characteristics. Built-up areas, uncultivated agricultural fields and the main riverbed filled with debris, which is only indirectly related to mass wasting processes, comprised the greatest number of misclassified objects. The texture features GLCM Mean and GLCM Entropy were then computed for the SAR image. A combination with gentle slope values proved efficient in removing settlement areas and agricultural fields from the landslide candidate class. Low relief values relative to the study area, and gentle slope values (< 5°) were used to differentiate the main river bed from debris flows, which have a high relative relief due to the location of their source area (Martha et al. 2010).

Morphometric criteria and local field knowledge were subsequently considered in order to classify landslides and debris flows according to their failure mechanisms. An analysis routine was built in eCognition that considered a range of landslide diagnostic features (e.g. NDVI, texture, shape features such as length/width ratio, morphometric features such as slope, curvature or flow accumulation).

Relatively low curvature values, a high length/width ratio and a moderate standard deviation of the mean slope were used to identify debris flows, including their runout tracks. The texture feature GLCM Dissimilarity calculated for the SAR image and combined with low relief values relative to the study site proved effective in identifying further debris flows, especially debris cones situated near the main riverbed filled with debris. Mean slope values were used to distinguish landslides from debris flows, whereby landslide candidates with mean slope values >30° were assigned to the class *landslide*, while those with a lower value were classified as *debris flow* (Chen and Yu 2011). Texture derived from SAR image layers combined with context and morphometric information was useful in the classification of large-scale landslides occurring on moderate slopes (e.g. the Xiaolin landslide). A couple of remaining false positives (mostly agricultural fields at lower elevations) were finally eliminated using high mean SAR brightness values and low relief values.

Identification of landslide prone areas with OBIA using optical, slope and SAR coherence information

The objective of the Iceland case study was to derive significant information from the integrated analysis of optical and multi-temporal SAR data for landslide mapping within OBIA. RapidEye data was combined with slope and coherence information to establish whether information derived from a SAR coherence image is beneficial in the detection of landslides. Two scenarios where coherence information could positively influence landslide detection based on optical and slope information were defined. For the first, we assumed that relatively fresh slope failures are also unstable between near-time SAR acquisitions, and thus characterized by low coherence, which is common for landslide-affected slopes. The correlation between optical data-based landslide delineation and low coherence areas attributed to possible landslide activity could be used to confirm the results derived from landslide mapping on the RapidEye image. For the second, we evaluated the possibility of detecting additional areas potentially affected by landslides through the loss of coherence that were not detectable based on optical and DEM data.

A simple analysis routine was built in eCognition to designate areas potentially affected by landslides in the first instance. A multi-resolution segmentation based on the RapidEye image was conducted to generate image objects, which were subsequently classified based on relatively low NDVI and relatively high brightness values. Based on local field knowledge, landslide candidates with a slope value of <20° were then removed from the classification. Next, the coherence values of the already detected landslide-affected areas were considered. A threshold <0.4 was used to determine landslide candidates that are also marked by a low coherence. For scenario II, the previously defined landslide candidates were again considered as a basis, yet all unclassified image objects with a coherence value <0.4 were classified as additional potentially landslide-affected areas in order to demarcate further landslide candidates. Vegetated areas and water bodies, which also tend to have low coherence between two SAR acquisitions, as well as landslide candidates on gentle to moderate slopes (<15 °) were then removed by incorporating NDVI, near infrared and slope thresholds.

Results

Mont-de-la-Saxe, northern Italy

The combined interpretation of the landslide boundaries detected through OBIA and surface displacements obtained from PSI, i.e. radar measurements, facilitated the updating of pre-existing landslide inventory maps (e.g. the Inventario dei Fenomeni Franosi in Italia - IFFI) (cf. Hölbling et al. 2012). About one-third of the OBIA polygons were covered by persistent scatterer (PS) data. For the unstable areas characterized by high densities of PS data within the OBIA landslide boundaries, the estimation of average velocities was performed as well as a classification of landslide types according to Cruden and Varnes (1996). Fig. 1 shows an example of the combined interpretation of OBIA results and radar measures.

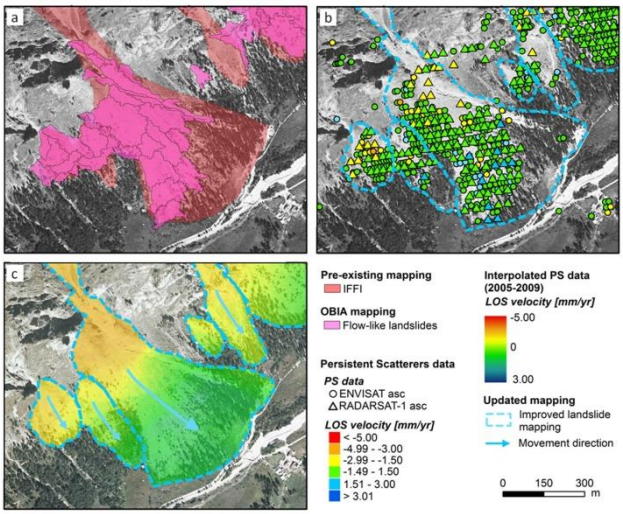

Figure 1 Combined interpretation of OBIA boundaries and SAR measurements for refining the IFFI landslide inventory. The figure shows the pre-existing IFFI inventory and the OBIA results (a), the updated landslide boundaries and PS data (b) and the interpolated Line of Sight (LOS) velocity of RADARSAT-1 PS in 2005–2009 (c). Negative velocities for the identified PS show LOS movements away from the sensor, while positive values depict movements towards the sensor. Modified after Hölbling et al. (2012).

Xiaolin, southern Taiwan

Approximately 29% of the test site is directly (landslides, debris flows) or indirectly (main riverbed filled with debris) affected by mass movements, with landslides making up the largest part (approximately 19%). Some land-

slides and their failed material remain on hillslopes, while others evolve into debris flows. In this sequential process, the landslide represents the source area and the debris flow transports the failed material downslope (Chiang et al. 2012), following drainage patterns that are formed naturally from terrain topography. Debris is mainly deposited along debris flow run-out tracks, but also in the main riverbed. Debris cones can be found near the main riverbed. Most of the classified mass movements show slope gradients between 20° and 40°. However, some mass movements appear on steeper slopes (>45°) or on more gentle slopes (<15°). This is consistent with the results of Tsai et al. (2010).

Fig. 2 depicts examples of the object-based landslide classification results derived from the combined analysis of optical, DEM and SAR data.

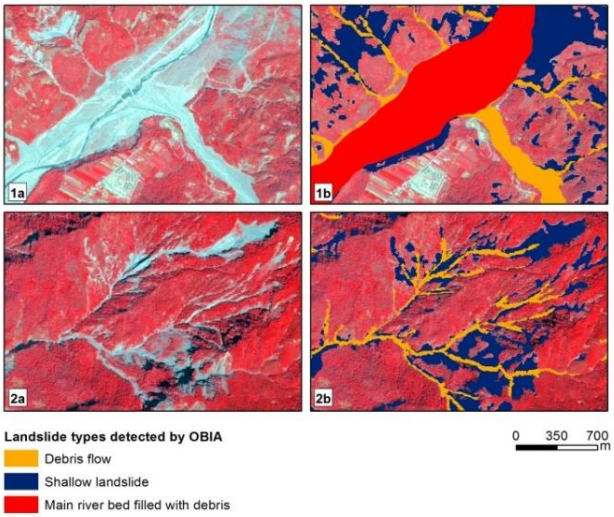

Figure 2 OBIA landslide mapping results based on optical, DEM and SAR data. The figure shows two subsets of the study area, with the unclassified SPOT-5 image (displayed in false colour composition) on the left (1a, 2a) and the respective classification of landslide types on the right (1b, 2b).

Öræfajökull, south-eastern Iceland

The coherence image of Öræfajökull derived from a TerraSAR-X image pair (22 days' time separation) reveals coherence magnitudes ranging from 0 (zero) (dark pixels) to 0.9 (bright pixels), with a mean coherence of 0.2. Further investigation showed that vegetated areas usually provide low to medium coherence (~0.1–0.5), while glaciers and water bodies exhibit low coherence (~0.1 or lower). The maximum coherence of 0.9 was identified over bare ground areas. Regarding scenario I, the classification outcome implies that major parts of the landslide-affected areas detected on optical and DEM data are also marked by a loss of coherence between the two SAR acquisitions. This indicates that there may be some kind of landslide activity on the identified slopes. Scenario II reveals slopes that may be landslide-prone and that could not be detected without the integration of the coherence layer. The classification results are shown in Fig. 3.

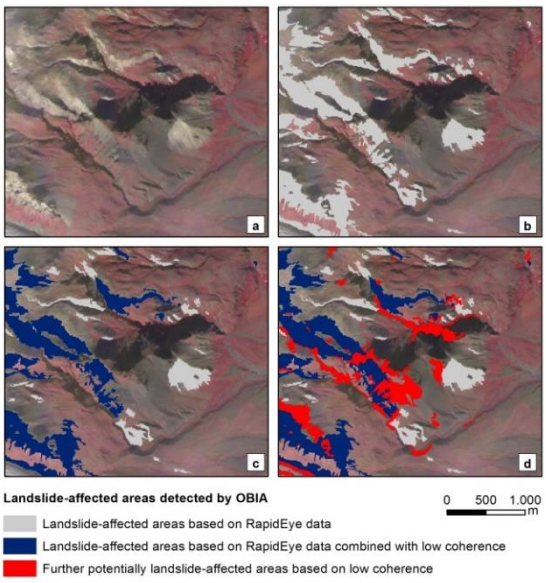

Figure 3 OBIA mapping of landslide-prone areas using optical, slope and SAR coherence information. The figure shows the RapidEye image (a), detected landslide-affected areas based on RapidEye (b), detected landslide-affected areas, which are also marked by low coherence (c) and further potentially landslide-affected areas derived from the loss of coherence between SAR acquisitions (d).

Discussion and Conclusion

For the Mont de la Saxe study area landslide mapping and interpretation was conducted by OBIA and by PSI. A 20 m DEM was used to support the mapping. The integration of a higher resolution DEM would probably improve the results; however, such data was not available. Landslide boundaries mapped on the optical image and displacements obtained from PSI data were combined to obtain detailed landslide information. More research, however, is needed to directly integrate PSI results into OBIA workflows for landslide mapping, for instance by joining PSI-derived information about moving rates and directions to image objects.

For the Taiwan case study, optical and DEM data were combined with SAR intensity in OBIA to semi-automatically classify different landslide types. Spectral features were most suitable for the detection of landslide-affected areas, whereas textural, morphometric, spatial and contextual characteristics proved effective in differentiating landslide types. The advantages of using the SAR data were most evident when combined with class descriptors from optical and DEM data. To fully exploit the potential of SAR data integration in OBIA, multi-frequency and multi-polarization data could be used to separate features with similar backscatter values.

Coherence information together with parameters such as brightness, NDVI and slope was synergistically analysed for the Öræfajökull case study. SAR coherence was used to confirm classification results obtained from optical and DEM data, as well as to identify additional landslide candidates. However, changes in the radar echo

between two SAR acquisitions can be affected by various driving mechanisms, which in turn result in a change of coherence. In Iceland, strong tectonic activity could lead to a loss of coherence between SAR acquisitions. Also, areas with high topographic variations are usually affected by radar layover or shadow, resulting in an underestimated or biased coherence. The integration of a layover-shadow mask could be useful for excluding these areas. Fine-tuning of coherence estimation parameters to minimize biases can be further considered (e.g. phase corrected coherence, temporal baseline of image pairs).

The combined interpretation of optical and SAR data offers remarkable possibilities for improved landslide mapping, even if existing semi-automated approaches still need to be optimized. Casagli et al. (2016) emphasized that integrated analysis of optical and SAR data should be intensively followed to fully exploit the potential of EO data from different sensors for landslide mapping and monitoring, with the aim of providing useful information for supporting disaster management.

Acknowledgments

This research has been supported by the Austrian Science Fund through the project MORPH (Mapping, Monitoring and Modelling the Spatio-Temporal Dynamics of Land Surface Morphology; FWF-P29461-N29), and by the EU's Seventh Framework Programme (FP7/2007–2013) under the SAFER (Services and Applications For Emergency Response) project, grant agreement no. 218802. Data for the Icelandic case study has been provided by the EMMIRS project funded by the Icelandic Research Fund (Rannis), Grant of Excellence No. 152266-052.

References

Auriac A (2014) Solid Earth response to ice retreat and glacial surges in Iceland inferred from satellite radar interferometry and finite element modelling. PhD thesis, University of Iceland, Reykjavik, Iceland.

Barlow J, Martin Y, Franklin, S E (2003) Detecting translational landslide scars using segmentation of Landsat ETM+ and DEM data in the northern Cascade Mountains, British Columbia. Canadian Journal of Remote Sensing. 29(4):510-517.

Berardino P, Fornaro G, Lanari R, Sansosti E (2002) A new algorithm for surface deformation monitoring based on small baseline differential SAR interferograms. IEEE Transactions on Geoscience and Remote Sensing. 40(11):2375-2383.

Casagli N, Cigna F, Bianchini S, Hölbling D, Füreder P, Righini G, Del Conte S, Friedl B, Schneiderbauer S, Iasio C, Vlcko J, Greif V, Proske H, Granica K, Falco S, Lozzi S, Mora O, Arnaud A, Novali F, Bianchi M (2016) Landslide mapping and monitoring by using radar and optical remote sensing: Examples from the EC-FP7 project SAFER. Remote Sensing Applications: Society and Environment. 4:92-108.

Chen C-Y, Yu F C (2011) Morphometric analysis of debris flows and their source areas using GIS. Geomorphology. 129(3-4):387-397.

Chiang S-H, Chang K-T, Mondini A C, Tsai B-W, Chen C-Y (2012) Simulation of event-based landslides and debris flows at watershed level. Geomorphology. 138(1):306-318.

Crosta G B, di Prisco C, Frattini P, Frigerio P, Castellanza R, Agliardi F (2014) Chasing a complete understanding of the triggering mechanisms of a large rapidly evolving rockslide. Landslides. 11(5):747-764.

Cruden D M, Varnes D J (1996) Landslide Types and Processes. In: Turner A K, Schuster R L (eds) Landslides: Investigation and Mitigation. Special Report 247, Transportation Research Board, National Research Council. National Academy Press: Washington, DC, USA. pp. 36-75.

Ferretti A, Prati C, Rocca F (2001) Permanent scatterers in SAR interferometry. IEEE Transactions on Geoscience and Remote Sensing. 39(1):8-20.

Friedl B, Hölbling D (2015) Using SAR Interferograms and Coherence Images for Object-Based Delineation of Unstable Slopes. FRINGE 2015 Workshop: Advances in the Science and Applications of SAR Interferometry and Sentinel-1 InSAR Workshop, 23-27 March 2015. Frascati, Italy. 6p.

Friedl B, Hölbling D, Füreder P (2012) Combining TerraSAR-X and SPOT-5 data for object-based landslide detection. Geophysical Research Abstracts, Vol. 14, EGU General Assembly 2012-8663, 22-27 April 2012. Vienna, Austria.

Hanssen F R (2001) Radar Interferometry: Data Interpretation and Error Analysis. Kluwer Academic Publishers, USA. 308p.

Hölbling D, Füreder P, Antolini F, Cigna F, Casagli N., Lang S (2012) A Semi-Automated Object-Based Approach for Landslide Detection Validated by Persistent Scatterer Interferometry Measures and Landslide Inventories. Remote Sensing. 4(5):1310-1336.

Liu J-K, Chang K-T, Rau J-Y, Hsu W-C, Liao Z-Y, Lau C-C, Shih T-Y (2009) The Geomorphometry of Rainfall-Induced Landslides in Taiwan Obtained by Airborne Lidar and Digital Photography. In: Ho P-G (eds) Geoscience and Remote Sensing. InTech. pp. 115-132.

Martha T R, Kerle N, Jetten V, van Westen C J, Kumar K V (2010) Characterising spectral, spatial and morphometric properties of landslides for semi-automatic detection using object-oriented methods. Geomorphology. 116:24-36.

Plank S, Hölbling D, Eisank C, Friedl B, Martinis S, Twele A (2015) Comparing object-based landslide detection methods based on polarimetric SAR and optical satellite imagery - a case study in Taiwan. 7th International Workshop on Science and Applications of SAR Polarimetry and Polarimetric Interferometry - POLinSAR, 26-30 January 2015. Frascati, Italy. 5 p.

Plank S, Twele A, Martinis S (2016) Landslide Mapping in Vegetated Areas Using Change Detection Based on Optical and Polarimetric SAR Data. Remote Sensing. 8(4):307.

Saemundsson T, Sigurðsson IA, Pétursson HG, Jónsson HP, Decaulne A, Roberts MJ, Jensen EH (2011) Bergflóðið sem féll á Morsárjökul 20. mars 2007 – Hverjar hafa afleiðingar þess orðið? Náttúrufræðingurinn. 81(3-4):131-141.

Scaioni M, Longoni L, Melillo V, Papini M (2014) Remote Sensing for Landslide Investigations: An Overview of Recent Achievements and Perspectives. Remote Sensing. 6(10):9600-9652.

Smith L C (2002) Emerging Applications of Interferometric Synthetic Aperture Radar (InSAR) in Geomorphology and Hydrology. Annals of the American Association of Geographers. 92(3):385-398.

Tsai F, Hwang J-H, Chen L-C, Lin, T-H (2010) Post-disaster assessment of landslides in southern Taiwan after 2009 Typhoon Morakot using remote sensing and spatial analysis. Natural Hazards and Earth System Sciences. 10:2179-2190.

Wu C-U, Chen S-C, Feng Z-Y (2013) Formation, failure, and consequences of the Xiaolin landslide dam, triggered by extreme rainfall from Typhoon Morakot, Taiwan. Landslides. 11(3):357-367.

Spatial engineering geological and geotechnical modelling of embankment with RNK-method and stability analyses of waste water treatment facility (UPOV) in Vukovar

Želimir Ortolan[(1)], Mensur Mulabdić[(1)], Krunoslav Minažek[(1)], Jelena Kaluđer[(1)], Jelena Matijević[(1)], Marko Ortolan[(2)]

1) J. J. Strossmayer University of Osijek, Faculty of Civil Engineering, 31000 Osijek, Drinska 16a, Croatia, krumin@gfos.hr

2) Croatian waters, Legal entity for water management, Sector for EU co-financed projects, Croatia

Abstract The RNK-method, or the Reference Level of Correlation method (RLC-method), is a procedure for spatial engineering geological and geotechnical modelling. The engineering geological (geotechnical) correlation column can be established in zones of limited extent (sometimes occupying tens of km²) using one or several characteristic layers, one of which is selected as the reference layer. In the established correlation column, a soil liquid limit and plasticity index appear as useful indicators of the peak, fully-softened and residual friction angle for coherent soils and soft rock formations. As a rule, maximum plasticity index and liquid limit values correspond to the minimum values of such friction angles. It offers the opportunity to produce for correct spatial engineering geological (geotechnical) modelling that differentiates between minimum shear strength zones (the weakest link in the "geotechnical chain of shear strength"), zones of different hydraulic conductivities, and zones of various degrees of natural compaction. The RNK method was tested on many landslides in Croatia, and in this paper the results obtained by applying the method on the potentially unstable area of the waste water treatment facility (UPOV) in Vukovar are shown. This project and its location are of special interest owing to the presence of loess soils, the vicinity of the river, relatively high seismic activity and warning signs of instability. In order to perform a correct stability analysis here the authors have put a lot of effort into creating an engineering geological (geotechnical) model based on the results of field and laboratory tests – tests planned not exclusively for stability analysis (most of the investigation works were previously planned for the foundations of the structures on the site).

Keywords liquid limit, plasticity index, RNK-method, spatial geotechnical model, slope stability

Introduction

Exact geotechnical modelling procedures aspire to full correlation of formations within a single geotechnical column. By using the possibilities provided by a detailed correlation of formations, which is actually quite common in geological sciences, it has been demonstrated (Ortolan 1990) that all results obtained using geotechnical testing in a relatively limited area of investigation may be interpolated in the corresponding part of the vertical sequence in the correlational geotechnical column. This is achieved by means of one or several reference layers, one of which is selected as the principal or reference layer. Ortolan (1996) proposed that this layer be called the reference level of correlation – RNK – while he defined it as a clearly recognizable bedding or any other reference plane, with respect to which it is possible to precisely determine the height position of all studied profiles with individual results obtained by point testing for any kind of material, in a single vertical lithostratigraphical or geotechnical sequence (correlational engineering geological column). This enables us to obtain a consistent engineering geological soil model in which is possible to logically attribute concrete numerical parameters to each individual layer along the entire height of the studied vertical layer sequence, which leads to the creation of a geotechnical model. With the correlational column devised in such way it is possible to differentiate, in a general way, parameters for zones of minimum residual shear strength, together with their thicknesses and continuities.

The correlational geotechnical column of the studied area is the "key" through which overall geotechnical relations are explained as per the required number of profiles and for two- and three-dimensional modelling. It has also been demonstrated that the presence of visually recognizable reference layers is not required. In fact, any reference plane can be selected as RNK, provided laboratory testing is performed with sufficient frequency by depth. Then the position of formations (layers) may be determined by an unequivocal positioning of the plane through three points, even in the zones where this was not possible by measuring the layer's position on the basis of visible outcrops.

The plasticity index has proven to be a reliable strength indicator for coherent materials (Ortolan 1996; Ortolan and Mihalinec 1998). The highest plasticity index values and those for the liquid limit correspond to the lowest expected values of friction angle. This fact allows for a new approach to exact geotechnical modelling.

The RNK method or the Reference Level of Correlation method (Ortolan 1996) is a fully developed method

for engineering geological and geotechnical modelling. It is primarily designed for analysis of the slope stability of soils and soft rock formations. The following supporting documents are most often used in the study of landslides: general geological map of the wider area under study, geotechnical correlation column and engineering geological map with slip plane contour lines, with clearly delineated slip areas and hydroisohypses or hydroisopiestic lines at the slip-plane level (Ortolan 1996, 2000). Consistent use of the RNK method from 1995 to the present day has resulted in the elaboration of three-dimensional geotechnical models for more than sixty landslides.

The Podsused landslide may be described as one of the most complex urban landslide projects in the world (Ortolan 1996; 2000). It is the project on which the RNK method has been developed in full detail, and the reliability of the model was confirmed using photogrammetric measurements (Ortolan et al. 1995) as well as three-dimensional stability analyses (Mihalinec and Stanić 1991).

Most of the studied landslides have been stabilized, in all cases with great success. The supervisory work conducted during the realization of improvement efforts provided positive feedback information regarding the correctness of the adopted engineering geological and geotechnical landslide models and about the reliability of the engineering geological (geotechnical) correlation column (design cross section). On some projects the reliability of the model was checked and confirmed on the basis of appropriate auscultation measurements using inclinometers, piezometers and benchmarks.

Overview of results and discussion

Over the past decade, parallel laboratory tests of residual shear strength, Atterberg plasticity limits and granulometry have all served to help numerous authors make correlations of residual or peak friction angles: using clay fraction content, liquid limit, plasticity index or a combination of all three indicators through experiments. Some authors have explored the influence of mineralogical composition on the residual strength of natural soils and mineral mixtures and numerous other influences on the residual shear strength of cohesive soil. Other authors have also explored and described in detail the residual shear mechanism and the reasons for possible deviations from determined principles. Skempton (1964; 1970) pointed to the relevance of peak, fully-softened and residual shear strength in some concrete cases. A detailed overview of these research efforts is presented in published papers (Ortolan 1996; Ortolan and Mihalinec 1998).

Despite some imperfections, a successful correlation between the plasticity index and the residual friction angle can clearly be noted in most of the above- mentioned papers. However, this fact is not sufficiently exploited in precise geotechnical modelling (Ortolan 1996). Ortolan and Mihalinec (1998) showed a practically usable correlation from which it was possible to determine the lowest peak and residual friction angle with the plasticity index of natural materials. On the basis of numerous tests of Atterberg limits and residual shear strength, the correlation diagrams of peak and residual friction angle with plasticity index and liquid limits have been updated.

An integrated approach to solving ground engineering problems

Bock (2006) writes: "Ground engineering is essentially a serial process directed towards the ground engineering structure. The process is characterised by an integration of all relevant aspects into a comprehensive scheme as depicted in Fig. 1." Writing about the degree of cooperation between engineering geologists and geotechnical engineers, he also remarked: "The requirement for formal linkages and feedback between the various professional practitioners within the field of ground engineering is project specific. It is highest in projects of the geotechnical category 3 as defined in Eurocode 7, encompassing the most demanding geotechnical projects. Such dominance gradually decreases with geotechnical categories 2 and 1. Accordingly, the degree of explicit cooperation between engineering geologists and geotechnical engineers can be linked to the geotechnical categories as specified in Tab. 1. Engineering geologists and geotechnical engineers are unified in their overall objective to create a geologically and technically sustainable, cost effective and safe engineering solution."

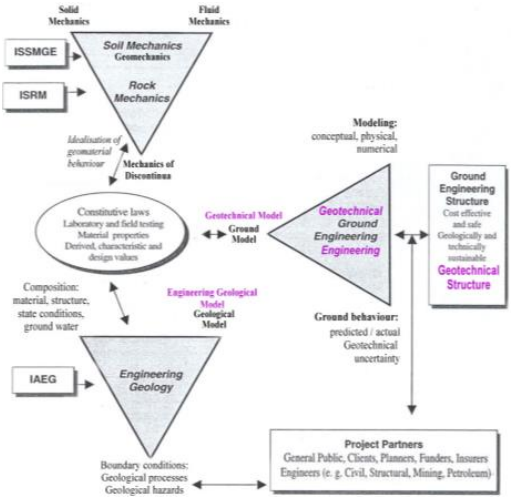

Figure 1 Position of soil mechanics, rock mechanics and engineering geology and the associated international societies within ground engineering (modified of Bock after JEWG 2004).

This integrated approach to solving ground engineering problems was applied, to the fullest possible extent, in all cases using the RNK method in the case of the spatial geotechnical modelling of the embankment and the stability analyses of the waste water treatment facility (UPOV) in Vukovar.

Table 1 Level of cooperation between engineering geologists and geotechnical engineers (after Bock 2006).

Geotechnical category Eurocode 7	Cooperation
1	Optional
2	Desiderable
3	Essential

Unfortunately, there were no piezometers installed in the area of interest on UPOV in Vukovar, so ground water levels are logically assumed in the geotechnical model.

Estimation of the shear strength of the materials at the site and similarities with Batina and Erdut

From 2010 to 2012, Ortolan explored landslides in Batina and Erdut (Croatia). The results of laboratory tests of loess and fossil humus from these areas are presented, among others, in Fig. 2. In the case of spatial geotechnical modelling of the embankment using the RNK method and a stability analyses of the waste water treatment facility (UPOV) in Vukovar it was particularly useful to know the residual shear strength of the same materials that build the Batina and Erdut areas. The similarity between the loess and fossil humus from Batina, Erdut and Vukovar is clearly visible on the plasticity diagram with samples of all three locations (Fig. 3). This fact allows the use of shear strength parameters from materials from Batina and Erdut and at Vukovar.

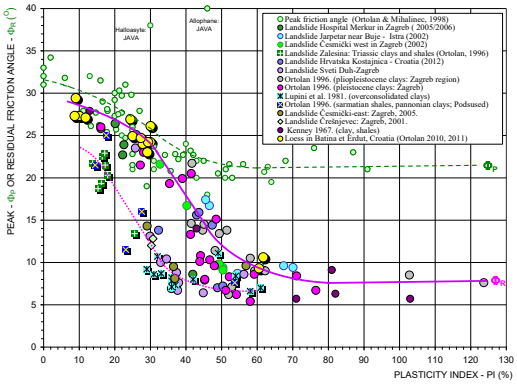

Figure 2 Correlation of the peak and residual friction angle with the plasticity index of natural materials.

Tiwari and Ajmera (2011) published a diagram that allows us to estimate the fully-softened friction angle by knowing the plasticity index (Fig. 4). For the investigated area, the curve for plasticity index values up to 80 % is appropriate. In the geotechnical column of the Vukovar region there are often clayey sands. For their display in the geotechnical column, the correlation is shown in Fig. 5. There are numerous indications of the instability of the natural slopes on the right bank of the Danube River in Vukovar; some of them are shown here (Fig. 6-9).

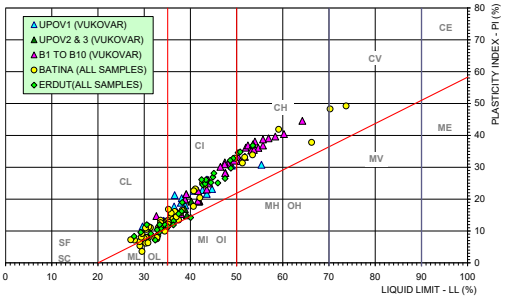

Figure 3 Similarity of loess and fossil humus samples from Batina, Erdut and Vukovar in the plasticity diagram.

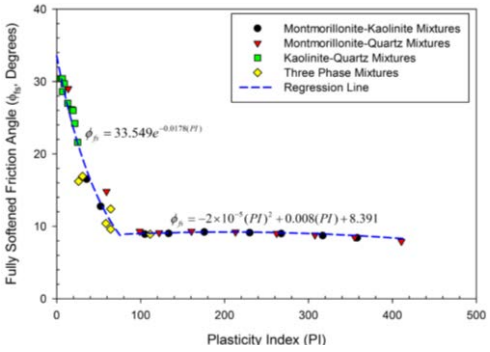

Figure 4 Variation of the fully-softened friction angle with the plasticity index (after Tiwari and Ajmera 2011).

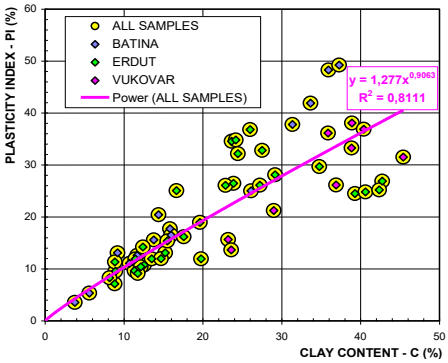

Figure 5 Correlation of the plasticity index with clay fraction content in Batina, Erdut and Vukovar. This is used for sandy materials for which only the granulometric composition is tested.

Landslides in Batina and Erdut were investigated by Ortolan (1984; 2012). The foreheads of these landslides were formed along deep tensile cracks. Similar cracks have been observed along the forefront of the very recent instability in Vukovar (Fig. 7, 8).

Geotechnical boundary conditions and the prognostic engineering geological model

Using all known engineering geological (geotechnical) boundary conditions, a correlation engineering geological (geotechnical) column has been constructed (Fig. 11).

Figure 6 Along the right bank of the Danube river are regular occurrences of landslides and escarpments.

Figure 7 Tensile cracks observed along the forefront of recent instability in Vukovar.

Figure 8 Landslide Velika Skela 57 activated in August 2008.

Figure 9 The crown of the stone embankment leaning back, warning of possible instability.

Figure 10 Construction of the planned embankment for the waste water treatment facility (UPOV) in Vukovar.

A critical breakdown zone is defined in the zone with the lowest shear strength values. Using the low shear strength of the clay layer zone in certain boreholes, the floor and roof of the critical layer of clay were determined. The ground floor and the roof of the clay layer were reconstructed on the basis of a detailed engineering geology map of the area (Fig. 14).

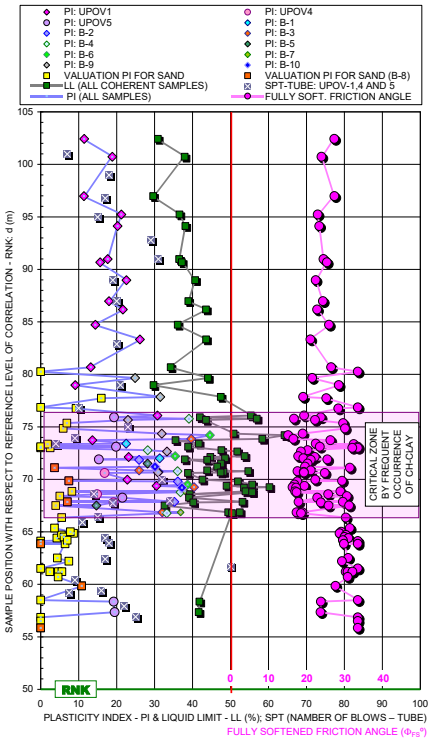

Figure 11 Engineering geological (geotechnical) correlation column for the investigated area in Vukovar.

In Batina it has been proven (Ortolan 1984) that the landslide at the church is activated after a sudden drop in the water level of the Danube River (Fig. 12). During investigation work on the landslide at the church in Batina, the dependence of cohesion and friction angle on moisture content in undisturbed loess samples was examined (Fig. 13).

The facts illustrated in Figures 12 and 13 for Batina can also be used for the design of a suitable geotechnical model in Vukovar owing to the remarkable similarities of the geotechnical boundary conditions.

Absolute level lines of underlying and overlying strata of critical clayey layers were used for the final design of the prognostic engineering geological (geo-technical) profile A-B with predefined sliding surfaces (Fig. 15). The presence of the Vukovar – Novi Sad reversal fault is a crucial factor in the selection of fully-softened friction angle.

Stability analyses

Based on prognostic engineering geological maps and profiles, geotechnical models for slope stability calculations for several cross sections were developed using the

conservatively selected shear strength parameters presented in Tab. 2.

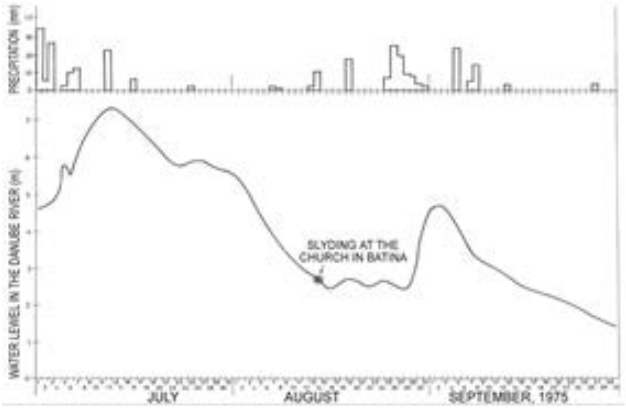

Figure 12 The moment of landslide activation at the church.

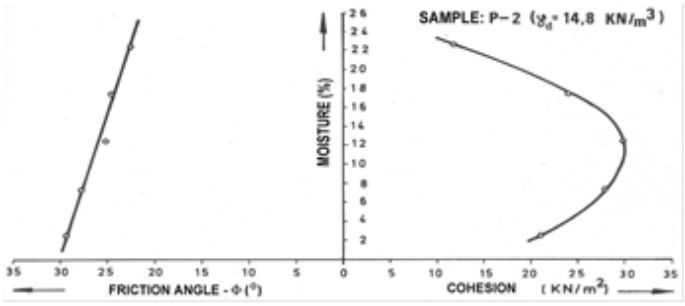

Figure 13 Dependence of cohesion and friction angle on moisture content in undisturbed loess samples (Ortolan 1984).

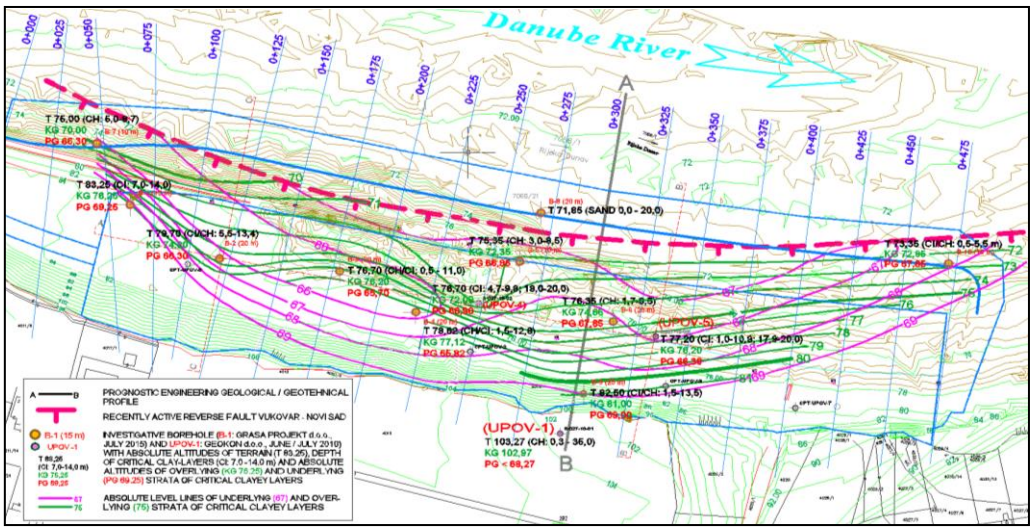

Figure 14 Detailed engineering geology map of the area.

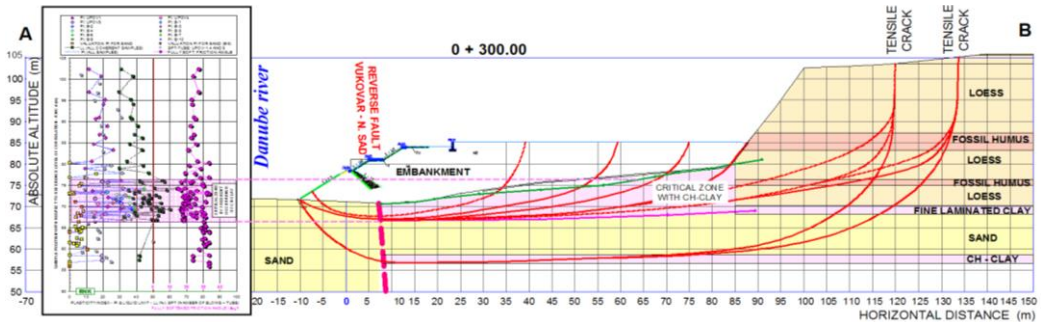

Figure 15 Prognostic engineering geological (geotechnical) profile A-B with predefined sliding surfaces.

The models and the results of the stability analysis at one of the analysed cross sections (0+300,00) before and after construction of the embankment to form a future plateau (necessary for complete structural construction) are shown in Fig. 16 and 17. A standard approach using safety factors in a stability analysis of the state prior to construction of the embankment (modeled with very conservatively selected shear strength parameters, pore pressures and the existence of tensile cracks) shows marginal (in)stability (factor of safety ≈ 1). Even for such a conservative model the stability is improved after the embankment is built to the required level (proven using stability analysis according to EC 7).

Table 2 Shear strength parameters for slope stability calculation.

	Soil	γ (kN/m3)	c (kPa)	Φ (°)
1	Clay	20.00	7.00	18.00
2	Sand	20.00	0.00	30.00
3	Tensile crack	20.00	0.10	0.10
4	Loess	20.00	5.00	25.00
5	Fossil humus	19.00	10.00	28.00
6	Fossil humus 2	19.00	5.00	24.00
7	Fine laminated clay	19.00	0.20	24.00
8	High plasticity clay	20.00	5.00	28.00
9	Hydraulic fill	19.00	0.00	32.00

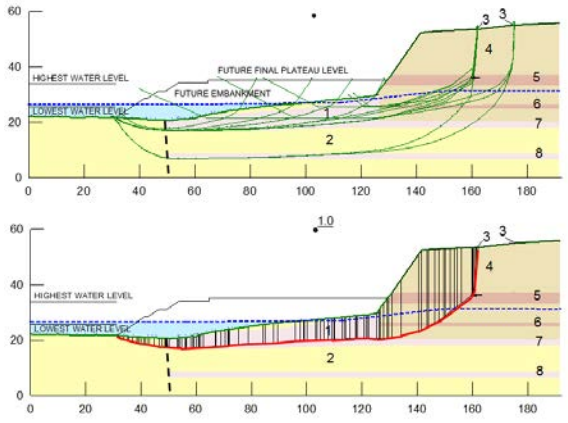

Figure 16 Model (upper figure) and the results (lower figure) of slope stability analysis on cross section 0+300 before embankment construction, rapid draw-down analysis, standard safety factor calculation approach.

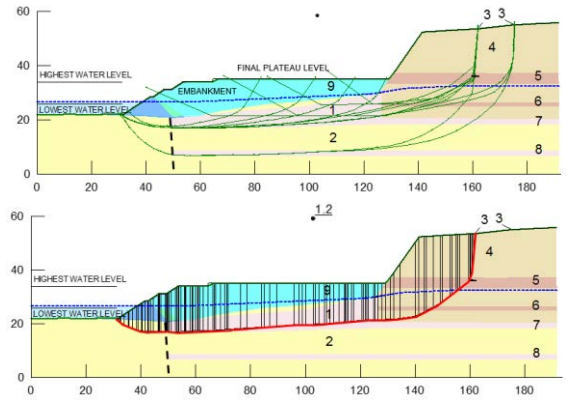

Figure 17 Model (upper figure) and the results (lower figure) of slope stability analysis on cross section 0+300 after embankment construction, rapid draw-down analysis, calculation according to EC7.

Conclusion

Considerable variability in ground conditions, water conditions and the overall complexity of an area possibly prone to landslides required extensive cooperation between engineering geologists and geotechnical engineers for the waste water treatment facility project in Vukovar. The results of such cooperation provided an opportunity to model complex geological conditions using the RNK method, although a more extensive investigation using a larger number of tested and better preserved samples, together with determined pore pressure distribution would provide more detailed results in the process of defining a geotechnical model of the location. However, the results obtained in the course of this project demonstrate that the method is well suited to the preparation of exact engineering geological and geotechnical models, and that the use of such a method is highly recommended. The complexity of the problem underlines the need for caution, so both additional investigations and observations during project execution in order to confirm the assumptions applied in the design process and a plan for eventual remediation is strongly recommended.

References

Bock H (2006) Common ground in engineering geology, soil mechanics and rock mechanics: past, present and future. Bulletin of Engineering Geolology and the Environment. 65: 209-216.

Jurak V, Ortolan Ž, Slovenec D, Mihalinec Z (2004) Verification of engineering geological/geotechnical correlation column and reference level of correlation (RNK) method by observations in the slip-plane zone. Geologia Croatica. 57(2): 191-203.

Kenney TC (1967) The influence of mineral composition on the residual strength of natural soils. In: Proc Geotech Conf on Shear Strength Prop of Nat soils and Rock, Oslo. pp. 123-129.

Lupini JF, A. E. Skinner & P. R. Vaughan 1981. The drained residual strength of cohesive soils. Geotechnique 31(2): 181-213

Mihalinec Z, Stanić B (1991) Three-dimensional stability analysis procedure. Građevinar. 9: 441-447. (in Croatian)

Ortolan Ž (1984) Evaluating stability and causes of landslide occurrences in loess formations of the region of Batina. In: Proc 81th Yugoslav Symposium on Hydrogeology and Engineering Geology, vol 2., Budva. pp. 177-190.

Ortolan Ž (1990) The role of correlation methods in determining zones of minimum parameters of the shear resistance. Proc 6th Int IAEG Congress, Balkema, Rotterdam. pp. 1675-1679.

Ortolan Ž (1996) The creation of a spatial engineering geological model of deep multi-layered landslide (on an example of the Podsused landslide in Zagreb). PhD thesis, Faculty of Minning, Geology and Petroleum Engineering, University of Zagreb, Zagreb, Croatia. 245p. (In Croatian)

Ortolan Ž, Mihalinec Z (1998) Plasticity index Indicator of shear strength and a major axis of geotechnical modeling. In: Geotechnical hazards, Proc. of the XI-th Danube-European conference on soil mechanics and geotechnical engineering, 25-29 May 1998. Poreč, Croatia. pp. 743-750.

Ortolan Ž (2000) A Novel Aproach to the Modelling of Deep Complex Landslides with Several Sliding Planes. Landslides in Research - Theory and Practice. In: Proc 8th Int Symp on Landslides, ISSMGE & BGS, vol 3., 26-30 June 2000. Cardiff, Wales. pp. 1153-1158.

Ortolan Ž, Mihalinec Z, Stanić B, Pleško J (1995) Application of repeated photogrammetric measurements at shaping the geotechnical models of multi-layer landslides. In: Proc. 6th Int Symp on Landslides, Balkema, Rotterdam. pp 1685-1691.

Skempton A W (1964) Long term stability of clay slopes. Geotechnique. 14: 77-101.

Skempton A W (1970) First-time slides in over-consolidated clays. Geotechnique. 120: 320-324.

Tiwari B, Ajmera B (2011) A new correlation relating the shear strength of reconstituted soil to the proportions of clay minerals and plasticity characteristics. Applied Clay Science. 53(1), 48–57.

Extreme precipitation events and landslide activation in Croatia and Bosnia and Herzegovina

Sanja Bernat Gazibara [(1)], Martin Krkač[(1)], Ivana Vlahek[(1)], Krešimir Pavlić[(1)], Hamid Begić[(2)], Sabid Zekan[(3)], Marin Sečanj[(1)], Snježana Mihalić Arbanas [(1)]

1) University of Zagreb, Faculty of Mining, Geology and Petroleum Engineering, Pierottijeva 6, 10000 Zagreb, Croatia, sbernat@rgn.hr

2) The Federal Institute for Geology, Ilidža, Bosnia and Herzegovina

3) Faculty of Mining, Geology and Civil Engineering, University of Tuzla, Bosnia and Herzegovina

Abstract This paper focuses on analysing the relationship between extreme precipitation conditions and rainfall-triggered landslides in Croatia and Bosnia and Herzegovina. During the winter and spring of 2013, extreme weather conditions (re)activated more than 900 shallow landslides in NW Croatia. In May 2014, the low-pressure cyclone Tamara (Yvette) affected a large area of Southeastern and Central Europe, causing floods and landslides, with the greatest damage incurred in Bosnia and Herzegovina. The most affected area was the central region of Bosnia and Herzegovina, with more than 7100 (re)activated landslides. Analysis of extreme precipitation conditions showed that both short- and long-duration rainfalls were responsible for the large number of landslide initiations in NW Croatia and central Bosnia and Herzegovina. Understanding the relationship between landslides, precipitation conditions and climate change are therefore crucially important in planning a proactive approach to landslide risk reduction.

Keywords landslides, precipitation conditions, ID threshold, Croatia, Bosnia and Herzegovina

Introduction

Landslides are common phenomena in Croatia and Bosnia and Herzegovina (BIH). Precipitation (rainfall and snowmelt) and manmade activities are two of the most frequent triggering factors (Mihalic Arbanas et al. 2017). Landslide activation for a given precipitation event can be analysed based on a database of precipitation events that resulted (or did not result) in landslides in the study area and neighbouring regions. The main problem with the current practice of landslide risk reduction in both countries is the lack of suitable landslide inventories and historical databases of landslide events.

The winter period of 2012/2013 in the continental part of Croatia saw extreme weather conditions that caused the (re)activation of more than 900 landslides (Bernat et al. 2014a). The highest number of reported landslide events was in the NW Croatian counties of Krapina-Zagorje County, Varaždin County and the City of Zagreb.

Over 13-17 May 2014, the low-pressure cyclone Tamara (Yvette) affected a large area of Southeastern and Central Europe, causing floods and landslides. Among the affected countries, BIH suffered the greatest damage from floods and landslides. The most affected areas include basins of the Bosna, Vrbas, Drina, Sana and Sava rivers. As a result of the flooding, 21 people died, more than 66,000 people were evacuated from their homes, more than 60,000 houses and buildings were damaged or destroyed, and more than 7100 landslides were (re)activated (Muhić 2015), with total damage estimated at more than two billion euros.

The aim of this paper is to present a preliminary analysis of antecedent precipitation conditions that have caused landslides and historical precipitation events in NW Croatia and central BIH, as well a comparison with global and national ID (Intensity-Duration) thresholds.

Study area

NW Croatia

The study area is located in the northwestern part of Croatia (Fig. 1), which occupies an area of approximately 10,500 km^2 with 1,659,169 residents (approximately 40% of the total Croatian population). NW Croatia includes 34 cities and 132 municipalities in six counties. Due to its geomorphological and geostructural position, NW Croatia belongs to the European Pannonian Basin. Relief changes from lower mountain areas, hilly areas to lowland areas (45% of total area; elevations <150 m a.s.l.) (Bernat Gazibara et al. 2017a). The lower mountain areas are constituted mainly of Mesozoic carbonate rocks, sporadically clastics and volcanoclastics and Paleozoic clastic rocks, sporadically carbonates, and metamorphic rocks. Hilly areas are composed of Pleistocene and Neogene sediments (i.e., engineering soils and soft rock-hard soils, mainly marls).

The climate is temperate continental with a mild maritime influence. Based on the precipitation data recorded

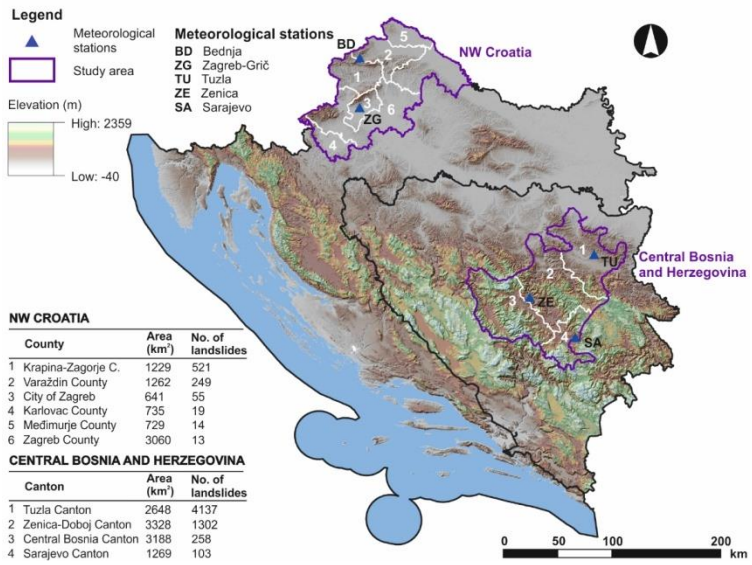

NW CROATIA

	County	Area (km²)	No. of landslides
1	Krapina-Zagorje C.	1229	521
2	Varaždin County	1262	249
3	City of Zagreb	641	55
4	Karlovac County	735	19
5	Međimurje County	729	14
6	Zagreb County	3060	13

CENTRAL BOSNIA AND HERZEGOVINA

	Canton	Area (km²)	No. of landslides
1	Tuzla Canton	2648	4137
2	Zenica-Doboj Canton	3328	1302
3	Central Bosnia Canton	3188	258
4	Sarajevo Canton	1269	103

Figure 1 Relief map of Croatia and Bosnia and Herzegovina with study area and meteorological station marked.

at Zagreb-Grič weather station for the past 154 years (from 1862 to 2014), this area received an average annual precipitation (MAP) of about 883.6 mm.

Central Bosnia and Herzegovina

The study area is located in the central part of Bosnia and Herzegovina and occupies approximately 10,000 km² (approximately or 20% of the land area) and includes 73 municipalities. Most of the territory of BIH in the area of the Internal Dinarides is comprised of mountains and hills (approximately 93%) (Mihalić Arbanas et al. 2017). Hills and lowlands are mostly present in the northern regions of BIH and are composed of various Pre-Neogene rocks of Dinaride Ophiolite Zone, in addition to Neogene clastic rock (marlstones) and carbonate rocks and Plio-Quaternary soils. The northern peri-Pannonian part of BIH belongs to a moderate continental climate zone with cold winters and warm summers. Generally, the MAP decreases from the west (1,500 mm) to the east (700 mm) (Abolmasov 2016).

Landslides

NW Croatia

Landslides are common phenomena in NW Croatia due to geomorphological, geological and climatic conditions and several anthropogenic factors, such as inadequate slope design, changes in land cover or slope gradients, and improper drainage of storm water (Mihalić Arbanas et al. 2017). The main triggering factors are rainfall and snowmelt, because most of the reported landslides in this area occur during months characterised by intense precipitation (Bernat Gazibara et al. 2017a). The hills and lowlands in NW Croatia are prone to small (10-10^3 m²) to medium-sized landslides (<10^5 m²) and superficial to moderately-shallow (<20 m) landslides (Bernat Gazibara et al. 2017b). In spite of their relatively small volume, soil slides cause significant damage to buildings and infrastructure because of the high landslide density involved. For example, Bernat Gazibara et al. (2017b) identified 676 landslides within the 21 km² area of Zagreb.

Information related to the (re)activation of landslides in the winter period of 2012/2013 was received from citizens who informed city administration personnel responsible for landslide remediation or civil protection throughout the period in question. Evidence of landslides is recorded in the City offices only in the form of lists with data on landslide location and date of activation. Fig. 1. shows the number of (re)activated landslides in the continental part of Croatia as a consequence of heavy precipitation events in winter 2012/2013 (Bernat et al. 2014a).

Bosnia and Herzegovina

Landslides are largely conditioned by morphological features and complex geological settings, resulting in sheared and jointed rocks with deep weathering zones (Mihalić Arbanas et al. 2017). Climatic conditions cause physical processes of prolonged high precipitation, rapid melt of deep snow and floods. Moreover, anthropogenic causal factors have had a major impact on changes in slope stability since 1990, given the large population migrations and illegal construction actions involved. According to Abolmasov (2016), landslides in BIH occurred most frequently in areas composed of volcanogenic-sedimentary deposits (diabase-chert series and Jurassic ophiolitic mélange) followed by Neogene clastic sediments, clastic sediments of Lower Triassic-Upper Cretaceous age and flysch-type sediments (from Jurassic to Eocene and Paleozoic shales). All Pre-Neogene and Neogene rocks are prone to slope movements, resulting in a wide

variety of landslide types, such as slides, debris/earth flows, rock falls and toppling.

The area of the Internal Dinarides in BIH experienced most of the landslides during the time of Cyclone Tamara in spring 2014, when more than 7,100 landslide activations were recorded. A general overview of landslides triggered by abundant rainfalls and floods in spring 2014 on the territory of BIH was given by Abolmasov (2016). The exact number of landslides is not known, except for Tuzla Municipality, where a landslide inventory exists (Abolmasov 2016) and contains more than 2,000 registered landslides (Mulać and Žigić 2017). Babić et al. (2017) reported the number of new landslides activated as a consequence of heavy rainfalls in May 2014 in the most-affected cantons in BIH (Fig. 1).

Extreme precipitation event in NW Croatia

Antecedent rainfall

Measurements obtained by the Zagreb-Grič and Bednja meteorological stations (Fig. 1) were used to analyse precipitation patterns in NW Croatia. Daily precipitation data for each meteorological station includes the amount of rainfall and snow. The Zagreb-Grič station has been measuring such conditions the longest of any station (154 years) in Croatia.

From 14 January to 5 April 2013, NW Croatia experienced prolonged and intense rainfall and snowmelt with cumulative values over the 82-day period exceeding 390 mm (at Zagreb-Grič) and 420 mm (at Bednja). Locally, the cumulative precipitation for the selected period exceeded 45% of MAP. In the selected period, significant precipitation episodes occurred on 14–25 January, 3 February–2 March, and 9 March–5 April (Fig. 2) and (re)activated large number of landslides. The first rainfall episode, 14–25 January, was characterized by cumulative precipitation of 130 mm, while the second precipitation episode, from 3 February–2 March, was less severe, with cumulative precipitation around 100 mm. The largest number of landslides was (re)activated during the third rainfall episode, 9 March–5 April, and was characterized by total precipitation in the range of 149.7 mm (at Zagreb-Grič) to 172.3 mm (at Bednja).

Historical rainfall data

The NW part of Croatia was particularly wet at the beginning of 2013. In the City of Zagreb, annual precipitation ranges from 550 mm to slightly over 1,100 mm, while MAP is 883.6 mm. In the Bednja area annual precipitation values are higher (MIN 618.5 mm, MAX 1222.3 mm, MAP 942.7 mm). At the Zagreb-Grič and Bednja meteorological stations, annual precipitation in 2013 (1092.4 mm and 1212.1 mm) was 23-28% higher than the MAP.

Fig. 3 shows the 3-month cumulative precipitation for January, February and March 2013 measured at the Zagreb-Grič and Bednja meteorological stations. Comparison showed that the 3-month cumulative precipitation for March 2013 was 136% (at Bednja) to 151% higher (at Zagreb-Grič) than the average 3-month value for the same month from 1862 to 2016. Based on the available historical data for the Zagreb-Grič meteorological station, analysis of the 3-month period from January to March showed that cumulative precipitation for the analysed period in 2013 was the highest ever recorded, and is unique for the period of the past 154 years.

Analysis of cumulative monthly precipitations for January-March 2013 at Bednja station showed that cumulative monthly rainfall ranged from 60% (in March), 95% (in January), to 188% (in February) higher than the average monthly values for the same period 2006–2016 (Fig. 3). For the selected period at the Zagreb-Grič station, monthly precipitation in 2013 was from 130% (February and March) to 190% (January) higher than the average monthly values for the period 1862–2016.

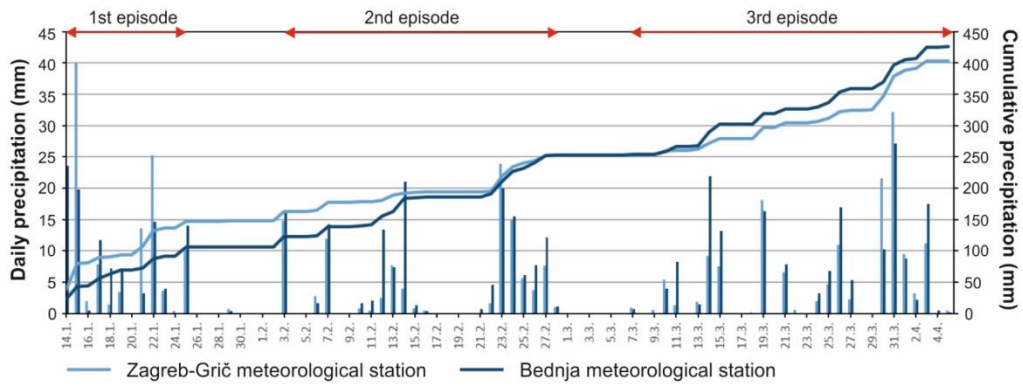

Figure 2 Daily and cumulative precipitation for winter period 2012/2013 (14 January – 5 April 2013) at Zagreb-Grič and Bednja meteorological station.

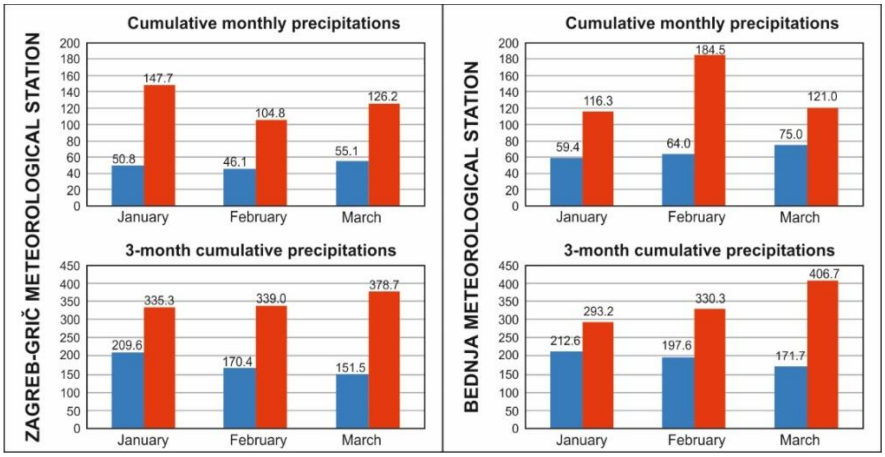

Figure 3 Analysis of cumulative monthly and 3-month cumulative precipitation data at Zagreb-Grič and Bednja meteorological stations. The red bars show values for 2013, and the blue bars show long-term averages over a period of 154 years (1862–2016).

Extreme precipitation event in central BIH

Antecedent rainfall

In order to investigate rainfall conditions that resulted in floods and landslides in central BIH in May 2014, we used rainfall measurements obtained at three meteorological stations – Sarajevo, Tuzla and Zenica (Fig. 1).

In central BIH, the rainfall event started after midnight on 12 May (Fig. 4), with moderately intense rain at the Sarajevo station (2.5 mm/h) and light rain at the Zenica station (0.86 mm/h), which stopped around 8:00 on 12 May. The rainfall event continued with moderately intense rain before noon on 13 May. Less than 20 mm of rain (at Tuzla) to more than 30 mm (at Sarajevo and Zenica) was measured in the 12-h period between 11:00 and 23:00 on 13 May. At Sarajevo meteorological station rainfall intensity increased significantly around midnight of 13/14 May (maximum intensity was 11.4 mm/h), and decreased after 2:00. At Tuzla station the period of moderately intense rainfall lasted 44 h, until 7:00 on 15 May, with an average intensity of 2.58 mm/h, and at Zenica station intense rain fell for 67 h, until 4:00 on 16 May, with an average intensity of 3.44 mm/h. The rainfall event continued at reduced intensity and ended at approximately 7:00 on 17 May. Precipitation event totaled around 140 mm in 93h at Sarajevo and Zenica station, while Tuzla station saw approximately 80% more rain (254.2 mm), with no difference in the duration of the rainfall event.

Historical rainfall data

The MAP in central BIH ranges from 787 mm (at Zenica) to slightly over 930 mm (at Sarajevo). Annual precipitation in 2014 at the Sarajevo station (1082.7 mm) was 16% higher than MAP. At the Zenica and Tuzla stations, annual precipitation in 2014 (1200.6 mm and 1353.1 mm) was 53-60% higher than the MAP. In addition, annual precipitation in 2014 was the highest annual precipitation recorded at the Zenica and Tuzla station over the last 66 years (1949–2015).

Fig. 5 shows the 3-month cumulative rainfall measured at the Sarajevo, Tuzla and Zenica meteorological stations for April and May 2014. A comparison of 3-month cumulative rainfalls for the month when floods and landslides occurred, with long-term 3-month cumulative averages showed that the 3-month cumulative rainfall for May 2014 ranged from 80% (at Sarajevo), 120% (at Zenica) to 180% (at Tuzla) higher than the average 3-month value for the same month 1949–2015 (Fig. 5). In addition, the 3-month cumulative rainfall values for May 2014 represents the highest cumulative rainfall for a 3-month period value in the last 66 years.

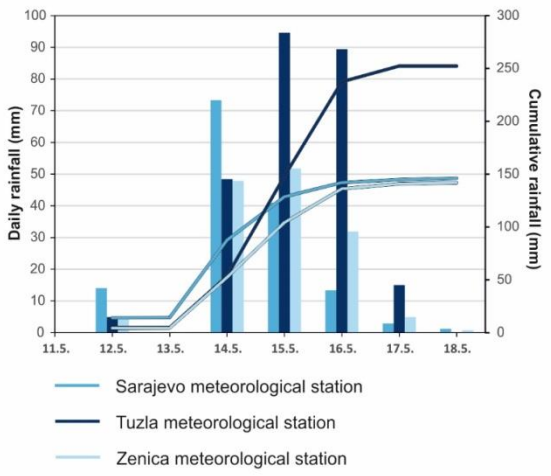

Figure 4 Daily and cumulative rainfall for cyclone Tamara (12 -17 May 2014) at Sarajevo, Tuzla and Zenica meteorological stations.

Analysis of cumulative monthly rainfalls showed that during April and May cumulative monthly rainfall was from 100-118% (at Sarajevo), 172-278% (at Tuzla) to 134-220% (at Zenica) higher than the average monthly figures for the same period 1949–2015 (Fig. 5). Cumulative monthly rainfall values for April and May 2014 at Sarajevo, Tuzla and Zenica station are the highest ever measured since 1949.

Comparison with global ID thresholds

Empirical rainfall thresholds are defined by past rainfall events that have activated landslides. Many thresholds combine mean rainfall intensity during a rainfall event with event duration (Caine 1980; Clarizia et al. 1996; Crosta and Frattini 2001; Guzzetti et al. 2007, 2008). Empirical ID thresholds are typically represented by a power law equation in the form of $I=\alpha D^{\beta}$, where I is mean rainfall intensity of an event, and D is determined as the time elapsed between the precipitation starting time and the time of landslide activation, and α and β are empirically derived parameters (Caine 1980). Precipitation events were bounded by periods of no rainfall lasting at least four days for late autumn and winter (October-April), and two days for other seasons (May-September) (Melillo et al. 2015). In order to reconstruct the rainfall conditions that resulted in landslides in NW Croatia in 2013 and central BIH in 2014 it is necessary to compare them with other global and national rainfall intensity-duration (ID) thresholds. For the comparison, all duration D and mean intensity I data was plotted together using a bi-logarithmic scale (Fig 6.). A comparison of the plotted precipitation conditions that caused landslides in NW Croatia with published global ID thresholds (Caine 1980; Crosta and Frattini 2001; Guzzetti et al. 2008) shows that precipitation conditions are lower than the threshold curves proposed by other authors. The exception is the global ID threshold for soil slips presented by Clarizia et al. (1996), which shows the best fit with precipitation data on landslide occurrence in NW Croatia in winter 2012/2013. The precipitation conditions that caused landslides in central BIH in 2014 exceeded all published regional and global ID thresholds for landslides, except one proposed by Caine (1980). Taken together, precipitation events from 2013 and 2014 that triggered landslides are in the duration range of $72<D<816$ h, and in the cumulative precipitation range of $29.5<E<252.7$mm.

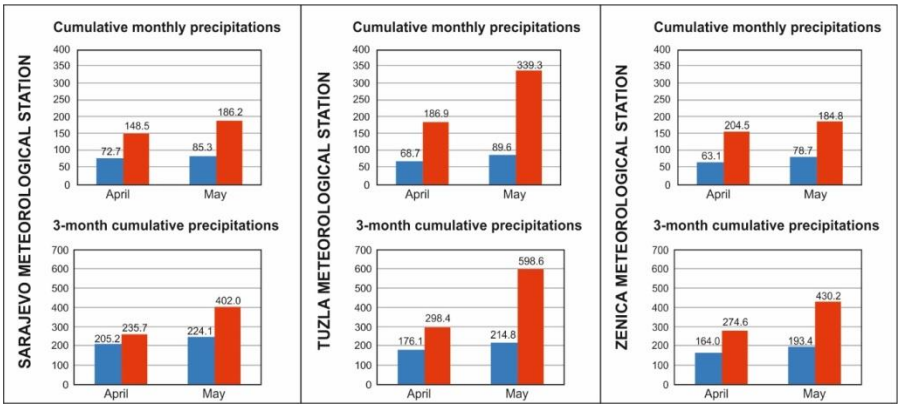

Figure 5 Analysis of monthly and 3-month rainfall data at Sarajevo, Tuzla and Zenica stations. The red bars show quantities for 2014, while the blue bars show long-term cumulative monthly and 3-month averages over a period of 66 years (1949–2015).

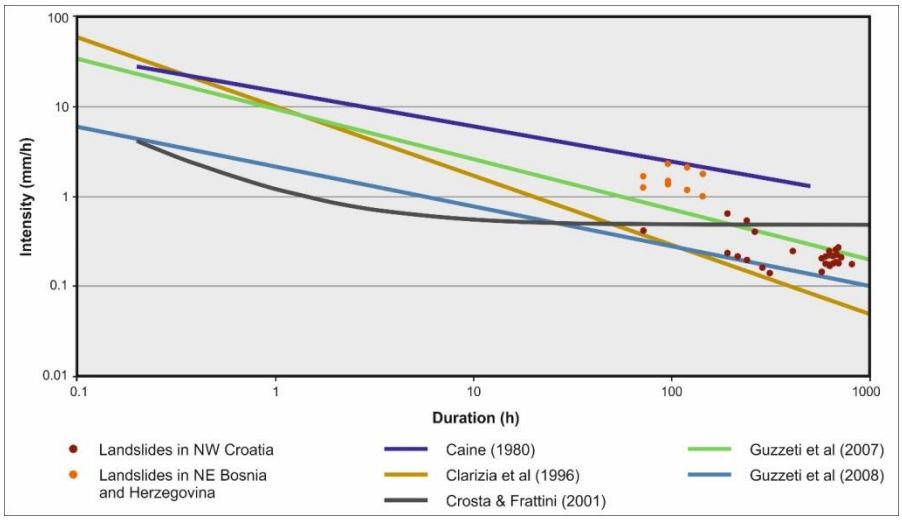

Figure 6 Comparison of the rainfall conditions (intensity-duration) that caused landslides in Croatia (winter 2012/2013) and Bosnia and Herzegovina (May 2014), with published regional and global ID thresholds.

Discussion and conclusion

The unusually large number of activated landslides in the hilly area of NW Croatia in winter 2012/2013 and central BIH in May 2014 is the result of extreme precipitation conditions. Analysis of cumulative monthly precipitation and 3-month cumulative precipitation figures showed that cumulative precipitation for the analysed period in 2013 in Croatia and 2014 in BIH are the highest ever recorded. A comparison of regional and global rainfall intensity-duration (ID) thresholds for landslides showed that precipitation conditions in central BIH and NW Croatia were likely to trigger landslides. Precipitation events in 2013 and 2014 have historical importance, i.e., these events were unique in the last 66 years (based on meteorological station data in central BIH) and 154 years (based on meteorological station data in NW Croatia) in terms of the influence of particular seasonal meteorological conditions on landslide activation in SE Europe.

Rainfall patterns that triggered landslides in NW Croatia and central BIH cannot be compared due to the great differences in their geotectonic, lithological and geomorphological characteristics and the climatic conditions in the given study areas (Pannonian Basin vs. Dinarides). Based on the available data related to the two precipitation events that triggered landslides in NW Croatia in 2013 and central BIH in 2014, it was impossible to define regional ID thresholds. Results of the preliminary analysis obtained in this study will be used for further study of empirical rainfall thresholds for landslides in Croatia and BIH. The first step is to create a catalogue of rainfall events that have triggered landslides, and that covers a longer period of time.

Understanding the relationship between landslides, rainfall patterns and climate change is therefore crucially important in planning a proactive approach to landslide risk reduction. Regional rainfall thresholds in combination with systematic rainfall measurements or forecasts can be used for landslide early warning systems (Jemec Auflič et al. 2016). Temporal changes of the climatic regime (e.g. increased intensities and frequencies of maximum daily rainfall in a given year) do not affect the precipitation threshold itself; rather, they only affect the frequency and intensity of severe rainfall events and therefore increase the frequency of landslide events in Croatia and BIH.

Acknowledgments

The authors would like to thank the DHMZ (Croatian Meteorological and Hydrological Service) and the FHMZBIH (Federal Hydrometeorological Institute in Bosnia and Herzegovina) for providing us with data. The dissemination/publishing process is supported by the Development Fund of the Faculty of Mining, Geology and Petroleum Engineering, University of Zagreb.

References

Abolmasov B (2016). Landslide risk management study in Bosnia and Herzegovina. URL: http://www.ba.undp.org/content/bosnia_and_herzegovina/bs/home/library/environment_energy/landslide-risk-management-study-in-bh.html [Last accessed: 4 January 2017]. (in Serbian)

Babić F, Begić H, Sorić I, Belić N, Sokolić Ž (2017) Categorization of landslides in the municipality of Vogošća activated in May 2014. In: Abolmasov B, Marjanović M, Đurić U (eds) Proceedings of the 2nd Regional Symposium on Landslides in the Adriatic-Balkan Region, 14-15 May 2015. Belgrade Serbia. pp. 233-238.

Bernat S, Mihalić Arbanas S, Krkač M (2014) Inventory of precipitation triggered landslides in the winter of 2013 in Zagreb (Croatia, Europe). In: Sassa K, Canuti P, Yin Y (eds) Landslide Science for a Safer Geoenvironment, Volume 2: Methods of Landslide Studies. Springer, Cham. pp. 829-836.

Bernat Gazibara S, Mihalić Arbanas S, Krkač M, Sečanj M (2017a) Catalog of precipitation events that triggered landslides in northwestern Croatia. In: Abolmasov B, Marjanović M, Đurić U (eds) Proceedings of the 2nd Regional Symposium on Landslides in the Adriatic-Balkan Region, 14-15 May 2015. Belgrade, Serbia. pp. 103-107.

Bernat Gazibara S, Krkač M, Sečanj M, Mihalić Arbanas S, (2017b) Identification and mapping of shallow landslides in the City of Zagreb (Croatia) using the LiDAR-based terrain model. In: Mikoš M, Tiwari B, Yin Y, Sassa K (eds) Advancing Culture of Living with Landslides, Volume 2: Advances in Landslide Science. Springer International Publishing. pp. 1093-1100.

Caine N (1980) The rainfall intensity-duration control of shallow landslides and debris flows. Geografiska Annaler, Series A, Physical Geography. (1/2): 23–27.

Clarizia M, Gulla G, Sorbino G (1996) Sui meccanismi di innesco dei soil slip. In: International Conference Prevention of Hydrogeological Hazards: The Role of Scientific Research. L'Artistica Savigliano. pp. 585-597. (in Italian)

Crosta GB, Fratini P (2001) Rainfall thresholds for triggering soil slips and debris flow. In: Proceedings 2nd EGS Plinius Conference on Mediterranean Storms, 1-3 October 2001. Siena, Italy. pp. 463-487.

Guzzetti F, Peruccacci S, Rossi M, Stark, CP (2007) Rainfall thresholds for the initiation of landslides in central and southern Europe. Meteorology and Atmospheric Physics. 98: 239-267.

Guzzetti F, Peruccacci S, Rossi M, Stark CP (2008) The rainfall intensity–duration control of shallow landslides and debris flows: An update. Landslides. 5:3–17.

Jemec Auflic M, Šinigoj J, Krivic M, Podboj M, Peternel T, Komac M (2016) Landslide prediction system for rainfall induced landslides in Slovenia (Masprem). Geologija. 59/2: 259-271.

Melillo M, Brunnetti M T, Peruccacci S, Gariano S L, Guzzetti F (2015) An algorithm for the objective reconstruction of rainfall events responsible for landslides. Landslides. 12: 311-320.

Mihalić Arbanas S, Sečanj M, Bernat Gazibara S, Krkač M, Begić H, Džindo A, Zekan S, Arbanas Ž (2017) Landslides in the Dinarides and Pannonian Basin – From the largest historical and recent landslides in Croatia to catastrophic landslides caused by Cyclone Tamara (2014) in Bosnia and Herzegovina. Landslides. 14/6: 1861-1876.

Muhić Š (2015) Case study. Maglaj – Floods, May 2014, Unpublished document. OSCE, Maglaj.

Mulać M, Žigić I (2017) The landslide causes and its zonation in Tuzla Region. In: Abolmasov B, Marjanović M, Đurić U (eds) Proceedings of the 2nd Regional Symposium on Landslides in the Adriatic-Balkan Region, 14-15 May 2015.Belgrade, Serbia. pp. 129-131.

Towards a Pan-European Database of Damaging Landslides

Gerardo Herrera[1,2], Eleftheria Poyiadji[1,3], Rosa María Mateos [1,2], Juan Carlos García- Davalillo [1,2], Juan López-Vinielles[1,2], Gilles Grandjean[1,4], Raluca Maftei[1,5], Tatiana- Constantina Filipciuc [1,5], Mateja Jemec Auflič[1,6], Jernej Jež[1,6], Laszlo Podolszki[1,7], Alessandro Trigila[1,8], Carla Iadanza[1,8], Hugo Raetzo[1,9], Arben Kociu[1,10], Maria Przyłucka[1,11], Marcin Kułak[1,11], Michael Sheehy[1,12], Xavier M. Pellicer[1,12], Charise McKeown[1,12], Graham Ryan[1,12], Veronika Kopackova[1,13], Michaela Frei[1,14], Dirk Kuhn[1,15], Reginald L. Hermanns[1,16], Kleopas Hadjicharalambous[1,17], Niki Koulermou[1,17], Colby A. Smith[1,18], Mats Engdahl[1,18], Pere Buxó Pagespetit[1,19], Marta Gonzalez[1,19], Claire Dashwood[1,20], Helen Reeves[1,20], Francesca Cigna[1,20], Pavel Liščák[1,21], Peter Pauditš[1,21], Vidas Mikulėnas[1,22], Vedad Demir[1,23], Margus Raha[1,24], Lídia Quental[1,25], Cvjetko Sandić[1,26], Balazs Fusi[1,27], Odd Andre Jensen[1,28], Jan Walstra[1,29], Philippe Steeghs[1,30], Aleksandra Gulan[1,31], Hjördis Löfroth[1,32], Boris Malyuk[1,33]

1) EuroGeoSurveys, The Geological Surveys of Europe, Earth Observation and Geohazards Expert Group (EOEG), Brussels, Belgium

2) Geological Survey of Spain (IGME), Geohazards Unit, Geohazards InSAR laboratory and modeling group, Madrid, Spain g.herrera@igme.es

3) Institute of Geology and Mineral Exploration, Engineering Geology Department, Athens, Greece

4) French Geological Survey (BRGM), Risk and Prevention Division, Orleans, France

5) Geological Institute of Romania, Bucharest, Romania

6) Geological Survey of Slovenia, Ljubljana, Slovenia

7) Croatian Geological Survey, Zagreb, Croatia

8) Geological Survey of Italy (ISPRA), Rome, Italy

9) Swiss Federal Office for the Environment, Bern, Switzerland

10) Geological Survey of Austria, Vienna, Austria

11) Polish Geological Institute – National Research Institute, Warsaw, Poland

12) Geological Survey of Ireland, Dublin, Ireland

13) Czech Geological Survey, Prague, Czech Republic

14) Federal Institute for Geosciences and Natural Resources (BGR), Berlin, Germany

15) Federal Institute for Geosciences and Natural Resources (BGR) on behalf of the participating SGS, Berlin, Germany

16) Geological Survey of Norway, Trondheim, Norway

17) Cyprus Geological Survey, Limassol, Cyprus

18) Geological Survey of Sweden, Uppsala, Sweden

19) Institut Cartogràfic i Geològic de Catalunya, Barcelona, Spain

20) British Geological Survey, Nottingham, United Kingdom

21) Geological Survey of Slovakia, Bratislava, Slovakia

22) Geological Survey of Lithuania, Vilnius, Lithuania

23) Federal Institute for Geology of Bosnia and Herzegovina, Ilidza, Bosnia and Hercegovina

24) Geological Survey of Estonia, Tallinn, Estonia

25) Laboratorio Nacional de Energia e Geologia, Amadora, Portugal

26) Geological Survey of the Republic of Srpska – Bosnia and Herzegovina, Zvornik

27) Geological Survey of Hungary, Budapest, Hungary

28) Norwegian Water Resources and Energy Directorate, Oslo, Norway

29) Geological Survey of Belgium, Brussels, Belgium

30) Geological Survey of the Netherlands, The Hague, Netherlands

31) Geological Survey of Serbia, Belgrade, Serbia

32) Swedish Geotechnical Institute, Linkoping, Sweden

33) Ukrainian State Geological Research Institute, Ukraine

Abstract The Earth Observation and Geohazards Expert Group (EOEG) from the Geological Surveys of Europe (EGS) has carried out a survey on the way geohazards, in particular landslides, are integrated into urban and land-use planning. This survey reveals heterogeneous policies across national borders, and a lack of knowledge about the actual socio-economic impacts of landslides in many of the countries reviewed. This overview stresses the need for a common legislative framework and a homogenization of national legislations, especially in the case of landslide hazards. With this long-term goal in mind, we analysed the landslide databases from the Geological Surveys of Europe, focusing on their interoperability and completeness. The 849,543 landslide records from the Geological Surveys allowed us to elaborate, for the first time, a landslide density map, including 210,544 km² of landslide-prone areas and 23,681 administrative areas where the Geological Surveys from Europe have recorded landslides. Comparison with the European landslide susceptibility map (ELSUSv1) allowed us to estimate that the completeness of the landslide databases (LDBs) from the Geological Surveys at some 17% on average, and varying between 1% and 55%. This variability arises out of the different landslide strategies adopted by each country. Hence, a greater coordination effort by all of the institutions working in landslide mapping is necessary in order to improve data integration and harmonization. In this framework, in 2015 EOEG compiled for the first time an annual report on damage landslides using data taken from Geological Surveys. The idea behind this initiative is to provide an annual landslide report based on a unified pan-European database that can provide information on spatial distribution, triggering events, types of landslides, and the social and economic impacts of such, making this geo-hazard visible to policymakers, decision makers and European citizens in order to reduce the impact of landslide disasters.

Keywords landslides, databases, damage, Europe

Introduction

Landslides are one of the most common and widespread geohazards in Europe, with significant social and economic impact. In past decades, the expansion of urban settlements has greatly increased risk of exposure to landslides. In view of growing urbanization, greater space requirements for settlements, various climate change scenarios and related consequences, the need for more security and protection from the risk of landslides is becoming increasingly important.

The Geological Surveys of Europe analysed the integration of geohazards into urban and land-use planning in 19 European countries (Mateos et al. 2017, Poyiadji et al. 2017). They found that 15% of countries do not include geohazards in spatial planning legislation, 40% still do not officially require geohazard maps in urban and land-use planning, and 50% lack official methodological guidelines for the production of maps. Moreover, there is scarce knowledge about the actual extent of the social and economic impacts related to geohazards and the transboundary nature of impacts is unevenly understood. Additionally, data fragmentation and data ownership restrictions in landslide inventories (Van Den Eeckhaut and Hervás 2012) hinder data integration and the development of strategies that could be used to understand and prescribe appropriate measures and thus reduce the risk of landslides in Europe. This is especially relevant with regard to landslide hazards, since there are no common guidelines or practices similar to Directive 2007/60/EC on the assessment and management of flood risks. Therefore, it is essential to develop a European Landslides Directive that provides a common legal framework for dealing with landslides.

The Geological Surveys of Europe, EuroGeoSurveys (EGS), is a not-for-profit organisation representing 37 National Geological Surveys and some regional Surveys in Europe, a workforce consisting of several thousand experts sharing their knowledge and expertise in the Geosciences through Expert Groups. In the first part of this manuscript results from the joint effort of 30 Geological Surveys (Herrera et al. 2017) are summarised. The annual report on destructive landslides gathered by the Geological Surveys in 2015 follows thereafter.

A review of landslides from the Geological Surveys

Landslide databases

LDBs in Europe from a variety of institutions, geological surveys, road & railroad authorities, water and energy authorities, national, regional and municipal authorities, and universities co-exist without being harmonized, integrated or simply being fully accessible. Herrera et al. (2017) reviewed the LDBs of 29 Geological Surveys of Europe from 24 countries accounting for 849,543 landslides (Fig. 1), of which 36% are slides, 10% falls, 20% flows, 11% complex landslides and 24% either unclassified or corresponding to other typologies. Most of them are located in Italy (62%) and 10 other countries. The majority of the LDBs (17) include landslides at 1:25.000 or larger, but others (10) report variable mapping scales ranging from 1:1.000 to 1:500.000. This is because their national LDBs integrate different landslide inventories mapped by different public institutions in different formats and scales. In order to obtain records of comparable quality the Geological Surveys apply standardized procedures in order to integrate different source LDBs into their own.

Landslide density map

The landslide density map of the Geological Surveys (LANDEN map) elaborated for 17 countries in Europe (Austria, Croatia, Cyprus, Czech Republic, France, Greece, Hungary, Ireland, Italy, Norway, Poland, Romania, Slovakia, Slovenia, Spain, Sweden and UK), provides

the first picture of the spatial distribution of the landslides recorded by the Geological Surveys over 3.65 million km² of European surface area (Herrera et al. 2017). The map reveals that approximately 6% are landslide prone areas, i.e., 1 km by 1 km cells with one or more landslide records. Note that they do not represent the real extent of mapped landslides (landslide area) but serve as an indicator of where landslides have been mapped. For instance, in Italy, which has the greatest density of landslides, landslide prone areas represent 35% of the Italian territory, whereas the landslide area represents only 7.3%. Taking this aspect into account, landslide prone areas occupy more than 10% of the Czech Republic, Slovenia, and Slovakia. In larger countries like the UK, Poland, France or Spain landside prone areas only represent 1-4% of the territory.

Landslide database completeness

Comparison of the LANDEN map with the ELSUSv1: the Landslide Susceptibility map of Europe (Günther et al. 2014) was successful for 70% of the area, whereas 28.9% of the area represents landslide susceptible areas without records from the Geological Surveys and 1.4% of the area represents areas not susceptible to landslides with records from the Geological Surveys (Herrera et al. 2017). Taking into account the results from the comparison of the LANDEN map with the ELSUSv1, the LDBs completeness has been evaluated. For this purpose, Herrera et al. (2017) calculate the relationship between landslide-mapped areas and the sum of ELSUSv1 susceptible areas with landslide-mapped areas that do not coincide with ELSUSv1. As a result, the estimated completeness of the landslide databases from the Geological Surveys is over 50% for Poland, Italy and Slovakia; for another five countries the figure varies from 10% to 30%; and for the rest of the countries the figure ranges between 6% and 1%. In countries like Spain or Greece the LDBs focus mainly on destructive landslides, whereas in Romania and Croatia we find only local and regional landslide databases held by the Geological Survey.

Annual report on damaging landslides 2015

Questionnaire

The idea behind this initiative is to provide an annual landslide report based on a unified pan-European database that can provide information on spatial distribution, triggering events, types of landslides and the social and economic impacts of such, making this geo-hazard visible to policymakers, decision makers and European citizens in order to reduce the impact of landslide disasters.

A questionnaire circulated among 38 Geological Surveys from Europe aimed at setting up a common database. This survey gathered simple, basic information about landslide events from 2015 that had significant consequences as recorded by Geological Surveys. The survey includes the following data: country, year, month, geographic coordinates (WGS84), type of landslide, triggering factor, affected area, deaths, injured, and source of information. Landslide types are divided into five classes according to Cruden and Varnes (1996): slides, falls, flows, complexes, other or unknown. The triggering factor is classified in earthquakes, precipitation, other or unknown. The affected area is classified as urban, road & rail networks, other or unknown. The source of information is classified as field survey, press or Internet, authorities or other.

A total of 22 Geological Surveys from 20 countries provided information. No landslide events occurred in Czech Republic and Sweden, whereas in the case of Bosnia and Herzegovina - Republika Srpska and Slovenia the damaging landslide events were not recorded by the Geological Surveys. In the case of Croatia, information on these events was provided only for the city of Zagreb.

Results

The damaging landslide database in 2015 includes 1,323 events from 17 countries (Fig. 1). Five countries including Austria, Italy, Serbia, Spain and the UK account for more than 90% of the total. The most common landslide type is the slide with 53% of the total, followed by falls (17%) and 3% both for flows and complex. In Italy 271 landslides (21%) were not classified, owing to the fact that at the time of the survey data of landslide damaging events provided by the Italian Geological Survey (ISPRA) was obtained from the media, online news and various reports. For this reason, the type of movement and the cause of the event were not then available, which was the task for the regional authorities to complete and provide ISPRA in order to update the Italian Landslide Inventory sometime later. Regarding the triggering factor, precipitation accounts for 80% of the records, 10% is unknown, 8% is other and 2% corresponds (mainly) to earthquakes triggering rock falls.

Recorded damaging landslides have mainly affected the road and rail network (48%), urban areas (20%) and 30% other areas. There were 56 fatal landslides (27 of them classified as rock falls) causing 21 deaths and injuring 37 people. The most heavily affected country is Italy, with 12 deaths and 25 injured (Fig. 9). Even though the main trigger in Italy is precipitation (30%) trigger information is not included for the majority of landslides (48%). Information on the locations where landslides hit victims reveals that urban areas and communication networks (roads and railways) represent 27% of the scenarios; “other” areas such as rural or coastal areas were more frequently affected. Note that slopes in urban areas and along road and rail networks are usually protected (reinforced and/or monitored), while “other” areas like the countryside (hiking trails) are not so strictly monitored.

Discussion and conclusions

EuroGeoSurveys's analysis of the integration of geohazards, in particular landslides, into urban and land-use planning, reveals heterogeneous policies across national borders, and a lack of knowledge regarding the actual extent of the social and economic impact of landslides in many of the countries under discussion. This overview stresses the need for a common legislative framework and homogenization of the national legislations, especially as regards landslide hazards.

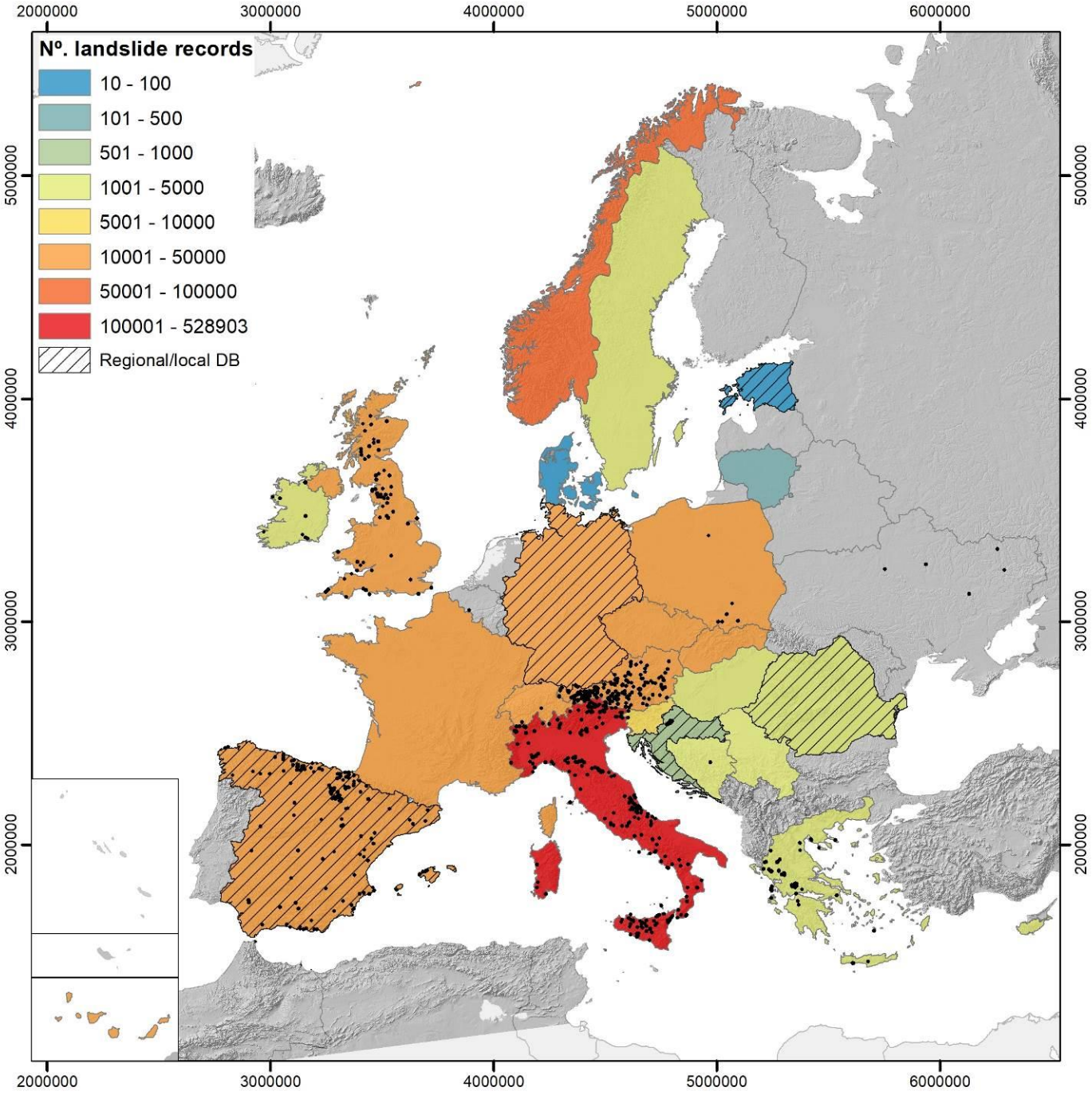

Figure 1 Number of landslides reported by the Geological Surveys of Europe. In black, the landslide damaging events occurring in 2015 as reported by 17 Geological Surveys.

The review of Landslide Databases (LDBs) from the Geological Surveys from 24 countries report 849,543 landslides, of which 36% are slides, 10% falls, 20% flows, 11% complex landslides and 24% either unclassified or corresponding to other typologies.

The landslide density (LANDEN map) elaborated for 17 countries in Europe reveals that there are approximately 210,000 km² of landslide prone areas, i.e. cells of 1 km² with one or more landslide records.

The completeness of the LDBs from the Geological Surveys is an estimated average of 17%, and varies from 1% to 50% among the analysed countries.

The Geological Surveys are working towards a European database of damaging landslides. To this end information was on 1,323 events occurring in 2015 from 17 countries was compiled. The most common landslide type is slide (53% of the total), with precipitation the main triggering factor. These largely affect infrastructure networks (road and rail), urban areas and others (countryside). The 56 fatal landslides (27 of them rock falls) caused 21 deaths and 37 injured, with Italy the most affected country.

This work has been useful in highlighting the need for a common legal framework to address landslide hazards in Europe and the existing gaps in terms of landslide database (in)completeness. In this context, the Geological Surveys of Europe would like to invite professionals and researchers from the Adriatic-Balkan region to help us improve this work through their participation in: (1) the landslide database review; (2) the landslide density map of Europe; (3) the damaging landslides database.

Acknowledgments

The Geological Surveys of Europe would like to sincerely thank all the scientists and technicians that worked to compile the landslide databases from each municipality, region and country over a period of years. This work, not always sufficiently acknowledged, constitutes the cornerstone of hazard and risk analysis necessary to reduce the impact of landslides and landslide hazard in Europe.

References

Cruden D M, Varnes D J (1996) Chapter 3 - Landslide types and processes. In: Turner A K, Schuster R L (eds) Landslides: Investigation and Mitigation. Special Report 247, Transportation Research Board, National Research Council. National Academy Press: Washington, DC, USA.. (ISBN 0-309-06151-2) pp. 36-75.

Günther A, Van Den Eeckhaut M, Malet J-P, Reichenbach P, Hervás J (2014) Climate13 Physiographically differentiated Pan-European landslide susceptibility assessment using spatial multi-criteria evaluation and transnational landslide information. Geomorphology. 224: 69-85.

Herrera G, Mateos R M, García-Davalillo J C, Grandjean G, Poyiadji E, Maftei R, ... Trigila A (2017) Landslide databases in the Geological Surveys of Europe. Landslides. In Press.

Poyiadji E, Kontogianni V, Nikolaou N (2017) Integration of Geohazards in Urban Planning and Management. Advanced Engineering Forum. 21: 557-563.

Mateos R M, Herrera G, García-Davalillo J C, Grandjean G, Poyiadji E, Maftei R, ... Trigila A (2017) Integration of Geohazards into Urban and Land-Use Planning. Towards a Landslide Directive. The Euro-GeoSurveys Questionnaire. Proceedings of the 4th World Landslide Forum, 29 May-2 June 2017. Springer, Cham. pp. 1067-1072.

Van Den Eeckhaut M, Hervás J (2012) State of the art of national landslide databases in Europe and their potential for assessing landslide susceptibility, hazard and risk. Geomorphology. 139: 545-558.

Analysis of rock falls on the Renke–Zagorje road section, Slovenia

Darja Rozina[(1)], Mateja Jemec Auflič[(2)], Timotej Verbovšek[(1)]

1) University of Ljubljana, Faculty of Natural Sciences and Engineering, Privoz 11, 1000 Ljubljana,Slovenia, timotej.verbovsek@ntf.uni-lj.si

2) Geological Survey of Slovenia, Ljubljana, Slovenia

Abstract The regional road section between the towns of Litija and Zagorje in central Slovenia is very problematic due to numerous rock fall events. These occur owing to the intensely fractured Triassic and Jurassic carbonates that form steep slopes above the road. Numerous accidents have been recorded by local police and road maintenance authorities, and field work was performed to measure the size and lithological composition of fallen rocks. Simulations of rock fall trajectories were performed on 14 profiles along the road section to calculate the trajectories, energies and locations of rocks using the RocFall 5.0 program. Results from the modelled problematic road sections are comparable with the field observations. Mitigation measures along the road include concrete walls, steel wire net barriers, crib walls, berms, gabions and road galleries; however, some damage occurs even in the protected areas, and some barrier nets are not cleaned regularly. Several further mitigation measures should be implemented in the future to avoid further accidents.

Keywords rock fall, Renke-Zagorje road, risk, Slovenia

Introduction

The regional road section between the towns of Litija and Zagorje in central Slovenia (particularly the eastern part of the road between Renke and Zagorje) is one of the most endangered sections in Slovenia, considering the amount of traffic, the very steep slopes and unfavourable geological conditions there (Ivnik and Ribičič 2014). Although numerous mitigation measures have already been implemented (concrete walls, steel wire net barriers, crib walls, berms, gabions, road galleries), the road is still prone to rock falls, as indicated by impacts on the asphalt, on the guard rails and rock fences, by car accidents and the appearance of rocks on the road. In order to identify the most prone sections a methodology combining fieldwork and computer modelling was applied. Rock fall modelling was performed using RocScience RocFall 5.0 software for 14 profiles along the road section to simulate the energy, velocity and bounce height of the falling rocks.

Geological setting

The analysed area belongs to the Sava folds, an intensely uplifted area composed of Permian-Carboniferous clastic rocks, Triassic and Lower Jurassic carbonates, Upper Cretaceous flysch and Quaternary deposits (Fig. 1; Premru et al. 1983a, 1983b). On the approximately 15 km road section, Middle and Upper Triassic limestones prevail, forming very steep slopes (Fig. 2). Tectonic fracturing and active tectonic uplift (Rižnar et al. 2005), which began in the Upper Miocene and Pliocene (Placer 1998), resulted in intensively fractured carbonates that serve to form many rock falls.

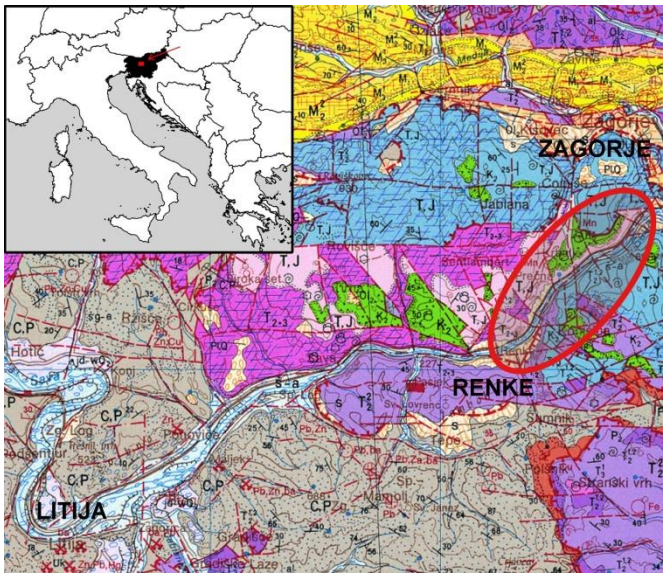

Figure 1 The geological setting of the studied area (from the Basic geological map OGK 1:100,000; Premru et al., 1983a). The studied area is shown inside the red ellipse, and major towns are written out in bold. Legend: *C, P*: Permian-Carboniferous clastic rocks, P_2: Permian sandstones, $T_2^{1,2}$, T_2^2, T_{2+3}, T_3^1: Triassic limestones and dolomites, *T, J*: Triassic and Jurassic limestones and dolomites, K_2: Upper Cretaceous flysch, M_1, M_2^2, M_3^1: Miocene clastic rocks, *s-a*: Quaternary slope deposits.

Materials and methods

Field measurements

In order to define the risk, the road was divided into smaller sections, each 500 m in length. Consequently, 14 sampling points and corresponding profiles (Fig. 3)

were selected to measure the blocks for the back analysis of the fallen blocks.

Figure 2 Steep slopes in Triassic dolomitized limestones above the road (road section between 12.500 and 13.000 km). The road is protected by a non-flexible net barrier and gabions.

On each such profile, the dimensions of 100 limestone and dolomite rocks were measured, and their lithological compositions determined. Also, all of the visible damage on the road and fence was documented, together with the geographical coordinates.

Data collection

Data on the location of road accidents related to rock falls was collected from the local police and road maintenance service. From the first source, data was collected for the full years of 2013, 2014 and 2015, which data included the location, time and type of recorded accident. From the second source, data was only available for the last full year of 2015, as the archives were only accessible from mid-2014 on for this road section. Data included the location, time and number of rock fall events on the road. A map showing the frequency of rock fall events and existing prevention measures on the selected road sections from both sources was prepared in GIS.

Rock fall modelling

Rock fall events were modelled in Rocscience software RocFall 5.0, by simulating limestone and dolomite rock falls of 100 rocks. Input block size was determined from the field measurements (back analysis), and 14 profiles were simulated along the road section. For the elevation layer, the digital terrain model (DTM) with a resolution of 1x1 m was used, and was obtained by national lidar scanning of Slovenian territory in the years 2014–15 (http://gis.arso.gov.si/evode/profile.aspx?id=atlas_voda_Lidar@Arso). Profiles were drawn in ESRI ArcGIS software as 3D lines and later exported into the RocFall program for simulations. Normal and tangential restitution coefficients were obtained from literature (Petje et al. 2005; Hoek 2007) and later calibrated to fit the measured locations along the road section.

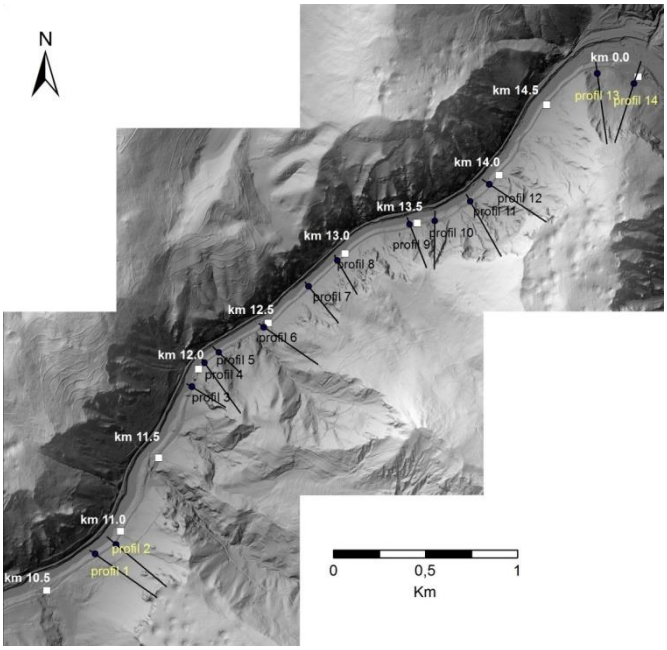

Figure 3 Locations of the simulation profiles and road sections in km.

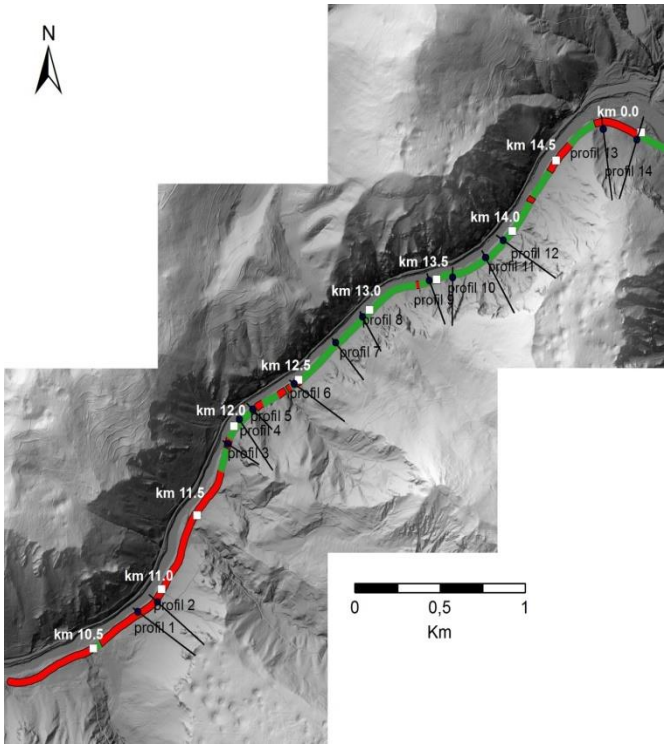

Figure 4 Status of protected road sections. Green: protected; red: unprotected.

Results and discussion

Field measurements

The average observed size of the carbonate blocks was about 35 x 30 x 50 cm, although far larger blocks were recorded. Field investigations of the protected road status showed that approximately half (55%) of the road length has some protection measures (Fig. 4); however, several of the net barriers were damaged or are not cleaned regularly.

Mitigation measures to protect the road largely consist in steel wire net barriers, concrete walls, crib walls, berms, gabions, and road galleries. In 2016 and 2017, dynamic net barriers were also installed in some sections.

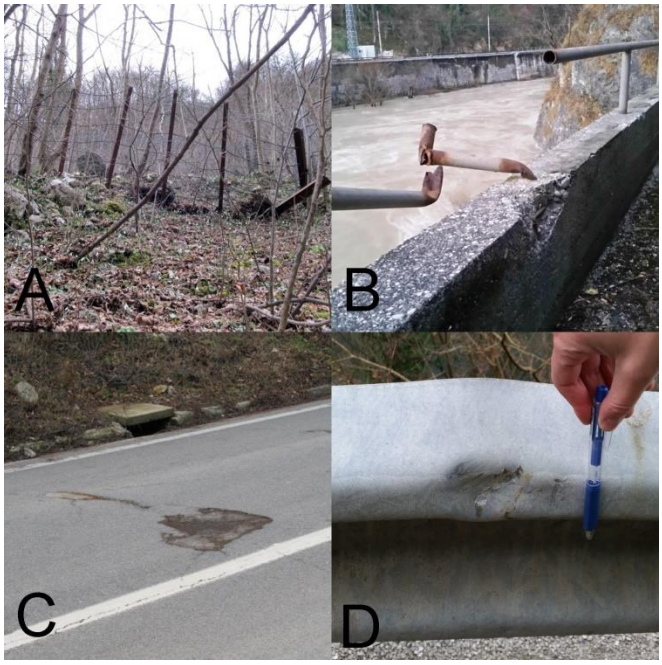

Figure 5 Selected observed damage. A: Fixed net barriers (note the large stopped blocks), B: Damaged concrete road fence along the river, C: Impact damage on the asphalt, D: Damaged road fence.

In the protected areas several cases of road damage were observed (Fig. 5). This problem can be attributed to insufficiently high existing barriers or the placement of such in inappropriate locations, thus allowing the rocks to avoid the net barriers. Some of the nets were also filled to approximately one-third their height, thus reducing their capacity to absorb impacts.

Police and maintenance data

Road maintenance service reported 269 rock falls in 2015, and police have reported 35 accidents for the past three years. However, not all accidents were reported. One should note that these numbers may actually be higher, as not all road damage and accidents are reported. People sometimes remove the fallen material themselves, and smaller instances of damage are not always reported. Most critical was the section from 13.400 to 14.300 m (north-eastern part, Fig. 6).

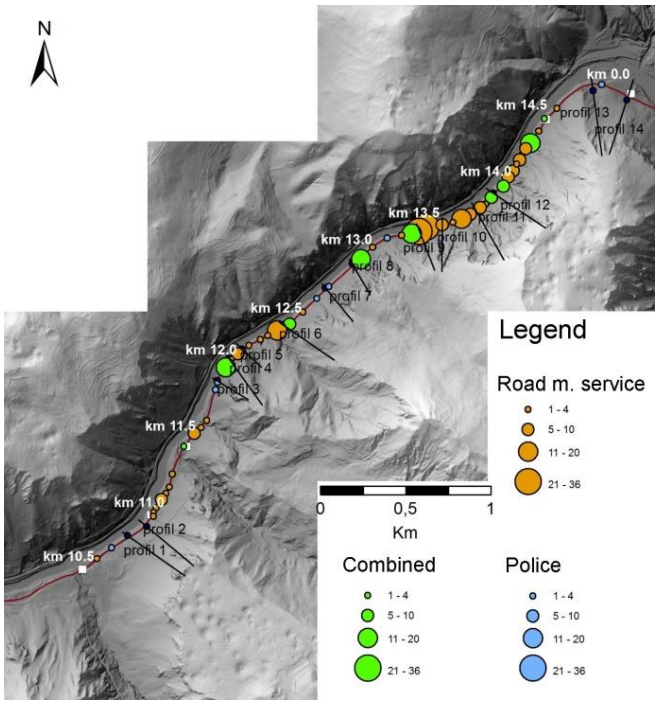

Figure 6 Numbers of detected road accidents and damage by local police (blue), road maintenance service (orange) and combined values (green).

Rock fall modelling

Rockfall simulations (Fig. 7) have shown most of the profiles to be problematic, as the majority of the rocks reached the road. These simulations are confirmed in the field, with many impact holes in the asphalt and road fences.

For the unprotected sections, rock fall simulations have confirmed the greatest impact of kinetic energies (maximum 297 kJ) for the most damaged sections. Larger energies were observed in profiles 11 and 12 in the most critical section, with the lowest values of approximately 15 kJ in the easternmost part of the road (profile 2) that features more gentle and vegetated slopes. Some exceptions regarding damage locations as extracted from the field observations compared to modelled locations were detected in profiles 6 and 7, which differences can be attributed to the 2D modelling, as the terrain is highly irregular and the trajectories of falling rocks can be complicated. Here 3D modelling would be more effective and appropriate (Li and Lan 2015).

According to these analyses, the road section was classified into four rock fall hazard classes, where the first class (no risk) represents only 1.5% of the road section. Over 90% of the road section was classified as high-risk classes 3 and 4, and indicate that this road section needs to be treated as one of the most dangerous road sections in the country. Results are presented on the map (Fig. 8; Tab. 1).

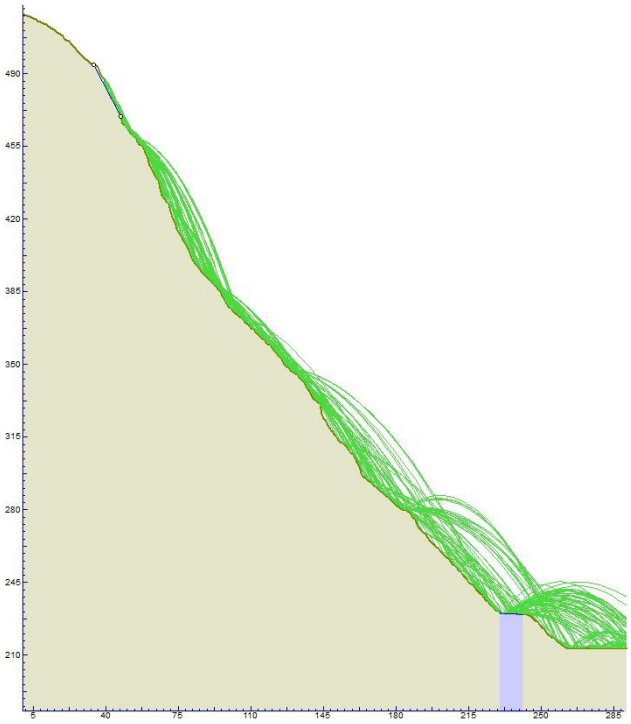

Figure 7 Example of simulated rock trajectories on profile #9 in Fig. 6. Violet colour: road.

Table 1 Risk classes with corresponding colours on the map and descriptions of them.

Class	Description
3 (red)	High risk. Drivers are highly exposed. Rock falls are numerous; road damage is common with bigger rocks along the road. Steep slopes.
2 (orange)	Moderate risk. Drivers are moderately exposed; rock falls are relatively common. Road is slightly damaged, small rocks appear along the road.
1 (yellow)	Low risk. Road and drivers are only slightly exposed; rock falls are rare. Road is not damaged, with no rocks along the road.
0 (green)	No risk. Drivers are not exposed, no damage on the road.

Recently, several mitigation measures (new steel wire net barriers) have been constructed in 2016 and 2017 on the most critical section (from gallery at 12.310 to 13.000 km; Fig. 9) and these measures will continue in the future along the other locations.

Conclusions

Despite the protection measures implemented, the investigated road section is still problematic due to the numerous rock fall events and accidents of recent years recorded by the local police and road maintenance services. Simulated trajectories and energies on the selected 14 profiles along the road based on their lithological compositions and steep slopes indicate that this is a problematic area that should be protected with additional measures, with regular maintenance provided for the already existing protective measures.

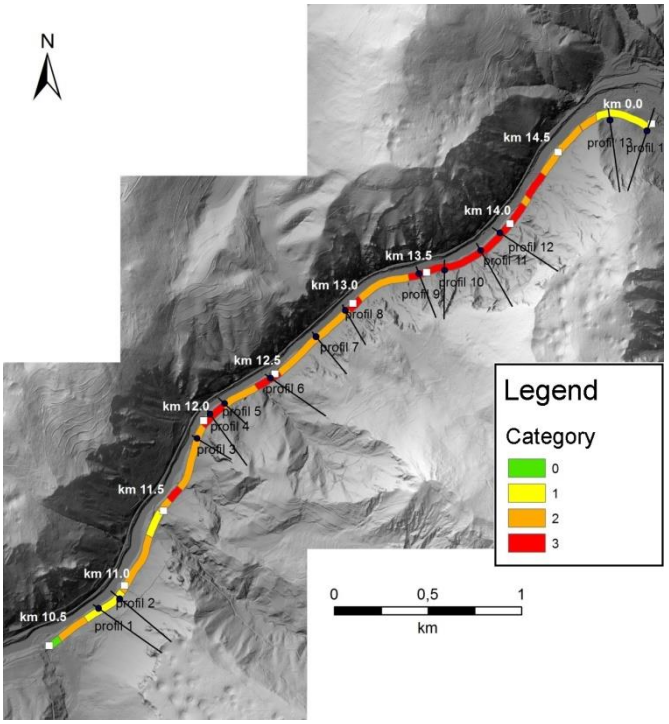

Figure 8 Map with four risk categories. For colour and number legend, see table 1.

Figure 9 New net barrier installed above the older protection measures.

Acknowledgments

This study was performed in the frame of a Bachelor thesis (Rock fall analysis on the road section Renke-Zagorje, Central Slovenia). The authors would like to thank the local police and road maintenance services for their help in providing vital data.

References

Hoek E (2007) Practical Rock Engineering (online), available on https://www.rocscience.com/documents/hoek/corner/Practical-Rock-Engineering-Full-Text.pdf [last accessed: 14th July 2017].

Ivnik M, Ribičič M (2014) Risk analysis from rock falls and other slope processes on the road G2 108 on the section 1183 Litija – Zagorje from km 12,000 to km 14,300 and on the section 1184 Zagorje – Trbovlje from km 2,200 to km 4,316. (Professional report.). Slovenian Infrastructure Agency. 68 p. (in Slovene)

Li L, Lan H (2015) Probabilistic modelling of rockfall trajectories: a review. Bulletin of Engineering Geology and the Environment. 74: 1163–1176.

Petje U, Ribičič M, Mikoš M (2005) Computer simulation of stone falls and rockfalls. Acta geographica Slovenica. 45(2): 93–120.

Placer L (1998) Structural meaning of Sava folds. Geologija. 41: 191–221.

Premru U (1983a) Basic Geological Map of SFRJ L33-66 1:100,000. Federal Geological Survey of Belgrade. Belgrade, Yugoslavia.

Premru U (1983b) Guide to the Basic Geological Map of SFRJ L33-66 1:100,000. Federal Geological Survey of Belgrade, Belgrade, Yugoslavia. 70 p.

Rižnar I, Koler B, Bavec, M (2005) Identification of potentially active structures along the Sava river using topographic, and levelling line data. Geologija. 48(1): 107–116.

Rozina D (2016) Rock fall analysis on the road section Renke-Zagorje, Central Slovenia. Diploma (BSc) thesis, University of Ljubljana, Faculty of Natural Sciences and Engineering, Department of Geology, Ljubljana. 78 p. (in Slovene)

GPR for detecting interlayer slides in turbidites – Anhovo (W Slovenia)

Marjana Zajc [(1)], Željko Pogačnik [(2)], Andrej Gosar [(3, 4)]

1) Geological Survey of Slovenia, Ljubljana, Dimičeva 14, 1000 Ljubljana, Slovenia, marjana.zajc@geo-zs.si

2) Georudeko, geology, mining and ecology d.o.o, Deskle, Slovenia

3) Seismology and Geology Office, Slovenian Environment Agency, Ljubljana, Slovenia

4) University of Ljubljana, Faculty of Natural Sciences and Engineering, Ljubljana, Slovenia

Abstract The ground penetrating radar (GPR) method was applied in order to differentiate rock layers within a heterogeneous turbidite, a multi-layered sedimentary formation that is formed by the re-sedimentation of vast amounts of material from underwater landslides and slope failures. The aim of the study was to determine the presence of discontinuities and unstable areas within this turbidite that have already proven capable of becoming sliding surfaces and producing landslides. The GPR results were correlated with the geological interpretation of partial outcrops as well as the lithostratigraphic map of the area. As our research area consists of heterogeneous materials with high signal attenuation, a low frequency 50 MHz rough terrain antenna (RTA) was used to ensure the depth penetration needed to reach different types of rock layers. The combination of geophysical and geological methods for the detection of layered bodies has shown to be very successful. Supported by adequate geological data, a systematic use of the GPR method can be effective in defining potentially and/or latently unstable rock masses, and can therefore be used to determine the scope of intervention needed for the construction and/or reconstruction of infrastructure.

Keywords landslides, interlayer slides, turbidites, ground penetrating radar (GPR), Rodež quarry, geohazard

Introduction

In the Rodež quarry in Anhovo, (W Slovenia, Fig. 1A), transport roads are being constructed perpendicular to the sediment transport axis, thereby increasing the possibility of geomechanical instability of the slopes (triggering sliding, rock fall and toppling). As this could create unsafe working conditions and have an economic impact as well, it is necessary to study the structural and lithological characteristics of the area in order to detect potentially unstable zones. New geological structures can often be detected in the ongoing process of mining the quarry banks and can help to plan safe excavation processes. One type of such structures found was the so-called multi-horse duplex parallel to the shear zone, which developed within the laminated shales between two thrusts in the Flysch Rodež (FR) succession (Ogata et al. 2014a; Fig. 1B). This unit contains channel-conditioned grain/debris flows (c-c g/df, Fig. 1B). Knowledge of those locations exhibiting such unstable sedimentological structures enables the quarry company to implement suitable safety measures and carefully plan their mining work strategies.

Along these complex heterogeneous horizons of subaquatic gravity flows slips as well as landslides (depending on the lithostratigraphy) have been triggered by blasting processes in certain orientations with regard to the axes of main gravity flows within the Rodež quarry. In order to prevent such hazardous events from happening in the future, detailed geologic mapping was carried out to study local geological features of the FR succession and define the discontinuities that could be reactivated as sliding surfaces. Low-frequency ground penetrating radar (GPR) was applied to determine whether it would be possible to detect these features in the wider quarry area where no outcrops are present.

The GPR method is an efficient and non-invasive geophysical method used for investigating the shallow subsurface. Its use in geological studies has been increasing rapidly, including in landslide studies (Barnhardt and Kayen 2000; Bichler et al. 2004; Sass et al. 2008; Mantovani et al. 2012; Kadioglu and Ulugergerli 2012). The method enables fast and easy data collection, while the results provide subsurface information also in areas where no outcrop or borehole data is available (Neal 2004). Electromagnetic waves are emitted from the transmitting antenna into the subsurface and reflected from boundaries between different types of material with different dielectrical properties (e.g. different types of strata, fractures, fault planes, water tables, cavity roofs and any other features that cause quick changes in electromagnetic properties in the material) back to the surface. The time it takes for the signal to travel from the transmitting antenna back to the receiving antenna after reflecting in the subsurface is measured in nanoseconds (ns) and later expressed as a function of depth (Blindow et al. 2007; Jol 2009). The depth range depends on the frequency of the antennas used; however, a number of other factors like signal attenuation, presence of water and clay fractions in the ground also have an impact on

the penetration (Davies and Annan 1989; Jol 2009). Detailed principles and use of the GPR method have been described in numerous publications (Davies and Annan 1989; Daniels 1996; Annan 2002; Milsom 2003; Neal 2004; Blindow et al. 2007; Jol 2009).

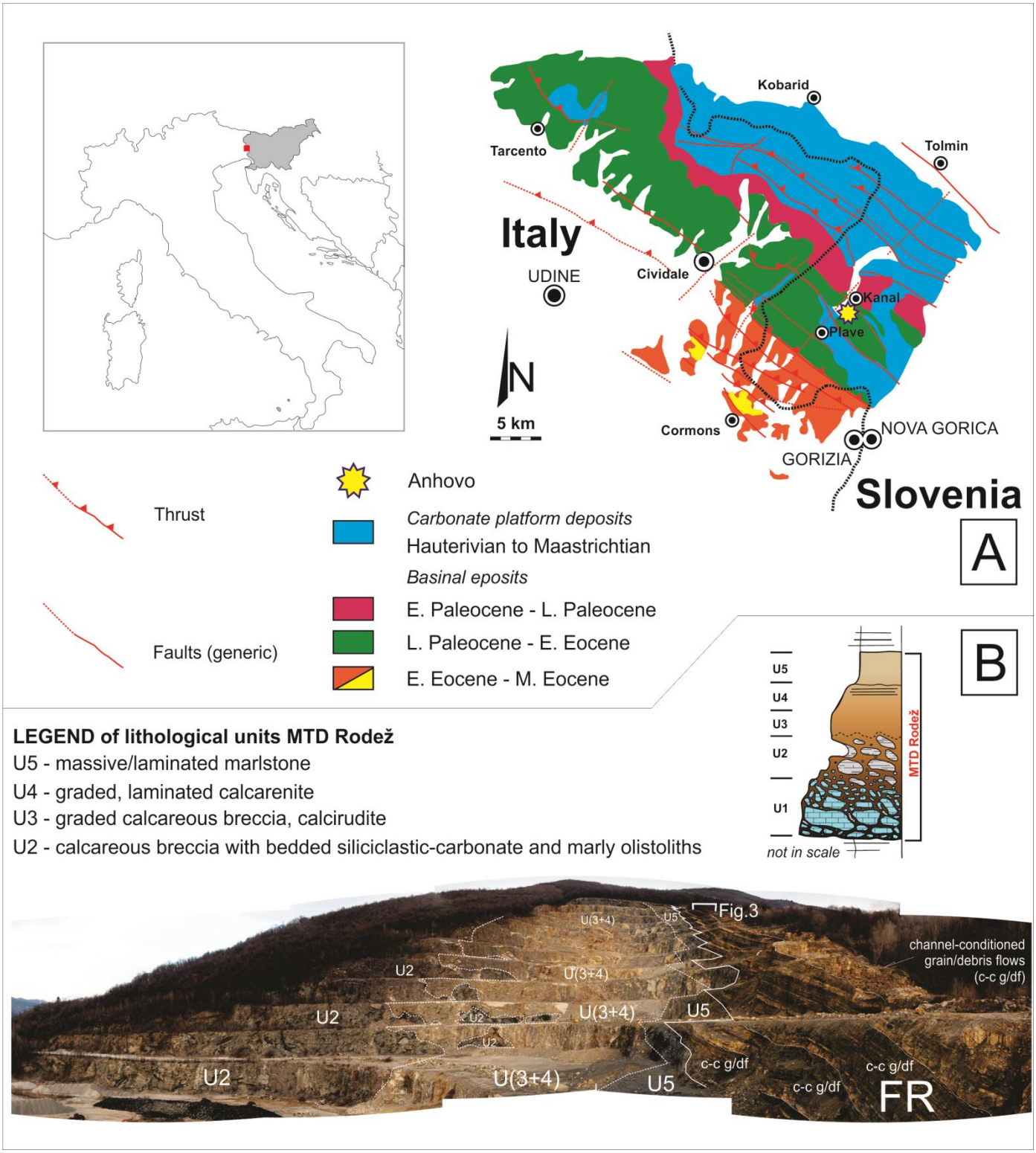

Figure 1 A – Geological map of research area (after Ogata et al. 2014a); B – photo of Rodež quarry with depicted lithological units of mass transport deposit (MTD) Rodež (U1 is not developed in this area) and FR succession with c-c g/df (photo: Kei Ogata) and indicated area of research (Fig. 3).

Structural integrity and the orientation of the lithological horizons play the key roles in determining the stability of the flysch layers. In determining the azimuth of the opening of the quarry banks, several structural and geomechanical properties of ductile rocks need to be taken into account (Marinos et al. 2005; Budeta and Nappi 2011): shear and residual shear angle, cohesion (Hajdarwish et al. 2013), chemical and mineralogical composition (Wan and Kwong 2002; Chen et al. 2010). Predicting the stability of the flysch slope (Azañón et al. 2010) is far more difficult when interlayer slides, which are largely the consequence of syngenetic deformations due to erosional gravity flows, are present. It is precisely the recognition and determination of these deformation structures that enable both safe and economically prudent planning of the exploitation fronts and the construction of infrastructure facilities (Pogačnik et al. 2015).

Study area

The research area is located in the central Soča Valley (W Slovenia, Fig. 1A), in the immediate vicinity of Anhovo, where the Salonit Anhovo cement factory has been operating for more than 90 years.

In geological terms the area belongs to the SW part of the northern Outer Dinarides (Ogata et al. 2014a; Placer 1981), namely the Friuli Basin. The rocks seen in outcrops are characterized by NW-SE orientated shear structural deformations as well as a monocline, which has a general incidence toward the SW in the investigated area and is kinematically linked to Dinaric thrusting, folding and faulting. In their final stage these features transform into reverse subvertical structural deformations (Fig. 1A). Formation of the Rodež single mass transport deposits (MTD; Ogata et al. 2014a) continues to the W and NW and is linked to the Ioanaz event on the Italian side (Ogata et al. 2014a).

The Julian-Slovenian basin and the Julian and Dinaric carbonate platforms developed from the late Campanian to the middle Eocene (Šmuc 2005; Rožič and Šmuc 2011) in the form of a composite foredeep system, which formed as the result of thrusting in the SW direction. Such dynamics caused the formation of elongated sedimentary depressions linked to shallow sedimentary environments with long axes in the SWS - NEN direction. Due to the progressive orogeny, the flysch units are younger toward the SW.

The Paleogene units stretch from eastern Friuli in Italy to western Slovenia, and represent the accumulation of heterogeneous carbonate debris. They extend over 100 km in width and represent a sequence of catastrophic events – underwater landslides that occurred when large parts of the shallow carbonate platforms collapsed and were re-deposited in deeper parts of the turbidity pool (Ogata et al. 2014a after Friuli Basin of Buser 1987 and Placer et al. 2010; Julian Basin, or Friuli Paleogene Basin of Selli 1953 and Gnaccolini 1968). Recent studies (Ogata et al. 2014a) show that there has been a sequence of catastrophic events with orthogonal transport orientations in this area: the Rodež MTD event (and other related events) with the transport direction from N to S, and perpendicular to this main transport sedimentation axis also proximal mass flows from the NE - E and SE sides (wedge – chain input, sensu Ogata et al., 2014a).

Methodology

Geological mapping

While mapping the outcropping FR unit, dips of proximal turbidite layers were measured and ductile deformations like intrafolial-hydroplastic folds, ductile shear zones, duplex-type/imbricated structures, asymmetric rootless folds, intra-block synformal and antiformal folds, intra-block and extra-block thrusts and mechanical lithologic mixing (e.g. stratal disruption) were studied (Fig. 2).

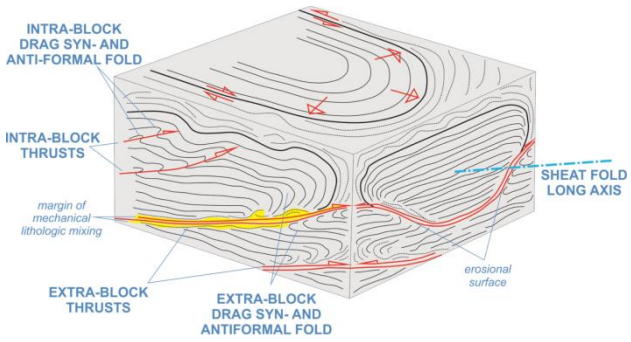

Figure 2 Main structural deformations in relation to flow direction of FR succession of the Rodež MTD (after Ogata et al. 2014b; 2016).

Ground penetrating radar (GPR)

The GPR profile was recorded along a horizontal road at the end of a quarry bench perpendicular to the estimated FR succession flow direction (Fig. 3). The Mala ProEx GPR recording unit was used with an unshielded 50 MHz rough terrain antenna (RTA) designed for difficult terrain and capable of depth penetration suitable for most geological studies. The time trigger mechanism with an interval of 0.2 s was used while recording, which requires steady movement along the profile lines. GPS coordinates of the start- and end-points of the profile were recorded in order to correctly calculate the profile length and for georeferencing purposes. Standard data processing was carried out using ReflexW from Sandmeier Software (DC shift, time-zero adjustment, background removal, gain, bandpass filtering and time to depth conversion).

Results

The results of the geological mapping gave two dipping angles of the c-c g/df sequence bedrock, i.e. 223/33 and

251/27, indicating the presence of two different flow directions. This means the structural deformations are probably synsedimental and linked to multiple erosional and synsedimentary events.

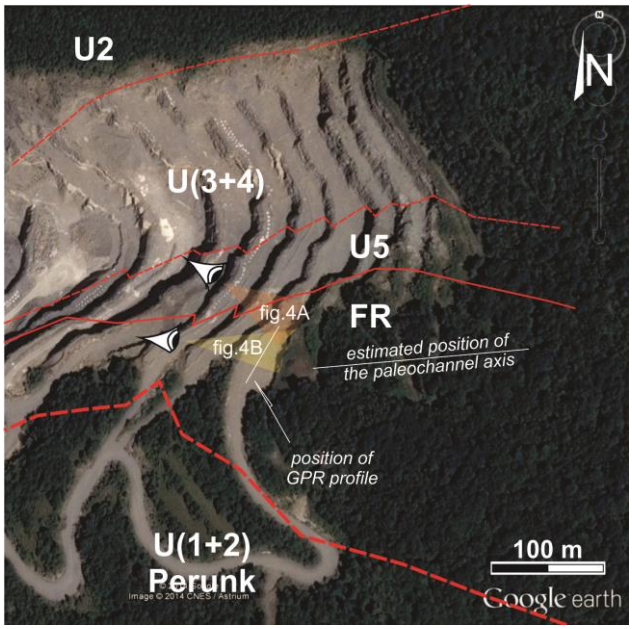

Figure 3 Position of the GPR profile in relation to the estimated orientation of the paleochannel/flow axis and views of Fig. 4.

Taking this new information into account it can be argued that the structural deformations are the result of ductile factors that show the mechanics of the erosion event of proximal carbonate turbidites that are conditioned by the paleotopographic channels (Unit 3 in Fig. 4).

By recording the GPR profile along the outcrop shown in Fig. 4 we were also able to gain information about the lithological and structural features in the shallow subsurface. Based on different reflection patterns seen in the GPR profile (Fig. 5), we can differentiate between different types of layers up to about 7 m in depth. The clearly seen linear reflectors that produce strong reflections consist of harder materials and represent the thicker graded calcareous breccia layer – one within Unit 1 and another within Unit 2 of the FR succession (yellow areas). Areas with weaker signal strength between these two breccia layers represent thinner and softer layers of claystones and siltstones, where signal attenuation is higher due to a far higher clay content (blue area). The irregular reflection pattern within this area suggests this is a structurally chaotic zone with stratal disruption. The last 10 m of the profile shows almost no reflections and represents a high signal attenuation area (red area). Here the upper limestone breccia layer already outcrops at the surface and the lower one is no longer visible. This part presents lateral changes and remains geologically and structurally undefined and therefore requires further investigation.

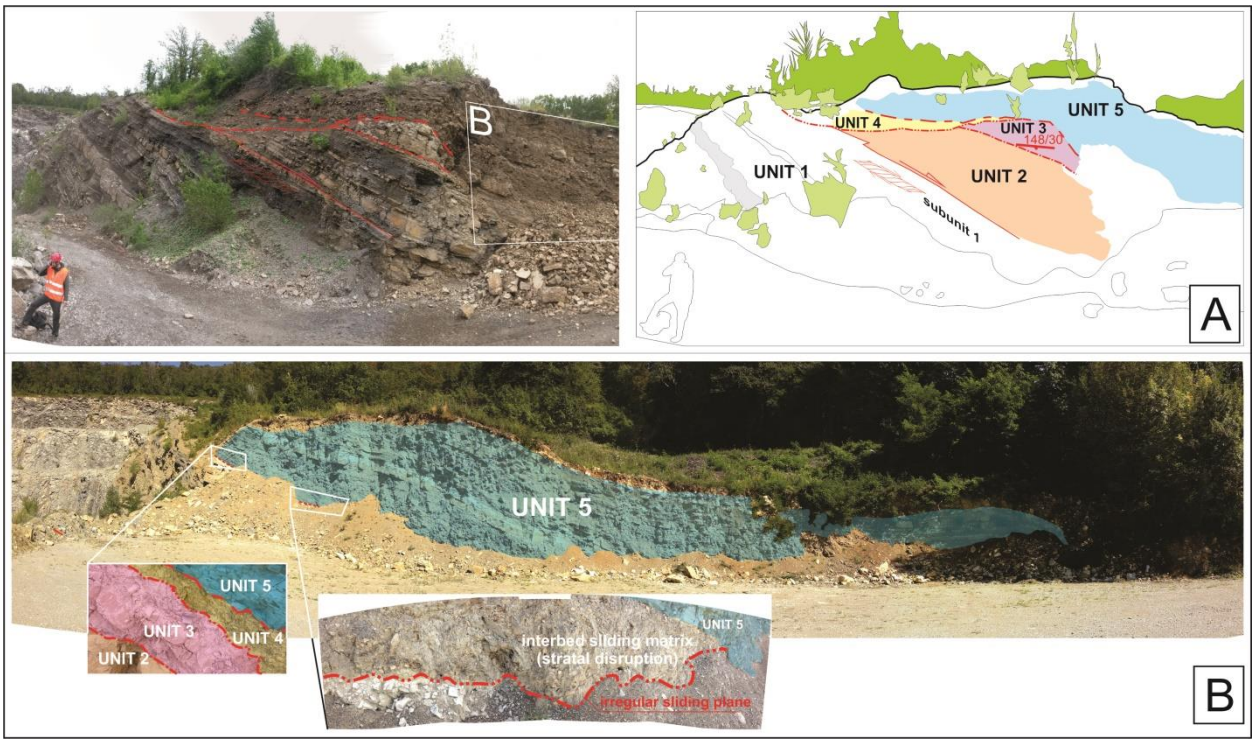

Figure 4 A – Units within the FR succession, SUBUNIT 1: unit with multi-horse duplex structure (Ogata et al, 2014a), UNIT 2: detached and bedded slide block of UNIT 1 along extra block thrust, UNIT 3: squeezed intra/extra block of FR succession, UNIT 4: marginal block with mechanical lithologic mixing structure, UNIT 5: extra block; B – view of UNIT 5 from W to E and its position on sliding plane.

Discussion

By comparing the GPR results in Fig. 5 with the geological mapping results in Fig. 4, the same strata in the subsurface as in the outcrop above can be defined. However, as the GPR profile was not recorded directly next to the outcrop (the distance between the profile and the wall is from 17.5 m to 19.8 m) and also due to the limited spatial resolution of the GPR, some features cannot be identified. For example, there is no certain way of defining the potentially present Unit 3 and Unit 4 on the GPR profile, as these units could be thinner than what the GPR is able to detect (based on the antenna frequency and rock type the minimum bed thickness would have to be around 1 m). Nonetheless, we were able to define the main features capable of producing hazardous events, i.e. the boundaries between different units (white dotted line in Fig. 5).

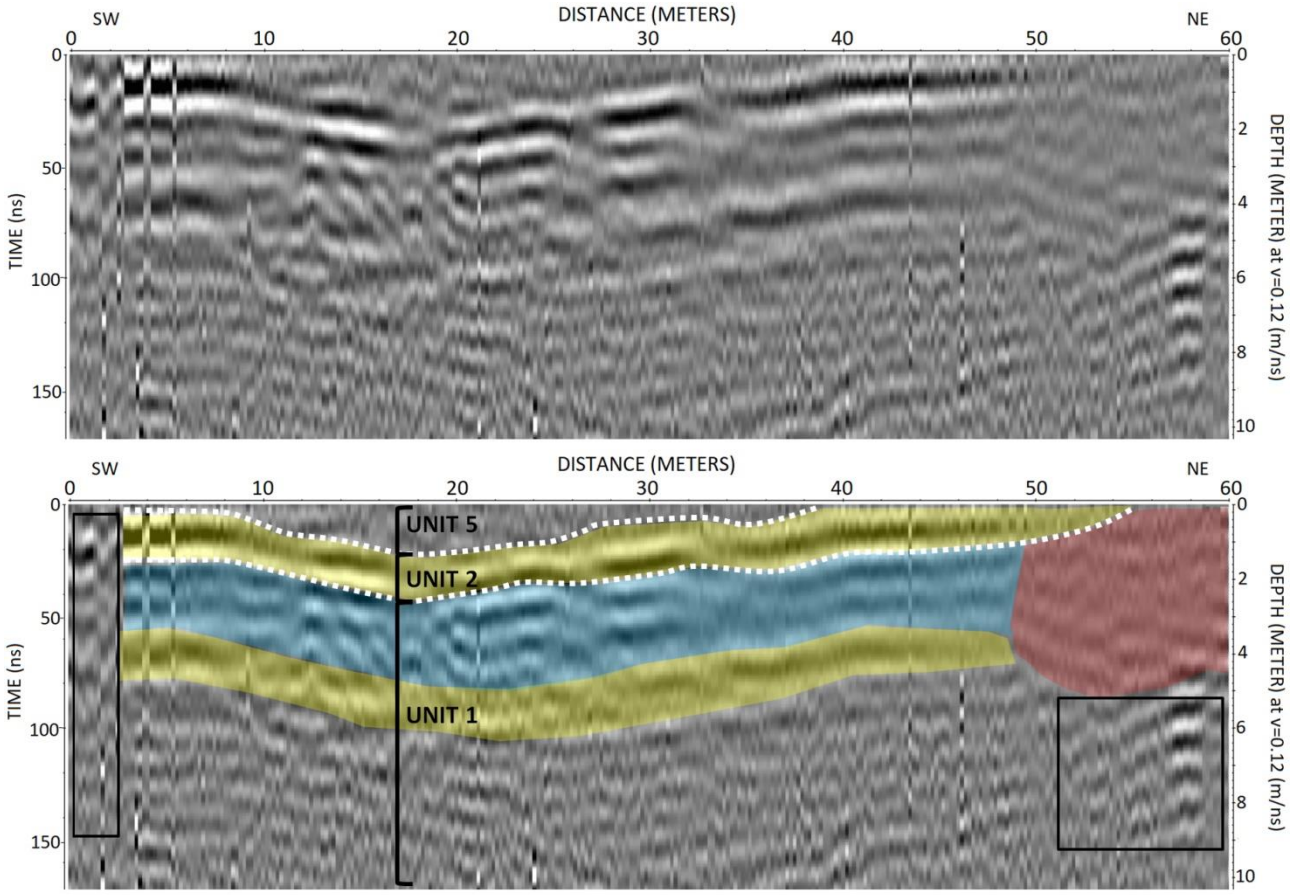

Figure 5 GPR profile without (top) and with (bottom) interpretation. Yellow area: harder and thicker layers of calcareous breccia, blue area: thinner softer layers with chaotic reflections due to strata disruption (Subunit 1), red area: high signal attenuation zone without reflections, white dotted line: potential sliding planes, black rectangles: noise dominates the radargram.

The chaotic reflections below the upper breccia layer of Unit 2 probably belong to the Subunit 1 (blue area in Fig. 4A), which has been proven to contain features related to micro-thrusting within its ductile layers. These interlayer deformation structures can be unstable during blasting and mining, as they represent the weakest parts of the FR succession and are capable of forming slip surfaces. Therefore, their geometry and spatial location need to be defined prior to excavation works. These are also structures along which landslides within the quarry have already occurred and therefore represent the most problematic features of the area.

Conclusion

Detailed geological mapping proved that the structural deformations within the FR succession were created synsedimentary and were thus formed during erosional processes of subsequent gravitational subaquatic events. The knowledge of subsurface features indicating the axes of such MTDs and the presence of past landslides within a quarry is crucial for ensuring a safe work environment and maintaining economically sound exploitation strategies. By locating unstable structures capable of reactivation as sliding planes future catastrophic events could be prevented. The use of GPR on heterogeneous layered turbidites of the Rodež quarry proved to be a suitable tool in recognizing such structures and could therefore be applied prior to mining works to ensure safer and better-planned new excavations.

References

Annan AP (2002) GPR – History, Trends and Future Developments. Subsurface Sensing Technologies and Applications. 3: 253-70.

Azañón JM, Azor A, Yesares J, Tsige M, Mateos RM, Nieto F, Delgado J, López-Chicano M, Martín W, Rodríguez-Fernández J (2010) Regional-scale high-plasticity clay-bearing formation as controlling factor on landslides in Southeast Spain. Geomorphology. 120: 26–37.

Barnhardt WA, Kayen RE (2000) Radar structure of earthquake-induced, coastal landslides in Anchorage, Alaska. Environmental Geosciences. 7: 38–45. (DOI: 10.1046/j.1526-0984.2000.71007.x).

Bichler A, Bobrowsky P, Best M, Douma M, Hunter J, Calvert T, Burns R (2004) Three-dimensional mapping of a landslide using a multi-geophysical approach: the Quesnel Forks landslide. Landslides. 1: 29–40. (DOI: 10.1007/s10346-003-0008 7).

Blindow N, Eisenburger D, Illich B, Petzold H, Richer T, (2007) Ground Penetrating Radar. In: Knödel K, Lange G, Voigt HJ (eds.)Environmental Geology, Handbook of Field Methods and Case Studies. Berlin, Heidelberg, New York: Springer. pp. 283-335.

Budetta P, Nappi M (2011) Heterogeneous rock mass classification by means of the geological strength index: the San Mauro formation (Cilento, Italy). Bulletin of Engineering Geolology and the Environment. 70: 585–593.

Buser S (1987) Osnovna geološka karta SFRJ, list Tolmin in Videm, L33-64 1:100.000 = Geological map of SFRJ 1: 100.000, sheet Tolmin and Udine. Zvezni geološki zavod, Beograd.

Chen NSh, Zhou W, Yang ChL, Hu GSh, Gao YCh, Han D (2010) The processes and mechanism of failure and debris flow initiation for gravel soil with different clay content. Geomorphology. 121: 222–230.

Daniels, DJ (1996) Surface Penetrating Radar. London: Institute of Electrical and Electronic Engineers. (ISBN: 0852968620). 300p.

Davies JD, Annan AP (1989) Ground-penetrating radar for high-resolution mapping of soil and rock stratigraphy. Geophysical Prospecting. 37: 531-51.

Gnaccolin M (1968) Sull'origine del "conglomerate pseudo-cretaceo" di Vernasso (Cividale del Friuli). Rivista Italiana di Paleontologia e Stratigrafia. 74: 1233-1254.

Hajdarwish A, Shakoor A, Wells, NA (2013) Investigating statistical relationships among clay mineralogy, index engineering properties, and shear strength parameters of mudrocks. Engineering Geology. 159: 45–58.

Jol HM (2009) Ground Penetrating Radar: Theory and Applications. Amsterdam, Oxford: Elsevier Science. (ISBN: 9780444533487). 544p.

Kadioglu S, Ulugergerli EU (2012) Imaging karstic cavities in transparent 3D volume of the GPR data set in Akkopru dam, Mugla, Turkey. Nondestructive Testing and Evaluation. 27: 263–271. (DOI: 10.1080/10589759.2012.694885).

Mantovani M, Devoto S, Forte E, Mocnik A, Pasuto A, Piacentini D, Soldati M (2012) A multidisciplinary approach for rock spreading and block sliding investigation in the north-western coast of Malta. Landslides. 10: 611–622. (DOI: 10.1007/s10346-012-0347-3).

Marinos V, Marinos P, Hoek E (2005) The geological strength index: applications and limitations. Bulletin of Engineering Geology and the Environment. 64: 55–65.

Milsom J (2003) Ground penetrating radar. In: Field Geophysics. 3rd Edition. West Sussex: John Wiley and Sons Ltd. pp. 167-78.

Neal A (2004) Ground-penetrating radar and its use in sedimentology: principles, problems and progress. EarthScience Reviews. 66: 261-330.

Ogata K, Pogačnik Ž, Pini, GA, Tunis G, Festa A, Camerlenghi A, Rebesco M (2014a) The carbonate mass transport deposits of the Paleogene Friuli Basin (Italy/Slovenia): Internal anatomy and inferred genetic processes. Marine geology. 356: 88-110.

Ogata K, Pini GA, Festa A, Pogačnik Ž, Tunis G, Mountjoy JJ, Senger K, Strasser M (2014b) High-resolution studies of mass transport deposits: outcrop perspective for understanding modern submarine slope failure and associated natural hazards. In: Lollino G et al. (eds) Engineering geology for society and territory, vol. 4: Marine and coastal processes. Cham: Springer. (ISBN: 978-3-319-08659-0). pp. 209-213.

Ogata K, Pini GA, Festa A, Pogačnik Ž, Lucente CC (2016) Meso-scale kinematic indicators in exhumed mass transport deposits: definitions and implications. In: Lamarche G et al. (eds) Submarine Mass Movements and their Consequences. Advances in Natural and Technological Hazards Research, vol 41. Springer, Cham. pp. 461-468.

Placer L (1981) Geološka zgradba jugozahodne Slovenije = Geologic structure of southwestern Slovenia. Geologija. 24/1: 27-60.

Placer L, Vrabec M, Celarc B (2010) The bases for understanding of the NW Dinarides and Istria Peninsula tectonics = Osnove razumevanja tektonske zgradbe NW Dinaridov in polotoka Istre. Geologija. 53/1: 55-86.

Pogačnik Ž, Ogata K, Pini GA and Tunis G (2015) Understanding the genesis of mass transport deposits (MTDs) for safe mining planning: Anhovo Quarry, Western Slovenia. In: Lollino G et al. (eds) Engineering Geology for Society and Territory - Volume 2. Springer, Cham. pp. 307-310. Rožič B, Šmuc A (2011) Gravity flow deposits in the Toarcian Perbla Formation (Slovenian Basin, NW Slovenia). Rivista Italiana di Paleontologia e Stratigrafia. 117: 283-294.

Sass O, Bell R, Glade T (2008) Comparison of GPR, 2D-resistivity and traditional techniques for the subsurface exploration of the Öschingen landslide, Swabian Alb (Germany). Geomorphology. 93: 89–103.

Selli R (1953) La geologia dell'alto bacino dell'Isonzo. Giornale di Geologia. 2/19: 1-153.

Šmuc A (2005) Jurassic and Cretaceous Stratigraphy and Sedimentary Evolution of the Julian Alps, NW Slovenia. Založba ZRC Publishing, Ljubljana, Slovenia. 98p.

Wan Y, Kwong J (2002) Shear strength of soils containing amorphous clay-size materials in a slow-moving landslide. Engineering Geology. 65: 293–303.

Photogrammetric monitoring of the Potoška Planina landslide

Vid Peterman

Modri Planet d.o.o., Vojkova 45, 1000 Ljubljana, Slovenia, vid.peterman@3dsurvey.si

Abstract The paper describes a practical example of mapping and monitoring of the landslide at Potoška Planina – a landslide above the village of Koroška Bela in the western Karavanke (mountain range of the Southern Alps) in north-west Slovenia. In order to assess the dynamics of the landslide we established a system of periodic 2-phase observation. In the first phase we conducted UAV-based periodic measurements twice per year – in mid-spring and mid-autumn – in order to measure the movement of the landmass. A geodetic survey network of stationary points was established around the landslide during each of the periodic measurements to determine the positions of photogrammetric ground control points. In the first phase, a hexacopter UAV was used to record overlapping aerial images of the landslide area; a photogrammetric 3D model of the area was then calculated, and displacements between consecutive measurements were also calculated.

The second phase was designed to determine whether displacements observed over 6-month periods occurred all at once or whether they occurred little by little. In order to acquire the necessary information, we placed two cameras at the foot of the landslide and programmed them to capture still photos of the landslide. From these observations we were able to determine the daily displacements of the landslide material, which ranged from 1 mm to several centimetres. Our observations indicated that the magnitude of the sliding of the material is commonly around 1 mm, with some larger daily displacements of up to 10 centimetres. In the paper we describe the process of calculating the landslide dynamics based on periodic still photo-captures, present the results, and draw conclusions from the problems we encountered and how we solved them.

Keywords close range photogrammetry, change detection, non-metric camera

Introduction

The Potoška Planina landslide is presumed to be a slow-moving slip that may eventually change into a debris flow. The area of the landslide is approximately 2000 square meters and is located at an altitude of 1200 meters. The relative altitude of the landslide is approximately 600 meters above the village of Koroška Bela, which makes the landslide quite remote and only barely accessible.

In the first phase, we conducted UAV-based periodic measurements twice per year – in mid-spring and mid-autumn (first measurement conducted in spring 2013) – in order to assess the magnitude of the movement of the landmass. Seven consecutive measurements were performed.

The determination of landslide dynamics is of great interest to geologists studying landslide activity. With this in mind, we have introduced a system of periodic observations involving two independent survey techniques: UAV photogrammetry based on a standard photogrammetric approach enhanced with automatic change detection (Niethammer et al. 2009; Karlsi et al. 2004) and classic tachymetry. Because it is fast, easy and inexpensive to deploy, UAV photogrammetry is able to systematically monitor landslide movement over time with tachymetric geodetic measurements, and provides accurate control of photogrammetrically assessed displacements.

In the area around the landslide we stabilized a geodetic network of stationary points to determine the positions of photogrammetric ground control points over the course of each measurement. A hexacopter UAV was used to record overlapping aerial images of the landslide area. A network of tachymetric control points moving with the landslide was also stabilized and measured each time, too. This scheme enabled us to independently control the photogrammetric observations of landslide activity. A comparison of displacement vectors shows that smaller displacement vectors can be observed more accurately than larger ones. In addition, the X and Y horizontal components of displacement vectors tend to be more reliable than the vertical Z component (Travelletti et al. 2010). Most importantly it shows that even low-magnitude displacement vectors (roughly 10 cm) can be successfully observed through photogrammetry.

UAV landslide activity surveys proved to be highly economically viable, requiring a day of work for a team of two people. In our case, we needed 3 hours for travel and the transport of equipment to and from the site, 1.5 hours to signalise and measure ground control point positions, and an additional half-hour to measure the positions of the tachymetric control points. A UAV flight performing aerial imaging is the fastest of the operations, taking only about 20 minutes. An additional 20 minutes, however, is required to plan the UAV flight mission. All together a little more than 5 hours of terrain work was required, followed by 2 days of office work to process and calculate all of the data and to write detailed technical reports.

During the periodic measurements we also encountered some problems. Most notable were the unfavourable weather conditions – strong, gusting wind – which forced us to interrupt the survey and land the UAV, return home and come back to perform the survey another day. During one of our later measurements, sliding land mass destroyed some of the tachymetric control points which then had to be re-signalised.

A detailed description of phase one from a photogrammetric point of view is available in Peterman 2015, while a description from a geologists' point of view is available in Peternel et al. (2016). A purely geological description of the landslide is available in Jež et al. (2008).

While in this paper we focus on the results of the second phase – determination of daily landslide displacements, where our goal was to determine whether displacements observed during 6-month periods occurred all at once or whether they occurred little by little. In order to acquire the necessary information we placed two cameras at the foot of the landslide and programmed them to capture still photos of the landslide. From these observations we were able to determine daily displacements of the landslide material, which ranged from 1 mm to several centimetres.

Determination of daily landslide displacements

Hardware used to determine daily landslide displacements

In the second phase our goal was to determine whether displacements observed during 6-month periods occurred all at once or whether they occurred little by little. In order to acquire the necessary information we placed two GoPro cameras at the foot of the landslide, and connected them to a Raspberry Pi miniature computer, which we programmed to take still photos of the landslide once every minute. In order to power the equipment we installed a photovoltaic panel nearby (Fig. 1).

Figure 1 Hardware used to determine daily displacements – 2 GoPro cameras, a photovoltaic panel, and a Raspberry Pi miniature computer.

Camera calibration

Before installing the cameras at the foot of the landslide the cameras need to be calibrated. Calibration was performed in our office, using a checkerboard calibration pattern. With each camera we made some 20 still photos of the pattern. The pattern corners were then detected using a corner-detection algorithm on all 20 photos (Fig. 2).

Parameters related to lens radial distortion were calculated (Hartley et al. 2003) and used to remove the distortion from the photographs from the GoPro cameras (Fig. 3).

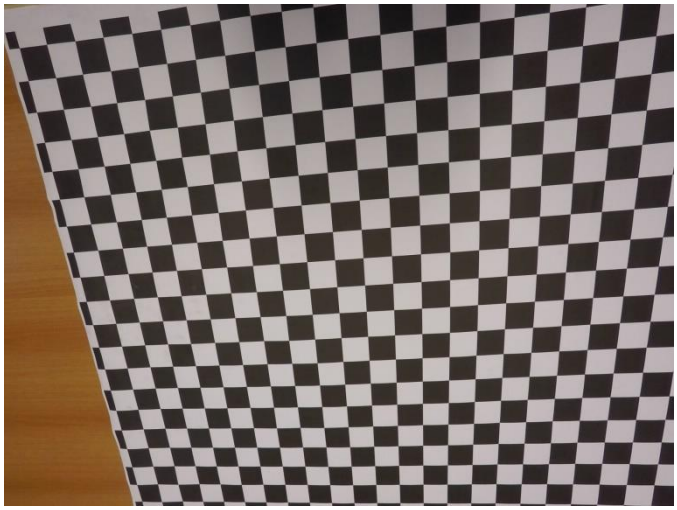

Figure 2 Sample of a photo of calibration pattern with de-tected corners.

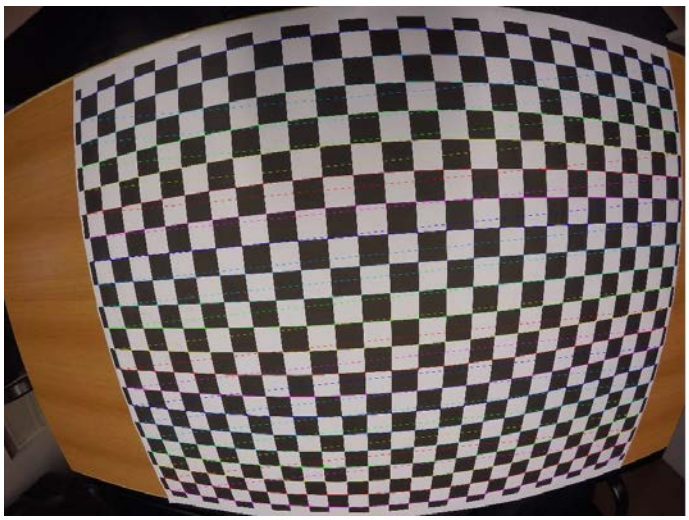

Figure 3 Example of undistorted photo of calibration pattern from figure 2.

Data acquisition

The cameras were placed at the foot of the landslide (Fig. 4), and were programmed to take still photos of the landslide area. Circular targets were signalized in the viewing range of the camera.

Figure 4 Sample landslide photo of landslide.

The same targets were used as were used in the process of taking UAV measurements (Fig. 5), only now they were oriented such that they were facing the GoPro cameras. Again their positions were measured using classical tachymetric survey techniques.

Figure 5 Subset of image from Figure 11 showing positions of photogrammetric targets using a Harris corner detector to detect well-defined points of interest on the landslide.

Data processing

The cameras produced a large number of photos of the landslide area. In order to process the data we developed an automated image processing algorithm. The algorithm automatically measured the positions of the signalized targets in images and used a Harris corner detector to detect well-defined points of interest on the landslide (Fig. 6). The positions of the targets were used to calculate camera position and orientation with relation to the landslide area, and this in turn enabled us to project the landslide digital terrain model on the camera view (Fig. 7). Subsequent daily photographs of the landslide area were compared, and an image-matching algorithm was used to measure 2D displacements between the subsequent photos (Fig. 8). Since non-metric consumer grade cameras were used to record still images, certain image displacements were also observed in areas that did not move, like signalized targets.

Figure 6 Detected target positions (red pluses) and well-defined points on the landslide (red dots).

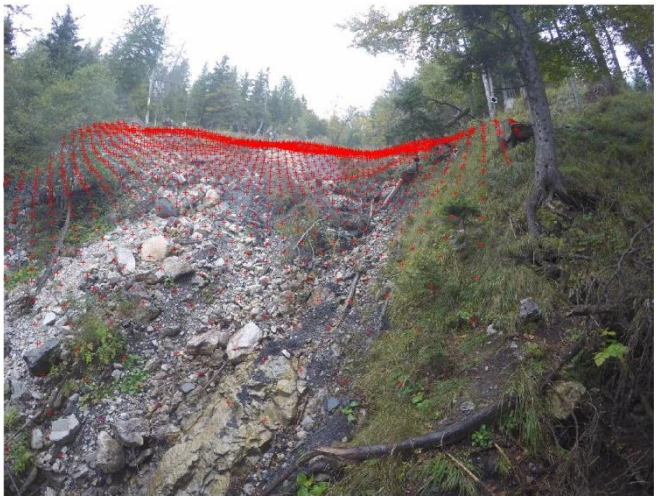

Figure 7 Digital terrain model projected on camera view.

Projective geometry was used first to assess how the image sensor had moved to record the displacements of the signalized targets. This information was then taken into account and the displacements of points of interest on the landslide were projected onto a digital terrain model in order to transform 2D projections into 3D real- world coordinates. From this data a regular grid of displacement vectors was calculated and overlaid atop a digital orthophoto map of the landslide area that was produced from the UAV measurements (Fig. 9). This methodology was repeated for daily pairs of subsequent images. A mean displacement vector was calculated for each daily measurement. The results of daily displacements are presented in Fig. 10. Our results demonstrated that larger displacements of landslide material occurred on rainy days which fact was easily determined, since weather con-

Figure 8 2D displacements of signalized targets (blue) and 2D displacements points of interest on the landslide (red). (All displacements are enlarged by a factor of 20x).

Figure 9 3D regular grid of landslide displacements displayed over the orthophoto map.

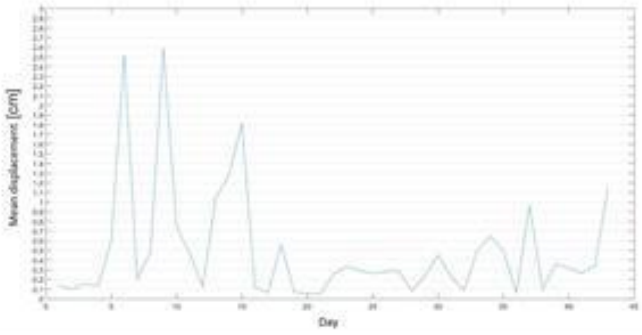

Figure 10 Mean amplitude of landslide material displacement by observation day.

ditions could easily be recognised from the recorded photos. In general, the landslide would move some two centimetres on wetter days, move only a couple of millimetres on others.

Conclusions

The process of using photogrammetry to measure displacements on the Potoška Planina proved effective and successful. One of the biggest advantages of using photogrammetric measurements compared to classic tachymetric measurements was the completeness of the data generated. Displacement vectors were calculated for the landslide for more than simply random points of interest. On the whole, the scheme employed and detailed here enabled geologists to accurately analyse the influence of meteorological events and their particular characteristics, such as rainfall, on landslide dynamics. The process of UAV-based landslide monitoring has already been repeated on the Slano Blato landslide, which is the largest landslide in Slovenia, and future monitoring of other landslides is also planned.

References

Hartley R, Zisserman A (2003) Multiple View Geometry in Computer Vision. Cambridge University Press, New York, USA. 657p.

Jež J, Mikoš M, Trajanova M, Kumelj Š, Budkovič T, Bavec M (2008) Koroška Bela alluvial fan—the result of the catastrophic slope events (Karavanke Mountains, NW Slovenia). Geologija. 51(2):219–227.

Karsli F, Yalcin A, Atasoy M, Demin O, Reis S, Ayhan E (2004) Landslide assessment by using photogrammetric techniques. In: Altan O (ed) International Archives of Photogrammetry, Remote Sensing and Spatial Information Sciences, XX ISPRS Congress, Commission VII, WG VIII/3, XXXV-B7, 12-23 July 2004. Istanbul, Turkey. pp. 736-739.

Niethammer U, Rothmund S, Joswig M (2009) UAV-based remote sensing of landslides. In: Mills JP, Barber DM, Miller PE, Newton I (eds) International Archives of Photogrammetry, Remote Sensing and Spatial Information Sciences, Vol. XXXVIII, Part 5 Commission V Symposium, 21-24 June 2010. Newcastle upon Tyne, UK. pp. 496-501.

Peterman V (2015) Landslide activity monitoring with the help of unmanned aerial vehicle. In: Armenakis C (ed) The International Archives of the Photogrammetry, International Conference on Unmanned Aerial Vehicles in Geomatics, Volume XL-1/W4, 30 August – 2 September 2015. Toronto, Canada. pp. 215-218.

Peternel T, Kumelj Š, Oštir K, Komac M (2016), Monitoring the Potoška planina landslide (NW Slovenia) using UAV photogrammetry and tachymetric measurements. Landslides. 14(1): 395 – 406.

Travelletti J, Malet J, Schmittbuhl J, Toussaint R, Bastard Delacourt C (2010) Multi-temporal terrestrial photogrammetry for landslide monitoring. In: Malet J (ed) Proceedings of the "Mountain Risks" International Conference, 24-26 November 2010. Florence Italy.

GPR facies determination – Pusto Brdo - Srebrnjak Hill's Recent and Historical Landslides

Željka Sladović, Zoran Mikić, Jakov Kalajžić

Geoda Consulting d.o.o., Zvonimirova 13, Zagreb, Croatia, zeljka@geoda.hr

Abstract Srebrnjak Hill and Pusto Brdo are situated at the eastern edge of the Samoborsko gorje mountains. Tectonic settings vary according to author, but common to all interpretations is the regional fault that passes through the nearby area. At the end of 2016 the landslide at the south part of the hill caused damage on the hangars and shades and only halted in the vicinity of the houses in the village of Mala Gorica. The reparation works were performed during 2016. Ground penetrating radar (GPR) surveying took place in 2017, with a shielded 80 MHz antenna in order to delineate landslide parts, primarily surface of rupture and its relation to rock body layers and fractures. The GPR signal is reasonably good for processing and analyses. Analyses workflow included data sorting, profile summaries, velocities calculated on the basis of diffraction hyperbola, and correction for elevation and interpretation. Alongside the colloquial workflow, GPR facies analyses based on Neal (2004) and multi-attribute analyses developed for seismic reflection were applied. GPR surveying enable 3D modelling of the 2016 landslide. The results were applied to the hill area, and some potential landslides were identified. They differ in type and volume. The most significant of them is situated on the eastern part of Srebrnjak hill, just 300 m from the 2016 landslide. The features of the historic landslide were also noted on several positions, with the landslide on Pusti Breg delineated in detail. GPR surveys enable 3D modelling of the landslides in detail, and serve as a basis for a discussion on mitigating the risks of the earth slide in the future. 4D modelling and monitoring with a GPR 80 MHz antenna with attribute analyses of the GPR signal is recommended, primarily owing to the fact that it is non-invasive and easy to operate.

Keywords GPR, Shielded 80MHz antenna, landslide, GPR facies, Hilbert transformation, multi-attribute analyses, Samoborsko Gorje

Introduction

Srebrnjak Hill and Pusto Brdo Hills are situated in Zagrebačka Županija at the eastern edge of Samoborsko Gorje Mountains and situated in the area of Sveta Nedelja settlements Jagnić Dol and Mala Gorica. It is a sparsely populated rural area, with hills covered with forests and meadows.

Former geological surveying implied pretty simple stratigraphic settings with minor lateral and vertical variation. Sedimentologic/stratigraphic units refer to upper Miocen shale and silts that could be according to Vrsaljko (2003), divided to Andrasevci and Medvednicki Bregi subunits overlain with Quarterly layer at the top of the hill (Fig. 1). Only regional fault that pass through nearby area is common in all interpretations.

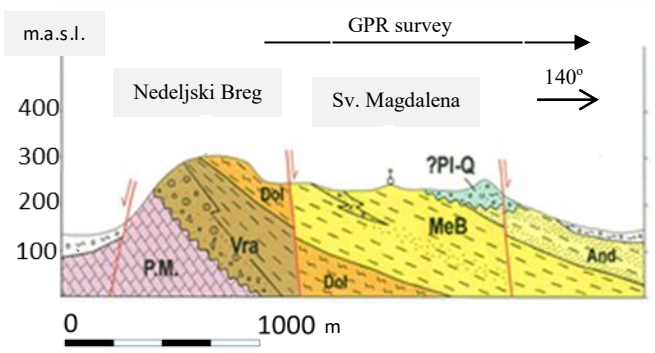

Figure 1 Geological settings (Vrsaljko, 2003). GPR surveying were conducted right of normal fault till the end of profile.

At the southern part of the part of the hill sliding occurred in 2016. The width of the landslide was around 100 m and with length of 150m it extended to the vicinity of the houses in Mala Gorica village.

Figure 2 Landslide on the southern part of the hill.

GPR data

GPR surveying

GPR surveying campaign (Fig. 3) took place in 2017 in order to describe the geological setting of the Srebrnjak and Pusti Breg Hills in detail. The campaign was conducted during February, the terrain was firm without vegetation or leaves on the ground, so the external requirements for surveying were optimal and enabled profiling as was designed.

Over 25 km of GPR profiles were recorded with a shielded GX 80 MHz antenna. The MALÅ GX solution consists of two separate components: the GX Controller and the GX antenna connected through a single data/power cable. Geopositioning was determined using a built-in DGPS and an external GPS.

Surveying of Samoborsko gorje was configured as a pull-system with an encoder wheel that was fitted to the mounting block on the back of the antenna. The recording time window of the antenna is 812 ns.

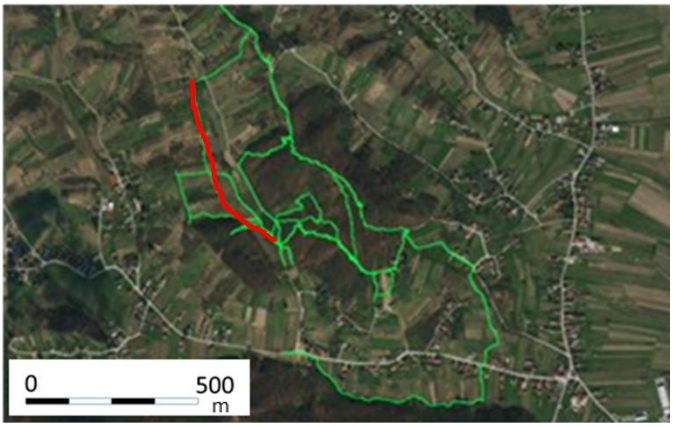

Figure 3 Part of GPR surveying campaign – Srebrnjak hill, profile 273 (red).

Detailed surveying of the 2016 landslide over a total length of approx. 1.5 km was performed as part of the campaign in order to delineate landslide parts, primarily surface of rupture and its relation to rock body layers and fractures.

GPR data processing

First step processing was performed during the surveying in order to QC recording data and repeat data collection when it was necessary.

GPR data was processed with ReflexW software and analysed. The processing workflow for the GPR signal included data sorting, summary profiles, velocities calculated based on hyperbolas, dewow, background removal and energy decay gain, and correction for elevation and interpretation. The processing workflow is shown on profile 273 (red line on Fig. 3), which was recorded from the bottom of Pusto Brdo from south to north.

Data was sorted and grouped (Fig. 4) based on profile quality when there were several records per profile. After the summation 30 profiles varying in length from 200 to 1000 m were prepared for further processing.

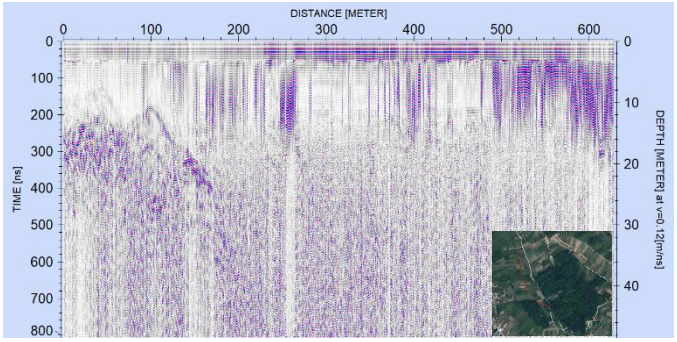

Figure 4 GPR data profile 273 after sorting and summation

Velocities were calculated based on hyperbolas ranging from 0.08 to 0.17 m/ns. Correction for elevation profiles was the final step in the initial processing (Fig. 5).

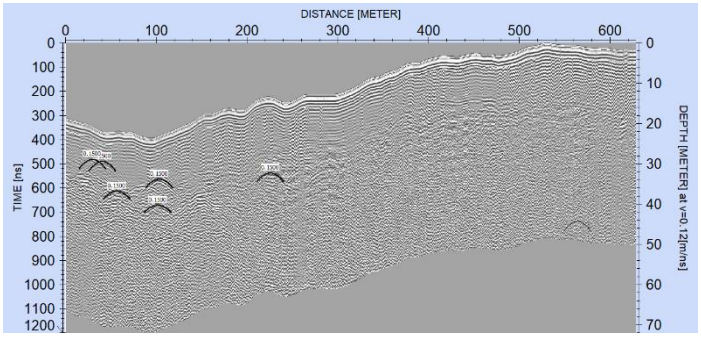

Figure 5 GPR data profile 273 corrected for elevation, with hyperbola velocities marked

Interpretation

GPR data is measured electromagnetically, but data processing is very similar to reflexive seismic processing.

Further analyses and interpretation were performed using OpendTect software owing to its wide choice of data attributes designed primarily for reflection seismic data and the workflow designed for seismic data was applied – interpretation supported by attribute analyses (Fig. 6) and facies recognition.

The attributes delineate the layers, frequency is best for fault and fold characterization, reflection strength is useful for details within facies, while shaded relief visualizes layers for non-technical users.

The GPR facies were visually delineated based on a method introduced by Neal (2004) and later adaptations of it.

Three main facies were extracted based on signal characteristics such as shape of signal, interrelationship, continuity and reflex strength, unit surface characteristics (concordant, erosional, onlap etc.) and unit scattering characteristics.

Analyses of all of the recorded data (Fig. 7) enabled the delineation of three main GPR facies (Tab. 1). The facies were classified according to Neal 2004 (Fig. 8).

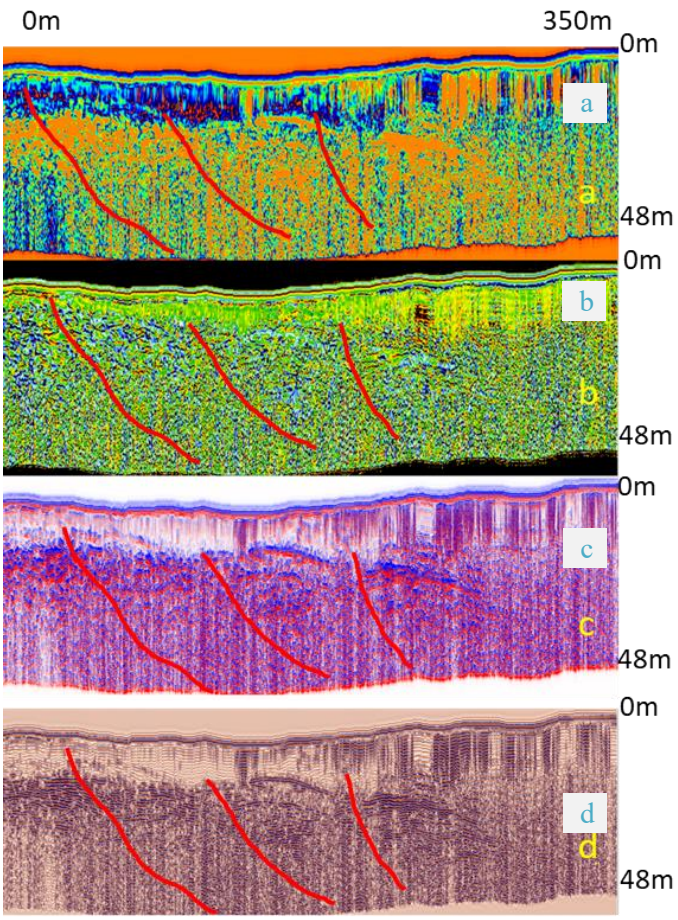

Figure 6 GPR attribute analyses, part of profile 273, enables fault and fold detecting, interpretation and facies analyses. a) Reflection strength attribute b) Instantaneous frequency attribute c) Shaded relief attribute d) Amplitude section.

Facies LF1 consist of a parallel well-defined layer with baselap and without the hyperbolas; Facies LF2 consists of well- defined hyperbolas and subparallel and sinusiondal GPR signal onlaps facies LF1; while Facies LF3 consists of sparse hyperbolas of non-defined subparallel reflex.

GPR facies were interpreted, but some sections required the subdivision of facies LF2 into three subgroups, from LF2A through LF2C.

Subgroups were divided primarily on the basis of hyperbola types. Subgroups LF2A and LF2C have coherent regular 'semi-reflecton', while subgroup LF2C is characterized by random incoherent hyperbolas due to bodies of mixed size. The facies boundary between LF2A and LF2C was set based on attributes like reflection strength and shaded relief and were confirmed by other attributes.

Together with facies determination young tectonic settings were detected in the area. The majority of faults and fractures are connected to facies LF2, and where facies LF 1 is very thin extend almost to the surface (Fig. 9).

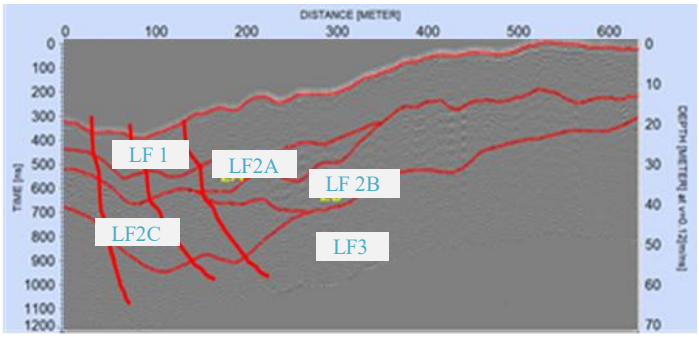

Figure 7 GPR facies analyses; profile 273.

Table 1 Facies definition based on Neal (2004). F – facies number; V – velocity; A - GPR signal characteristics; B - unit surface characteristics; C - scattering characteristics.

F	V (m/ns)	A	B	C
1	0.1	parallel, continuous, coherent , well defined	concordant top, baselap	without hyperbolas, vertical amplification
2	0.15	sinusoidal, subparallel, 2B semi- continuous, 2A i 2C better defined	2A onlap, 2C, 2B baselap	2A and 2C continuous well-defined hyperbolas, semireflex
3	0.1	no defined wavy reflex, subparallel	facies 2 onlap	sparse occurrence of hyperbolas

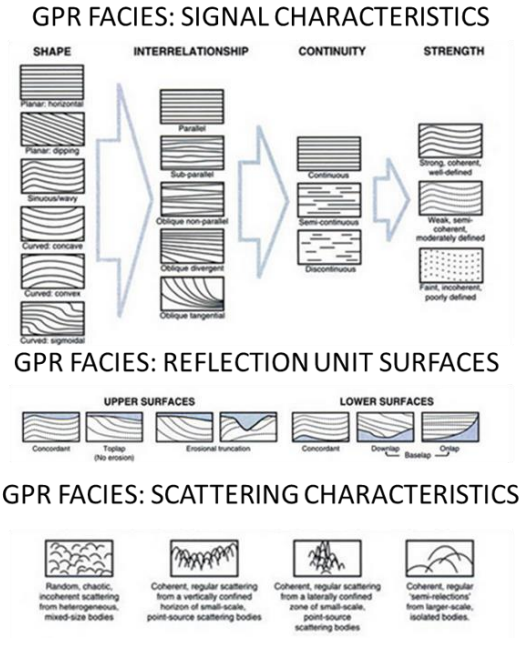

Figure 8 GPR signal characteristics (Neal 2004).

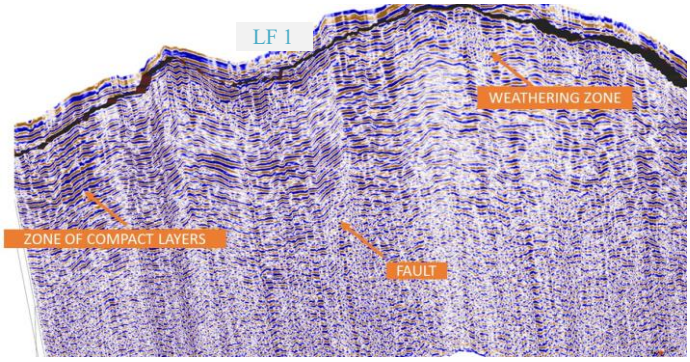

Figure 9 Profile 180 Detected faults, weathering zone and zone of compact layers within GPR facies 2.

Landslides

Part of the surveying campaign covered a previously repaired landslide with a 8 GPR profile in the regular grid (Fig. 10).

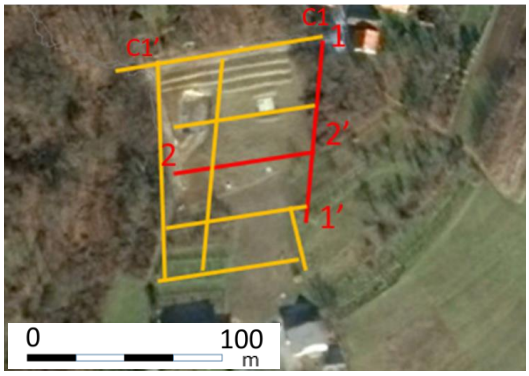

Figure 10 Landslide covered by GPR grid.

There were no significant hyperbolas except the one caused by the construction of an object built during landslide mitigation. On the rough GX Controller section before processing the water niveux on crown profile C1 – C1' of the landslide was apparent (Fig. 11), even on GX controller terrain data.

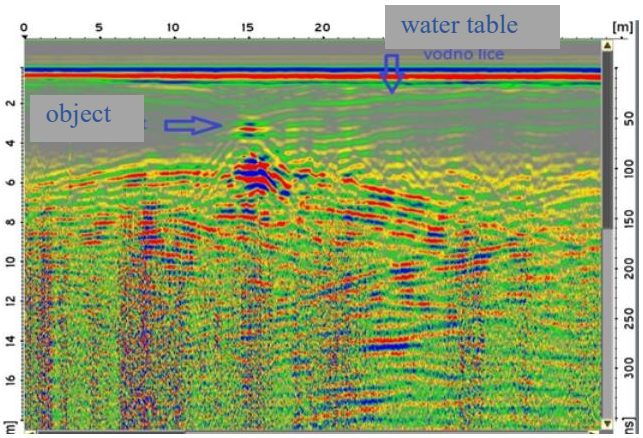

Figure 11 GX Controller output – part of profile C1-C1'.

The GPR signal at the 2016 landslide area is good for processing and analyses.
GPR surveying allows us to gain an inside view of the 2016 landslide.

Signal detection is as high as 800 ns. After the processing, the signal visibility reached the detection depth level and enabled recognition of the surface of rupture, the main landslide body, and the landslide foot. GPR facies LF1 and LF3 were easily interpreted; LF 2 is interpreted as LF2B. Several layers are interpreted within that GPR facies.

The landslide figures after reparation are connected to facies 2B (Fig. 12) Detected young faults at the backside of the landslide opened up the possibility of a fault-triggered landslide (Fig. 13).

The landslide features were also recognised on several profiles in the area, and differ in type and volume. The most significant of them is located on the eastern part of Srebrnjak hill just 300 m from the 2016 landslide. On Pusti Breg, an historic (Fig. 14) landslide was detected within facies 2. As the landslide is covered, after Vrsaljko with Quaterny horizontal layers (LF 1), dating of the land sliding is pre-Quarterly. Multi-attribute analyses improved the visibility of the profiles and enabled us to determine the timing and extension of the landslide.

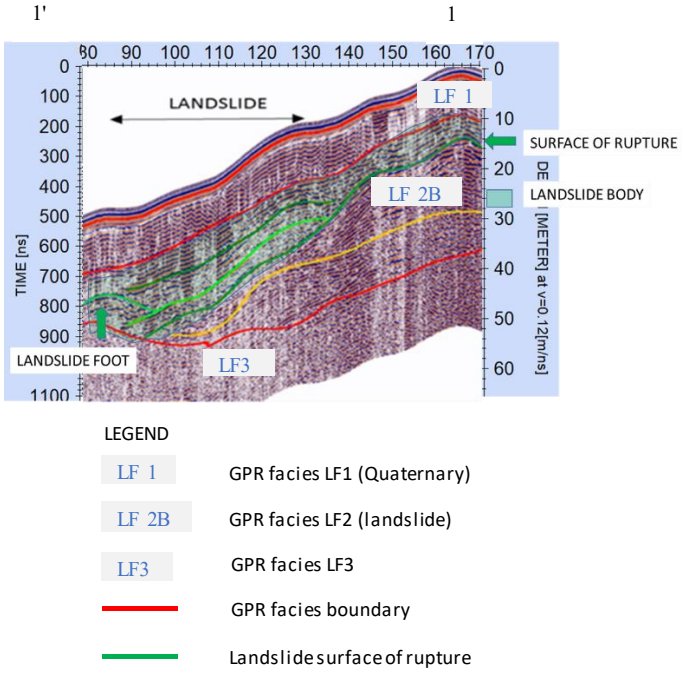

Figure 12 GPR Profile 1-1'.

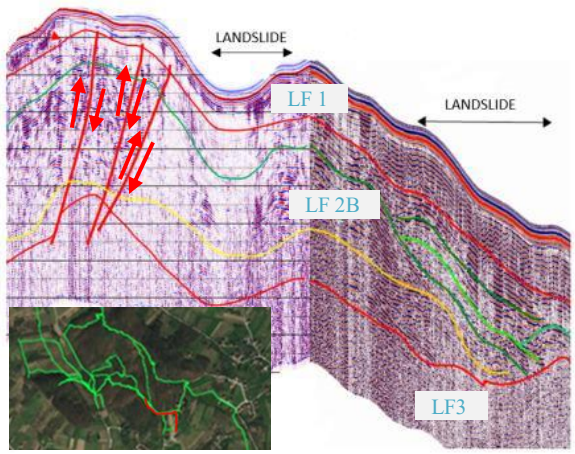

Figure 13 Composite profile with map: Faults at the back of the landslide; red lines LF1 and LF3 are boundaries; green and yellow is the subdivision of LF2.

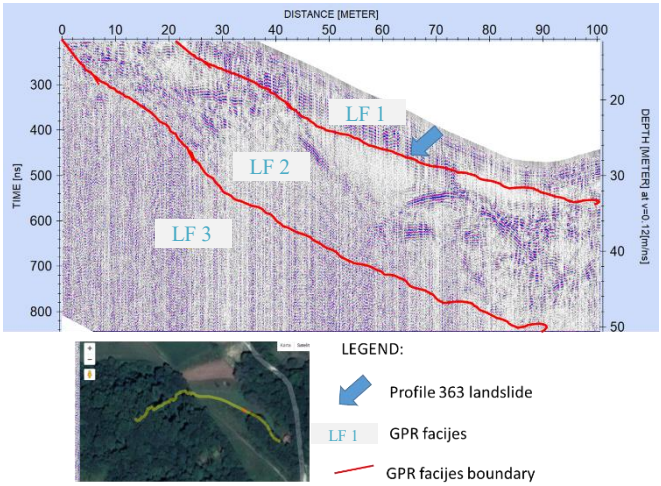

Figure 14 Historic landslide on Pusti Breg hill, profile 363

Conclusion

GPR surveying, because it is non-invasive and easy to operate, has proven to be an effective tool for shallow geological surveying. New georadar of the GX generation with its penetration depth (recorded time 812 ns) could be used to monitor already repaired and potential landslides. The method enables 3D modelling of the landslides in detail, which can in turn form the basis for discussions related to mitigating risks associated with the earth slide in the future. 4D modelling and monitoring with a GPR GX80 MHz antenna, together with attribute and facies analyses of GPR signals is recommended.

References

Neal A (2004) Ground-penetrating radar and its use in sedimentology: principles, problems and progress. Earth-Science Reviews. 66: 261–330.

Vrsaljko D (2003) Biostratigrafija miocenskih naslaga Žumberačkog i Samoborskog gorja na temelju mekušaca [Biostratigraphy of Miocene deposits of Žumberačko and Samoborsko gorje Mts. on the basis of molluscs]. Unpubl. PhD Thesis, Faculty of Science, University of Zagreb, Zagreb, Croatia. 147p. (in Croatian, abstract in English)

Visibility analysis for planning landslide alert systems with webcams

Florian Albrecht[(1)], **Mateja Jemec Auflič** [(2)], **Daniel Hölbling**[(1)]

1) Department of Geoinformatics – Z_GIS, University of Salzburg, Schillerstraße 30, 5020 Salzburg, Austria, florian.albrecht@sbg.ac.at

2) Geological Survey of Slovenia, Ljubljana, Slovenia

Abstract New approaches to landslide alert systems are necessary, because the current systems cannot cover all aspects that users in emergency response and infrastructure maintenance need. Here we present a concept for estimating the capability of a landslide alert system based on webcams. Such an alert system could be installed to monitor inaccessible areas that exhibit high susceptibility to landslides. We present visibility analysis models for mapping the webcam coverage on the basis of a digital elevation model (DEM). Preliminary results are promising, but also show that the ability of webcams to identify landslides has to be better understood in order to advance the visibility analysis model towards a tool for choosing optimal webcam locations.

Keywords landslides, landslide susceptibility, webcam images, alert system, emergency response, visibility analysis

Introduction

In mountainous regions like the Alps, landslides frequently cause damage and pose a risk to the population and infrastructure. Thus the collection of information on landslides is essential for purposes of prevention and emergency response. On one hand there is a clear need to monitor known landslides, and on the other hand a need for rapid documentation of rainfall-triggered landslides and related damage, particularly after heavy rainfall events (Albrecht et al. 2016). An automatic system for immediate alert would be most relevant and important for emergency response procedures and the coordination of infrastructure maintenance activities. Key for any alert system would be the shortest possible response time after a landslide has been triggered and the size of the region the alert system can cover, i.e., if a region with high landslide-susceptibility can be comprehensively monitored.

Webcam images can provide a timely source of information for landslide alert systems. They can be collected frequently and have the advantage over remote sensing data from optical Earth Observation (EO) satellites that they are less weather-dependent and less susceptible to conditions like cloud cover and similar, which requires clearing prior to data collection. Nevertheless, remote sensing data has real potential for mapping and monitoring landslides quickly and efficiently. This applies to webcams as well. While conventional image interpretation is time-consuming and depends considerably on the experience and skills of the investigator, it is still the most widely used method for landslide detection and inventory preparation. Recent studies show that semi-automated landslide mapping methods can produce reasonably good results and are both faster and less subjective (e.g. Hölbling et al. 2017). Both aerial photography and optical satellite imagery are commonly used in landslide recognition efforts (Scaioni et al., 2014). Webcam images, however, have not yet been used for (semi-automated) landslide mapping. But they have proven valuable for extracting information related to phenology (Bothmann et al. 2017) and snow cover (Dizerens 2015).

Alongside the issue of extracting information from images, the main challenge associated with using webcams for landslide alert systems is their ability to cover a specific region. In order to keep the number of webcam installations on the ground to a minimum, the target area to be monitored has to be narrowed down primarily to those areas that are susceptible to landslides.

Over the past years landslide susceptibility maps have become considered a standard tool in landslide hazard management (Guzzetti et al. 1999; van Westen et al. 2008). They are usually based on comparisons of previously registered landslides and the conditional or preparatory causal factors. In susceptibility analyses, triggering factors (rainfall intensity, earthquakes, volcanoes, etc.) are often not considered (Corominas et al. 2014). Susceptibility maps identify locations as susceptible where similar conditions prevail as were identified at known landslide locations. In combination with a Geographic Information System (GIS), landslide susceptibility maps can be obtained at different scales that depend largely on the resolution of input data. Landslide susceptibility maps describe the relative likelihood of future landsliding based on variables such as derivatives from a digital elevation model (DEM), soil type and rainfall patterns.

Apart from knowledge related to the area to be monitored, the ability to cover said area depends on the webcam's viewing capabilities and its location. When webcams are installed on the ground, including an offset, their viewing perspective relative to the terrain limits the area they can cover. A constellation of multiple webcams is required to ensure coverage of regions that are susceptible to landslides, and thus are relevant for alert systems. Visibility analysis methods enable us to estimate webcam

coverage and the coverage of webcam constellations. Visibility analysis is a highly versatile set of methods that has been used for analysing the visual exposure of landscape features in general (Llobera 2003) and for providing visual impact maps for landscape planning for entire regions (Lienhard and Binna 2013). Visibility analysis has a long tradition in the design of monitoring systems for natural hazards, specifically wildfires (Amidon and Elsner 1968; Lee 1991; Fischer 1996; Denau 2014), but has not yet been used for the design of landslide monitoring systems. Terrain visibility is modelled using the viewshed method (cf. Fisher 1996), which estimates the visibility for each location in a DEM and is capable of incorporating observer parameters that describe the viewing capabilities of a camera. Information on camera distance, terrain slope and aspect enable us to include terrain exposure in the modelling of webcam viewing capabilities and terrain coverage with respect to specific target features like landslides. Therefore, visibility analysis provides a valuable tool for gaining a better understanding of webcam-based landslide alert systems.

This research presents a visibility analysis model that estimates webcam viewing capabilities for detecting landslides as part of a larger concept for modelling the optimal distribution and required camera coverage needed to monitor the landslide susceptible areas of a region. The concepts, materials and methods section investigates the requirements of the visibility analysis model and describes the essential components of the implementation of such based on the investigation of a webcam that is installed in the region of Montafon, Austria, and which contains landslides within its view. The results present a visibility analysis profile for the webcam relative to landslides viewed and area covered. The discussion addresses the value of the visibility analysis model in the design of landslide alert systems.

Concepts, Materials and Methods

Visibility analysis model design

Any type of model, including visibility analysis models, is a representation of a real-world situation or scenario, e.g., a possible future in the real world. In this study, the target visibility analysis model is taken to represent a real world situation whereby webcams provide observations of the environment employed in monitoring landslide activity. The first step in designing a visibility analysis model is to describe the situation where the observer acts within the scene. This situational concept identifies all relevant parameters that play a role in the next step involved in modelling visibility. Within the visibility analysis model landslides are assigned the role of viewed targets, the webcam the role of the observer, and the other environmental features the role of obstacles. These obstacles are the terrain and elevated objects (trees, buildings) that may block the observer's view of the target.

Each role provides parameter inputs to the visibility analysis model that are dependent on the objects' properties and capabilities. The webcam's, i.e., observer's, visually relevant properties (viewing height, vertical and horizontal view angles) and capabilities (stationary, horizontal turning) result in the following viewing parameters: vertical view angle α, horizontal viewing angle β (or β_2), and an offset h from the ground (Fig. 1).

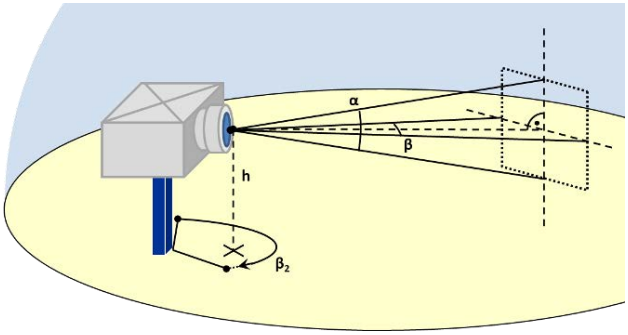

Figure 1 The webcam and its visually relevant properties that determine the field of view: viewing height h, vertical view angle α, horizontal view angle β, and extended horizontal view angle β_2 as a result of the webcam's turning capability.

The landslide's, i.e., target's visually relevant properties consist in its vertical and horizontal extent, which determine its surface area as well as its slope and exposure to the northerly direction (i.e., aspect). These are the parameters that, in relation to the observer's, i.e., the webcam's, viewing inclination and orientation to the northerly direction and distance to the target determine how large the landslide appears in the field of view of the observer (Fig. 2).

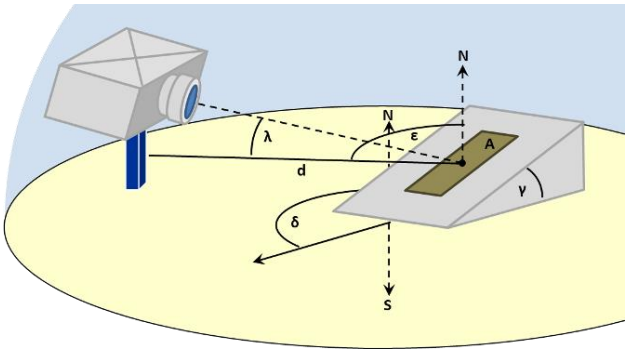

Figure 2 The landslide's size in the webcam's field of view is a function of the landslide surface area A, its inclination γ, its northward orientation δ, the webcam's slope and orientation angles ε and λ in the direction of the landslide, and the distance d between the landslide and the webcam.

Definition of the scene and set-up completes the description of the situation for which visibility analysis is to be performed: prior to more complex scenarios with multiple webcams we model a single webcam within its sur-

rounding landscape to evaluate its capacity to cover susceptible areas with a view to detecting new landslides. This could come to form a basis for modelling the setting-up of multiple webcams at their respective locations and an area of landslide-susceptible locations, i.e., an area where landslides potential is high, which can then be seen in the webcam view.

Study area and data

This study models a visibility analysis for the situation described above for an area in Montafon, Austria (Fig. 3).

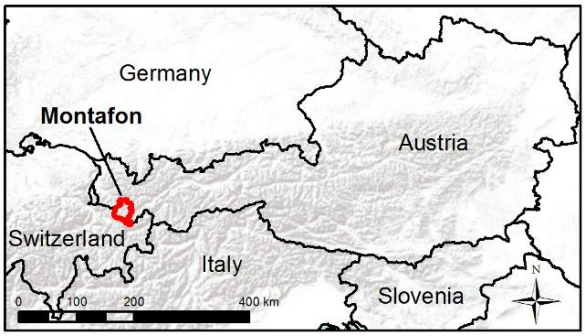

Figure 3 Location of study area Montafon, Austria.

The investigated webcam is located in the ski resort of Silvretta. It can be viewed on the Panomax website (https://silvretta-montafon.panomax.com/nova-stoba; Fig. 4). The webcam has a coverage resolution of 13088 x 2048 pixels and covers a horizontal view angle β_2 of 260°, i.e., reaching from the cardinal direction of 205° on its left and passing over due north (0°) to 125° on its right. If we assume that the webcam pixels represent square angular grid cells, the vertical view angle α is 40.7°. Further technical information about the webcam is available from the Panomax website (www.panomax.com). Several landslide locations can be identified from the webcam view. No further information on landslide susceptibility was available. Therefore, for purposes of this study, the entire area was considered the target-observation area, where landslides may potentially occur. In order to model the landscape and thereby also the target area, an airborne laser scanning-based DEM with 5 m resolution provided by the federal government of Vorarlberg was used. For verification purposes, a WorldView-2 optical satellite image with a resolution of 0.5 m, acquired on 29/08/2015, was available.

A simple viewshed calculation illustrates which regions of the study area in general are in the sight of the webcam and which are not (Fig. 5).

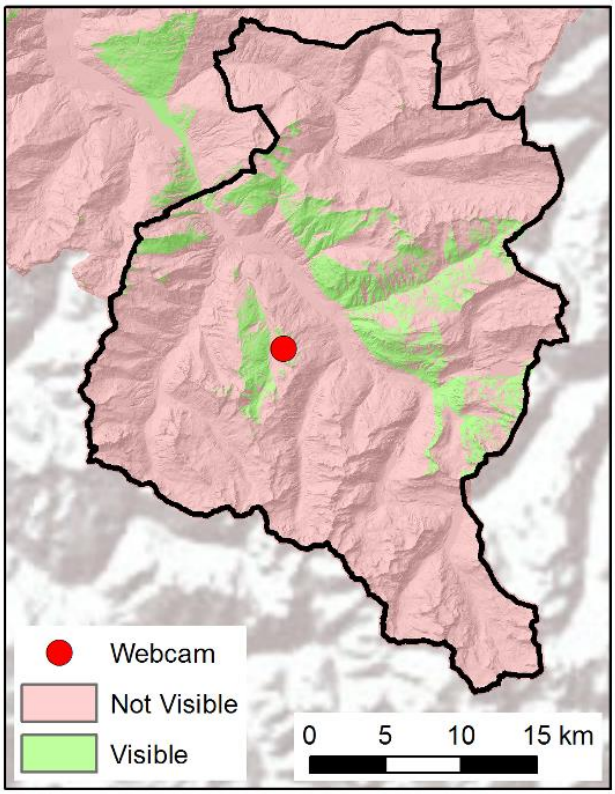

Figure 5 Viewshed for webcam "Silvretta" in Montafon, Austria.

Visibility analysis model

The viewshed calculation already excludes the locations in the area defined as out of sight of the webcam and therefore cannot be monitored by the webcam. Locations visible to the webcam, however, have to be further distinguished in order to acknowledge the webcam's resolution in relation to the size of the landslides that can be monitored. In order to incorporate the webcam's specific capabilities, a method was developed that relates the pixel size of the webcam image to the size of the area covered on the ground – which represents an analogy to the ground resolution of EO satellite images. However, in EO data, this parameter is more or less the same over the entire image, while, for webcams, it varies with distance and exposure to the sensor.

The viewshed-based visibility analysis model analysed coverage of the landscape and subdivided the field of view of the webcam into 180 x 360 tiles of 1° x 1°, assuming a panoramic view. For each tile where the terrain was in view, the ratio of the perceived surface area to the real surface area was calculated, and represents a meas-

Figure 4 Webcam view in Silvretta, Montafon, Austria, 25/08/2016.

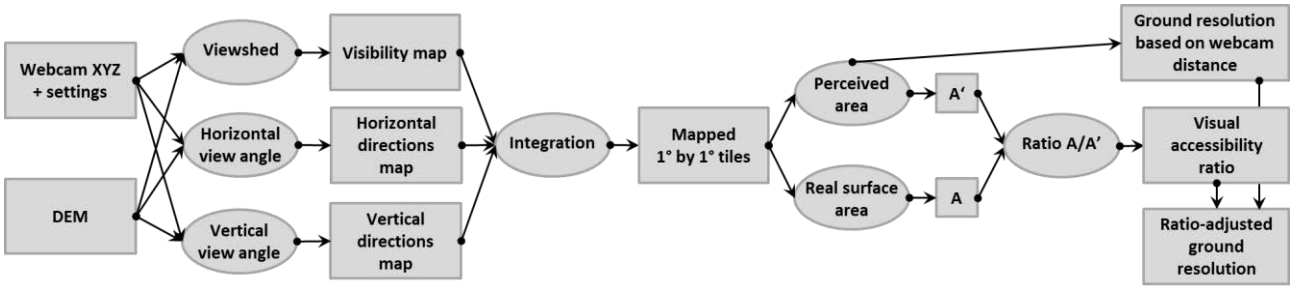

Figure 6 Visibility analysis model for mapping visual accessibility ratio and ratio-adjusted ground resolution used to evaluate the land-slide viewing capability of a webcam.

sure of visual accessibility. This measurement was then figured in with the webcam distance to achieve a ratio-adjusted ground resolution for the perceived locations within each 1° x 1° tile. The model uses the DEM and the webcam coordinates as an input (Fig. 6), and can be broken down into the following processing steps:

- Constructing tile boundaries (for the 1° x 1° tiles of the webcam's field of view) projected onto the visible terrain surface, by:
  - Calculating the visibility of a DEM location from the webcam location using the viewshed function. The results of subsequent calculations are only considered for visible areas.
  - Calculating the horizontal view angle (based on Euclidean direction) from the webcam location to the target location to identify to which tile column a target location belongs (resulting in an angular direction integer value).
  - Calculating the vertical viewing angle (in relation to the webcam viewing height, the target location terrain height, and the distance between the locations) to determine to which tile row a target location belongs (resulting in an angular direction integer value).
  - Integrating these calculated results into groups of DEM locations associated with 1° x 1° tiles of the field of view that cover them.
- Estimate the perceived locations' visual accessibility for each tile, by:
  - Calculating the perceived area A, i.e., the size of the tile's field of view at the mean distance from the webcam to the target location (that the tile covers).
  - Calculating the real surface area A that accounts for the slope at a DEM location; then summarize for each tile's perceived cells.
  - Calculating the ratio between the real surface area A of each tile to the perceived surface area A of each tile.
- Calculate ground resolution:
  - Calculate the ground resolution of a webcam pixel at the distance of each tile.
  - Calculate the ratio-adjusted ground resolution to account for the real surface area covered.

The final outcomes of the visibility analysis model are, for all of the visible target locations on the terrain dataset, the visual accessibility ratio and the ratio-adjusted ground resolution.

Results

The visual accessibility ratio and the ratio-adjusted ground resolution have been calculated for the webcam location and the DEM in the study area of Montafon. Results of the analysis are displayed both as a map, i.e., as a geographic projection, and as an overlay with the field of view of the webcam (Fig. 7 and Fig. 8). The field of view overlay was generated using the 1° x 1° tile index to associate the value calculated for each tile with a grid 360 cells in width and 180 cells in height, which represents the field of view with an angular grid. The webcam view was geo-referenced to the field of view, which enabled the overlaying of the analysis results with the webcam view (Fig. 7 and Fig. 8).

Fig. 7 shows that the webcam resolution decreases as the represented terrain grows more distant. Also, the terrain locations are represented at lower resolution as soon as the direction deviates from the direct sight line of the webcam. The calculation of the ratio-adjusted ground resolution described above, however, has certain drawbacks, as it produces excessively high values whenever the 1° x 1° tile covers a mountain ridge. Nevertheless, the other areas show plausible values that are useful for purposes of interpretation. The detailed picture presented in Fig. 8 shows an area covered by the webcam where landslides are present. They can be discerned by the bare soil that became visible after the landslide removed the vegetation layer. The large landslide n° 1 to the west (Fig. 8, lower left), however, is blocked from the view of the webcam (Fig. 8, upper left) by a mountain ridge in the foreground. Fig. 8, upper right in combination with the lower right, shows that the larger landslides n° 2 and n° 4 are located in the tiles with 2-5 m ratio-adjusted ground resolution and are well visible in the webcam view. But the webcam reaches its limits when it comes to the two small landslides marked as n° 3. Of these two, only one is clearly identifiable on the webcam view. Also, the south-

ern landslide n° 2 is surrounded by forest that partially occludes it from view. As a result, it is not as easily visible as landslide n° 4. Nevertheless, landslides the size of n° 2 and n° 4 ought to be detectable within the areas with a ratio-adjusted ground resolution of 5 m or finer. Landslides like n° 3 would need a ratio-adjusted ground resolution of at least 2 m.

Discussion and Conclusion

In this study we developed a visibility analysis model that calculates the ratio-adjusted ground resolution of a webcam for the visible surrounding terrain. The procedure and measurements help estimate the webcam's ability to identify landslides. This allows us to evaluate the webcam's effective coverage in monitoring areas suscep-

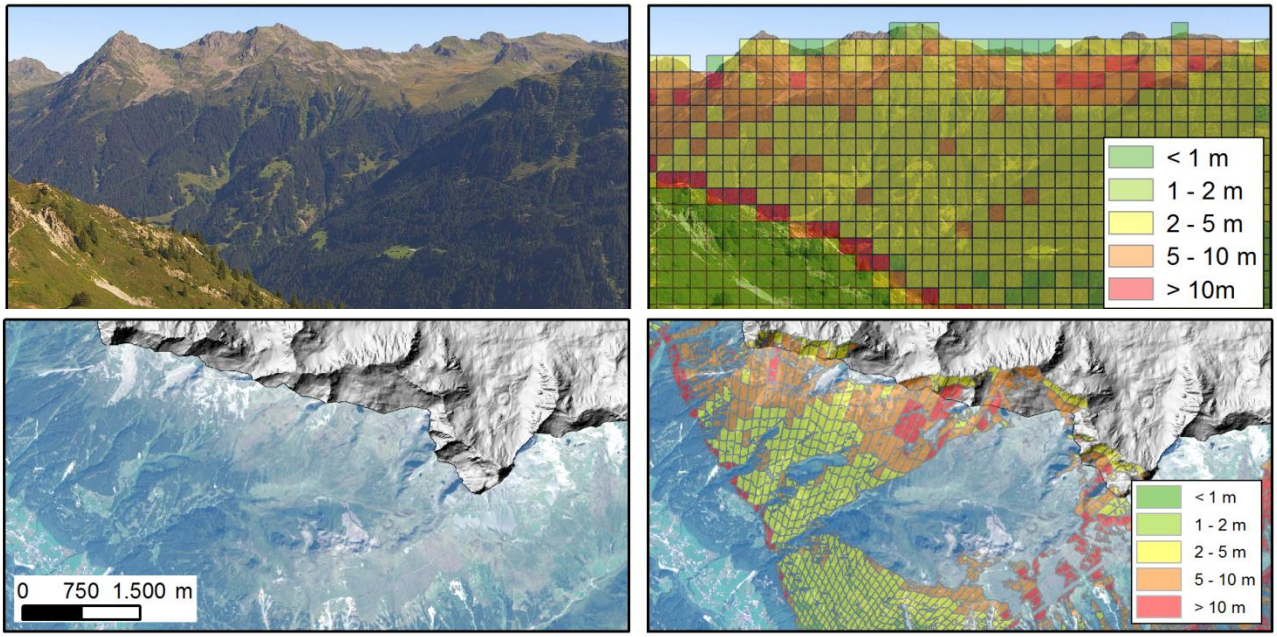

Figure 7 Webcam view (upper left) and the webcam view overlaid by 1° x 1° tiles with the ratio-adjusted ground resolution (upper right); map view of study area with WorldView-2 image (lower left) overlaid with mapped webcam tiles containing the ratio-adjusted ground resolution (lower right).

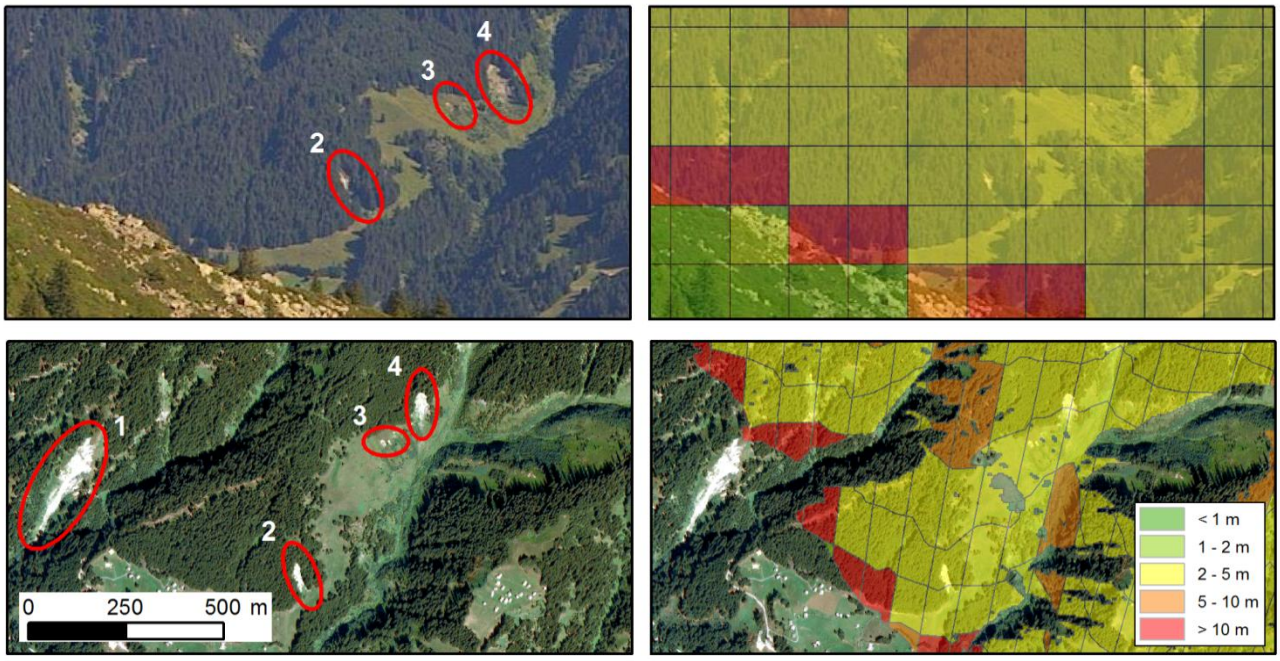

Figure 8 Zoom of webcam view (upper left) and zoom of webcam view overlaid by 1° by 1° tiles with ratio-adjusted ground resolution (upper right); detailed map view of study area with WorldView-2 image (lower left) overlaid by mapped webcam tiles containing the ratio-adjusted ground resolution (lower right). Landslides are circled in red.

-tible to landslides. The visualization employed included transformation of the results map to the webcam's per-spective view for the overlay with the webcam image. This way of visualising the webcam data and EO refer-ence data was highly valuable in visually validating the visibility analysis model and in evaluating the webcam's capabilities. In order to better determine the relation be-tween the size of the measured landslide and the ratio-adjusted webcam resolution, a more detailed visibility analysis model can be developed that calculates a ratio-adjusted ground resolution for every single webcam pixel and for each single DEM raster cell, as opposed to using coarse 1° x 1° tiles. Also, the use of input DEM data with higher resolution digital surface models (DSMs) that in-clude obstacles on the terrain, or the use of land cover maps indicating forest areas would improve the results of the visibility analysis.

According to the modelled visibility information in this study, webcams and the presented concept have real potential as a possible cost-effective landslide alert system. But the scheme still requires more research in order to determine the technical feasibility of such a system. The visibility analysis model needs to be extended to analyse the capability of a system employing constellations of multiple webcams and which may follow an approach similar to Bao et al. (2015) designed to plan constellations of fire watchtowers. Also, the cost of installing webcams in the field has so far been disregarded. A further challenge is the integration of the webcam network into a web service architecture capable of automatically extracting landslide information from webcam images in order to produce fast processing and good, workable response times in the issuing of alerts.

Acknowledgments

This research has been supported by the Austrian Research Promotion Agency FFG in the Austrian Space Applications Program (ASAP 11) through the project Land@Slide (contract n° 847970).

References

Albrecht F, Hölbling D, Weinke E, Eisank C (2016) User requirements for an Earth Observation (EO)-based landslide information web service. In: Aversa S, Cascini L, Picarelli L, Scavia C (eds) Landslides and engineered slopes: Experience, theory and practice: Proceedings of the 12th International Symposium on Landslides, 12-19 June 2016. CRC Press, Napoli, Italy. pp. 301–308.

Amidon EL, Elsner GH (1968) Delineating landscape view areas - a computer approach. U.S.D.A. Forest Service Research Note PSW-180.

Bao S, Xiao N, Lai Z, Zhang H, Kim C (2015) Optimizing watchtower locations for forest fire monitoring using location models. Fire Safety Journal. 71: 100–109.

Bothmann L, Menzel A, Menze BH, Schunk C, Kauermann G (2017) Automated processing of webcam images for phenological classification. PLoS ONE. 12(2): e0171918.

Corominas J., van Westen C, Frattini P, Cascini L, Malet JP, Fotopoulou S, Catani F, Van Den Eeckhaut M, Mavrouli O, Agliardi F, Pitilakis K, Winter MG, Pastor M, Ferlisi S, Tofani V, Hervás J, Smith JT (2014) Recommendations for the quantitative analysis of landslide risk. Bulletin of Engineering Geology and the Environment. 73(2): 209–263.

Daneu V (2014) Einsatz von Sichtbarkeitsanalysen und heuristischer Optimierungsverfahren bei der Routenplanung von Aufklärungsflügen zur Waldbranddetektion in Südportugal. Master Thesis, University of Salzburg, Salzburg, Austria.

Dizerens C (2015) Georectification and snow classification of webcam images: potential for complementing satellite-derived snow maps over Switzerland. Master Thesis, University of Bern, Bern, Switzerland.

Fisher PF (1996) Extending the applicability of viewsheds in landscape planning. Photogrammetric Engineering and Remote Sensing. 62(11): 1297–1302.

Guzzetti F, Carrara A, Cardinali M, Reichenbach P (1999) Landslide hazard evaluation: a review of current techniques and their application in a multi-scale study, Central Italy. Geomorphology. 31: 181–216.

Hölbling D, Eisank C, Albrecht F, Vecchiotti F, Friedl B, Weinke E, Kociu A (2017) Comparing manual and semi-automated landslide mapping based on optical satellite images from different sensors. Geosciences. 7(2): 37.

Lee JAY (1991) Analyses of visibility sites on topographic surfaces. International Journal of Geographical Information Systems. 5(4): 413–429.

Lienhard A, Binna T (2013) VisibilityMap, innovative GPU-Programmierung zur Sichtbarkeitsberechnung. In: Strobl J, Blaschke T, Griesebner G, Zagel B (eds) Angewandte Geoinformatik 2013. Wichmann Verlag, Austria. pp. 332–337.

Llobera M (2003) Extending GIS-based visual analysis: the concept of visualscapes. International Journal of Geographical Information Science. 17(1): 25–48.

Scaioni M, Longoni L, Melillo V, Papini M (2014) Remote sensing for landslide investigations: an overview of recent achievements and perspectives. Remote Sensing. 6: 9600–9652.

van Westen CJ, Castellanos Abella EA, Sekhar LK (2008) Spatial data for landslide susceptibility, hazards and vulnerability assessment: an overview. Engineering Geology. 102: 112–131.

Tools for the real time visualization and analysis of Ground-based SAR data: application to the monitoring of landslides

Giovanni Nico[(1)], **Uroš Kostić** [(2)], **Andrea Di Pasquale**[(3)]

1) Consiglio Nazionale delle Ricerche, Istituto per le Applicazioni del Calcolo, Via Amendola 122/O, 70126 Bari, Italy
g.nico@ba.iac.cnr.it

2) Aalta doo, Solkan, Slovenia

3) DIAN srl, Z.I., Matera, Italy

Abstract This paper is focused on visualization of the information extracted by GBSAR data acquired in landslide areas. It describes the way Graphical Processing Units (GPUs) can be used to generate and visualize accurate GBSAR images and displacement maps in near real time. Examples of GBSAR images, as radar coordinates and rendered on Digital Surface Models (DSMs), coherence and displacement maps are shown.

Keywords Synthetic Aperture Radar (SAR), GBSAR, SAR interferometry, landslide, Graphical Processing Unit (GPU)

Introduction

The application of Ground-Based Synthetic Aperture Radar (GBSAR) to monitor natural disasters and man-made infrastructures has been demonstrated in the recent past (for example see Leva et al. 2003; Takahashi et al. 2013; Mascolo et al. 2015; Nico et al. 2015). The working principle revolves around SAR interferometry, which has been applied extensively in geology using space-borne SAR images (see Massonet and Feigl 1998). Oliveira et al. (2015) describes the application of space-borne SAR interferometry to the survey of landslide-prone areas. In many cases, as for continuous monitoring operations, GBSAR can produce a near-continual stream of high-dimensional data, and this explosion in the amount of collected information introduces new processing challenges, mainly during real-time monitoring applications where high spatial resolution information is required. In recent years, GPUs have evolved into highly parallel multi-core processors with tremendous computing power and high memory bandwidth that provide an increase in magnitude on the order of two to three times that of CPUs. A cost-effective GPU computer has become an affordable alternative to an expensive CPU computer cluster for many researchers performing various scientific and engineering applications. In this work we present the first results of a project aiming to demonstrate the usefulness of GPUs in real-time measurement of displacements by GBSAR. User requirements, in terms computational power and processing times, depend on the observation configuration, i.e. the maximum range of the monitored area from the GBSAR location and the irradiation pattern of antennas, which are chosen based on the landslide's characteristics. The generation of accurate high-resolution GBSAR images rendered on a 3D digital surface of the monitored area requires specific processing techniques. The issue of the quality of the time series of GBSAR images also represents key information to be visualized during monitoring operations. This is usually assessed using interferometric coherence, which is useful in estimating the local precision of the displacement measurement. The generation of SAR images from raw data, a processing step called focusing, is a key factor in the whole processing chain since it sets the possibility of easily distinguishing close targets in the scene that have different displacement histories. The computational complexity of SAR image focusing depends on the maximum range of the monitored area. In practice, the quality of SAR images is determined by the observation configuration. For far range configurations, raw data consists of large matrices that call for the use of approximate fast-focusing algorithms, such as the Time Domain algorithm (TDA) based on FFTs, in order to reduce computational times, which in turn provides less accurate results. Applications where near-range configurations are used can benefit from the more accurate Frequency Domain Back propagation algorithm (FDBA) to focus GBSAR raw data, which also provides the possibility to visualize GBSAR images on a Digital Surface Model (DSM) of the scene. The use of Graphical Processing Units (GPU) ignores this distinction and provides the user with the most accurate focused GBSAR images, and also offers the possibility of visualizing on the DSM both GBSAR images and all of the images produced in the interferometric processing of GBSAR data, including displacement maps and temporal profiles during the monitoring campaign. In this work, a few case studies are shown related to landslides of different spatial extension and an average distance from the GBSAR installation site ranging up to 4 km. Details related to the visual inspection of landslides required in order to choose the most useful location of the installation of the GBSAR, the data acquisition process and processing of GBSAR data up to the generation of displacement

maps are all provided. In particular, the processing chain of GBSAR data is detailed from the point of view of geologists and geotechnical engineers. The critical points, where a real-time (or near real-time) visualization and analysis of GBSAR are required are described in detail. In particular, the computational times for FDBA-focused images on both GPUs and CPUs are reported, together with the quality of the focused image compared to that of TDA-focused images provided by GBSAR systems currently available on the market.

Acquisition and processing of GBSAR images

A GB-SAR consists in a stepped frequency continuous wave (SF-CW) radar moved along a rail of finite length that changes its position in a constant step, while a burst of pulses characterized by different progressive frequencies are transmitted and the corresponding backscattering echoes are received. The raw data structure consists of a matrix with the number of columns given by the acquisition positions along the rail and the number of rows given by the transmitted frequencies. The Frequency-Domain Back Propagation (FDBA) provides the exact focusing method of GBSAR. It performs a coherent sum of the different frequency contributions for each radar position, corrected for the phase delay (Fortuny-Guasch 2009)

$$S(\rho,\psi)=\sum_n\sum_m d(x_n, f_m)\cdot\exp\left\{i4\pi f_m\frac{R}{c}\right\} \quad [1]$$

where $d(x_n, f_m)$ is the raw data matrix, x_n and f_m the acquisition position and transmitted frequency, respectively, R is the distance of each point in the scene with respect to the center of the synthetic aperture, c is the speed of light and $S(\rho,\psi)$ the focused image expressed as polar coordinates (see Figure 1). Although the FDBA provides a precisely focused GBSAR image implementation is very heavy. Its computational load is given by $O(M_R,N_R,M_F,N_F)$ with $O(M_R,N_R)$ and $O(M_F,N_F)$ – the dimensions of the raw data matrix and focused image, respectively. Approximated solutions have been proposed in literature ensuring computational efficiency (e.g., see Zonno et al. 2013 and reference therein). The spatial resolution of GBSAR images depends on the frequency bands of the GBSAR employed and the distance of the landslide from the radar. The range resolution is commonly 0.50 m and angular distance between targets that can be resolved is 0.5 degrees. The interferometric processing of a time series of GBSAR images consists in computing phase images, called interferograms, as

$$\Delta\varphi=\arctan\{S_i\cdot conj(S_{i+1})\} \quad [2]$$

where S_i is the i-th GBSAR image, a complex-value matrix. The displacement image is computed as

$$D=\frac{\lambda}{4\pi}\Delta\varphi \quad [3]$$

where λ is the radar wavelength. Displacement measurements have a sub-millimetre precision that depends on the local interferometric coherence γ of the target, defined as

$$\gamma=\frac{\left|\langle S_i\cdot conj(S_{i+1})\rangle\right|}{\sqrt{\langle|S_i|^2\rangle\cdot\langle|S_{i+1}|^2\rangle}} \quad [4]$$

with $\gamma\in[0,1]$ and the operator $\langle\cdot\rangle$ denoting the spatial average within a NxM window sliding over the image.

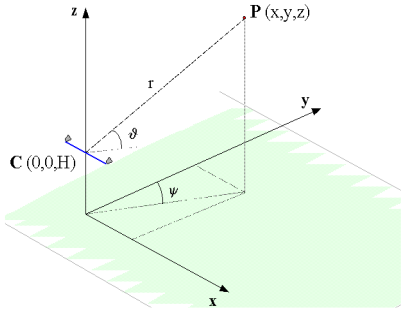

Figure 1 Reference system of GBSAR images.

GPU implementation of estimation of FDBA algorithm and coherence

The calculations required to focus a GBSAR image using a FDBA algorithm are independent for each pixel of the focused image or point of the target DSM. That means that they can be very efficiently performed in parallel, i.e. one processor can be used for each pixel on the SAR image. Usually, CPU clusters are used for such tasks; however, we parallelized the algorithms in such a way as to take advantage of the large number of cores in a Graphical Processing Unit (GPU). The FDBA algorithm has been coded in CUDA (Compute Unified Device Architecture), which is a parallel programming and computing platform developed by NVidia. The main differences between a CPU and a GPU code are:

1) the input data are copied beforehand from RAM to GPU memory, and
2) the serial algorithm (on CPU) requires a loop that runs through all the data points; however, on a GPU, one thread is dedicated to each data point on the focused image, thus reducing the number of loops to those on the raw data matrix.

This way, each thread calculates only one point of the image. Since GPUs can typically run hundreds of independent threads, hundreds of image points are

calculated concurrently, thus, speeding up the calculations significantly. All these properties made GPU an interesting tool for Earth Observation applications (e.g. see Baier and Zhu 2016 and Xingxing and Seok-Bum 2012). Analogously to the FDBA focusing algorithm, the computation coherence, too, is an intrinsically parallel processing operation, since it can be computed in parallel on different pixels since its values does not depend on the coherence of the adjacent pixel. Furthermore, this approach can also allow an adaptive computation of the coherence, choosing the window size MN that locally minimizes the estimation bias instead of using the window size for the whole image as currently done in GBSAR processing. This results in more accurate coherence maps, with higher possible spatial resolutions for a given allowed bias. Table 1 summarizes the technical specifications of the GPU used in this work.

Table 1 GTX 760 technical specifications.

Variable	Value
Number of Compute Units	6
Number of CUDA cores	1152
CUDA cores per Compute Units	192
Graphics Clock	1 GHz
Memory Clock	3 GHz
Global Memory	2 GB
Peak single precision Flops	2.25 TF/s

Results

In this section, we summarize a few of the results. In the first example, we compare the FDBA focused GBSAR image to that obtained by the commonly used TDA. The execution times of the FDBA on both GPU and CPU are reported. Figure 2 shows the GBSAR Normalized Radar Cross Section (NRCS) images referring to the landslide area, which required monitoring an area up to a maximum range of 1 km. Raw data has been weighted using a Hamming function. As expected, the image obtained by FPBA has a better spatial resolution than that provided by TDA. Note in particular the capability to better differentiate buildings in the landslide area (see also the picture of the monitored area in Figure 3-a). Table 2 summarizes the execution times of the FDBA algorithm on GPU and CPU, for both single and double precision operations: the increased speeds obtained with GPU code compared to the single-threaded CPU code (running on Intel i7-4770 @ 3.40GHz) are 85x–185x and 44x–79x for single and double precision arithmetic, respectively. A second example is reported in Fig. 2. A corresponding scene is shown in Fig. 3. It refers to a small village affected by a slow landslide, where it was necessary to discriminate stable buildings from those slowly being displaced over time. Figure 3-b also shows the displacement map rendered on the DSM of the area, which is a useful visualization tool with which to identify the targets in the scene and provide an interpretation of the measured displacements that can be made in near real-time with the use of GPUs. Figure 4 shows a second example referring to a larger landslide area still affecting an urban area. In this case it was necessary to acquire GBSAR data up to a maximum range of 4 km. The FDBA focusing of GBSAR images and the adaptive computation of the coherence maps on CPU hinder any near real-time interpretation of data during monitoring operations. Nevertheless, the observation of the GBSAR image and the coherence map, shown in Figure 4(b) and 4(c), respectively, makes clear the importance of generating them in near real time, also comparing with data acquired in previous campaigns.

Table 2 Execution times of GPU and CPU-based FDBA algorithm for the two case studies. The single and double precision codes are compared.

CPU [s]		GPU [s]	
Single precision	Double precision	Single precision	Double precision
43885	50119	202	383

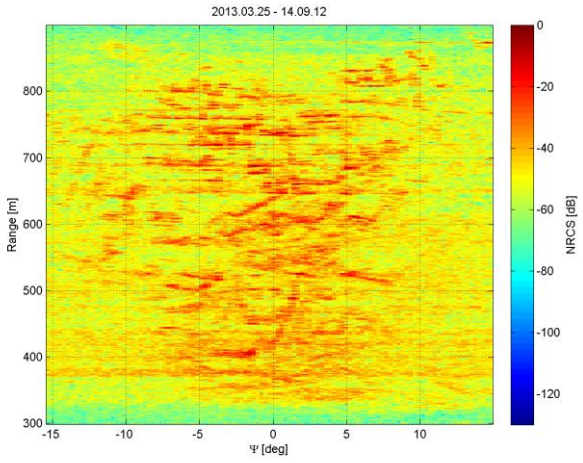

(a)

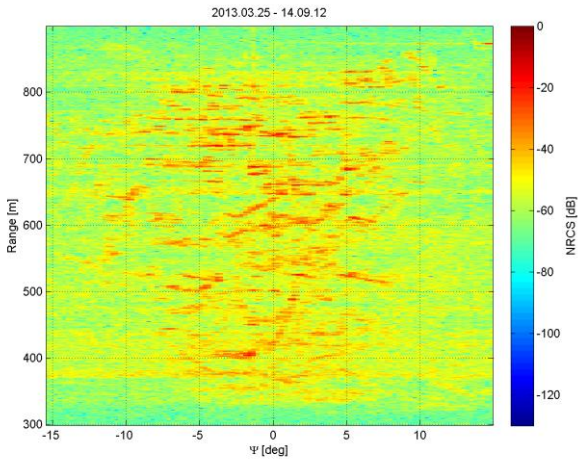

(b)

Figure 2 Amplitude of SAR image focused with (a) TD algorithm, on CPU, and (b) BPDA algorithm on GPU. The corresponding scene is shown in Figure 3-(a).

The use GPU-based visualization tools can be make this possible and open new perspectives for the real time computation of coherence maps between all possible pair of acquired GBSAR images in order to get rid off of less uncorrelated images and provide more accurate displacement time series of target of interest.

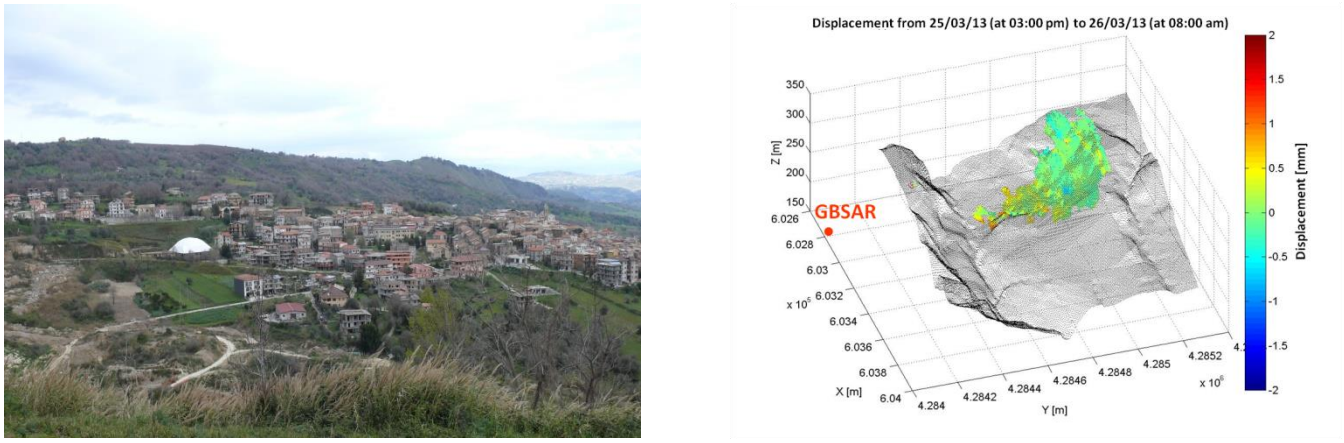

(a) (b)

Figure 3 (a) Picture of the landslide area; (b) Rendering of the amplitude of GBSAR images on a Digital Elevation Model of the monitored area.

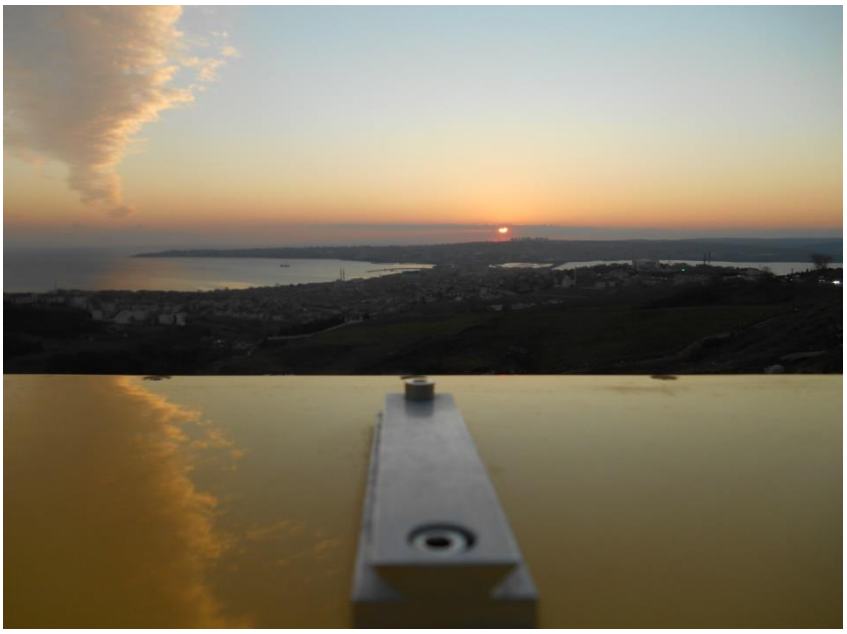

(a)

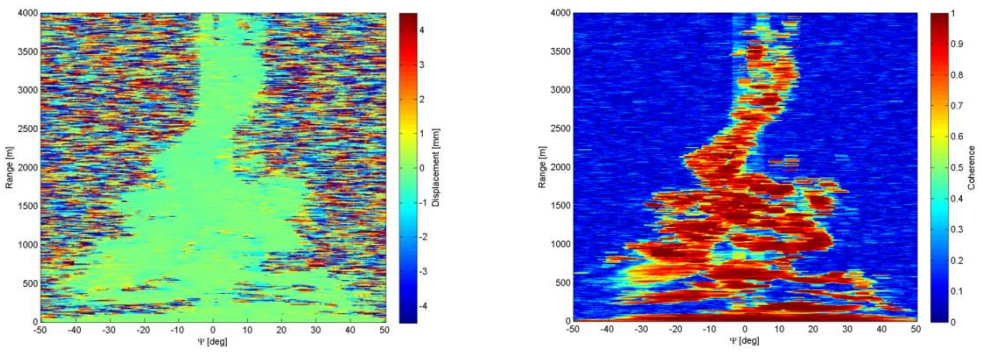

(b) (c)

Figure 4 (a) Picture of the landslide area; (b) Amplitude of GBSAR images and (c) Interferometric coherence in radar coordinates.

Conclusions

In this paper the results, which we have obtained by generating GBSAR images by a FDBA and coherence maps by adaptive algorithm, both implemented on GPU, are described. Taking into account the characteristics of FDBA and coherence algorithms, we can be certain that, if a larger number of GPUs were used, the speed-ups would be even greater opening new perspective to thereal-time in-depth analysis of GBSAR data.

References

Baier G, Zhu X (2016) GPU-based nonlocal filtering for large scale SAR processing. In: Proceedings of the IEEE International Geoscience and Remote Sensing Symposium, 10-15 June 2016. Beijing, China. pp. 7608-7611.

Fortuny-Guasch J (2009) A fast and accurate far-field pseudopolar format radar imaging algorithm. IEEE Transactions on Geoscience and Remote Sensing. 47(4): 1187-1196.

Leva D, Nico G, Tarchi D, Fortuny J, Sieber AJ (2003) Temporal analysis of a landslide by means of a ground-based SAR interferometer. IEEE Transactions on Geoscience and Remote Sensing. 41(4): 745-752.

Massonnet D, Feigl KL (1998) Radar interferometry and its application to changes in the earth's surface. Review of Geophysics. 36(4): 441-500.

Mascolo L, Nico G., Di Pasquale A, Pitullo A (2014) Use of advanced SAR monitoring techniques for the assessment of the behavior of old embankment dams. In: Michel U, Schulz K (eds) Proceedings of SPIE Remote Sensing, vol. 9245,23-24 September 2014. Amsterdam, Netherlands. pp. 92450N-92450N-10.

Nico G, Borrelli L, Di Pasquale A, Antronico L, Gullá G (2015) Monitoring of an ancient landslide phenomenon by GBSAR technique in the Maierato town (Calabria, Italy). In: Lollino G et al. (eds) Engineering Geology for Society and Territory, vol. 2. Springer International Publishing, Switzerland. pp. 129-133.

Oliveira SC, Zezere JL, Catalao J, Nico G (2015) The contribution of PSInSAR interferometry to landslide hazard in weak rock-dominated areas. Landslides. 12(4): 703-719.

Takahashi K, Matsumoto M, Sato M (2013) Continuous observation of natural-disaster-affected areas using ground-based SAR interferometry. IEEE Journal of Selected Topics in Applied Earth Observations and Remote Sensing. 6(3): 1296-1294.

Xingxing J, Seok-Bum K (2012) GPU-based parallel implementation of SAR imaging. In: Proceedings of the IEEE International Symposium on Electronic System Design, 19-22 December 2012. Kolkata, India. pp. 125-129.

Zonno M, Guccione P, Nico G (2013) Study of ground-based SAR imaging algorithms. In: Proceedings of the IEEE International Symposium on Geosciences and Remote Sensing, 21-26 July 2013. Melbourne, Australia. pp. 3895-3898.

Automated GNSS monitoring of Umka landslide – review of seven years' experience and results

Biljana Abolmasov[(1)], Marko Pejić[(2)], Mileva Samardžić-Petrović[(1)], Uroš Đurić[(2)], Svetozar Milenković[(3)]

1) University of Belgrade, Faculty of Mining and Geology, Đušina 7, 11000, Belgrade, Serbia, biljana.abolmasov@rgf.bg.ac.rs

2) University of Belgrade, Faculty of Civil Engineering, Belgrade, Serbia

3) The Highway Institute, Belgrade, Serbia

Abstract The Umka landslide is the biggest and deepest active landslide in the Republic of Serbia, and has been investigated and monitored using various geotechnical techniques for decades. This paper focuses on the results and experience gained using the automated Global Navigation Satellite System (GNSS) monitoring network of the Umka landslide introduced in March 2010. It remains the longest continuous period of any landslide monitoring in Serbia; however, many operational and maintenance problems were addressed over seven years of monitoring. The main problems were related to the GNSS network's functional operation, such as the replacement of the reference station position and the relocation of the object point station to a different location. The shape of the GNSS network was changed as the result of replacing the reference stations which was implemented by the Republic Geodetic Authority (RGA) in 2011. The GNSS sensor (object point) placed in the landslide body also had to be relocated after December 2013 for technical reasons and was moved to a nearby location after in May 2014. Precipitation data on the Belgrade Main Meteorological Station (MMS) and the level of the Sava River from a Beljin water level station was continuously collected throughout the entire period on a daily basis. The results and experience gained through the automated GNSS monitoring of the Umka landslide over the past seven years will be presented and discussed.

Keywords landslide, GNSS, automated, permanent monitoring

Introduction

The development of geodetic instruments for data acquisition and technology for data processing in real time has encouraged and increased the use of complex automated monitoring systems across an array of engineering disciplines. Consequently, over the past decade a wide range of different types of landslide monitoring systems have been used in an attempt to assess the dynamics of landslides and potentially prevent possible disasters. One widely used system, which has proven to be an effective and reliable tool for landslide monitoring, is the Global Navigation Satellite System (GNSS). In 2000 Gili et al. (2000) provided a general overview of the Global Positioning System (GPS) principles and discussed its applicability to landslide monitoring of the Vallcebre landslide in Spain. Since then, many research papers have presented successful landslide monitoring using GNSS and the integration of such with other observations (gained using other geodetic instruments like totally automated stations and laser scanners) from around the world (Coe et al. 2003, Malet et al. 2002, Zhou et al. 2005, Castagnetti et al. 2013).

According to the European Joint Research Centre's Institute for Environment and Sustainability (JRC-IES) the largest part of the Balkan Peninsula lies in the high to very high class of landslide susceptibility (Erić et al. 2015). Due to climate change and expected increasingly heavy rains, which are one of the main triggers that activate landslides, several countries in the Balkan region have established landslide monitoring systems in order to provide early warning system and prevent possible disasters. The Republic of Croatia, within the Japanese-Croatia five-year (2009–2014) project, designed GNSS- based real time monitoring systems on the two largest landslides in the country – Kostanjek (Krkač et al. 2014, Krkač et al. 2017) and Grohovo (Arbanas et al. 2012, Arbanas et al. 2014).

The first automated GNSS monitoring project in Serbia was established in March 2010, on the Umka landslide (near Belgrade), the biggest active landslide in Serbia (Abolmasov et al. 2013). This seven-year project represents the longest continuous monitoring of any landslide in Serbia and probably one of the longest-running in the Balkan region. The objectives of this paper are to present the results and some of the main issues of the automated GNSS monitoring system used at the Umka landslide. In view of the high correlation between the movement of the landslide with precipitation and the proximity of the Sava River, two additional data sets were analysed: precipitation data from Belgrade (MMS) and data on the level of the Sava river from a Beljin station, which were collected throughout the entire period (2010–2017), on a daily basis (Fig. 1).

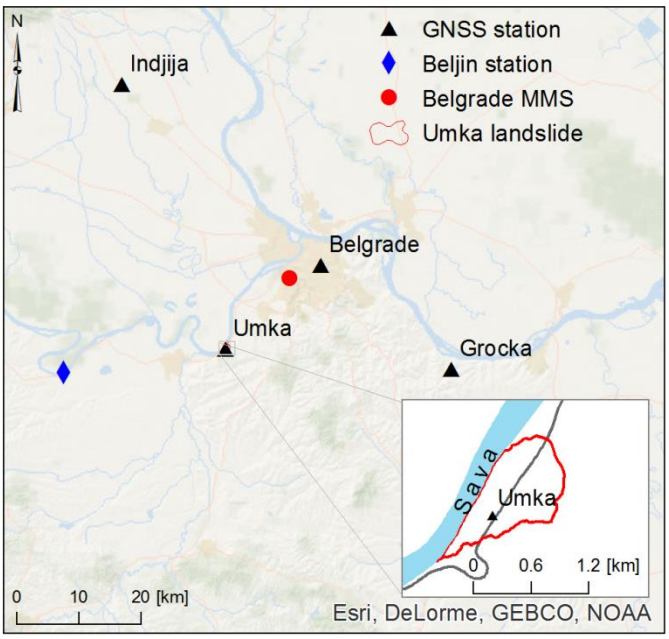

Figure 1 Locations of GNSS stations, Belgrade MMS, Beljin water level station and Umka landslide area.

Study area – Umka landslide

The Umka landslide represents one of the largest inhabited landslides in Serbia. The landslide is formed on the right bank of the Sava river, 22 km southwest of Belgrade, and comprises part of the suburban Belgrade settlement of Umka. Mali Zvornik, part of the important state road IB26, Belgrade crosses the landslide body (1.7 km) (Fig. 1). According to the available data for annual traffic volumes (http://www.putevi-srbije.rs) an average of 13,000 vehicles crossed the landslide body daily in 2016. According to geotechnical investigations performed in 2005 by the Highway Institute – Belgrade (the last phase of investigations for the Preliminary Design of the E-763 motorway) the landslide surface is 0.83 km^2, with a maximum length of cca. 1.66 km, and a maximum width of cca. 0.88 km, with a maximum slip surface depth of 26 m.

The results of these extensive geotechnical investigations of the Umka landslide were published in Vujanić et al. (1981, 1984), Ćorić et al. (1994, 1996). Dangić et al. (1997), Hadžiniković (1988). Results of the conventional geotechnical monitoring of the landslide can be found in Jelisavac (1995), Jelisavac et al. (2006). A recent summary of GNSS monitoring results was published (Abolmasov et al. 2012b and Erić et al. 2015) and overview of landslide geotechnical modeling was presented in Jelisavac et al. 2006, Đurić et al. 2011, Đurić 2011 and Abolmasov et al. 2014a, Abolmasov et al. 2015. Reports on the IPL-ICL project related to the Umka landslide can be found in Abolmasov et al. 2014b, 2017 as a part of IPL 181 Project results.

Automated GNSS monitoring system

The main characteristics of the system

The Umka monitoring system consists of a GNSS network and supporting software solutions. Generally, the network consists of reference and object (monitoring) points on which GNSS stations (sensors) are mounted. Highly precise, multi-channel, multi-frequency systems (receivers and antennas) are used on all network points (Abolmasov et al. 2012b, Abolmasov et al. 2014b). During the seven years of ongoing monitoring the GNSS network has changed twice, but the concept has remained the same. The reference points used comprise an integral part of the Active Geodetic Reference Network of Serbia (AGROS network), which is a permanent GNSS service providing accurate data on satellite positioning over the Republic of Serbia territory. All reference points used are located outside the landslide area, and their movements are not significant over time (Erić et al. 2015). The Umka landslide area is represented by a single object point, which is located in the landslide body on the roof of a house there (Abolmasov et al. 2011, Abolmasov et al. 2012b).

The second essential part of the automated GNSS monitoring system is the supporting software solution. The system used two Leica Geosystems software solutions in order to continuously monitor the dynamics of the Umka landslide, remotely control and communicate with other GNSS stations, store, evaluate and post-process collected data and perform analysis: GNSS Spider and GeoMoS (Geodetic Monitoring System), which was further comprised of two main applications: GeoMoS Monitor and GeoMoS Analyzer. All observed GNSS measurements, with an observation rate of 30 s, are collected by the GNSS Spider and forwarded, in the form of RINEX files, to the GeoMoS Monitor and GeoMoS Analyzer for processing and further analysis, respectively. Detailed descriptions of the system can be found in Erić et al. (2015).

Changes and some of the main issues of system

During the more than seven years of continuous monitoring of the Umka landslide two major changes occurred in the system, together with various technical problems that caused operational problems.

Firstly, the system underwent two main changes. Initially, the GNSS monitoring network consisted of three GNSS points: two reference points, Belgrade and Lazarevac, which are included in the AGROS network, and the Umka point that is placed in the Umka landslide area (Fig. 2). In June 2011, the Republic Geodetic Authority (RGA) made changes on the AGROS network and excluded the permanent station Lazarevac (Abolmasov et al. 2014). In response, a new GNSS monitoring network was established in December 2011, consisting of the initial reference point Belgrade and the Umka point, and the two new reference points – Indjija and Grocka – both of which were also included in the AGROS network. Given that the observations from the Indjija and Grocka reference points were not logged prior to the detection of RGA

changes, i.e. December 2011, it was not possible to reanalyze the measurements in order to form a continuous data set. It was possible to acquire the data from RGA for post-processing, but there were no funds available at the time. Thus, this change resulted in the loss of almost six months of continuous monitoring.

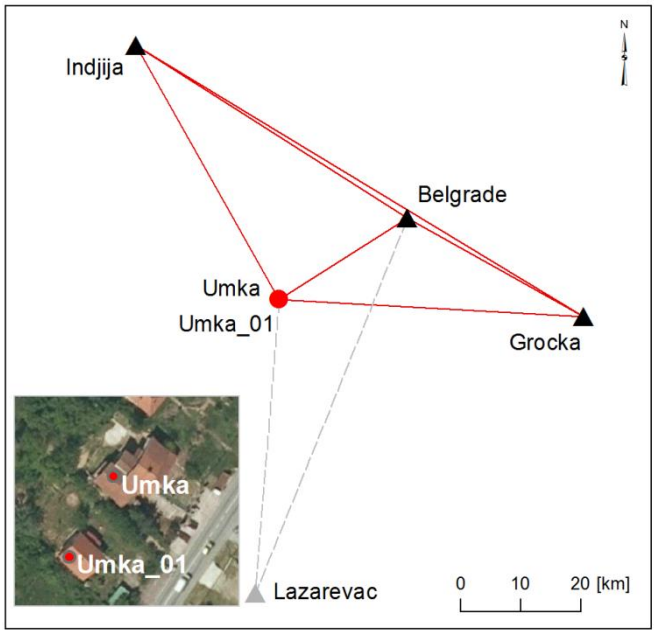

Figure 2 Location of all GNSS network points used from March 2010 to the present.

The second significant change occurred as the result of relocating the Umka point (station) (Fig. 2). This resulted in the loss of more than nine months of continuous monitoring, from the end-December 2013 through September 2014 and the establishing of a new monitoring point. Namely, the house on which roof the Umka monitoring station receiver was placed changed owners, resulting in the relocation of the receiver to the roof of a neighboring house (Fig. 2).

All told, the system did not record data for some 31 months over the seven-year monitoring period: more than 15 months owing to the changes outlined above, and an additional 16 months of interruptions caused by various technical problems. Those additional gaps in monitoring occurred at different time intervals, lasting several days to a full one-and-a-half months, depending on the problem. Generally, the main problem lay in the interrupted communication with the sensors (especially with the sensor on Umka) caused by difficulties with the Internet connection, loss of power (technical problems and human error), replacement of the modem due to malfunction and similar. Due to the complexity of the monitoring system, which requires the parallel (synchronized) operation of all system components, the gaps in monitoring caused by these kinds of technical problems are to be expected and are practically unavoidable. Despite the numerous interruptions during the seven years of continuous monitoring the dynamics of the Umka landslide can be determined and analyzed through time.

Analysis of the observed data

The Umka object point (sensor) changed location (from one house to another, i.e. from Umka to Umka_01). Given that the sensor was not working for a longer period of nine months, during which the relocation was finalized, the data derived from the continuous monitoring is analyzed for two time periods, separately: the first, from the beginning of the monitoring, from March 2010 to December 2013; and the second, from September 2014 to end-2016. The results of displacements for both time periods as well as the data collected on precipitation, from the Belgrade MMS, and the level of the Sava River from a Beljin station, are presented in Fig. 3. The data shown in the lower graphs (Fig. 3) represents longitudinal (northing displacement component), transverse (easting displacement component) and height displacements of the Umka (bottom right figure) and the Umka_01 (bottom left figure) points from the first and second observation periods, respectively. Data on precipitation and level of the Sava River, from January 2010 to end-December 2016 are presented in the upper graph. Unfortunately, during times of extreme precipitation and very high river levels caused by the Cyclone Tamara that affected the Balkans in May 2014, the automated GNSS monitoring system was not functional.

Generally, both graphics for displacements indicate that the Umka landslide is continuously moving, most significantly towards the northwest, i.e. towards the Sava River (Fig. 1). During the first 45 months (Fig. 3) the object point Umka moves 0.46 m north and 0.70 m west. Based on these results it can be concluded that the total 2D displacement is 84 cm towards the northwest. Furthermore, during the same period, the vertical displacement of the Umka sensor was nearly -0.30 m.

Results from September 2014 to end-2016 indicate that the Umka_01 object point has moved 0.25 m north and 0.46 m west, i.e. the total 2D displacement is 52 cm towards the northwest, while the vertical displacement during those 28 months was approximately -0.15 m.

As already concluded in the previously published results by Abolmasov et al. (2015), the movement of the Umka landslide can be characterized as slow to very slow. Furthermore, it can be concluded that landslide velocity varied during both observed periods (displacement velocity of both monitoring points, Umka and Umka_01). Nevertheless, considering the cumulative displacements velocity of both monitoring points, Umka and Umka_01). Nevertheless, considering the cumulative displacements and the duration of the monitoring for both periods, it can be stated that the velocities for those time periods are in general very similar. The average annual 2D displacement was approximately 22 cm for both presented periods, except for two periods – in early 2011 (January– May).

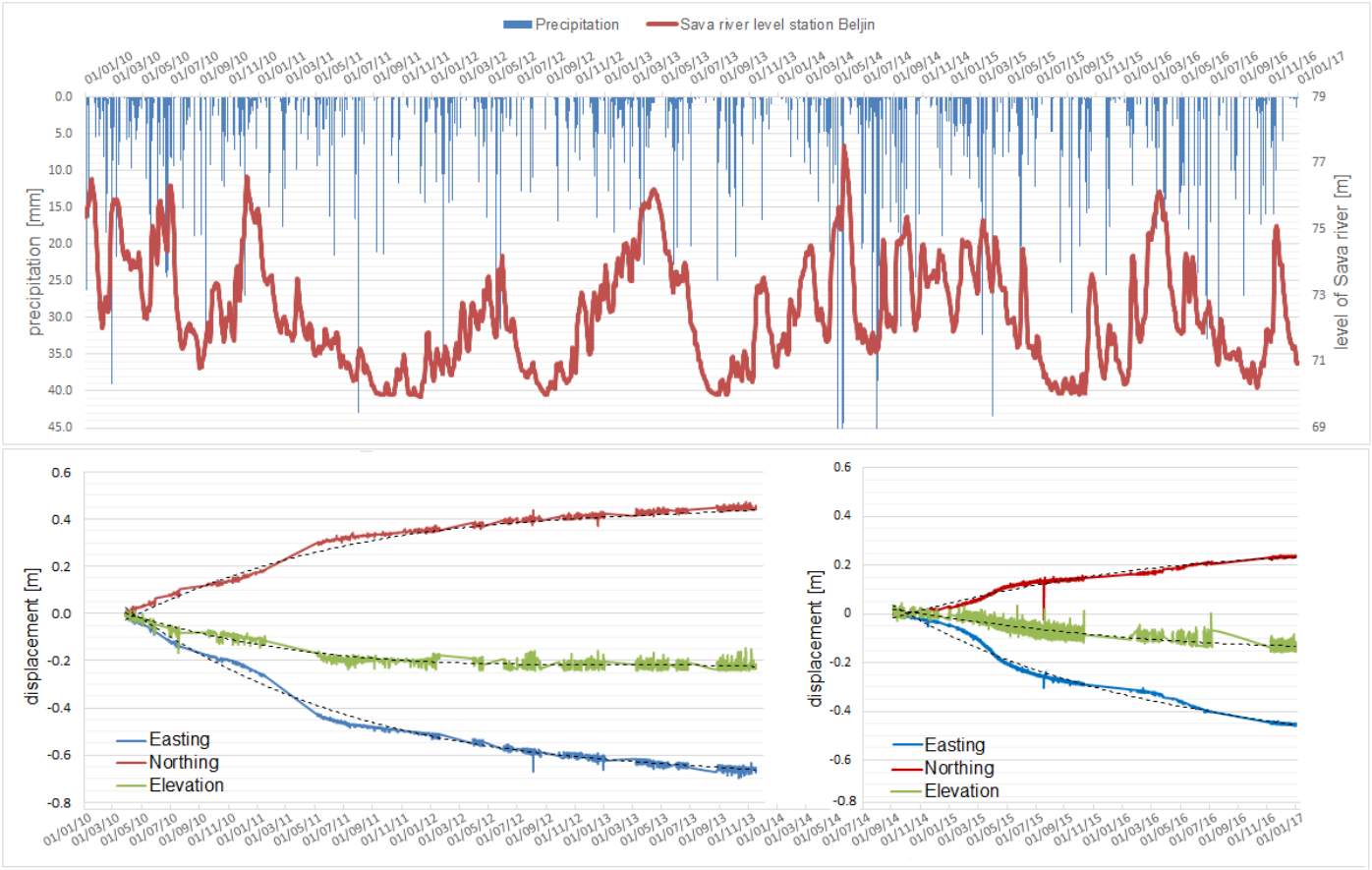

Figure 3 Precipitation and level of the Sava river (upper figure) from January 2010 to end-December 2016, displacement of Umka point from March 2010 to December 2013 (bottom right figure) and displacement of Umka_01 point from September 2014 to end-December 2016 (bottom left figure).

Both periods are characterized by intensive fluctuations in the level of the Sava river level (well-known drop-down effects) and both started with a high river level (76–77.8 m). During 2010 the Sava river twice reached those levels (June 2010 and November 2010), and obvious acceleration began in the early summer of 2010 and continued through May 2015. Said fluctuation in the river level in 2015 was followed by the highest river discharge rates during the floods of May 2014 and after, the drop-down effects caused by the empting of the Djerdap dam accumulation.

Conclusion

The experience gained during the seven years of monitoring and measuring the Umka landslide indicates the advantages of this type of monitoring and monitoring system, with said advantages already highlighted in previous publications (Abolmasov et al. 2012, Abolmasov et al. 2013, Abolmasov et al. 2015, Erić et al. 2015). The consequent analyses and derived results indicate that the points from the permanent GNSS reference systems, which exist in almost all countries (like AGROS in Serbia), can be used as points of reference networks for real time monitoring of slowly moving landslides. They are sufficiently spatially accurate (within several centimeters), and are both economical and reliable for purposes of long-term observation where greater accuracy is not necessary. In other words, using points from such GNSS networks located outside landslide areas as reference points represent an optimal solution – especially in terms of the cost of the system.

The main drawback of such a system is the single observed object point, which drawback is also highlighted and discussed in previous publications. Furthermore, during the seven years of monitoring the Umka landslide the GNSS monitoring network underwent two major changes, together with various technical problems resulting in interruptions in the continual real time monitoring process. However, it can be concluded that the observations collected represent reliable data, and that an established automated system can be used for permanent monitoring. Seven years of monitoring shows that the Umka landslide is moving continuously towards the Sava River, with an average annual displacement of approximately 22 cm.

Acknowledgments

This research is part of Project TR36009 and funded by the Ministry of Education, Science and Technological Development of the Republic of Serbia (Project No TR36009). We are very grateful to VekomGeo d.o.o. for all their support and to the Hydrometeorological Service of Serbia for sharing precipitation and hydrological data.

References

Abolmasov B, Đurić U, Pavlović R, Trivić B (2012a) Tracking of slow moving landslide by photogrametric data-a case study. Landslides and Engineered Slopes: Protecting Society through Improved Understanding, Proceedings of the 11th International and 2nd North American Symposium on Landslides and Engineered Slopes, 3-8 June 2012. Banff, Canada 1(2). pp.1359-1363.

Abolmasov B, Marjanović M, Milenković S, Đurić U, Jelisavac B, Pejić M (2017) Study of Slow Moving Landslide Umka Near Belgrade, Serbia (IPL-181). In: Mikoš M, Tiwari B, Yin Y, Sassa K (eds) Advancing Culture of Living with Landslides, vol 2: Advances in Landslide Science. Springer International Publishing, Switzerland.pp.75-80.

Abolmasov B, Milenković S, Jelisavac B., Vujanić V (2013) Landslide Umka: The First Automated Monitoring Project in Serbia. In: Margottini C, Canuti P, Sassa K (eds) Landslide Science and Practice. Springer, Berlin Heidelberg, Germany. pp. 339-346.

Abolmasov B, Milenković S, Jelisavac B, Đurić U, Marjanović M (2014a) IPL Project 181: Study of Slow Moving Landslide Umka Near Belgrade, Serbia. In: Sassa K, Canuti P, Yin Y (eds) Landslide science for a safer geoenvironment - the international pro- gramme on landslides (IPL) (1). Springer International Publishing, Switzerland. pp.75-80.

Abolmasov B, Milenković S, Jelisavac B, Vujanić V, Pejić M, Pejović M (2012b) Using GNSS sensors in real time monitoring of slow moving landslides-a case study. Land- slides and Engineered Slopes: Protecting Society through Im- proved Understanding, Proceedings of the 11th International and 2nd North American Symposium on Landslides and Engineered Slopes, 3-8 June 2012. Banff, Canada 1(2). pp. 1381-1385.

Abolmasov B, Milenković S, Marjanović M, Đurić U, Jelisavac B, (2015) A geotechnical model of the Umka landslide with reference to landslides in weathered Neogene marls in Serbia. Landslides. 12 (4): 689-702.

Abolmasov B, Pejić M, Šušić V (2014b) The analysis of landslide dynamics based on automated GNSS monitoring. In: Proceeding of the 1st Regional Symposium on Landslides in the Adriatic-Balkan Region - 1st ReSyLAB 2013, 6-9 March 2013. Zagreb, Croatia. pp. 187-191.

Arbanas Ž, Sassa K, Marui H, Mihalić S (2012) Comprehensive monitoring system on the Grohovo Landslide, Croatia. In: Proceedings of the 11th International and 2nd North American Symposium on Landslides: Landslides and Engineered Slopes: Protecting Society through Improved Understanding, 2-8 June 2012. Banff, Canada. pp. 1441-1447.

Arbanas Ž, Jagodnik V, Ljutić K, Vivoda M, Jovančević Dugonjić S, Peranić J (2014) Remote Monitoring of a Landslide Using an Integration of GPS, TPS and Conventional Geotechnical Monitoring Methods. In: Proceeding of the 1st Regional Symposium on Landslides in the Adriatic-Balkan Region - 1st ReSyLAB 2013, 6-9 March 2013. Zagreb, Croatia. pp. 39-44.

Arbanas Ž, Tofani V (2017) Introduction: Landslide Monitoring and Warning. In: Mikoš M, Arbanas Ž, Yin Y, Sassa K (eds) Advancing culture of living with landslides, vol 3: Advances in Landslide Technology. Springer International Publishing, Switzerland. pp. 23-31.

Castagnetti C, Bertacchini E, Corsini A, Capra A (2013) Multi-sensors integrated system for landslide monitoring: critical issues in system setup and data management. European Journal of Remote Sensing. 46(1). pp. 104-124.

Coe J A, Ellis W L, Godt J W, Savage W Z, Savage J E, Michael J A, Kibler J D, Powers P S, Lidke D J, Debray S (2003) Seasonal movement of the Slumgullion landslide determined from Global Positioning System surveys and field instrumentation, July 1998–March 2002. Engineering Geology. 68 (1-2): 67-101.

Ćorić S, Božinović D, Vujanić V, Jotić M, Jelisavac B (1994) Slope instability analysis in Neogene clays and marls. In: Oliveira R, Rodrigues LF, Coelho AG, Cunha AP (eds) Proceedings of 7th International IAEG Congress, 5–9 September 1994. Balkema, Rotterdam, Netherlands. pp. 1759–1770.

Ćorić S, Božinović D, Vujanić V, Jotić M, Jelisavac B (1996) Geotechnical characteristics of old landslides in Belgrade area. In: Senneset K (ed) Proceedings of the 7th International symposium on landslides, 17–21 June 1996.Balkema, Rotterdam, Netherlands. pp. 689–694.

Dangić A, Vujanić V, Josipović J, Joticć M, Jelisavac B (1997) Geochemical and geotechnical study of complex landslide in vicinity of Belgrade, Yugoslavia. In: Marinos P, Koukis GC, Tsiambaos GC, Stournaras GC (eds) Proceedings of the International Symposium on Engineering Geology and Environment, 23–27 June 1997. Balkema, Rotterdam, Netherlands. pp. 581–566.

Đurić U (2011) Primena GIS-a u praćenju dinamike klizišta „Umka". Diploma thesis, Univeristy of Belgrade, Faculty of Mining and Geology, Belgrade, Serbia. 75p. (in Serbian)

Đurić U, Petrović B, Gogić A (2011) Primena DEM-a za morfometrijsku analizu klizišta. Zbornik radova Rudarsko-geološko-građevinskog fakulteta Tuzla - posebno izdanje (XXXV). Tuzla, Bosnia and Herzegovina. pp.61-69. (in Serbian)

Erić V, Božić B, Pejić M, Abolmasov B, Pandžić J (2015) Permanent geodetic monitoring of the Umka Landslide using GNSS techonology and GeoMoss system. Abstract book - 2nd Regional Symposium on Landslides in the Adriatic-Balkan Region-2nd ReSyLAB 2015, 14-16 May 2015. Belgrade, Serbia. pp 39-39.

Gili J A, Corominas J, Rius J (2000) Using Global Positioning System techniques in landslide monitoring. Engineering Geology 55 (3):167–192.

Hadžiniković G (1998) Slope stability analysis in complex geotechnical conditions. In: Moore D, Hungr O (eds) Proceedings of 8th international IAEG congress, 21–25 September 1998. Balkema, Rotterdam, Netherlands. pp. 11523–11529.

Jelisavac B (1995) Prilog istraživanju dinamike pomeranja aktivnih klizišta u glinama. Zbornik radova, Drugi simpozijum istraživanje i sanacija klizišta, 1995. Donji Milanovac, Serbia. pp. 113-119. (in Serbian)

Jelisavac B, Milenković S, Vujanić V, Mitrović P (2006) Geotechnical investigations and repair of the landslide Umka—Duboko on the route of motorway E-763 Belgrade–South Adriatic. International workshop-Prague geotechnical days, 2006. Prague, Czech Republic.

Krkač M, Mihalić Arbanas S, Nagai O, Arbanas Ž (2014): The Kostanjek landslide – Monitoring system development and sensor network.– In: Mihalić Arbanas S, Arbanas Ž (eds.): Landslide and Flood Hazard Assessment, Proceedings of the 1st Regional Symposium on Landslides in the Adriatic-Balkan Region, 6–9 March 2013. Croatian Landslide Group, Zagreb, Croatia. pp. 27–32.

Krkač M, Mihalić Arbanas S, Arbanas Ž, Bernat Gazibara S, Sečanj M (2017) Prediction of the Kostanjek landslide movements based on monitoring results using random forests technique. In: Mikoš M, Arbanas Ž, Yin Y, Sassa K (eds) Advancing culture of living with

landslides, vol 3: Advances in Landslide Technology. Springer International Publishing, Switzerland. pp. 267-275.

Malet J P, Maquaire O, Calais E (2002) The use of Global Positioning System techniques for the continuous monitoring of landslides: application to the Super-Sauze earthflow (Alpes-de-Haute-Provence, France). Geomorphology. 43 (1-2): 33– 54.

Vujanić V, Livada N, Božinović D (1984) On an old landslide in Neogene Clays on the right bank of the Sava near Belgrade. Proceedings of 4th international symposium on landslides, Toronto, Canada. pp. 227–233.

Vujanić V, Livada N, Jotić M, Gojković S, Ivković J, Božinović D, Sunarić D, Šutić J (1981) Klizište "Duboko" na Savi kod Beograda. Zbornik radova Simpozijuma istraživanje I sanacija klizišta, 1981. Bled, Slovenija. Knjiga 1:119–134. (in Serbian)

Zhou P, Zhou B, Guo J, Li D, Ding Z, Feng Y (2005) A Demonstrative GPS-aided Automatic Landslide Monitoring System in Sichuan Province. Journal of Global Positioning Systems. 4 (1-2): 184-191.

Challenges for operational forecasting of rainfall-induced landslides in Slovenia

Mateja Jemec Auflič, Jasna Šinigoj, Matija Krivic

Geological Survey of Slovenia, Dimičeva ulica 14, 1000 Ljubljana, Slovenia, mateja.jemec@geo-zs.si

Abstract In this paper we will discuss the challenges for operational forecasting of rainfall-induced landslides in Slovenia. The forecast system for rainfall-induced landslides is based on the landslide susceptibility map, landslide triggering rainfall threshold values and the precipitation forecasting model. Through the integrated parameters a detailed framework of the system, from conceptual to operational phases, is shown. Using fuzzy logic landslide prediction has been calculated twice daily, in the morning and in the afternoon for the 24 hours ahead. Due to the sparse density of rain gauge networks in Slovenia the rainfall thresholds were statistically defined. Thus the system integrates two different rainfall thresholds. Although in general the landslides areas are overpredicted and largely do not correspond to the landslide inventory, the overall performance indicates that the system is able to capture those factors crucial in determining landslide location. Additional calibration of input parameters and the landslide inventory as well as improved spatially distributed rainfall forecast data can further enhance the model's predictive capabilities.

Keywords rainfall, landslides, forecasting, Slovenia

Introduction

The spatial-temporal prediction of landslide hazards is one of the most important fields of geoscientific research. The aim of these methods is to identify landslide-prone areas in space and/or time based on knowledge of past landslide events and terrain parameters, geological attributes and other information. In the last 25 years many countries, regions and cities have been affected by intense precipitation that led to catastrophic landslides (Haque et al. 2016). Therefore, public awareness of extreme events has improved considerably around the world in different sectors. Also, the development of information systems has led to progress in the design of landslide forecasting systems that through the input rainfall data reflect possible scenarios or situations that have occurred in nature. The high certainty models developed serve as useful tools with which to predict landslide areas where rainfall exceeds the defined threshold and as a warning system for the population against the increased probability of the occurrence of landslides.

In Slovenia, the system for landslide prediction was developed in 2013 for the whole of the country in the frame of the MASPREM project, financed by the Administration of the Republic Slovenia for Civil Protection and Disaster Relief (ACPDR) and the Ministry of Defense (Komac et al. 2013, Komac et al. 2014, Šinigoj et al. 2015, Jemec Auflič et al. 2016). The operational system that was designed is based on real-time rainfall data, rainfall threshold values and a landslide susceptibility map. The landslide forecasting system developed informs inhabitants and responsible authorities of any increased probability of landslide occurrence as a consequence of heavy precipitation that exceeds the landslide triggering values. At the moment, MASPREM predicts landslide probability at a national scale (1: 250,000) and at the local level (1: 25,000) for five selected municipalities where the potential exposure of inhabitants, buildings and different types of infrastructures is displayed, twice daily for both for the 24 hours following. The system is now in the validation phase, which presents the important task of demonstrating that the model reasonably represents actual conditions in nature. The quality and reliability of each model should be properly verified to satisfy analysis objectives. When a rainfall-induced landslide is reported the reliability of the prediction models is evaluated.

This contribution focuses on the main conceptual and technological challenges faced in the design, implementation, and daily operation of MASPREM. Several typical elements of an operational landslide forecasting system are considered, including: (i) observation parameters (better quality of input parameters), (ii) methods for defining rainfall thresholds, (iii) quality of the rainfall information used for operational forecasting, (iv) optimal system architecture used to calculate complex data, (v) validation and (vi) communication to end users.

Quality of input parameters

Landslide susceptibility map

Landslides in Slovenia occur in almost all parts of the country. Based on the extensive landslide database that has been compiled and standardized at a national level, and based on analyses of landslide spatial occurrences in relation to the spatio-temporal precondition factors (lithology, slope inclination, slope curvature, slope aspect,

distance to geological boundaries, distance to structural elements, distance to surface waters, flow length, and land-cover type), a landslide susceptibility map of Slovenia at scale 1:250,000 was produced (Komac and Ribičič 2006). The map was updated in 2011 using the new landslide database and marginally adjusted weights in the linear weighted model for spatio-temporal precondition factors (Tab. 1).

Table 1 Different weights of spatio-temporal precondition factors in the linear weighted models.

Spatio-temporal precondition factors	LSM 2006	LSM 2011
Lithology	0.33	0.30
Slope inclination	0.23	0.25
Type of land cover	0.27	0.25
Slope curvature	0.08	0.10
Slope aspects	0.05	0.05
Distance to structural elements	0.05	0.05

Precipitation forecasting model

The ALADIN system has been used in Slovenia as an operational weather forecast system since 1997 (Pristov et al. 2012). A regional ALADIN model for Slovenia predicts the status of the atmosphere over the area of Slovenia up to 72 h ahead. The model simulates the precipitation (kg/m^2), snowfall, water in snow pack, and air temperature data. ALADIN/SI is a grid point model where the horizontal distance between the grid points is 4.4 km and which runs in a 6-h cycling mode for the next 54 h by the Environmental Agency of the Republic of Slovenia (ARSO 2017).

Landslide triggering rainfall threshold values

Due to the sparse density of the rain gauge networks in Slovenia (1 rainfall gauge per 460 km^2) and the related uncertainty, the rainfall threshold values (RT1) have been defined using the non-parametric statistical method chi-square ($\chi 2$) for each lithological unit. In this order we separately cross-analysed the occurrence of landslides within each unique class derived from the spatially cross-analysis of lithological units and classes of 24-hour maximum rainfall. Maximum daily rainfall above 100 mm proved to be critical for landslide occurrence, especially in looser soils and in less resistant rocks (e.g., Quaternary, Tertiary, Triassic, and Permo-Carbonian rocks). According to the past analyses (Jemec and Komac 2013; Rosi et al. 2016) the RT1 is slightly corrected such that some lithological units have lower rainfall thresholds as shown by statistical approach (Tab. 2). This is due to the significant number of landslides in the last 10 years (annual technical reports and bulletins, ACPDR) that have not been registered in the landslide database owing to imprecise information on their location.

Table 2 Landslide triggering rainfall threshold values for each litostratigraphic unit (RT1-statistical defined; RT2-corrected in accordance to annual landslide reports). Critical 24-h rainfall intensities are presented only for litostratigraphic units for which the number of observed landslides was statistically higher than the number of expected landslides.

Lithostratigraphic unit	RT1	RT2
predominantly clay soils	-	-
marsh and lake sediments (clay, silt, peat)	-	-
alluvium, fluvial loose sediments in terraces	-	-
clayey – diluvial, proluvial	90 - 120	60 - 90
gravely with a clayey component	150 - 180	150 - 180
gravely (predominantly thick fraction), moraines	210 - 240	210 - 240
clayey	90 - 120	60 - 90
alternation of fine and coarse grain soils	90 - 120	60 - 90
pebbly	90 - 120	60 - 90
mine tailings – gangues	120 - 150	120 - 150
clayey, marly rocks	90 - 120	60 - 90
clayey, marly and limestone	90 -120	90 -120
alternation of different materials (marl, sand, sandstone, conglomerate pebble, clay)	90 - 120	60 - 90
conglomerate	90 - 120	90 - 120
(slaty) claystones with inclusion of other rocks	120 - 150	120 - 150
marl and sandstone (flysch) with inclusion of other rocks	210 - 240	150 - 180
sandstones and conglomerates with inclusion of other rocks	120-150	120 - 150
stratified and cliff limestones	-	-
flat limestones	-	-
limestones and dolomites	-	-
dolomites	-	-
limestones with marls	90 - 120	90 - 120
limestones with inclusions of other rocks	210 - 240	210 - 240
limestone conglomerates and breccia	120 - 150	120 - 150
phyllites, schists and slate	180 - 210	180 - 210
amphibolite and gneiss	120 - 150	120 - 150
diabase and other magmatic rocks with tuff	120 - 150	120 - 150
amphibolites, serpentinites, diaphthorites	120 - 150	120 - 150
tonalite, dacite, granodiorite	-	-

Method for defining warning

The prediction model highlights the fuzzy logic that allows a gradual transition between the variables (Krol and Bernard 2012). The precise boundaries of the rainfall threshold over which a landslide always occurs are very difficult to define. In this order, the model considers continuous rainfall threshold values for each engineering geological unit. The minimum threshold defines the lowest level, below which a landslide does not occur. The maximum threshold is defined as the level above which a landslide always occurs (White et al. 1996). Below a certain value the probability of the triggering event is almost nul, while above a certain value the probability of a triggering event is almost certain. Between the two values the probability of triggering increases from 0 to 1, depending on the membership function that defines the transition (Jemec Auflič et al. 2016).

System architecture

The landslide prediction system is a fully-automated system based on open source software (PostgreSQL, PostGIS, Java) and web applications for displaying the results (MapServer, OpenLayers). First ALADIN/SI and INCA models are transferred to the GeoZS server, then the conversion process to raster data starts and stores data in a PostgreSQL database is followed by a calculation of the landslide prediction model. Based on that the WMS service for distribution of data is created and displayed in a web application. When the probability of a landslide occurrence increases, the system automatically sends an email to those responsible for disaster management at ACPDR and to landslide experts at the Geological Survey of Slovenia. Fig. 1 shows a calculation of the landslide prediction model using two days antecedent measured near-real-time rainfall data (INCA) and a prediction rainfall forecast (ALADIN) for the next 24 hours.

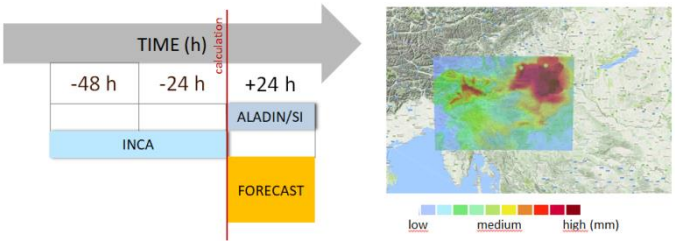

Figure 1 Calculation of the landslide prediction model using two days antecedent measured near-real-time rainfall data (INCA) and a prediction of rainfall forecast (ALADIN) for the next 24 hours.

Validation

In the observed period, from September 2013 to December 2017, the system for calculating landslide prediction triggered an alert on the probability of landslide occurrence in 124 cases. Overall validation of rainfall thresholds is hindered by the lack of information on landslide occurrence and will be completed when representative landslide events are collected. In this paper we highlight the rainfall event that lasted from 25 June to 27 June 2016 with the peak during the night between 26 and 27 June when more than 50 mm of rainfall was recorded in the northern part of the country (Fig. 2). Some 70 landslides were triggered in the two municipalities (Fig. 3).

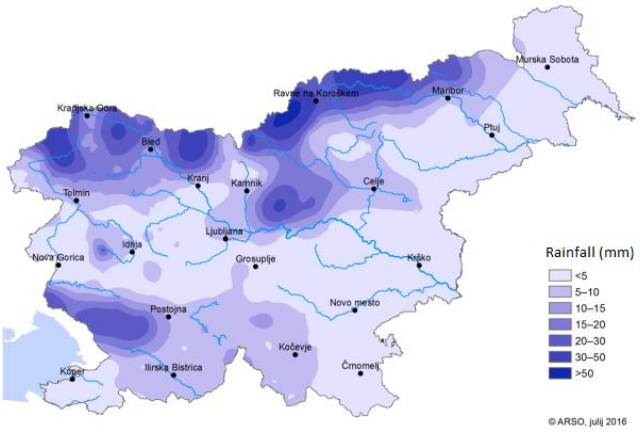

Figure 2 24-hours, amount of rainfall measured on 27 June at 8 am, that was further interpolated based on meteorological stations (ARSO 2017).

Fig. 3 shows landslide prediction models from 25 June afternoon to 27 June 2018 morning using two different rainfall thresholds: (RT1) landslide triggering rainfall threshold values, statistically defined; (RT2) landslide triggering rainfall threshold values, corrected in accordance with the annual landslide reports. Blue dots represent landslide events that were triggered during the night between 26 and 27 June 2016.

Communication to end users

One very important part of a warning system is also the communication plan to end users. In Slovenia, the ACPDR is fully responsible for the task of sending an alert to regional branches that are responsible for further coordination, actions and measures (Official Gazette of the Republic Slovenia, number 51/2006-ZVNDN-UPB1). In the case that a natural or other disaster or other is too extensive, the responsible party is the national centre that also activates occupational units like fire brigades and different rescue teams. In the case of the landslide warning system, ACPDR does not have any systemic procedures for warnings. Since September 2013, when MASPREM became operational, landslide prediction models support the ACPDR. According to the level of prediction (at a national or regional level) experts from the Geological Survey send a warning to the national media by email. These

warnings serve as a general warning to citizens in the particular endangered region with a message that warns people to be careful around visible signs of landslide activity (cracks, subsidence, etc.). All special recommendation and prevention actions are also available on the ACPDR and GeoZS web pages.

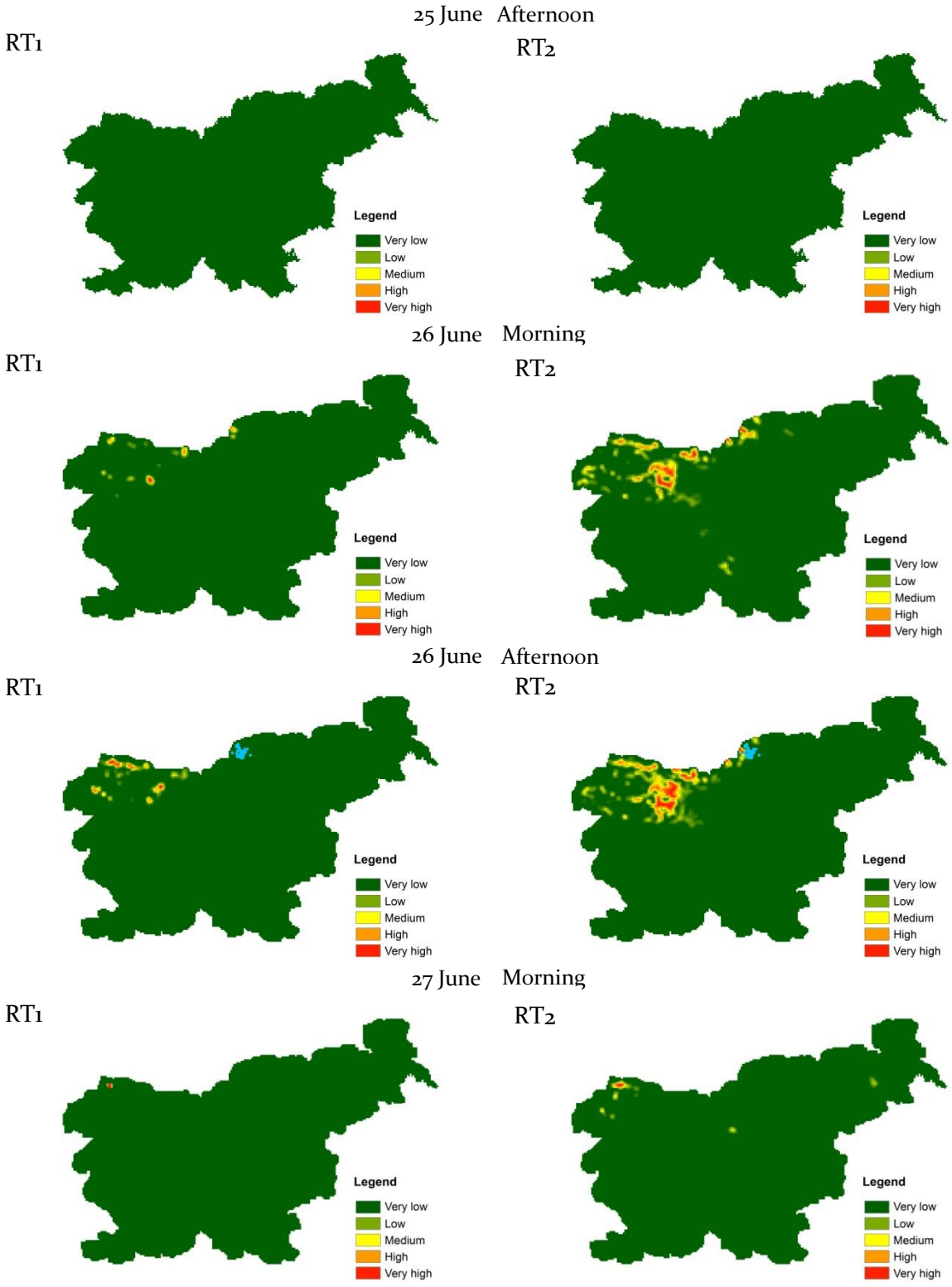

Figure 3 Landslide prediction models from 25 June afternoon to 27 June 2018 morning. RT1- landslide triggering rainfall threshold values, statistically defined; RT2 - landslide triggering rainfall threshold values, corrected in accordance with annual landslide reports. Blue dots represent landslide events that were triggered during the night between 26 and 27 June 2016.

Acknowledgments

The authors would like to thank the Administration for Civil Protection and Disaster Relief and the Ministry of Defense for financing the MASPREM project, and the Slovenian Environment Agency (ARSO) for providing ALADIN-SI and INCA data.

References

ARSO (2017) National Meteorological Service of Slovenia. Ministry for Environment and Spatial Planning, Environmental Agency of the Republic of Slovenia, available on http://meteo.arso.gov.si/met/en/app/webmet/ (19.10.2017).

Haque U, Blum P, da Silva PF et al. (2016) Fatal landslides in Europe. Landslides. 14 (1): 1545-1554.

Jemec Auflič M, Komac M (2013) Rainfall patterns for shallow landsliding in perialpine Slovenia. Natural Hazards. 67(3): 1011-1023.

Jemec Auflič M, Šinigoj J, Krivic M, Podboj M, Peternel T, Komac M (2016) Landslide prediction system for rainfall induced landslides in Slovenia (Masprem) = Sistem opozarjanja na nevarnost prožen-ja zemeljskih plazov v Sloveniji (Masprem). Geologija. 59/2: 259-271.

Komac M, Ribičič M (2006) Landslide susceptibility map of Slovenia at scale 1:250,000. Geologija. 49/2: 295-309.

Komac M, Šinigoj J, Jemec Auflič M (2014) A national warning system for rainfall-induced landslides in Slovenia. In: Sassa K, Canuti P, Yin Y (eds) Landslide science for a safer geoenvironment, 2, Methods of landslide studies. Springer, Cham. pp. 577-582.

Komac M, Šinigoj J, Jemec Auflič M, Čarman M, Krivic M (2013) Landslide hazard forecast in Slovenia - MASPREM. In: Mihalić Arbanas S, Arbanas Ž (eds) Landslide and flood hazard assessment, 1st Regional Symposium on Landslides in the Adriatic Balkan Region with the 3 rd Workshop of the Croatian-Japanese Project "Risk Identification and Land-Use Planning for Disaster Mitigation of Landslides and Floods in Croatia", 6-9 March 2013. Zagreb, Croatia . pp. 225-230.

Krol O, Bernard T (2012) elDeWaS – Online early warning system for landslide detection by means of dynamic weather nowcasts and knowledge based assessment. In: Seppelt Rl, Voinov AA, Lange S, Bankamp D (eds) International Environmental Modelling and Software Society (iEMSs) 2012 International Congress on Environmental Modelling and Software Managing Resources of a Limited Planet: Pathways and Visions under Uncertainty, Sixth Biennial Meeting. Leipzig, Germany. pp. 212-219.

Pristov N, Cedilnik J, Jerman J, Strajnar B (2012) Priprava numerične meteorološke napovedi ALADIN-SI. Vetrnica. pp. 17-23.

Rosi A, Peternel T, Jemec Auflič M, M Komac, S Segoni, N Casagli (2016) Rainfall thresholds for rainfall-induced landslides in Slovenia. Landslides. 13(6): 1571-1577.

Šinigoj J, Jemec Auflič M, Kumelj Š, Krivic M, Požar M, Podboj M, Tukić, M, Peternel T, Prkić N (2015) Nadgradnja sistema za obveščanje in opozarjanje v primeru proženja zemeljskih plazov – Masprem 2: poročilo ob prvem mejniku. Geološki zavod Slovenije, Ljubljana. 42p. (In Slovene)

White ID, Mottershead DN, Harrison SJ (1996) Environmental Systems, 2nd edition. Chapman & Hall, London. 616p.

Observing surface movement patterns of the Potoška planina landslide using geodetic techniques

Tina Peternel[(1)], **Marko Komac**[(2)]

1) Geological Survey of Slovenia, Dimičeva ulica 14, 1000 Ljubljana, Slovenia, tina.peternel@geo-zs.si

2) Marko Komac s.p., independent researcher, Ljubljana, Slovenia

Abstract This paper focuses on the observation of surface movement patterns at the Potoška planina landslide (NW Slovenia), which has the potential to mobilize the material into debris flow. The Potoška planina landslide is located in the Karavanke mountain ridge, above the settlement of Koroška Bela, which lies on the outskirts of the town of Jesenice. In order to observe surface movement patterns it was crucial to set up a flexible and reliable monitoring system to monitor visible surface changes through time and space, including displacement rates and extent, changes in elevation and changes in volume. The monitoring of changes on the surface and observation of surficial displacements can be accomplished using different surveying techniques. In order to estimate the surface movement pattern of the Potoška planina landslide periodic monitoring was performed on the basis of the results of independent surveying techniques: photogrammetry using unmanned aerial vehicles (UAV), terrestrial laser scanning (TLS) and tachymetric measurements. The upper part of the landslide at the main scarp and the part immediately below it are dominated by rockslides and runoff of the scree material. The main body of the landslide is formed by heavily deformed and weathered clastic rocks and is presumed to be a rotational, deep-seated slow-motion slide that has accelerated predominately as the result of percolation of surface and ground water. The toe of the landslide is considered to be the most active part. It is crossed by the Bela torrent and features gully-type morphology. The movement patterns in this part represent a combination of steadily sliding mass towards the torrent gully as well as localised superficial surge slips. Sliding material is moving downslope towards the bottom of the landslide toe, where the material is being fed into the stream.

Keywords surface movement pattern, monitoring, geodetic techniques, Potoška planina, Slovenia

Introduction

The hillslope morphology, unfavourable geological and tectonic conditions as well as climatic diversity all contribute significantly to the high susceptibility of slope mass movements in Slovenia. The Landslide Susceptibility Map (at scale 1:250,000) shows that one-third of Slovenian territory is highly susceptible to landslides, while the Debris Flow Susceptibility Map (at scale 1:250,000) has shown that approximately 15% of Slovenia is highly susceptible to debris flows (Komac et al. 2006; Komac et al. 2009). Consequently, almost one-fifth of Slovenia's population lives in areas that are highly susceptible to slope mass movements (Komac 2012).

This fact underlines the need for more systematic observation and monitoring of landslides in Slovenia, with the ultimate aim of defining prevention measures and reducing the hazards associated with slope mass movements in the future.

In order to recognize and understand the slope mass movements and their dynamics it is crucial to apply an engineering-geological approach. It is also essential to set up a flexible and reliable monitoring system to monitor visible surface changes through time and space, including displacement rates and extent, changes in elevation and changes in volume. Monitoring of changes on the surface and observation of surficial displacements can be accomplished using different surveying techniques.

Recent research on landslide monitoring has demonstrated that remote sensing techniques are commonly used to monitor visible surface changes through time, and can be particularly useful in cases of remote, mountainous and difficult-to-access landslide areas where the installation of more sophisticated in-situ monitoring equipment is difficult or impossible (Oppikofer et al. 2009; Tofani et al. 2013; Raspini et al. 2015, Mihalič Arbanas and Arbanas, 2015). Remote sensing techniques allow the rapid measurement of quantitative surface changes, primary indicators key to understanding the development of landslides and correlations with triggering factors (Rosi et al. 2013; Agostini et al. 2014; Scaioni et al. 2014).

In order to estimate the surface movement pattern of the Potoška planina landslide periodic monitoring was performed on the basis of the results of independent surveying techniques: photogrammetry using unmanned aerial vehicles (UAV), terrestrial laser scanning (TLS) and tachymetric measurements.

Periodic monitoring was performed over a period of 46 months (July 2013–April 2016).

Study area

This research work focuses on the observation of slope

mass movements at the Potoška planina landslide (NW Slovenia), which has the potential to mobilize into debris flow. The Potoška planina landslide is located in the Karavanke mountain ridge, above the settlement of Koroška Bela, which lies on the outskirts of the town of Jesenice (Fig. 1).

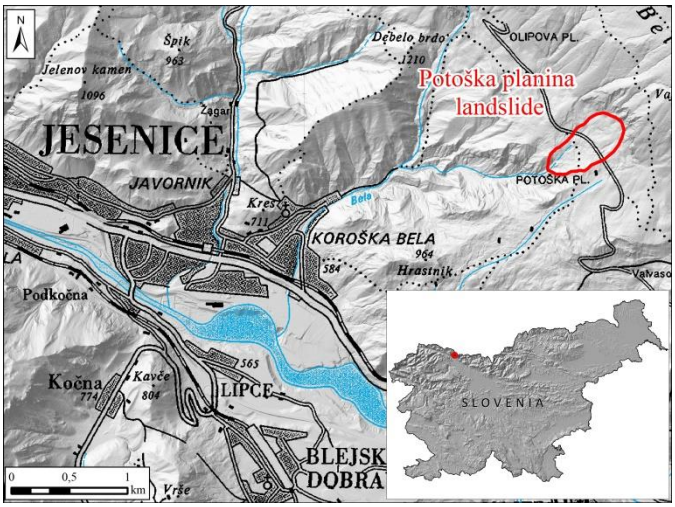

Figure 1 Location of Potoška planina landslide.

The geological and tectonic setting of the wider Potoška planina area is fairly complex. The landslide is situated at the contact between the Upper Carboniferous and Permian clastic rocks, which consists of alternating shale, quartz sandstone and conglomerate; and Upper Triassic to Lower Jurassic carbonate rocks. The contact is represented by a reverse fault dipping approximately 70° to the NE (Jež et al. 2008). In terms of tectonics, the area is part of the Košuta fault zone and is bisected by numerous NW-SE faults linking two major fault zones (the Sava and Periadriatic fault zones) (Jež et al. 2008).

Due to its geological and tectonic features the Potoška planina area is highly prone to different slope mass movements (Peternel et al. 2017; Peternel 2017). The upper part of the landslide at the main scarp and the part immediately below it are dominated by rockslides and runoff of the scree material. The main body of the landslide is formed by heavily deformed and weathered clastic rocks and is presumed to be a rotational, deep-seated slow-motion slide that has accelerated predominately as the result of percolation of surface and ground water (Jež et al. 2008; Komac et al. 2014; Peternel et al. 2017; Peternel 2017). The morphology of this part is characterized by irregular and hummocky terrain comprising protrusions and depressions of various sizes. This activity is evidenced by "pistol butt" trees, erosion slumps and ponds on the surface, as well as the deformation of local roads. Locally, large unstable boulders are present (Peternel et al. 2017; Peternel 2017).

A greater spatial density of springs and wetlands is evident at the contact between scree and clastic rocks, partly supplied by the infiltration. One of the most significant is the Urbas spring (1,275 m.a.s.l) of the Bela torrent that runs through the landslide. Past research (Jež et al. 2008), which focused on the alluvial fan of this torrent, has demonstrated that this torrent periodically (on a geologic scale) produces devastating debris flows.

Methodology

In order to estimate the surface movement pattern of the Potoška planina landslide periodic monitoring was performed on the basis of results of independent surveying techniques: photogrammetry using unmanned aerial vehicles (UAV), terrestrial laser scanning (TLS) and tachymetric measurements. UAV photogrammetry and TLS enabled us to create detailed surface models (DEMs, orthophotos, etc.), while the classic and highly accurate tachymetric measurements using a total station were used to determine accurate displacements of object points and to assess the reliability of the photogrammetric data (Fig. 2). Periodic monitoring was performed over a period of 46 months.

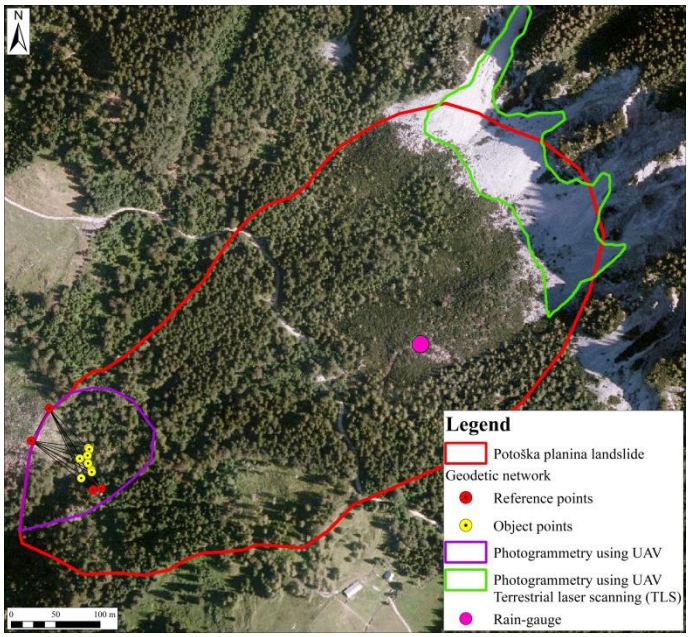

Figure 2 Spatial coverage of used methods.

On the basis of the results obtained from the monitoring system, the following derived data was used:

- accurate displacements of object points;
- orthophotos and
- digital elevation models.

Periodic monitoring (in different time periods) was performed over a period of 46 months. Periodic monitoring enabled:

- determination of surficial displacements,
- comparison of DEMs and elevation and volume changes,
- determination of erosion and accumulation areas,
- estimated transported volumes.

UAV photogrammetry

UAV photogrammetry is a remote sensing platform used to perform photogrammetric surveys and to acquire high-resolution spatial data.

Recently, UAV photogrammetry has become an increasingly popular alternative technique for collecting remote sensing data for landslide monitoring. The key advantage of this method is that it enables high spatial resolution imaging of difficult-to-access or inaccessible areas and is relatively inexpensive. Furthermore, UAV photogrammetry bridges the gap in scale, resolution, and viewing angle between terrestrial observation and satellite sensors (d'Oleire-Oltmanns et al. 2012; Lucieer et al. 2014).

UAV imaging of the monitoring site has been ongoing since July 2013 (Tab. 1). Five acquisitions using UAV photogrammetry were performed from July 2013 through end-September 2014 and are presented in Tab. 1.

Table 1 An overview of UAV acquisitions of lower part of Potoška planina landslide.

UAV photogram.	1st measurement	2nd measurement	3rd measurement	4th measurement	5th measurement	6th measurement	7th measurement
Date	7/2013	10/2013	4/2014	9/2014	5/2015	10/2015	4/2016
Area (m2)	120 x 100	85 x 80	180 x 100	100 x 100	210 x 190	200 x 185	175 x 170
Images	59	27	82	70	155	315	154
Image overlap (%)	> 60	> 60	> 60	> 60	> 60	> 60	> 60
GCPs	8	8	8	9	9	9	10

Tachymetric measurements using total station

In order to assess the reliability of the photogrammetrically assessed displacements it is essential to compare resulting surfaces and displacements with existing reference measurements (Stumpf et al. 2013). In order to verify displacement vectors that were obtained using UAV photogrammetry and to determine the absolute displacements of the monitoring site, classic tachymetric geodetic measurements using a Leica TC803 power (R400) theodolite were performed simultaneously with the UAV data acquisitions.

The geodetic network was established in November 2012, and all further measurements were conducted simultaneously with the UAV acquisitions. The network initially consisted of ten object points (1-10), which were largely located in the upper part of the monitoring site owing to the extremely difficult access to the lower part. Three reflecting prisms were installed on steel rods and seven prisms were installed on boulders.

Terrestrial laser scanning (TLS)

Additionally, in order to obtain reliable extent and to understand the dynamics of the landslide it was also necessary to perform periodical monitoring in the main scarp of the Potoška planina landslide. The main scarp has been formed in the scree below a very steep slope of limestone, and covers an area of 270 x 170 m. The main scarp consists of a large amount of talus material that is highly prone to instability and represents the source area of the sliding mass. Owing to the extent of the main scarp, the configuration of the site and the surface conditions, and with aim of determining near-real time reliable superficial displacement rates and changes in the surface topography including analysis of the discontinuity sets and fold axes, scanning of the main scarp of the Potoška planina landslide have been performed using a terrestrial laser scanner (TLS) in different acquisition periods.

The geodetic network, consisting of nine points stabilized in the solid rock, was established around the major scarp to provide uniform georeferencing of the point clouds from different periods. The coordinates of all points in the network were measured with a tachymeter. In order to determine the coordinates in the national coordinate system, four points were measured with GNSS. So far, two data acquisitions using TLS technology were performed in June 2014 and June 2015.

Results

In order to determine a movement pattern for the lower part of Potoška planina landslide over the entire monitoring period (from July 2013 to April 2016) the cumulative displacements (Fig. 3) were calculated, and average elevation and volume differences (Fig. 4) for the (same) monitoring period were estimated.

The surface displacement pattern for the entire monitoring period of 33 months (July 2013 to April 2016) were analysed based on the sum of the displacement vectors for all observation periods. The assessed displacements over the 33-month monitoring period ranged from 1.2 to 19.0 m with a significant SW directional orientation.

In order to estimate average erosion and accumulation rates for the sliding material at the main scarp over the entire monitoring period, elevation changes were observed between the DEM of July 2013 and the DEM of April 2016 (Fig. 5). An area of 1130 m^2 (approximately 57% of the analysed area) was identified as the zone of greatest decrease, with an average increase of 0.5 m and a maximum of 1.5 m. Conversely, an area of 732 m^2 (~37% of the analysed area) was characterized by an increase in

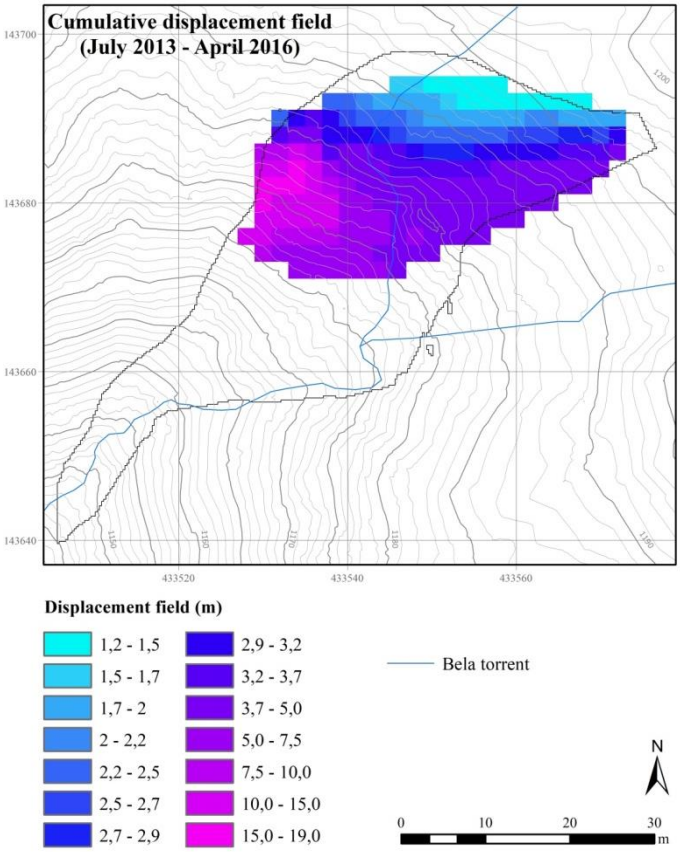

Figure 3 Cumulative displacement of lower part of Potoška planina landslide for the observation period July 2013 – April 2016.

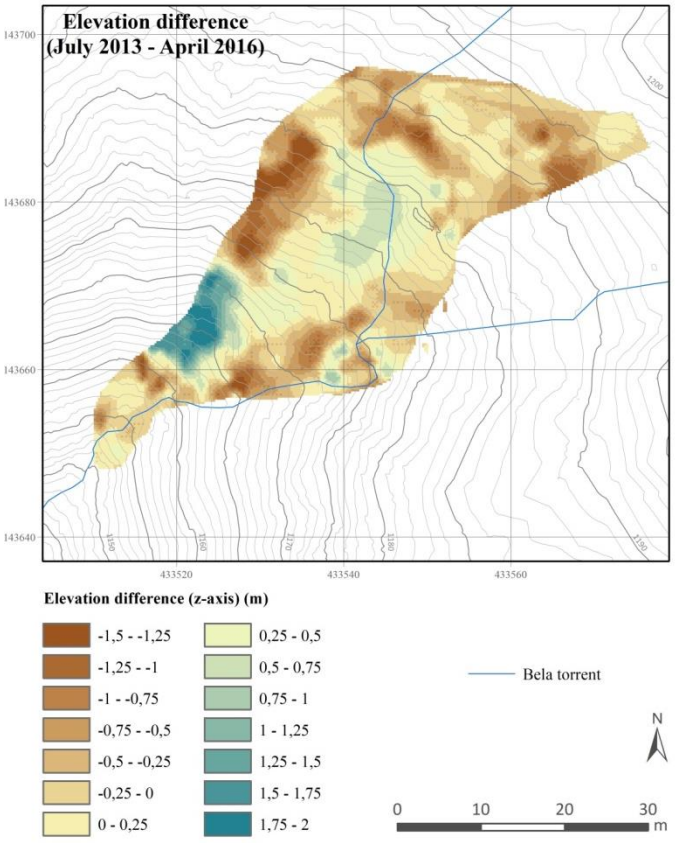

Figure 4 Elevation difference (z-axis) of the lower part of the Potoška planina landslide obtained by subtracting the DEM values (April 2016 and July 2013).

height, where an average of 0.5 m of mate-rial accumulated, with some areas peaking at an increase of up to 2.0 m. No elevation changes were detected with-in the area of 107 m² (~6% of the analysed area). The estimated volume loss for the entire monitoring period is approximately 308 m³; meanwhile the volume gained was estimated at 273 m³.

The difference in change between the DEMs of July 2013 and April 2016 shows that approximately 561 m³ of material was transported over a period of 33 months. The comparison shows dominant erosion in the central part of the analysed area.

Additionally, a comparison of DEMs obtained by TLS was used to evaluate surface changes and estimate transported volumes at the main scarp of the Potoška planina landslide.

The comparison showed that the total area of ablation within the study site was approximately 19.000 m² (~15% of analysed area), while the total area of accumulation was 4.000 m² (~85% of study site) (Fig. 5).

From Fig. 5 it can be seen that the dominant ablation occurred in the middle part of the study area; meanwhile sediment accumulation was observed at the foot zones. The volume of the eroded surface material was estimated at approx. 2000 m³, while accumulated material was estimated at approximately 400 m³.

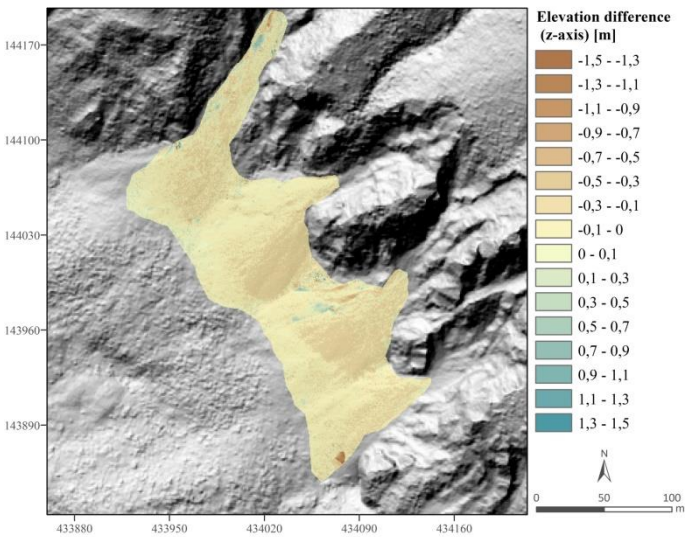

Figure 5 Elevation difference (z-axis) at the main scarp of the Potoška planina landslide obtained by subtracting the DEM values (July 2014 and July 2015).

Conclusions

Historical sources and previous investigations describe the broader area of the Potoška planina landslide as known to have experienced severe debris-flow events in the recent geological past. The most recent of these events occurred in the 18th century, and caused the partial or total destruction of more than 40 buildings and cultivated areas in a village down-slope (Koroška Bela) located in the area of the alluvial fan. Presently, some 2,200 inhabitants live in the alluvial fan area of past debris flows. With this risk potential in mind, monitoring of the sliding mass and assessment of the displaced material volumes is even more important than the purely scientific value of any assessment efforts.

In order to recognize and understand the slope mass movements and their dynamics it was crucial to set up a flexible and reliable monitoring system to monitor visible surface changes through time and space, including displacement rates and extent, and changes in elevation and volume. Monitoring of changes on the surface and observation of surficial displacements can be accomplished using different surveying techniques.

In order to estimate the surface movement pattern of the Potoška planina landslide periodic monitoring was performed on the basis of the results of independent surveying techniques: photogrammetry using unmanned aerial vehicles (UAV), terrestrial laser scanning (TLS) and tachymetric measurements. Periodic monitoring was performed over a period of 46 months.

Based on our results, we can conclude that current available modelling data, such as displacement rates, assessments of elevation changes and estimated transported volumes all contribute significantly to a better understanding of the behaviour and dynamics of the Potoška planina landslide.

References

Agostini A, Tofani V, Nolesin, T, Gigli G, Tanteri L, Rosi A, Cardellini S, Casagli N (2014) A new appraisal of the Ancona landslide based on geotechnical investigations and stability modelling. Quarterly journal of engineering geology and hydrogeology. 47(1): 29-43.

D'Oleire-Oltmanns S, Marzolff I, Klaus DP, Ries BJ (2012) Unmanned Aerial Vehicle (UAV) for Monitoring Soil Erosion in Morocco. Remote Sensing. 4: 3390–3416.

Jež J, Mikoš M, Trajanova M, Kumelj Š, Budkovič T, Bavec M (2008) Koroška Bela alluvial fan – The result of the catastrophic slope events (Karavnke Mountains, NW Slovenia). Geologija. 51(2): 219–227.

Komac M, Ribičič M (2006) Landslide susceptibility map of Slovenia at scale 1:250,000. Geologija. 49(2): 295–309.

Komac M, Kumelj Š, Ribičič M (2009) Debris-flow susceptibility model of Slovenia at scale 1: 250,000. Geologija. 52(1): 87–104.

Komac M. (2012) Regional landslide susceptibility model using the Monte Carlo approach – the case of Slovenia. Geological Quarterly. 56(1): 41–54.

Komac M, Holly R, Mahapatra P, Van der Marel H, Bavec M (2014) Coupling of GPS/GNSS and radar interferometric data for a 3D surface displacement monitoring of landslides. Landslides. 12(2): 241 – 257.

Lucieer A, De Jong SM, Turner D (2014) Mapping landslide displacements using Structure from Motion(SfM) and image correlation of multi-temporal UAV photography. Progress in Physical Geography. 38(1): 97–116.

Mihalić Arbanas S, Arbanas Ž (2015) Landslides: A Guide to Researching Landslide Phenomena and Processes: In: Gaurina-Međimurac N (ed) Handbook of Research on Advancements in Environmental Engineering. Hershey : IGI Global. pp. 474–510.

Oppikofer T, Jaboyedoff M, Blikra L, Derron MH, Metzger R (2009) Characterization and monitoring of the Aknes rockslide using terrestrial laser scanning. Natural Hazards and Earth System Sciences. 9: 1003–1019.

Peternel T (2017) Dynamics of the slope mass movements in the Potoška planina with analyses of results of remote sensing and terrestric surveys techniques and in-situ measurements. PhD thesis, University of Ljubljana, Ljubljana, Slovenia. 183p.

Peternel T, Kumelj Š, Oštir K, Komac M (2017) Monitoring the Potoška planina landslide (NW Slovenia) using UAV photogrammetry and tachymetric measurements. Landslides. 14(1): 395–406.

Raspini F, Ciampalini A, Del Conte S, Lombardi L, Nocentini M, Gigli G, Ferretti A, Casagli N (2015) Exploitation of Amplitude and Phase of Satellite SAR Images for Landslide Mapping: The Case of Montescaglioso (South Italy). Remote Sensing. 7: 14576–14596.

Rosi A, Vannocci P, Tofani V, Gigli G, Casagli N (2013) Landslide Characterization Using Satellite Interferometry (PSI), Geotechnical Investigations and Numerical Modelling: The Case Study of Ricasoli Village (Italy). International Journal of Geosciences. 4: 904–918.

Scaioni M, Longoni L, Melillo V, Papini M (2014) Remote Sensing for Landslide Investigations: An Overview of Recent Achievements and Perspectives. Remote Sens. (DOI: 10.3390/rs60x000x).

Stumpf A, Malet JP, Kerle N, Niethammer U, Rothmund, S (2013) Image-based mapping of surface fissures for the investigation of landslide dynamics. Geomorphology. 186: 12–27.

Tofani V, Raspini F, Catani F, Casagli N (2013) Persistent Scatterer Interferometry (PSI) Technique for Landslide Characterization and Monitoring. Remote Sensing. 5(3): 1045-1065.

Rockfall monitoring and simulation on a rock slope near Ljig in Serbia

Miloš Marjanović[(1)], Biljana Abolmasov[(1)], Marko Pejić[(2)], Snežana Bogdanović[(1)], Mileva Samardžić-Petrović[(1)]

1) University of Belgrade, Faculty of Mining and Geology, Đušina 7, 11000 Belgrade, Serbia, milos.marjanovic@rgf.bg.ac.rs

2) University of Belgrade, Faculty of Civil Engineering, Belgrade, Serbia

Abstract This paper addresses a rock slope on the M-22 road, one of the main regional corridors in Serbia. One of the critical points on the road is a medium-sized rock slope located near the town of Ljig. It is composed of a flysch complex dominated by a brittle and compact sandstone, interlayered by laminae of less-competent, ductile marly-shales. Rockfalls on this slope are mainly represented by larger sandstone blocks, as well as weathered, crumbly crust atop the uppermost sandstone layers. These source areas were precisely identified over the course of a 5-year process of slope monitoring based on terrestrial LiDAR scanning. However, the runouts and accumulation zone were never precisely determined. To this end, typical back-analysis is herein performed. Firstly, the source areas were analysed by comparing point-clouds of the first and the latest scanning epoch. Four main source areas were identified and adopted for the model. Secondly, potential rockfall block sizes and shapes were adopted based on the measurements over the first epoch point-cloud. Subsequently, some mechanical and physical properties of the rock were determined. These three steps included known and documented facts related to the present rock slope. The last step was to simulate the most probable trajectories in order to obtain runout distances and possible threats to the road asset. The results show that source area No. 4 is potentially the most critical, because its runouts can reach the road infrastructure. Simultaneously, the kinetic energy, componential velocities and forces of falling blocks were simulated. The calculations showed that rockfalls could be easily controlled, as none of the trajectories resulted in energies or forces that would be too much for standard structural remediation measures.

Keywords rockfall, LiDAR, Monitoring, simulation

Introduction

The highest road categories in Serbia's road network are labelled class I state roads. These are further divided into IA – motorways, and IB state roads. The M-22 road (marked as IB22 according to the most recent categorization) is the most heavily trafficked among the IB-class roads. It stretches meridianally, about 300 km, from Belgrade to the border with Montenegro (Fig. 1). Its southernmost part passes through the Ibar River valley, hence the colloquial name "the Ibar Highway". The average daily traffic volume is approximately 10,000 vehicles/day, composed of 85% passenger vehicles, 13% heavy-duty vehicles, and 2% public transport shuttles (http://www.putevi-srbije.rs, accessed 25.5.2017). This transit corridor is also notorious for its high rate of traffic accidents, one of the highest in the country. According to the national automobile and motorcycle association, four accident blackspots mark the M-22. It is a strategically important route, as it connects the state capital with several larger cities: Lazarevac, Ljig, Gornji Milanovac, Čačak, Kraljevo, Raška, and Novi Pazar. It is also part of European routes E763, E761, E65, and E E80.

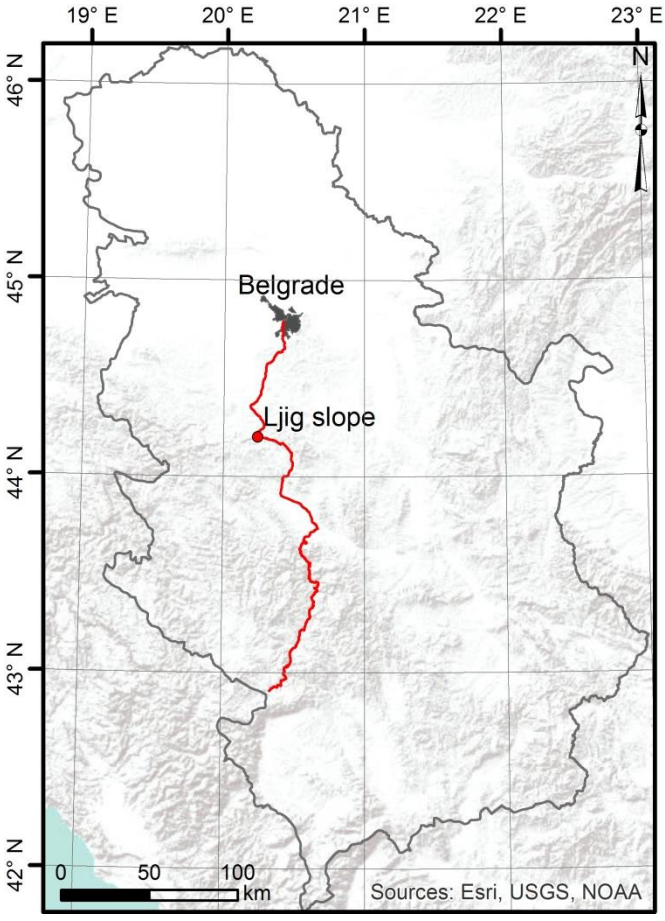

Figure 1 Location of area of interest along the M-22 road.

The location of interest is located along the M-22 highway, some 5 km to the south of the town of Ljig. It is a medium-sized rock slope, about 30 m in height and 60 m long, with average slope of 30–40° (Fig. 2).

Several structural elements were distinguished, including one set of stratification discontinuities *ss* (orientation 39/44°) and two conjugated joint sets (orientation 187/62° and 148/79°). Kinematic analysis showed a potential for

Figure 2 Panoramic view of the rock slope of interest near Ljig (approximate dimensions 60x30m), brighter light-grey parties are sand-stone strata, while less competent parties are dark-greyed (photo B. Abolmasov).

Historically, it is a road cut that was designed in the 1970s during the re-routing of an earlier road that was built close to the local riverbed and having suffered considerable damage and interruptions due to flooding. The new road was built on higher ground but required cutting into the hillside. Opening this rock face resulted in intensive weathering and deformations related to stress release, thereby allowing for the relatively vivid dynamics of the rock face. However, the volume and runout distances of the fallen rock are anticipated, and do not pose an imminent threat to the road. The slope is therefore left open without any remedial measures.

In the present research, key rockfall elements (block volumes and their trajectory runouts) were finally quantified for this rock slope, which has only been estimated thus far. Quantification was targeted at verifying whether there was still a need for some remedial measures.

Previous research

The slope was identified as a typical succession of Cretaceous flysch formation, represented by thick sandstone strata (fine-grained, with carbonate cementing), interlayered with thin laminae of less-competent, ductile marly-shales (Marjanović et al. 2015). It was systematically monitored for roughly 5 years using the terrestrial LiDAR scanning technique. First, its kinematic potential and joint distribution were analysed (Marjanović et al. 2015).

block and wedge failures along the joint planes, while stratification acts as a stabilizing element (daylighting into the rock mass). Basic geometric elements were estimated by calculating average spacing and joint density per each discontinuity set (Bogdanović et al. 2014). Further on, the slope was monitored for rockfalls using consecutive LiDAR scanning (Bogdanović et al. 2015), wherein several detachment zones were distinguished. These zones, slightly modified, were used in this research as rockfall source inputs. Volumes of detached blocks were also estimated, but accumulation zones could not be determined by LiDAR scanning, because the road maintenance authority removes the surface accumulated debris from the slope foot immediately after a rockfall event.

Finally, some basic mechanical parameters were determined using uniaxial testing. The emphasis was on the most competent rocks, i.e. sandstone, which were sampled along the lower parts of the slope. Peak compressive strength was determined at around 80-100 MPa, while tensile strength was around 30-40 MPa. Strength parameters c and φ were 34 MPa and 30°, respectively. Bulk density was 25 kN/m^3. These are yet unpublished lab reports performed before this research. It is also interesting to mention that these are relatively fresh parties of flysch formations. Their equivalents in the location of the nearby tunnel, which is under construction (2016–), are far more weathered and looser, with much weaker mechanical properties.

Methodology

Monitoring rockfall sources

LiDAR scanning was performed using a Leica Scan Station (model P20, target resolution up to 2 mm at 100 m, range up to 120 m, point positioning accuracy 3mm at 50m distance, scan rate up to 1M points/s) in several consecutive epochs. All epochs over the course of 2013–2017 were taken every year in early spring, before the vegetation begins to appear. Given the slope width, 4 ground stations were necessary (view-angles were optimized according to the target slope features to minimize the shadowing effect). This resulted in 4 sub-clouds, which were then registered together into a single point-cloud and reduced to 5 cm resolution. Such point-clouds were created for every epoch. For this research, only the first (2013) and last (2017) epochs were used to map the biggest changes between the two point-clouds, thereby revealing the source areas of the rockfalls. Both point-clouds were automatically cleaned of any vegetation and other screening objects (vehicles and figurants during the scanning) by using the CANUPO filtering plugin tool (Brodu and Lague 2012). Finally, prepared point-clouds for 2013 and 2017 were compared using the Cloud to Cloud Distance tool. All processing was done in the open-source software Cloud Compare 2.8.

Rock properties

Rock properties were determined using 12 standard cylindrical samples for uniaxial rock strength testing (Bieniawski and Bernede 2007), in the ToniNORM modular system with a 2000kN pressure rig. Rock blocks were first taken from the field, within a single sandstone layer at 2 different locations in the accessible part of the slope. A total of 3 samples for each block were cored from these blocks for the Unconfined Compressive Strength test, and an additional 3 for the Brazilian test. Samples were measured for their dimensions and weights. By averaging results from multiple samples at two different sampling points, strength parameters c (cohesion) and φ (friction angle) were determined analytically, as was bulk density. Therein, Coulomb-Mohr's failure criteria (Equation 1: τ is the shear strength, and σ the normal stress), and the Brazilian test correction (Equation 2: F is the failure force, R is the sample diameter, and h its height) were adopted. Final true unconfined tensile strength value was determined analytically (Equation 3). This true value was required to establish fragmentation criteria. These sandstones might be prone to fragmentation owing to their natural fracturing into blocks by three main joint sets.

$$\tau = c + \sigma \tan\varphi \qquad [1]$$

$$\sigma_1 = \frac{6 \cdot F}{\pi \cdot R \cdot h}; \quad \sigma_3 = -\frac{2 \cdot F}{\pi \cdot R \cdot h} \qquad [2]$$

$$\sigma_t = \frac{2c \cdot \cos\varphi}{1 + \sin\varphi} \qquad [3]$$

Trajectory simulation

Simulation of rockfall trajectories was required to input previously acquired bulk density, Digital Terrain Model (DTM) and target block size. The latter was achieved by measuring blocks from the 2013-point-cloud, but was missing in 2017-point-cloud (directly in Cloud Compare software), while DTM was generated by converting the point-cloud data into a raster model, and resampled to 30-cm resolution, which was more convenient for running simulations yet sufficiently detailed. Simulations were performed in RAMSS Rockfall software (Christen et al. 2012), based on the physics of a rigid body with hard unilateral constraints. The software generates trajectories as sets of XYZ points at each desired time interval of the rockfall. In addition it generates numerous kinetic and dynamic parameters at each of these trajectory points (componential velocities; total, potential and kinetic energy; and their translational and rotational components, normal and tangential forces, jump heights, etc.). Although the original software does not offer the option to simulate rock fragmentation, the option to examine a trajectory at any desired moment was used to check if the fragmentation criterion was met at any point along the trajectory. Given the block size, i.e. its cross-section surface, the criterion was such that a normal force at a given point divided by the block cross-section area has to overcome at least the tensile strength of the rock (previously calculated) to fragment the rock block and split it in half.

All these analyses allowed a reconstruction of the rockfall that took place sometime in 2013-17, including identification of their critical runouts and critical points along each trajectory that might require remediation measures.

Results

Four major source areas were identified by computing cloud to cloud difference (Fig. 3a-b). The depletion zones mainly involve larger sandstone blocks (source area 1, 3, and 4), as well as weathered, crumbly crust atop the uppermost sandstone layers (source area 2). Source area 3 has the highest position on the slope (around 20 m above the road level), while 1 and 2 are at approximately similar elevations. The last source area is the lowest, at ~10 m of relative elevation difference to the road level. This is a good proxy to anticipate which source areas are going to be the most critical, given that the average slope is the same across the entire rock face, and equals about 35°. Logically, the highest source area (3) will provide the longest trajectories and runouts, with the largest energies and forces.

Block volumes are defined by the spacing of the corresponding discontinuity sets (stratification ss, and two

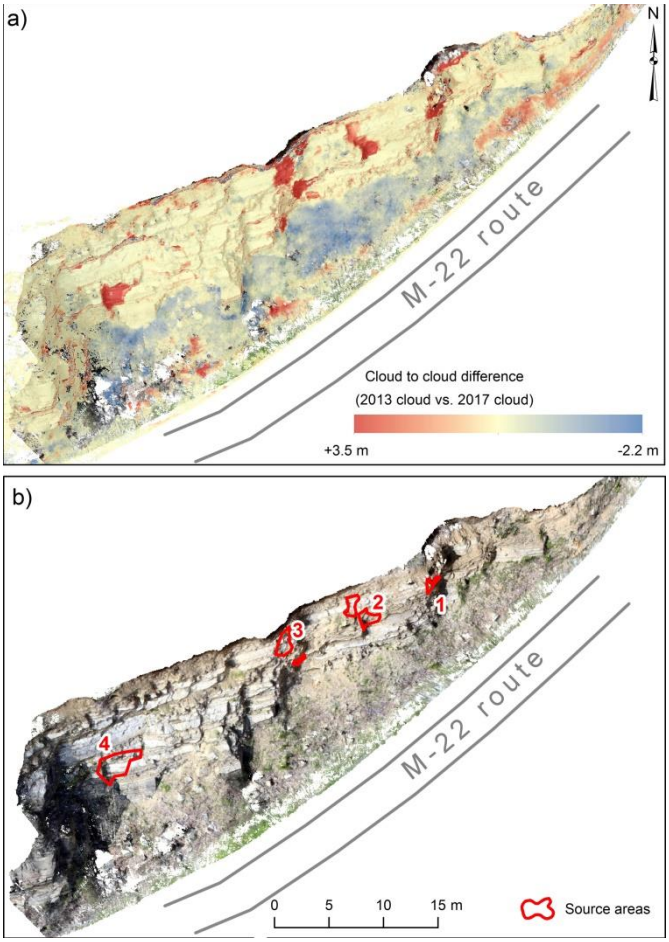

Figure 3 Top view of the rock slope: a) Difference between the 2013 and 2017 point-clouds, delineating missing volume (positive values) in red and accumulated material (negative values) in blue; b) identified source areas of rock fall depletion zones (numbered 1-4). Scale is the same in a and b.

Table 1 Averaged spacing per each source area (sandstone).

Source area	*ss* spacing [m]	Joint set 1 spacing [m]	Joint set 2 spacing [m]
1	0.30	0.30	0.50
2	0.40	0.30	0.50
3	0.65	0.60	0.50
4	0.70	0.70	0.60
av. block size	0.50	0.50	0.50

conjugated joint sets). These spacing values were measured on the point clouds, averaged to obtain a general block size and shape, and input into simulations. Tab. 1 depicts these spacing values, and based on their averages a block size of 0.5 x 0.5 x 0.5 m was adopted with an apparent cuboid shape. The cross-section area for first-order fragmentation (splitting the original cuboid block into two equal prismatic blocks) criterion was practically related to the normal forces over the 0.5 x 0.5 m area (0.25 m^2). According to this criterion, these should exceed 40 MPa of tensile strength (Equation 3) to induce block fragmentation. The simulated trajectories indicate the highest potential for adverse rockfall influence on the road for source area 3 (Fig. 4-5). It has the largest runouts and highest energies along the trajectory (parts of trajectories are indicated in red). For this reason source area 3 was examined in greater detail. Source area 1 trajectories ex-tend very close to the road but the velocities and energies of these blocks quickly drop after the first contact of the depleted rock block. It can be assumed that existing de-tritus and the road's drainage system are sufficient to neutralize their effects. The remaining two areas (2 and 4) do not pose a threat.

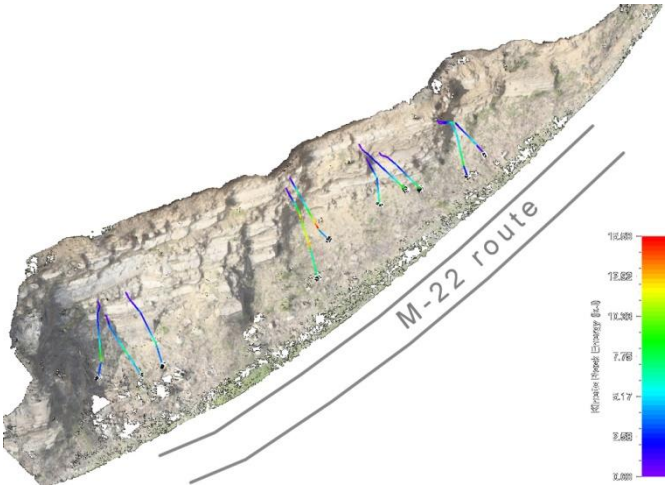

Figure 4 Top view of the rock slope with projected trajectories from all 4 source areas (trajectory paths are coloured according to their kinetic energy). Same scale as in Fig.3.

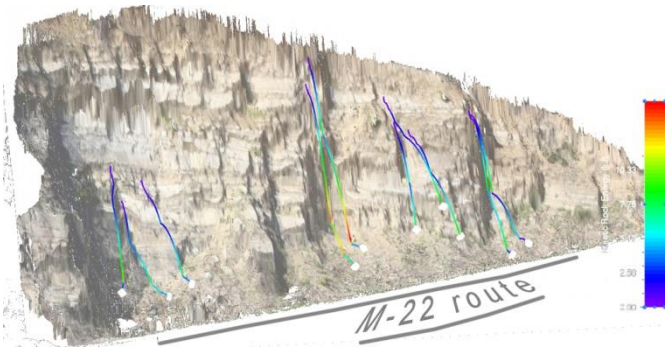

Figure 5 Oblique view of the rock slope with projected trajectories from all 4 source areas (trajectory paths are coloured according to their kinetic energy).

Detailed analysis of the source area 3 included more simulations with more initial positions of the cuboid rock block (4 instead of 1 initial position). As a result, various geometric settings were examined. The simulation (Fig. 6) shows that there are 4 critical trajectories. Their maximal kinetic energy amounts to some 10 kJ, which is easily handled by a number of remediation measures, such as road nets, barriers, or simple solutions like side trenches. The critical trajectories were also examined for their potential fragmentation. If fragmentation is likely, then the given simulation needs to be extended and the danger po-

sed to the road further examined. It is likely that the fragmented block would have longer runout than the non-fragmented parent block. However, before they come to a standstill, fragments will exert smaller forces and energies than would their parent blocks. The simulations showed that the impact forces of these 4 critical trajectories were no larger than 60 kN (given the area of 0.25 m^2, with normal stress of around 0.2 MPa), which is insufficient to overcome the approximated tensile strength of 30–40 MPa.

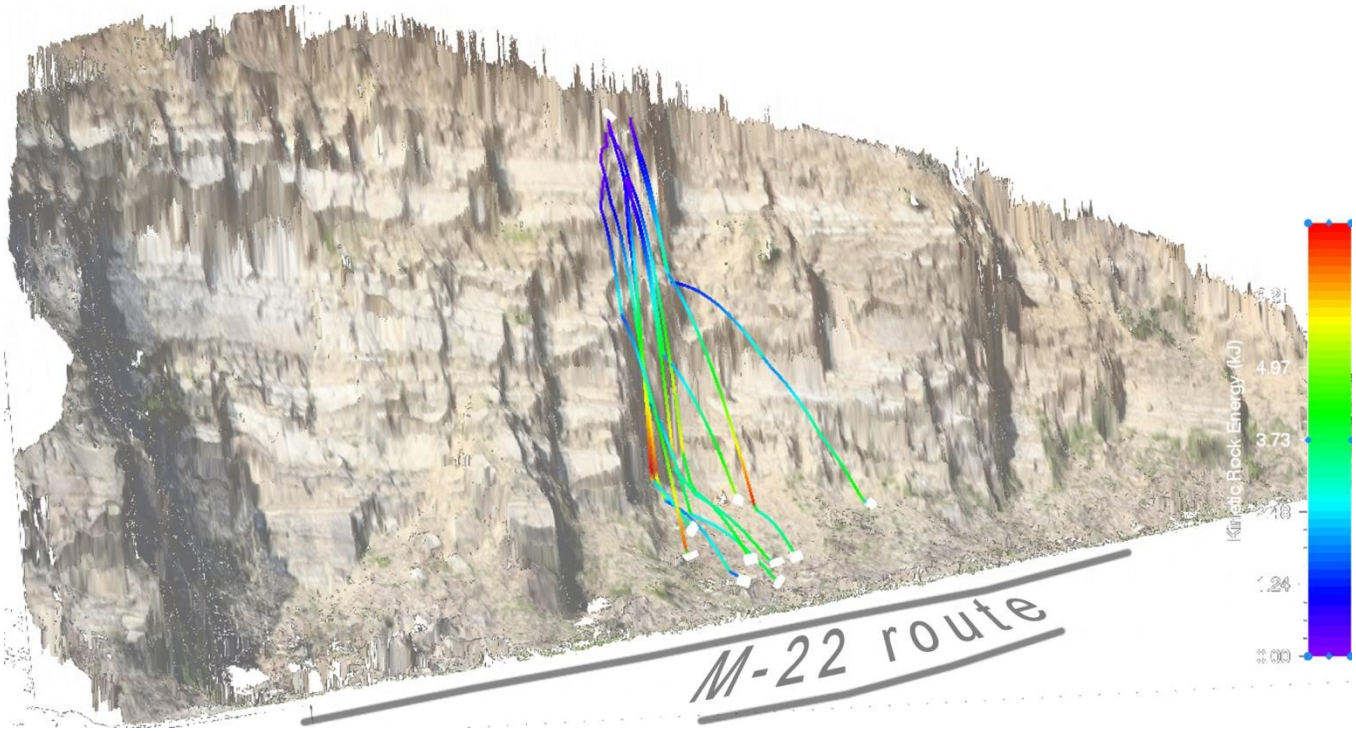

Figure 6 Oblique view of the rock slope with projected trajectories from source area 3 (trajectory paths are colour-scaled).

Conclusions

This article examines the application of LiDAR data on rock slope analyses in combination with some conventional mechanical rock testing. First it exploits the possibilities of identifying the critical depletion zones of the rockfalls by analyzing the point-clouds from different monitoring epochs. These are further used as the source areas for simulations of rockfall trajectories. Rock block sizes and shapes are also determined on the basis of the LiDAR point-cloud data.

The results indicate that the highest source area is the most critical in terms of energy balance along the trajectory and the trajectory runout distance. However, most of the simulated blocks come to a standstill far before the road infrastructure zone. It is also apparent that the velocities, energies and forces generated along the trajectories are low, and can be easily managed using a number of remedial measures. Some simple and economical solutions include the use of road nets and side trenches, which if properly maintained can serve as a long-term solution for this rock slope.

Acknowledgments

This research was supported by the project of the Ministry of Science and Technological Development of the Republic of Serbia No. TR36009. The authors would like to thank Daniel Bohnsack and Carola Wieser from TUM for their assistance with laboratory tests.

References

Bieniawski ZT, Bernede MJ (2007) Suggested methods for determining the uniaxial compressive strength and deformability of rock materials. In: Ulusay R, Hudson JA (eds) The complete ISRM suggested methods for rock characterization, testing and monitoring 1974–2006. ISRM Turkish National Group, Ankara, Turkey. (ISBN: 978-975-93675-4-1). pp. 151–156.

Bogdanović S, Marjanović M, Abolmasov B, Đurić U, Basarić I (2015) Rockfall Monitoring Based on Surface Models. In: Růžičková K, Inspektor T (eds) Surface Models for Geosciences. Springer International Publishing. pp. 37-44.

Bogdanović S, Marjanović M, Abolmasov B, Đurić U, Pejić M (2014) Applying terrestrial laser scanning in geotechnical engineering. Proceedings of the 4th Symposium of Macedonian Association for Geotechnics, 25-28 June 2014. Struga, FYR of Macedonia. pp. 337-342.

Brodu N, Lague D (2012) 3D Terrestrial LiDAR data classification of complex natural scenes using a multi-scale dimensionality criterion: applications in geomorphology. ISPRS journal of Photogrammmetry and Remote Sensing. 68: 121-134.

Christen M, Bühler Y, Bartelt P, Leine R, Glover J, Schweizer A, Graf C, McArdell BW, Gerber W, Deubelbeiss Y, Feistl T, Volkwein A (2012) Integral hazard management using a unified software environment: numerical simulation tool "RAMMS" for gravitational natural hazards. Proceedings of the 12th Congress Interpraevent, 23-26 April 2012. Grenoble, France. pp. 77-86.

Marjanović M, Đurić U, Abolmasov B, Bogdanović S (2015) Preliminary Analysis and Monitoring of the Rock Slope on the M-22 Highroad Near Ljig in Serbia, Using LiDAR Data. In: Lollino G, Giordan D, Crosta GB, Corominas J, Azzam R, Wasowski J, Sciarra N (eds) Engineering Geology for Society and Territory - Landslide Processes, Volume 2: Landslide Processes. Springer International Publishing. pp. 147-150.

Karst structures in heterogeneous lithological units as a potential geo-engineering hazard factor for mining and civil infrastructures

Željko Pogačnik[(1)], Kei Ogata[(2)], Gian Andrea Pini[(3)], Giorgio Tunis[(3)]

1) Georudeko, geology, mining and ecology, d.o.o., Anhovo 1, 5210 Deskle, Slovenia, zeljko.pogacnik@georudeko.si

2) Vrije Universiteit, Faculty of Science, Amsterdam, Netherland

3) Università di Trieste, Dipartimento di Matematica e Geoscienze, Trieste, Italy

Abstract The planning of civil engineering infrastructures and the exploitation of mineral resources in lithologically and structurally heterogeneous carbonate-dominated rock assemblages should take into account associated complex karst structures as potential geohazards. A recent study on the Paleocene-Eocene sedimentary succession outstandingly exposed in the Anhovo quarry (Outer NW Dinarides, Slovenia) points out the occurrence of paleokarst structures that are the result of localised dissolution processes along phreatic channels. These fluid flow pathways follow the directional anisotropy provided by a complex network of lithological matrix/clasts contacts in a matrix-rich depositional unit of ancient, large-scale submarine landslides (mass transport deposits; MTDs), which is in turn originated by specific sedimentary and post-sedimentary processes. Among primary sedimentary processes, down-slope gravitational transport favoured the lithological disaggregation and mixing of slide blocks and clasts into a marly-silty matrix, which later played an important role in controlling subsequent diagenetic processes on such exhumed MTDs. In this framework, groundwater flow followed different lithological and structural contacts, and block/clast boundaries, allowing the formation of contact karst structures, consequently providing favourable conditions for the formation of geomechanical labile systems in heterogeneous lithological units. The complex "worm-like" network of such phreatic channels, with certain anatomical features defined by the shape and orientation of structures and slide block/clast contacts, represents a zone potentially prone to gravitational collapse. The presented results suggest that the correct interpretation of syn-sedimentary structures, backed up by e.g. georeferencing of the contacts and the orientation of the slide blocks axes, allows us to identify or predict potential geomechanically weak areas of the quarry slopes where landslides could well be activated, and thereby contributes to better, more efficient decision-making on issues related to safe mining and/or civil engineering practices.

Keywords paleo submarine landslides, karst structures, geohazard

Introduction

Mass-transport deposits (MTD) or mass-transport complexes (MTC) are highly heterogeneous bodies/units deriving from *en-mass* subaqueous sedimentary processes, such as rock avalanches, hyperconcentrated flows, slides and slumps, acting in a sedimentary basin and often related to continental margins located at the edges of lithospheric plates and seismic zones (Pini et al. 2012; Festa et al. 2014; Festa et al. 2016).

The understanding of sedimentary and post-sedimentary processes (Ogata et al. 2014; Petkovšek et al. 2011) occurring within these geological bodies exhumed in orogenic belts (Pogačnik et al. 2015) allows for a proper spatial planning strategy (Cano and Tomás 2013) for the construction of infrastructures, as well as for the prevention and remediation of natural disasters.

The investigated MTDs, which occur in W Slovenia, are related to the Mesozoic and Cenozoic sedimentation in the north (Šmuc 2005; Rožič and Šmuc 2011) and central (Ogata et al. 2014) Soča Valley (Fig. 1).

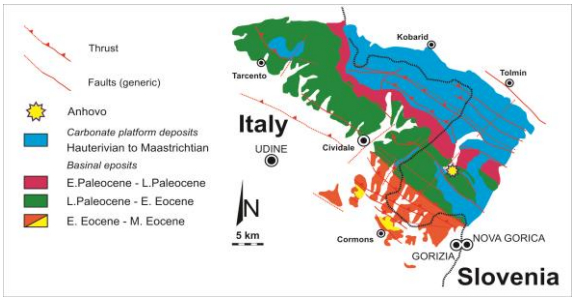

Figure 1 Position of Anhovo MTDs and generalised geological situation (after Ogata et al. 2014).

In the Anhovo region, a sequence of very thick MTD bodies of Middle Paleocene age crops out with an average dipping of 28° towards SW. Each body displays a sequence of lithological intervals corresponding to the internal depositional units (Fig. 2) defined by Tunis and Venturini (1992): calcareous breccia with oversized carbonate olistoliths (U1), calcareous breccia with bedded siliciclastic-carbonate and marly olistoliths (U2), graded calcareous breccia, calcirudite (U3), graded and laminated calcarenite (U4) and massive/laminated marlstone (U5).

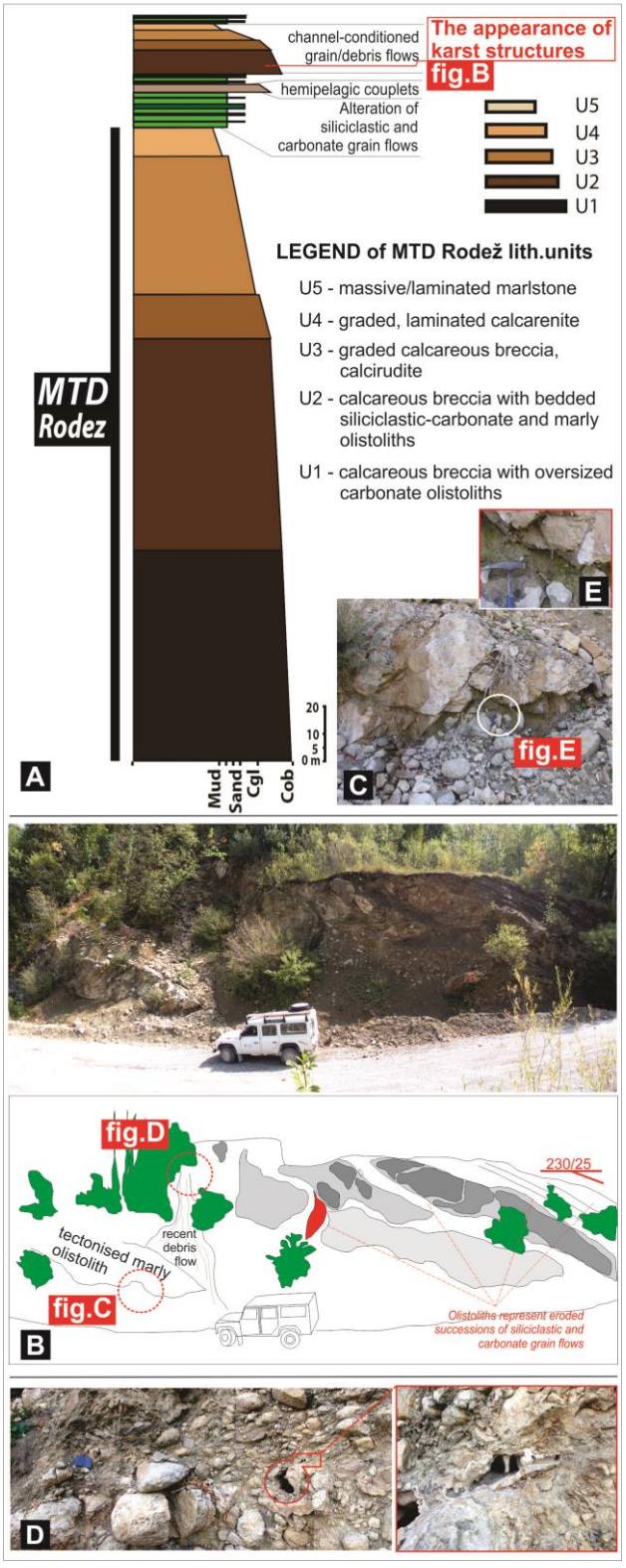

Figure 2 (A) Schematic lithostratigraphic succession of MTD Rodež with appearance of karst structure; (B) Field outcrop view of unit U2 with structurally deformed marly olistolith as conduits for groundwater percolation, different structurally damaged pebble-boulder and pebble conglomerate (dark grey), olistoliths with muddy sand matrix (light grey), and plastic deformed eroded successions of siliciclastic and carbonate grain flows; (C and E) NE-oriented tectonic deformation and travertine stalactite (location in B); (D) Typically oriented pebbles and boulders with their mutual contact and evidence of karst structures.

Due to the specific internal organisation of individual units such as the orientation of clast long axes (Enos 1977; Major 1998), their mutual contacts and the permeability of contact surfaces, these rocks represent a potentially significant geohazard to be considered in the design and proper use of mining space. Internal organisation depends on rheological and palaeotopographic factors (occurring during sedimentation) and early (as compaction structures) and late diagenetic activation of labile zones.

The overall impact of meteoric water (Pánek et al. 2011) and groundwater in structural and lithological heterogeneous rocks like those of the MTDs creates specific structures such as karst contact caves (Mocchiutti 2001; Zupan 2004; Mocchiutti and Maddalena 2005; Knez et al. 2005; Kenz and Slabe 2009, 2016; Pánek et al. 2011) of various shapes (Margielewski and Urban 2005; Pánek et al. 2011; Urban and Margielewski. 2013; Lenart et al. 2014; Lenart 2015) and sizes (Margielewski and Urban 2005).

The U2 unit represents a heterogeneous assemblage from a structural, textural and compositional point of view, with a specific internal organisation that requires a complex approach in order to study the individual and interrelated causal effects that originate peculiar types of speleothem. This paper addresses the factors influencing the formation of karst structures, which are responsible for a triple porosity aquifer (conduits, fractures and matrix) (White 1999) and the potential impact of such structures on the geohazard.

Materials and methods

At the stage of sedimentation, unit U2 can be described as a mixture of solid heterogeneous materials and fluids with different mechanical properties in which a great number of momentum-transfer mechanisms operate, from bulk transitional to grain vibrational kinetic energy and fluid pressure energy (Iverson 1997). In the outcrop, where the karst structures (detail on Fig. 2D) have been detected, a detailed structural, stratigraphic and compositional study has been done, with special attention paid to the type of contact between clasts of different facies and the type of matrix (sandy-muddy), in order to establish a meaningful interpretation of the speleothem occurrence.

Results

Rudist limestone breccia (Fig. 3B), with pronounced karstic structural planes, eroded clasts of sandy matrix, which include angular marly clasts (Fig. 3A), and fine-grained sandstones (Fig. 3D) predominantly display an angular shape, as opposed to resedimented radiolitic breccias, where a rounded shape prevails. Defining the contact geometries among pebbles and boulders (Fig. 3E), a tangential (point) contact (point 1 and 3 on Fig. 3E) appears in its greatest extent, probably related to the

primary depositional processes. It is followed in importance by long axes contacts (point 2 and 4 on Fig. 3E), with the latter probably originating in post-depositional burial and compaction of the U2 unit. A concavo-convex contact between ductile eroded hemipelagic couplets (yellow dashed line-point 5 on Fig. 3E) and/or harder limestone clasts can be found around larger pebbles.

In the empty space between clasts (Fig. 4A, 4B and 4C), the observed speleothems indicate a continuous connection (Fig. 4B, point 2 and 3) of the karst cave system (Fig. 4C; red dashed line). The flame-shaped sandy matrix injections (Fig. 4D, yellow dotted line) between angular pebbles indicate a lithological contact between olistoliths with different muddy-sandy and muddy matrices in unit U2. The traces (Fig. 4E; arrows) of multistage, phreatic channel development are evident on the now exposed walls (Fig. 4E; dashed line) of a phreatic channel (Fig. 4D) opened in a boulder of Rudist limestone breccias.

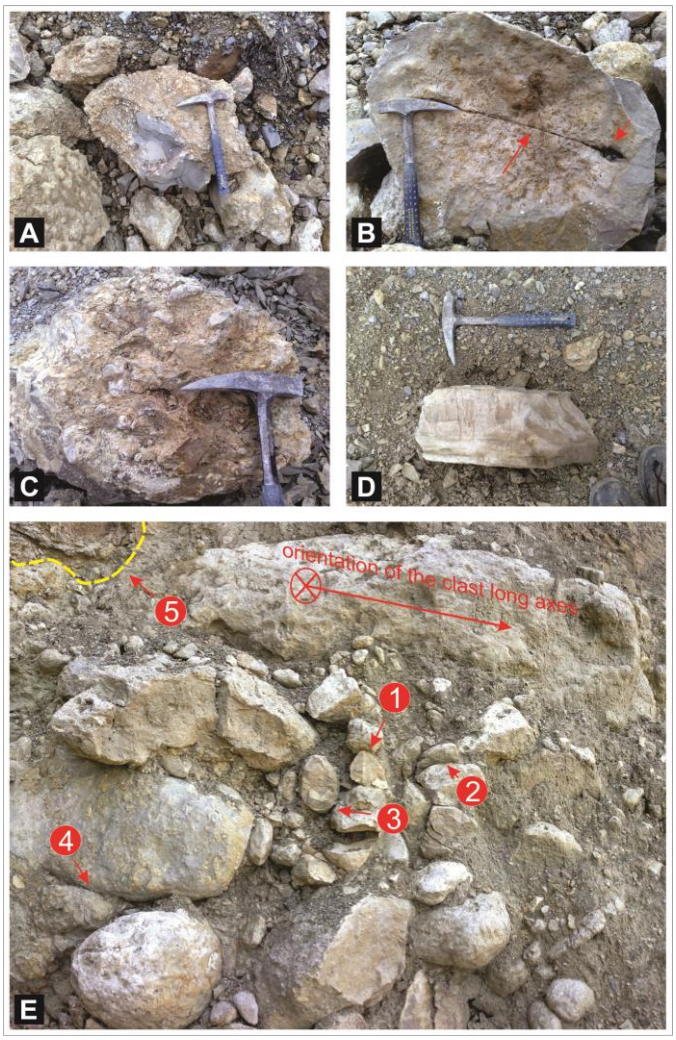

Figure 3 Lithological and geometric diversity (A-D) of clasts, some of them with pronounced karstic structures (red arrows, B); (E) Different types of contacts: tangential-point contact (1 and 3), long axes contact (2 and 4) and concavo-convex contact (5).

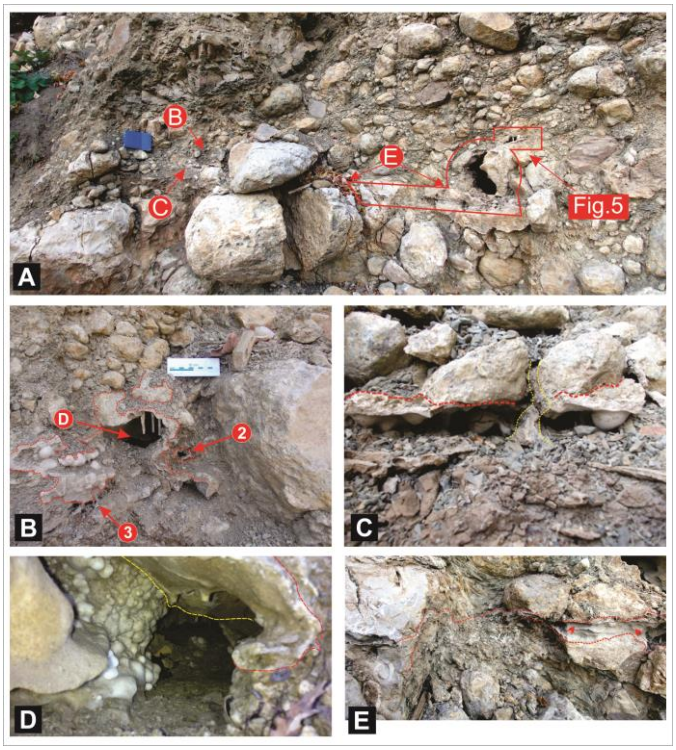

Figure 4 (A) An outcrop with speleothems; (B) Close-up view of worm-shaped cave; (C) Crystallisation of calcite on the concave/half-moon shaped channel ceiling; (D) Crystallisation of calcite on the walls forms a bubbly surface and broken stalactites on the channel ceiling; (E) broken boulder reveals the worm-connected system (broken red line).

Discussion and Conclusions

The crystallisation processes developed in the pore spaces of unit U2 indicate active late diagenetic activity, which can be assigned to either small-scale accommodation processes as a consequence of matrix weathering or the sudden movement of rock masses triggered by a subaerial landslide (Dugonjič Jovančević and Arbanas 2012; Berisavljević et al. 2015; Berti et al. 2017) or other events (Cano and Tomás 2013).

Hypothetically, the U2 unit can be conceived as a "blend" of different matrices (each with its own rheological properties) surrounding clasts that are of uneven shape and size (Fig. 5A) and are oriented in the same direction as the axes of the sedimentary mass transport. To illustrate the fluid transmissivity factors impacting the speleogenesis in unit U2, we have used a combined approach of clasts rotating around their own axes (as a consequence of a directional simple shear during post-depositional tectonics/slide events) and percolation (opening/closing of channels due to rotation of clasts, creating new contacts by extruding the homogeneous matrix).

In unit U2, there are cracks and interconnected cracks (Fig. 4B to 4D), which allow the flow of saturated waters with carbonate ions and the consequent formation of speleothems in micro-environments in interparticles and larger channel porosity. If a lithological horizon such

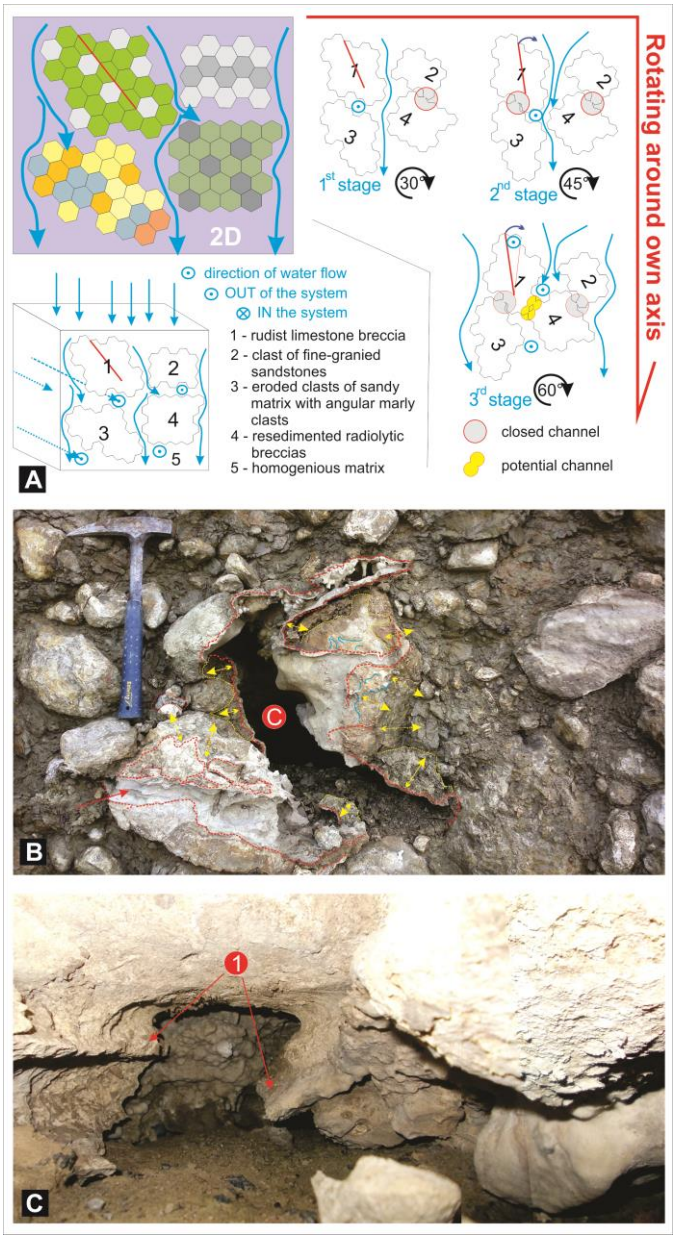

Figure 5 (A) Rotation of clasts around their own axes in a homogeneous muddy-sand matrix and the formation of percolation bulkheads as a consequence of new grain contact types and squeezing of the surrounding matrix; (B) Type of vuggy channel porosity (red dotted line) and diagenetic transformed matrix (yellow dotted line) with orientation of the contact of the speleothem (double yellow arrow). The blue line on the rudist limestone breccia indicates traces of the previous karst system, which was destroyed during diagenesis. The red arrow shows the fasetes, which indicate the process of the corrosion of the rock as the result of the water vortex flow on the rock and the erosion gut, in turn the result of the spilling of low water flow; (C) Part of the keyhole cave system, a result of downcutting from an initial phreatic tube. The width of the system varies depending on the solubility of the wall rock (red arrows as point 1).

as unit U2 is overloaded with a simple shear force (as late diagenetic processes), the clasts and surroundings matrix repack in order to establish a new balance andform a new channel – vuggy porosity (Fig. 5B), where water can form new speleothems. Ductile matrix deformation develops as a result of the new balanced state (Fig. 5B dotted red line) and is characterised by radical degradation of porosity (detail C on Fig. 5B) due to compaction and compaction-related processes (yellow dotted line on Fig. 4C). This can cause additional pore clogs to form a percolation barrier. At that moment in the MTD, a hydrostatic pressure zone may develop, forming new latent mesogenic and/or talogenic landslide structures that destroy the worm-shaped karst caves connected through the channel (Fig. 5C) and/or giant vuggy porosity of unit U2 and trigger a new potential rupture surface on the slope. In order to check this proposed explanation, a geochemical analysis of the speleothems "chemostratigraphy" must be performed (from the matrix to the inside of the structure), to determine whether the various channels and stalactites can be stratigraphically bundled. Positive results would open a new chapter on the geomechanical interpretation of the heterogenous units that form large MTDs and the appropriate interpretation of the geohazards connected with them.

References

Berisavljević Z, Berisavljević D, Čebašek (2015) Shear strength properties of Dimitrovgrad flysch, Southeastern Serbia. Bulletin of Engineering Geolology and the Environment, 74: 759-773. (DOI 10.1007/s10064-014-0678-5).

Berti M, Bertello L, Bernardi A R, Caputo G (2017) Back analysis of a large landslide in a flysch rock mass. Landslides. 14: 2041. (DOI 10.1007/s10346-017-0852-5).

Cano M, Tomás R (2013) Characterization of the instability mechanisms affecting slopes on carbonatic Flysch: Alicante (SE Spain), case study. Engineering Geology. 156: 68–91.

Dugojnić Jovančević S, Arbans Ž (2012) Recent landslide on the Istrian Penisula, Croatia. Natatural Hazards, 62: 1323-1338. (DOI 10.1007/s11069-012-0150-4)

Enos P (1977) Flow regimes in debris flow. Sedimentology. 24(1): 133-142.

Festa A, Dilek Y, Gawlick HJ, Missoni S (2014) Mass-transport deposits, olistostromes and soft-sediment deformation in modern and acient continental margins and associated natural hazards. Marine Geology. 356: 1-4.

Festa A, Ogata K, Pini GA, Alonso JL (2016) Origin and significance of Olistostromes in the Evolution of Orogenic Belts: A Global Synthesis. Gondwana Research. 39: 180-203.

Gams I (2001) Notion and forms of contact karst = Pojem in oblike kontaktnega krasa. Acta Carsologica. 30/2(2): 33-46.

Iverson M (1997) The physics of debris flows. Reviews of Geophysics. 35(3): 245-296.

Knez M, Slabe T, Šebela S (2005) Smognica – a cave developed in upper cretaceous breccia. Acta Carsologica. 34/2: 425-438.

Knez M, Slabe T (2009) Caves in breccia and flysch below Mount Nanos in the Vipava valley (Slovenia). Annales Ser. hist. nat., 19: 85-94.

Knez M, Slabe T (2015) Development and Karstification of the Karst Aquifer as Discovered between Klanec and Črni Kal. In: M. Knez M, Slabe T (eds) Cave Exploration in Slovenia. Cave and Karst Systems of the World. Springer, Cham. pp. 19-29. (DOI 10.1007/978-3-319-21203-6_2).

Lenart J, Pánek T, Dušek R (2014) Genesis, types and evolution of crevice-type caves in the flysch belt of the Western Carpathians (Czech Republic). Geomorphology. 204: 459-476.

Lenart J (2015) Morphological patterns of crevice-type caves in sedimentary rocks of the outer western Carpathians (Czech Republic). Journal of Cave and Karst Studies. 77(3): 165-176.

Major JJ (1998) Pebble orientation on large, experimental debris flow deposits. Sedimentary Geology. 117: 151-164.

Margielewski W, Urban J (2003) Crevice-type caves as initial forms of rock landslide development in the Flysch Carpathians. Geomorphology. 54: 325-338.

Margielewski W, Urban J (2005) Pre-existing tectonic discontinuities in the rocky massifs as initial forms of deep-seated mass movements development: case studies of selected deep crevice-type caves in the Polish Flysch Carpathians. In: Senneset K, Flaate K, Larsen J O (eds) Landslides and Avalanches ICFL 2005, Proceedings of the 11th International Conference and Field Trip on Landslides, vol 1, 1-10 September 2005. Norway.pp. 249-256.

Mocchiutti A (2001) Contact caves in flysch formations – Friuli Region – Northeast Italy. Acta Carsologica. 30/2: 157-164.

Mocchiutti A, Maddaleni P (2005) Chemical, geomechanical and geomorphological aspects of Karst in sandstone and marl of flysch formation in north east Italy. Acta Carsologica. 34/2: 349-368.

Ogata K, Pini G A, Pogačnik Ž, Tunis G, Monutjoy J, Senger K, Strasser M (2014) High-Resolution Studies of Mass Transport Deposits: Outcrop Perspective for Understanding Modern Submarine Slope Failure and Associated Natural Hazards. In: Lollino G et al. (eds) Engineering Geology for Society and Territory – Volume 4. Springer, Cham. pp. 209-213.

Pánek T, Tábořík P, Klimeš J, Komárková V, Hradecký J, Šťastný M (2011) Deep-seated gravitational slope deformations in the highest parts of the Czech Flysch Carpathians: Evolutionary model based on kinematic analysis, electrical imaging and trenching. Geomorphology. 129: 92-112.

Pánek T, Margielewski W, Tábořík P, Urban J, Hradecký J, Szura C (2010) Gravitationally induced caves and other discontinuities detected by 2D electrical resistivity tomography: Case studies from the Polish Flysch Carpathians. Geomorphology. 123: 165-180.

Pánek T, Brázdil R, Klimeš J, Smolková V, Hradecký J, Zahradníček P (2011) Rainfall-induced landslide event of May 2010 in the eastern part of the Czech Republic. Landslides. 8: 507-516.

Petkovšek A, Fazarinc R, Kočevar M, Maček M, Majes B, Mikoš M (2011) The Stogovce landslide in SW Slovenia trigered during the September 2010 extreme rainfal event. Landslides. 8: 499-506.

Pini G A, Ogata K, Camerlenghi A, Festa A, Lucente C C, Codegone G (2011) Sedimentary Mélanges and Fossil Mass-Transport Complexes: A Key for Better Understanding Submarine Mass Movements? In: Yamada Y et al. (eds) Submarine Mass Movements and Their Consequences. Springer, Cham. pp. 585-594.

Pogačnik Ž, Ogata K, Pini G A, Tunis G (2015) Understanding the genesis of mass transport deposits (MTDs) for safe mining planning: Anhovo Quarry, Western Slovenia. In: Lollino G et al. (eds) Engineering geology for society and territory, vol. 2: Landslide processes. Springer, Cham. pp. 307-310.

Rožič B, Šmuc A (2011) Gravity flow deposits in the Toarcian Perbla Formation (Slovenian Basin, NW Slovenia). Rivista Italiana di Paleontologia e Stratigrafia. 117: 283–294.

Šmuc A (2005) Jurassic and Cretaceous Stratigraphy and Sedimentary Evolution of the Julian Alps, NW Slovenia. Založba ZRC Publishing, Ljubljana, Slovenia. (ISBN 961-6568-15-9).98 pp.

Urban J, Margielewski W (2013) Types of non-karst caves in Polish Outer Carpathians – Historical review and perspectives. In: Michal F, Bosak P (eds) Proceedings of the 16th International Congress of Speleology, 21-28 July 2013. Brno, Czech Republic. pp. 21-28.

White W B (1999) Conceptual models of karstic aquifers. In: Palmer A N et al. (eds) Karst Modeling, Special Publication 5.. Karst Waters Instutute, Charles town, West Virginia. (ISBN 978-0-9640258-4-4). pp. 11-16.Zupan N H (2004) The caves of the kontact karst of Beka and Ozicla, the SW Slovenia. Acta Carsologica. 33/2: 91-105.

Preliminary results of debris flow modelling in RAMMS - a Case Study

Jelka Krušić, Katarina Andrejev, Biljana Abolmasov, Miloš Marjanović

University of Belgrade, Faculty of Mining and Geology, Belgrade, Đušina 7, Serbia, jelka.krusic@rgf.bg.ac.rs

Abstract This paper will introduce the preliminary results of the numerical modelling of the Selanac debris flow, Municipality of Ljubovija, Serbia as the largest debris flow triggered during an extreme rainfall event in May 2014. The model was created using RAMMS software, which actually uses a one-phase approach (similar to avalanches, Voellmy-Fluid). Input data included pre-event DEM (30x30m resolution) and analysis of Pleiades satellite data (from June 2014). RAMMS® software provides the opportunity to simulate maximum values of flow height, velocity and pressure in different parts of the process. After calibration, some models were chosen as the most representative, and a discussion of various scenarios is presented for comparison.

Keywords debris flow, extreme rainfall, numerical modelling, RAMMS

Introduction

Debris flows occur when masses of poorly sorted sediment, agitated and saturated with water, surge downslope as the result of gravitational pull (Iverson, 1997). Their high flow velocity, impact forces, and long runout combined with poor temporal predictability make debris flows and debris avalanches one of the most hazardous types of landslides (Hungr, 2005). Today there are many approaches to debris flow modelling, some of them more empirical-statistical (Rickenmann, 1999, Legros, 2002), while others are based on physical-deterministic approaches (Savage and Hutter, 1989; Hungr, 1995; Iverson, 1997; Takahashi, 2007; Wu, 2015). Numerical modelling of debris flows is a complex process, because it is important to include many parameters that define the initial area and the dimensions of the triggering process, as well as the most important rheological param-eters. In this case study, we used RAMMS debris-flow software based on the Voellmy (1955) approach, which was specially designed for snow avalanches (Bartelt, 2015; Christen et al., 2007; 2010a; 2010b); nevertheless, it is also suitable for modelling other processes such as rock avalanches and debris flows (Schraml, 2015; Sosio, 2007; Frank, 2016).

In the third week of May 2014, the massive low-pressure Cyclone Tamara (Ivette) swept through the Western Balkans, resulting in an extreme precipitation event that saw some 230 mm fall over a period of 72 h, causing floods, flash floods and massive landslides in western and central Serbia. Some of the locations in western Serbia were affected by many flow-type landslides, which had never previously been reported in these areas. These flow-type landslides caused severe damage in and to local municipalities (residential areas, roads, infrastructure facilities, cultivated land, pastures, and forests). In the framework of the post-disaster recovery led by the United Nations Development Programme (UNDP) office in Serbia, a post-event landslide inventory was conducted. Analysis of Very High Resolution satellite images resulted in 691 recognized debris flows in the affected areas (about 2,3 km^2 of visually recognized landslides)(Đurić et al., 2017).

In this paper we present the first results of calibrating Voellmy friction parameters, which produced comparable results with field observations. The case study presented in this paper represents the largest debris flow ever observed in Serbia – Selanac (about 1.5 km long and more than 350 m wide), activated during the May 2014 event.

Study area

The Municipality of Ljubovija is situated in the western part of Serbia, which covers 331.47 km^2 (Fig. 1) with a population of 14,424 inhabitants according to the 2011 census. Most of the territory experiences a mid-continental climate with an annual precipitation average of 800–900 mm and an average temperature of 8.1–10.0 C^o (1981–2010). The topography is a typical low mountainous to hilly relief landscape (185–1268 m a.s.l.) with predominantly gentle to moderate slopes (10°-21°) and many micro-relief forms enclosed in relatively small catchments.
The Selanac debris-flow study area is located in the northern part of the Municipality of Ljubovija, and during the May 2014 event was affected by different types of landslides – predominantly slides and flows or complex slope movements. The greatest 48h rainfall was recorded at the nearby Loznica Main Meteorological Station, which exceeded 160 mm in 48h, which corresponds to an extreme rainfall event with a 1000-year return period. These extreme levels of soil saturation – especially when coupled with the antecedent cumulative effects of rainfall causing a gradual yet constant deterioration of soil strength by diminishing the effective stress factors – resulted in numerous massive landslides in the area (Fig. 2).

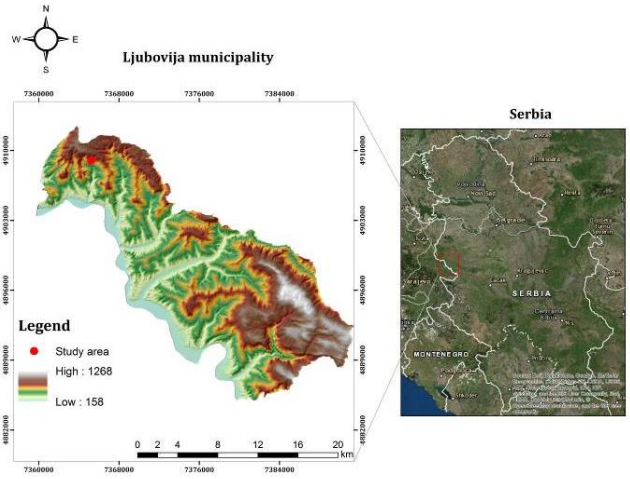

Figure 1 Geographical location of the study area.

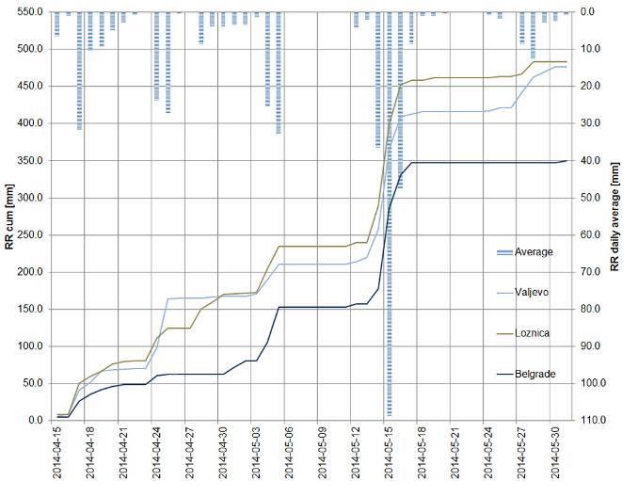

Figure 2 Average precipitation in mm (April 15 – May 30, 2014) from the two nearest Main Meteorological Stations, at Valjevo and Loznica, and Belgrade.

Geological settings

The geological setting of the study area is very complex (Fig. 3). The "Drina formation" is the oldest Palaeozoic formation in the area. It is a complex of Lower ($^1C_{1,2}$) and Middle Carboniferous age ($^2C_{1,2}$) phyllite, metasandstone, clay and graphitic schists, limestone, diabase, tuff and tuffite. In the "Jadar formation" the Paleozoic formation is developed as a complex of sandstone, argillophyllite and black limestone. Both formations are transgressively overlain by sandstone, shale and limestone of the Permian, which pass into the block bituminous limestone of the Upper Permian (P_3). Lower Triassic (T_1) and Middle Triassic (T_2), consisting of dolomite, dolomitic limestone, sandstone, limestone, and andesite with pyroclastics. The Jurassic ($J_{1,2}$) consists of oolitic to nodular, limonitized to siliceous limestones, sandstone, shale, conglomerate, chert, spilite, amphibolite, gabbro and serpentinite. The Jurassic ($J_{1,2}$) weathered offiolitic melange is the main formation involved in the debris flow process.

Large masses of magmatic rocks were formed during the Tertiar (Tc) – granodiorite, dacite, andesite, quartz-latite and basalt. Dacite and andesite are partly propylitized and hydrothermally altered (like the surrounding Palaeozoic rocks).

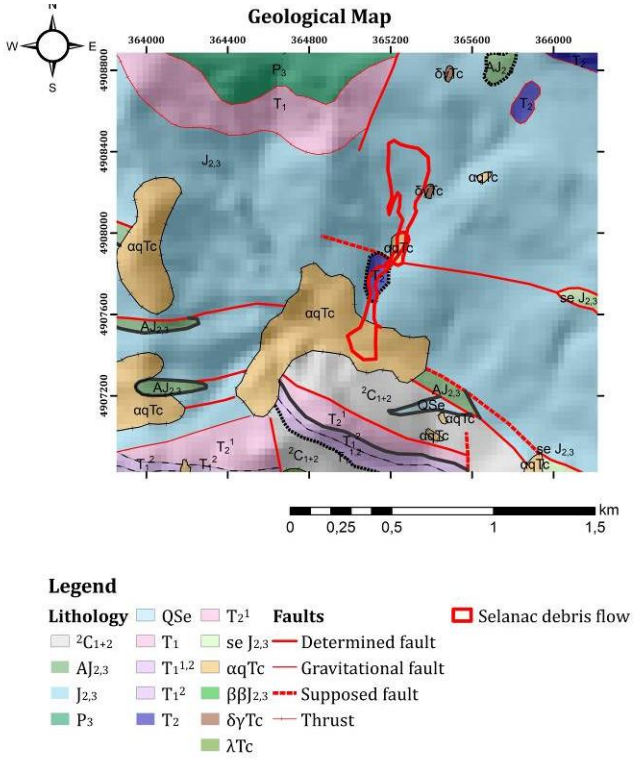

Figure 3 Geological map of the study area with the position of the Selanac debris flow.

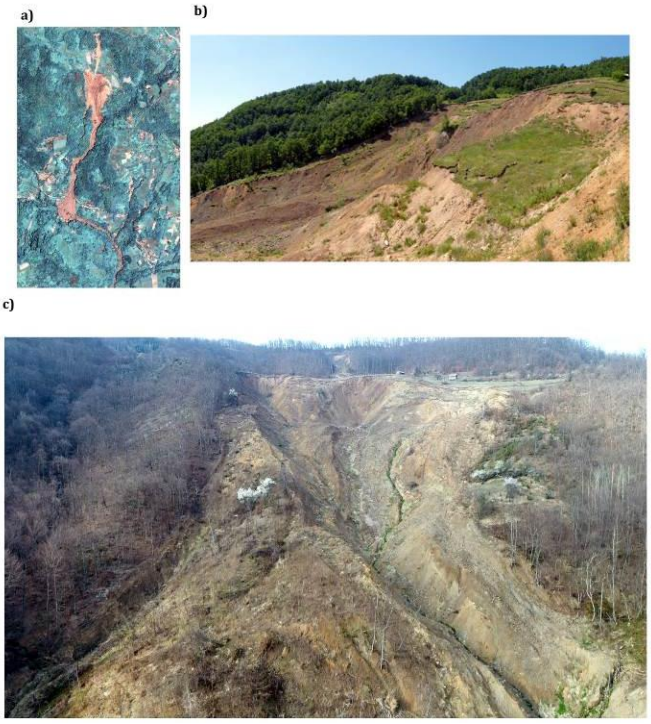

Figure 4 a) Pleiades image (June 2014), b) Main scarp photo (June 2015), c) UAV photo of the source area (April 2017).

Debris flow

Debris flow was triggered on May 15, 2014 and flowed continuously for the next 2 days (personal communication with habitants from the village of Selanac). The debris flow stretched 1.5 km with a width of more than 350 m. A large amount of material (estimated at 750,000 m^3) started to flow between two existing gullies. The source area is estimated at 25,000 m^2 , with the main scarp height at 30 m as its deepest part (Fig. 4). The zone of the main scarp is composed of weathered material (limestone, sandstone and diabase), with heterogenious fragments ranging from some cm^3 to some m^3 in volume. A lot of material was transported from the bottom of the slope to the Selanačka river (1.5 km), forming a landslide dam. It is supposed that this dam was destroyed after a short time by the Selanačka river torrent flow (at the time), and the debris material was transported another 1 km further downstream. In the middle part of the debris flow the material was very wet, with a lot of clay component between boulders. In the deposition zone a lot of heterogeneous fragments ranging in size from a few cm to huge blocks over 2 m in diameter were registered. The very high heterogeneity of the entire debris flow material mass prevented regular geotechnical drilling and sampling efforts.

Methodology

RAMMS Debris Flow software is specially designed for the numerical modelling of debris flow processes from initiation to run-out over three-dimensional terrain. RAMMS was developed in 2005 by the Swiss Federal Institute for Forest, Snow and Landscape Research (WSL, Birmensdorf) and the Swiss Federal Institute for Snow and Avalanche Research (SLF, Davos). For debris flow simulation, RAMMS actually uses a one-phase approach (similar to snow avalanches, Voellmy-Fluid). The Voellmy-Fluid model assumes no shear deformation. The flow body moves as a plug with the same mean velocity (u) everywhere over the flow depth (H); a simplified representation of the total resistance S [Pa] is as follows:

$$S_f = \rho g H \cos\varphi + \frac{\rho g u^2}{\xi} \qquad [1]$$

where ρ is the density, g the gravitational acceleration, φ the slope angle, H the flow depth, and u the flow velocity (Fig. 5).

The normal stress on the running surface, $Hgcos(\varphi)$, can be summarized with a single parameter N. The Voellmy model accounts for the resistance of the solid phase (μ is sometimes expressed as the tangent of the internal shear angle) and a viscous or turbulent fluid phase (ξ was introduced by Voellmy using hydrodynamic arguments). The friction coefficients are responsible for the behaviour of the flow. The tangent of the effective internal friction angle of the flow material can be defined for the resistance of the solid phase (the term containing μ) which extensively controls the deceleration behaviour of a slower moving flow. On the other hand, the resistance of the viscous or turbulent fluid phase (the term including ξ) prevails for a quicker moving flow (Bartelt et al., 2013).

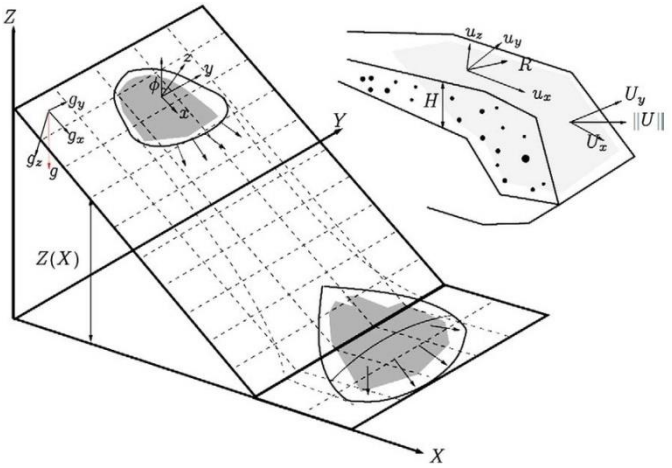

Figure 5 The topography Z (X, Y) is given in the Cartesian framework, X and Y being the horizontal coordinates. The surface induces a local coordinate system x, y, z. It is discretized such that its projection onto the X, Y plane results in a structured mesh (from Christen et al., 2010a).

The vertical information within the Voellmy-Salm model is given as an ananysotropic Mohr-Coulomb relation, using the earth pressure coefficient ka/p as a proportionality factor for vertical and normal stresses (Christen et al., 2010). The earth pressure coefficient ka/p is given by the Rankine equation:

$$ka = \tan^2\left(45° \mp \frac{\varphi}{2}\right) \qquad [2]$$

The active earth pressure coefficient ka characterises a dilatant flow and contracting, causing an increase in change of velocity or passive kp, where the flow is compressive and the change in velocity of the flow decreases. Within our study, we used the default fixed value of $ka = kp = 1$ in simulations.

Model input

RAMMS uses basic data inputs to numerically calculate the *Digital Elevation Model (DEM)*. The DEM used for simulations has a resolution 30x30m, which is not particularly precise for these kinds of simulations, but was up until now the only pre-event DEM data that was available, which we found acceptable for the preliminary results.

Defining the *source area* is the first step in RAMMS modelling, which offered the choice of two approaches: defining an input hydrograph or a block area. Using an input hydrograph rather than a block release certainly

enhances the simulation results – if data is available. It is assumed that the model input parameters are well known and represent the measured field data. For hillslope debris flows, which typically occur in open, unchannelized topographies, a block release produces better results (Bartelt, 2013). In such cases a block release zone is defined, since there are no measurements, and because it is assumed that the material initially begins to move as a huge block of mass, and then rapidly flows due to the (great) amount of rainfall. The assumed initial block is on average some 30 m deep, and has a total volume of about 730,000 m^3 (estimated from field observations).

The main step in debris-flow modelling in RAMMS consists in calibrating *resistance parameters* μ – Coulomb frictional parameter, and an εviscous-turbulent parameter. Final models were made using literature value ranges for debris flow tested in many case studies of different types of processes (Tab. 1).

Table 1 Typical values ranges for the rheological parameters adopted from the literature for the frictional and Voellmy rheologies (Sosio et al., 2008).

Voellmy friction parameters	Frictional coefficient, μ	Turbulent coefficient, ξ(ms^{-1})
Rock avalanches	0.1–0.25	450–1000
Debris avalanches	0.07–0.1	200–250
Rockslide-debris avalanches	0.05–0.2	200–400
Ice-rock avalanches	0.03–0.1	1000
Debris flows	**0.05–0.2**	**200–500**
Volcanic-rock avalanches	0.05–0.1	100–140

The parameter λ, i.e. *ka*/*kp*, has been assumed to be equal to 1, as the default fixed value. Also, the density value is taken as the default, at 20 KN/m^3.

Results and discussions

The RAMMS model was calibrated by separately changing each Voellmy input parameter, μ and ε, as well as the release block volume, while keeping the other parameters constant. As interpreted from the literature, we use a range of 0.05–0.2 for μ and 200–500m/s for ξ, while the volume of the initial area was increased 2 to 3 times according to the depth and surface of the source area.

Larger friction parameter values yielded more unrealistic results, thus the minimum value is considered the most reasonable. Larger friction parameter values result in a far larger amount of deposited debris material in zones where field observations did not yield any information about transportation and deposition.

Calibrating the turbulent parameter did not produce as much of a difference as that of the friction parameter. So on Fig. 7 a) and c) the results are almost the same, even if that parameter is different by 200 m/s.

Finally, the results of the volume and the surface of deposited debris material served as the parameters indicating the accuracy of the model. The best model has parameters of μ=0.05 and ε=500, (Fig. 7d), which resulted in a debris flow volume of 125,000 m^3, and an average deposition height of 5 m (Fig. 6). These values are within the range of values observed in the field. The final model also gives a wider area of transportation and deposition; we assume that a better DEM with higher resolution would yield better results using these calibrated parameters.

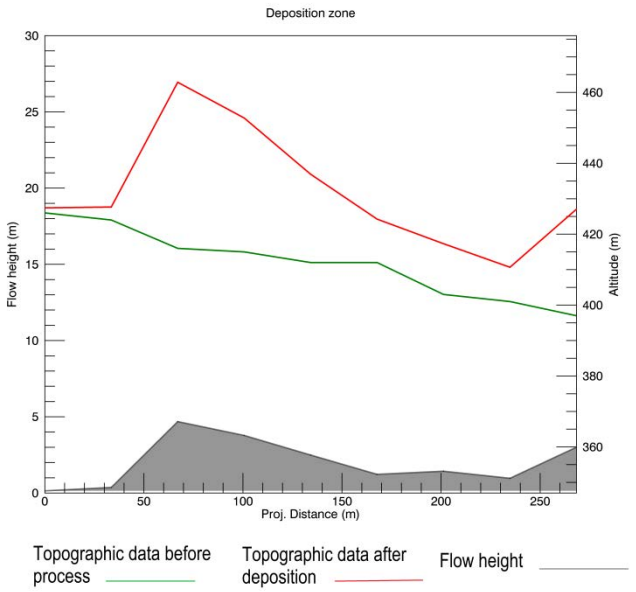

Figure 6 Cross section of the model with parameters μ=0,05 ξ=500 m/s in the debris-flow deposition zone.

Conclusions

The results of the numerical modelling of the Selanac debris flow using RAMMS were considered acceptable for the preliminary analysis stage. The main goal of the study was to model the debris-flow process with a limited amount of data, especially without using any basic rheological data obtained in a laboratory. The RAMMS model input parameters were assumed from recognised field engineering geological data and data from the UAV survey. It is obvious that a simple back analysis and calibration of the Voellmy input parameters could provide a realistic model of a debris flow like the Selanac debris flow. It is assumed that existing ERT geophysical survey data, and laboratory test data, which is in the planning, will provide more acceptable model input parameters and yield a better numerical/simulation model of the Selanac debris flow.

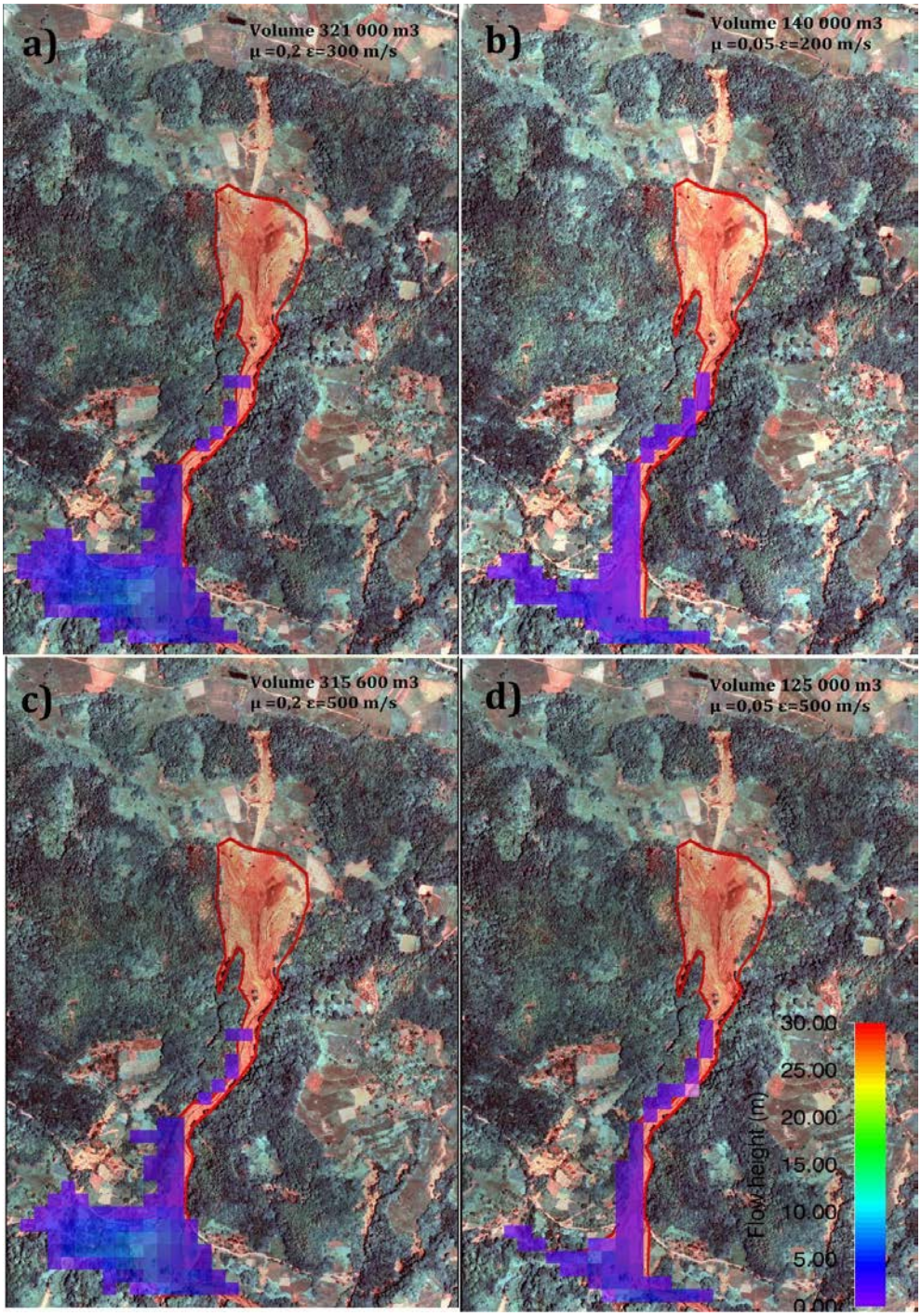

Figure 7 Calibrated models with input parameters: a) μ=0.2, ξ=300 m/s; b) μ=0.05, ξ=200 m/s; c) μ=0.2, ξ=500 m/s d) μ=0.05, ξ=500 m/s.

Acknowledgments

This study was part of Project BEWARE (BEyond landslide aWAREness) funded by the People of Japan and the UNDP Office in Serbia (grant No 00094641). The Project was implemented by the Geological Survey of Serbia, and the University of Belgrade, Faculty of Mining and Geology. All activities were supported by the Ministry for Energy and Mining, the Public Agency for Reconstruction, and the Ministry for Education, Science and Technological Development of the Republic of Serbia Project No TR36009.

References

Bartelt P, Buehler Y, Christen M, Deubelbeiss Y, Graf C, McArdell B W (2013) RAMMS–rapid mass movement simulation, A modeling system for debris flows in research and practice, user manual v1.5, debris flow. Institute for Snow and Avalanche Research SLF. pp. 126.

Christen M, Bartelt P, Kowalski J, Stoffel L (2007) Calculation of dense snow avalanches in three-dimensional terrain with the numerical simulation program RAMMS. Differential Equations. vol. Proceeding. pp. 709-716.

Christen M, Kowalski J, Bartelt P (2010a) RAMMS: Numerical simulation of dense snow avalanches in three-dimensional terrain. Cold Regions Science and Technology. 63: 1–14.

Christen M, Bartelt P, Kowalski J (2010b) Back calculation of the In den Arelen avalanche with RAMMS: Interpretation of model results. Annals of Glaciology. 51(54): 161-168.

Đurić D, Mladenović A, Pešić-Georgiadis M, Marjanović M, Abolmasov B (2017) Using multiresolution and multitemporal satellite data for post-disaster landslide inventory in the Republic. Landslides. 14: 1467- 1482.

Frank F, McArdell BW, Oggier N, Baer P, Christen M, Vieli A (2017) Debris flow modeling at Meretschibach and Bondasca catchment, Switzerland: sensitivity testing of field-data-based entrainment model. Natural Hazards and Earth System Sciences. 17: 801-815.

Hungr O (1995) A model for the runout analysis of rapid flow slides, debris flows, and avalanches. Canadian Geotechnical Journal. 32 (4): 610-623.

Iverson RM (1997) The physics of debris flows. Reviews of Geophysics. 35(3): 245-296.

Jakob M, Hungr O (2005) Debris-flow hazards and related phenomena. Blondel, P. Springer Praxis Book in Geophysical Sciences, Chichester, UK. 1723p.

Rickenmann D (1999) Empirical relationships for debris flows. Natural Hazards. 19: 47-77.

Savage SB, Hutter K (1989) The motion of a finite mass of granular material down a rough incline. Journal of Fluid Mechanics. 199 (1): 177-215.

Schraml K, Thomschitz B, Mcardell BW, Graf C, Kaitna R (2015) Modeling debris-flow runout patterns on two alpine fans with different dynamic simulation models. Natural Hazards and Earth System Sciences. 15(7): 1483-1492.

Sosio R, Crosta GB, Hungr O (2008) Complete dynamic modeling calibration for the Thurwieser rock avalanche (Italian Central Alps). Engineering Geology. 100(1-2): 11-26.

Takahashi T (2007) Debris Flow: Mechanics, Prediction and Countermeasures. Annual Review of Fluid Mechanics. 13(1): 57-77.

Voellmy A (1955) Über die Zerstörungskraft von Lawinen. Schweizerische Bauzeitung. 73: 212–285.

Wu W (2015) Recent advances in modeling landslides and debris flows. Wu W (ed). Springer Series in Geomechanics and Geoengineering, Springer Verlag. (ISBN 978-3-319-11053-0). 322p.

Dealing with the risk posed by rock spreading phenomena

Lisa Borgatti

University of Bologna, DICAM, Bologna, Viale Risorgimento 2, Italy, lisa.borgatti@unibo.it

Abstract Among deep-seated gravitational slope deformations, rock spreading phenomena normally develop where rigid rock blocks are overlying plastic terrains. They are frequently associated with secondary slope instability processes such as rock falls, topples and slides occurring at the edges of the plateaus, while earth slides and/or flows involve the underlying terrains, enhancing erosion at the base of the cliffs and further slope processes. Long periods of deformation, cracks opening and very slow movements on the entire scale of the slope lead up to rapid landslides, which may imply hazard and high risk conditions. A relevant example, for which a large data set is available, is the historic village of San Leo, a medieval town built on the top of a calcarenitic slab in Val Marecchia (northern Italy). On the 27 February 2014 a volume of roughly 330,000 m^3 of rock detached from the NE side of the plateau, resulting in the evacuation of several houses, a school and a police station. After the event, field investigations and lab tests, and remote-sensing techniques together with numerical modelling and monitoring procedures were used to delineate possible predisposing factors and related failure mechanisms. The results demonstrate that the slope processes are tightly linked to groundwater processes related to infiltration, weathering and erosion both in the short- and long-terms. In particular, the undermining of the rock slab as the result of progressive remoulding and erosion of the clay shales at its base lead to an opening of the cracks in the rock mass and to the final failure that is the toppling of the outer portions of the plateau.

Keywords deep-seated gravitational slope deformation, lateral spreading, rock fall-toppling, predisposing factors, failure

Introduction

Deep-seated gravitational slope deformations (Pasuto and Soldati 2013) can involve entire sections of high-relief mountain chains that are eventually over-steepened by glacial erosion or uplift. They have been described as giant, non-catastrophic landslides (Crosta et al. 2013), or as an intermediate class of slope instability processes that lie somewhere between gravitational movements and gravitational tectonic phenomena (Ambrosi and Crosta 2006; Margielewski 2006; Kellerer-Pirklbauer 2010). Even if they typically display very slow and discontinuous displacements (0.4–5 mm y^{-1}, Agliardi et al. 2009), they can evolve into catastrophic events and may themselves represent the predisposing factor of relatively smaller but rapid secondary landslides, such as rock falls and rock avalanches (Brideau et al. 2009; Jaboyedoff et al. 2009; Brideau et al. 2011; Zerathe and Lebourg 2012; Zorzi et al. 2014; Spreafico et al. 2017). Detailed investigations are still lacking in the field of lateral spreads and related landslides in weak rock masses, and more research is required to properly assess the hazard and design appropriate mitigation measures (Pasuto and Soldati, 2013).

Several causal factors control the initiation and evolution of these phenomena (Crosta et al. 2013): predisposing factors are related to the structural setting of the slope, the characteristics of the rock mass, and the valley geometry, whereas preparatory factors include glaciation and deglaciation effects, topographic stresses, changes in valley geometry, uplift rate and distribution, and regional seismicity. Prolonged rainfalls and earthquakes are recognized as triggering factors. As far as predisposing factors are concerned, these large-scale slope processes occur in moderately strong and anisotropic rock masses and are thus influenced by structural features such as bedding planes, foliation and fractures (Agliardi et al. 2001; Kellogg 2001; Massironi et al. 2003; Agliardi et al. 2009). In fact, deep-seated gravitational slope deformations are described in different geological contexts: sackungen (Zischinsky 1969) or rock flows (Cruden and Varnes 1996) typically occur in schistose metamorphic rocks, whereas lateral spreading normally develops in the presence of rigid blocks overlying a plastic sequence and is more common where antiformal structures are associated with extensional regimes and thrust structures (Cruden and Varnes 1996). Where lateral rock-spreading phenomena involve brittle rock units overlying a more ductile substratum, associated secondary slope instability processes such as rock falls, topples and slides may occur at the edges of the plateau, while earth slides and/or flows can impact the underlying terrains. Several examples have been described in Europe, i.e. Maltese archipelago (Mantovani et al. 2013), Slovakia (Vlcko, 2004), in the Alps (Cinque Torri Group, Viero et al., 2010) and particularly in the Apennines of Italy, where historical villages were often built atop rocky plateaus, such as Orvieto and Radicofani (Bozzano et al. 2008), Civita di Bagnoregio (Margottini and Di Buduo, 2017), and Pitigliano (Fanti et al. 2013).

On the 27 February 2014 a large landslide threatened the historical centre of San Leo, a medieval town built on the top of a calcarenitic slab in Val Marecchia (northern Italy, Fig. 1). A volume of some 330,000 m^3 of rock de-

tached from the north-eastern side of the plateau, resulting in the evacuation of several houses, a school and a police station. Prior to the failure, severe undermining of the rock slab was observed due to the progressive removal of the underlying clay shales. Mass wasting processes associated with surface runoff and shallow landslides occurring in small-scale catchments at the base of the cliff were thought to be the controlling factors. Thus, countermeasures such as earthen dams and retaining walls set on piles were adopted in recent decades to avoid further slope instability, together with extensive bolting of the rock face (Ribacchi and Tommasi 1988; Caturani et al. 1991; D'Ambra et al. 2004; Benedetti et al. 2011).

After the most recent catastrophic event, numerical modelling, together with field investigations, laboratory tests and monitoring were all used to delineate possible predisposing factors and related failure mechanisms. In particular, back analysis of the San Leo 2014 landslide complements the understanding of secondary instability phenomena that develop at the edges of the plateau and the recognition of those mechanisms that lead to catastrophic failure in the medium- to long-term (Borgatti et al. 2015; Spreafico et al. 2015; 2016; 2017).

The overall results provide data that can be used to plan effective and low impact interventions in target sections of the unstable slope. In fact, in this outstanding cultural landscape, conservation of the assets must be ensured, together with safe access to the area by means of adequate landslide risk mitigation measures with low environmental and visual impacts.

Geographical, geological and geomorphological settings

San Leo is the best known among the towns and castles of the historical region of Montefeltro (northern Apennines, Italy, Fig. 1). Throughout centuries, it gained great fame as an invincible military fortress, owing to its extraordinary geographical position and its massive fortifications. In fact, the town of San Leo rises from the top of a calcarenite and sandstone slab bordered by subvertical and overhanging cliffs up to 100 m in height overlying clayey gentle slopes (Fig. 1). This site is particularly relevant, because it combines unique geological and geomorphological features and historical and artistic assets. The rock slab and the surroundings are, owing to these particular geological and morphological features, also affected by slope processes.

In fact, the fortress underwent remarkable restoration works over the course of many centuries, mainly as the result of the effects of a number of landslides, most of which are well documented in various chronicles, paintings and other historical documents (Benedetti et al. 2011). Even as recently as in 2006 and 2014, large rockfalls (50,000 and 300,000 m^3 respectively) affected the northern and eastern cliffs of the plateau (Fig. 2). The San Leo rocky plateau is located on the south side of the Marecchia River Basin. The structural setting is characterized by alloctonous geological units belonging to the so-called "Val Marecchia Sheet", a nappe overlying the autoctonous geological units of the "Umbria-Marche-Romagna" geological sequence. The "Val Marecchia Sheet" encompasses several geologic units, from the older Ligurian units to the younger Epiligurian units, dating back to the Oligocene and Pliocene. The Epiligurian units are formed by hard rocks and are well differentiated from the Ligurian units that are characterized by a dominant clayey fraction. The outcropping of resistant rocks embedded in clay-rich terrains promotes the process of selective erosion resulting insteep cliffs and spurs. The enhanced erosion of the clayey substratum leads in turn to the progressive undermining of the resistant rocks and accelerating the cliff retreat. Accordingly, the San Leo rock slab can be considered a typical example of these rock slabs (Conti and Tosatti 1996). The rock plate is made of limestone belonging to the "San Marino" unit at the base and glauconitic arenaceous-calcareous sediments of the "Monte Fumaiolo" unit at the top. Bedding layers in the rock slab are mainly WSW dipping. The whole cliff lies above scaly clays called "Argille Varicolori" with a tectonic contact (Fig. 3). The whole rock slab is affected by rock spreading and related phenomena (opening of cracks on the top of the slab, differential movements, bulging at the base, squeezing of clayey material). Moreover, due to their lithological and mineralogical composition (smectite is predominant), varicoloured clays undergo swelling and are subject to rapid erosion and unloading phenomena. Landslide processes such as slumping and earth flows concentrate both at the foot of the rock plate and in the surrounding badlands. As a consequence, the cliff base is progressively undermined and the stability of the rock plate is compromised by rock falls and topples, so that periodic and expensive maintenance and consolidation works are required to avoid damage to the old town and castle (Ribacchi and Tommasi 1988; Caturani et al. 1991; D'Ambra et al. 2004; Benedetti et al. 2011).

2014 San Leo landslide: field and lab investigations, numerical modelling and monitoring

On 27 February 2014 a failure occurred in the north-eastern cliff involving a volume of about 330,000 m^3 of rock. Efforts to determine possible triggering factors noted only average weather conditions, with no seismic events recorded in the days preceding the landslide. After the 2014 event, an extensive civil protection plan was established by the Emilia-Romagna Region in order to assess and mitigate landslide risk. In particular, numerical modelling, together with field investigations, laboratory tests and monitoring were all used to delineate possible predisposing factors and related failure mechanisms acting on the slope in the medium- to long term. In particular, surveys conducted before the failure highlighted the presence of undermining in the area, with natural caves

Figure 1 San Leo village and rocky plateau, view of the south cliff (Rimini Province, Emilia-Romagna Region, northern Apennines).

Figure 2 Village of San Leo and rocky plateau. The 2014 landslide scarp and deposit are visible in the foreground. The 2006 landslide affected the northern cliff, visible on the right. (Photo courtesy of C.C. Lucente)

extending at least 20 m associated with springs originating under the slab. Moreover, after the event, a major discontinuity plane some 65 m long and 40 m wide was recognized in the upper part of the landslide scarp (Fig. 2). Considering the intense weathering of the surface, the discontinuity is understood to have already been open before the failure, like other discontinuities with similar orientation crossing the north-eastern cliff area, with a mean spacing of 20–22 m. In the lower area of the landslide scarp, the failure propagated along the joints and through the fracture of intact rock bridges, demonstrating a backward-propagation. Based on these observations, the principal objective of the San Leo 2014 failure back-analysis was to investigate the failure mechanisms acting at the borders of rock slabs affected by lateral spread phenomena. Two main potential predisposing factors were considered: the softening of a clay shale layer some 5 m thick, and the undermining of the cliff due to the erosion of the clay shales, enhanced by groundwater seepage and related chemical and physical weathering.

Several numerical models were built based on the reference geological model using 2D and 3D commercial codes and adopting either Finite Elements (FEM) or discrete Elements (DEM) approaches (Borgatti et al. 2015; Spreafico et al. 2015b; 2016; 2017). Among them a set of simulations was conducted using the 2D FEM code Phase2 in order to analyse the role played by the major pre-existing discontinuity and by groundwater hosted within the rock slab.

Even in the days following the 2014 event, a large intervention plan has been ongoing in order to guarantee safe access to the castle and to reduce the movement of earth, debris and large rock blocks in the valleys at the base of the cliff. A monitoring system records displacement data using a total of 13 wire crackmeters, 4 jointmeters, and 2 borehole rod extensometers installed across the main fractures as individuated during the field surveys. Starting from August 2014, the system has been set to activate the civil protection emergency plan if strain-rates exceeding the fixed thresholds are detected. To date, displacementis related to changes in daily and seasonal temperatures (Lucente 2015).

Discussion and conclusions

The 2D FEM modelling provided a realistic simulation of the 2014 San Leo failure, highlighting the onset and evolution of secondary toppling phenomena at the edges of the plateau and the role of groundwater-related processes, i.e. softening of the clay shales (Fig. 4) and undermining (Fig. 5). In the first stages of the simulations the progressive removal of layers at the base of the rock mass promotes unloading and consequential stress-induced deformation in the clay shales, with squeezing and shear yielding. All of those simulations performed that do not take into account the discontinuity at the top of the slope do not lead to realistic results. In particular, a larger volume of rock mass is involved and no backward propagation of the failure surface occurs. On the contrary, with the main discontinuity a failure surface is generated that resembles that measured in post-event surveys (Fig. 5). Due to its relatively higher secondary permeability relative to the lower clay-rich materials, the groundwater hosted within the fractured slab feeds perennial and ephemeral springs at the contact between the two units. In particular, three perennial springs have been mapped (Fig. 3), of which one has been monitored in continuous since April 2014, showing maximum discharge in the order of 0,0025 m^3/s (Spreafico et al. 2015a).
Chemical and physical processes mainly associated with the interaction of clay shales with groundwater itself promote the softening of a basal layer which, associated with seepage erosion and groundwater sapping processes, lead to the accelerated removal of material at the toe of the slab. In the bedrock headwall, where favourable joint intersections are present, caves develop, leading to a progressive undermining, collapse and retreat of the headwall itself from its base.

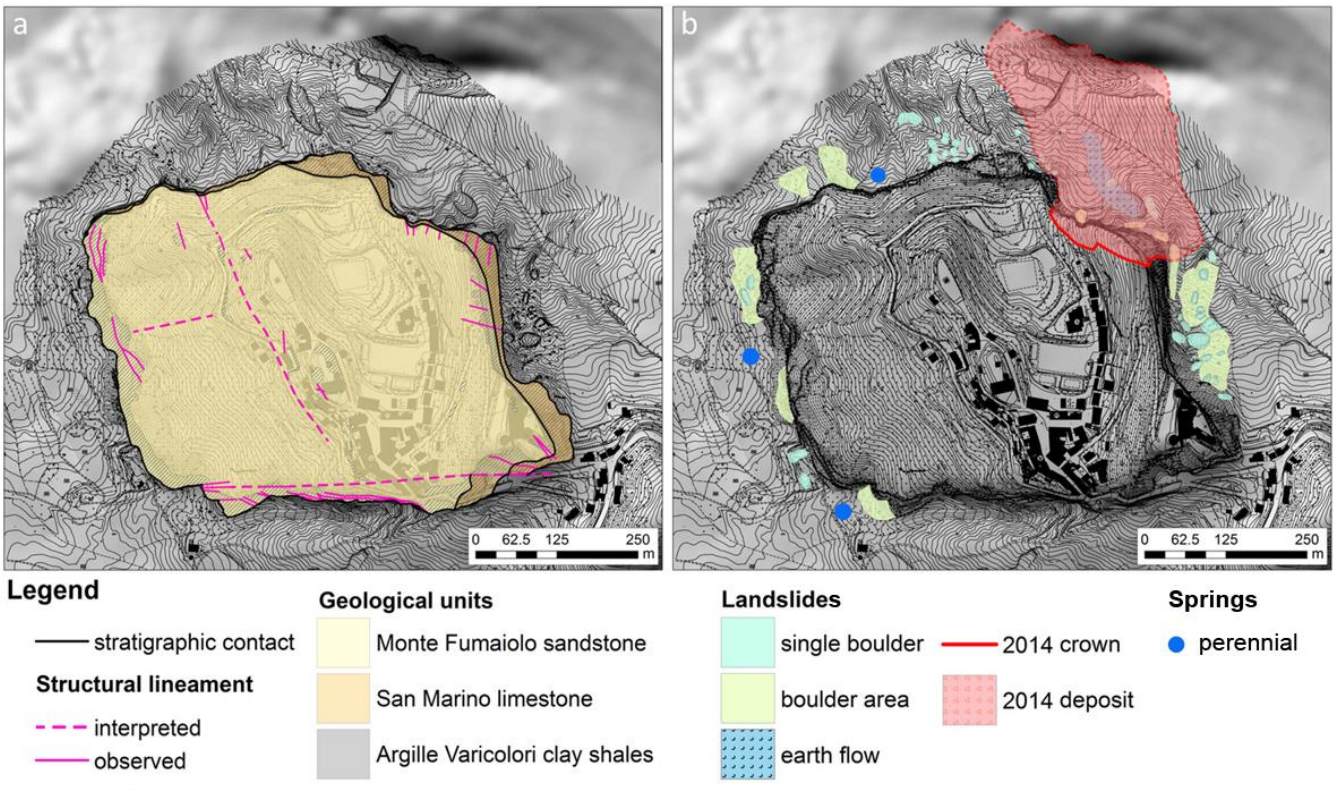

Figure 3 Pre-event maps of the San Leo rock plateau. a) Geological and structural map. b) Landslide landforms and deposits and perennial springs (modified after Badioli 2012; Spreafico et al. 2015a; 2017).

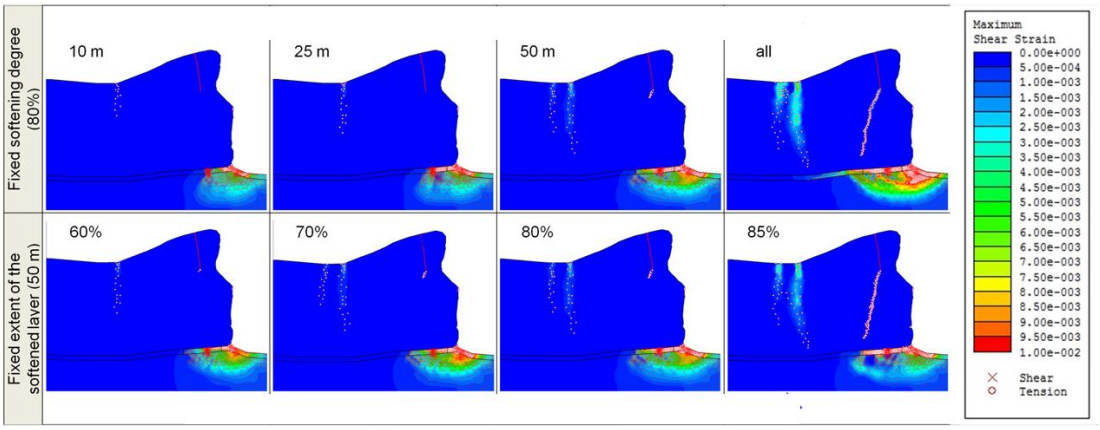

Figure 4 Softening of the clay shales. Upper row: fixed degree of softening plus increasing extent of the softened layer. Lower row: fixed extent of softened layer plus lowering of its mechanical properties (modified after Spreafico et al., 2017).

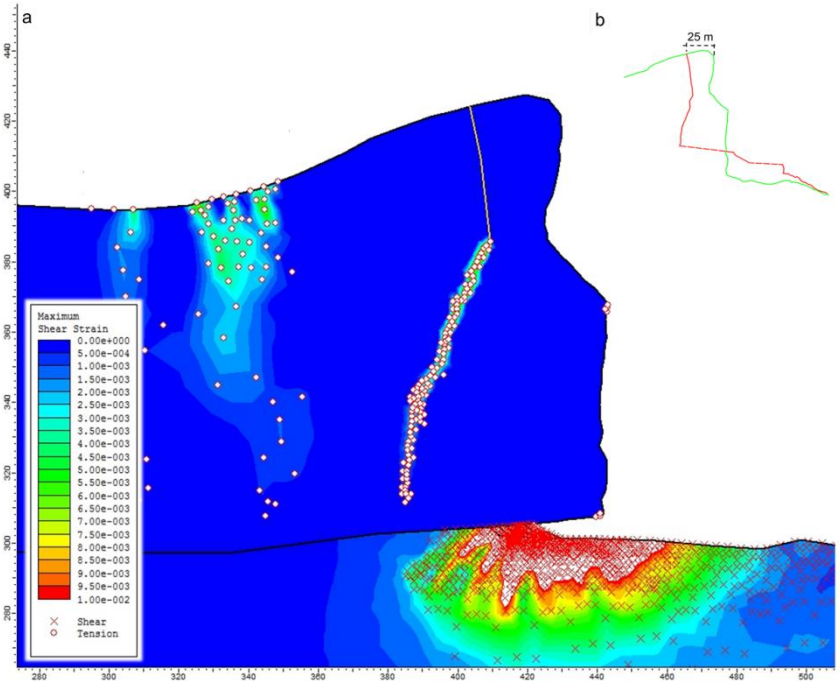

Figure 5 Undermining: a) Maximum shear strain prior to failure; b) Pre- and post-landslide sections extracted from TLS point cloud (modified after Spreafico et al., 2017).

Moreover, creep and shallow landslides contribute to the removal of material. The cliff becomes progressively unstable and undergoes large-scale landslides due to falls or topples. The resulting landslide deposits may exert an undrained loading on clay-rich units (both on bedrock and on loose landslide and slope deposits), which in turn leads to the reactivation or acceleration of slow-moving earth slides or flows in gullies. In addition, the stress related to massive failures may contribute both to the breaking of intact rock and to the opening of pre-existing fractures, promoting future slope processes.

Back analyses through numerical modelling can lead to a better understanding of rock slope failure mechanisms. In particular, the work carried out so far on the San Leo case study allowed the long-term evolution of lateral spreads where brittle rock masses overlie a soft substratum to be reproduced. In particular, the onset of secondary rock fall-toppling mechanisms developing at the edges of fractured plateaus has been successfully captured through back analysis of the 2014 event. Moreover, the role of groundwater flow in the fractured rock mass, in the form of enhancing weathering and subsequent geomorphological processes at the base of the cliffs in the clay shale unit, has been clarified. The results imply that, in order to effectively mitigate long-term slope processes driving the evolution of the rocky plateau, tailored countermeasure works could be designed (drainage tunnels and sub-horizontal drains, sealing of major fractures on the top of the slab etc.) beyond the classical engineering approaches of trimming and bolting the hard rock, retaining walls in the soft rocks and similar measures.

Acknowledgments

This work represents no more than a very short summary of the very extensive activities carried out together with several colleagues and friends in the area of Val Marecchia over the course of almost ten years: M. Bacenetti, G. Benedetti, P. Berry, G. Bitelli, F. Cervi, S. Devoto, F. Franci, M. Francioni, M. Gabrielli, M. Ghirotti, V.A. Girelli, C. Guerra, M. Guerra, A. Landuzzi, C.C. Lucente, E. Mandanici, G. Marcato, G. Marchi, O. Nesci, M. Pellegrini, L. Perotti, G.A. Pini, R.W. Romeo, T. Schanz, M.C. Spreafico, D. Stead, M.A. Tini, F. Veneri, M. Vincent. The data set was made available by Agenzia regionale per la sicurezza territoriale e la protezione civile, Servizio Area Romagna, in the frame of ongoing joint works.

References

Agliardi F, Crosta GB, Zanchi A (2001) Structural constraints on deep-seated slope deformation kinematics. Engineering Geology. 59: 83-102.

Agliardi F, Crosta GB, Zanchi A, Ravazzi C (2009) Onset and timing of deep-seated gravitational slope deformations in the eastern Alps Italy. Geomorphology. 103: 13-129.

Ambrosi C, Crosta GB (2006) Large sackung along major tectonic features in the central Italian Alps. Engineering Geolology. 83: 183-200.

Badioli L (2012) Analisi strutturale della rocca di San Leo. Diploma (BSc) thesis, University of Bologna, Italy. (unpublished).

Benedetti G, Bernardi M, Borgatti L, Continelli F, Ghirotti M, Guerra C, Landuzzi A, Lucente CC, Marchi G (2011) San Leo: centuries of coexistence with landslides. In: Margottini C Canuti P Sassa K (eds) Landslide science and practice. Springer-Verlag Berlin Heidelberg, Germany. pp. 529-537.

Borgatti L, Guerra C, Nesci O, Romeo RW, Veneri F, Landuzzi A, Benedetti G, Marchi G, Lucente CC (2015) The 27 February 2014 San Leo landslide (northern Italy). Landslides. 12: 387-394.

Bozzano F, Bretschneider A, Martino S (2008) Stress–strain history from the geological evolution of the Orvieto and Radicofani cliff slopes (Italy). Landslides. 5: 351-366.

Brideau MA, Yan M, Stead D (2009) The role of tectonic damage and brittle rock fracture in the development of large rock slope failures. Geomorphology. 103: 30-49.

Brideau MA, Pedrazzini A, Stead D, Froese C, Jaboyedoff M, van Zeyl D (2011) Three-dimensional slope stability analysis of South Peak Crowsnest Pass Alberta Canada. Landslides. 8: 139-158.

Caturani A, Ribacchi R, Tommasi P (1991) The San Leo Cliff (Italy): stability conditions and remedial measures. In: VII ISRM International Congress on Rock Mechanics, Aachen, Germany. pp. 853-858.

Crosta GB, Frattini P, Agliardi F (2013) Deep seated gravitational slope deformations in the European Alps. Tectonophysics. 605: 13-33.

Cruden DM, Varnes DJ (1996) Landslides types and processes. In: Turner AK Schuster RL (eds) Landslides: investigation and mitigation, Special Report 247. National Research Council, Transportation Research Board, Washington DC. pp. 36-75.

D'Ambra S, Giglio G, Lembo-Fazio A (2004) Interventi di sistemazione e stabilizzazione della Rupe di San Leo. 10° Congress INTERPRAEVENT, 2004, Riva del Garda. 2: IV/103-114.

Fanti R, Gigli G, Lombardi L, Tapete D, Canuti P. (2013) Terrestrial laser scanning for rockfall stability analysis in the cultural heritage site of Pitigliano (Italy). Landslides. 10: 409-420.

Jaboyedoff M, Couture R, Locat P (2009) Structural analysis of Turtle Mountain (Alberta) using digital elevation model: toward a progressive failure. Geomorphology. 103: 5-16.

Kellerer-Pirklbauer, A Proske H, Strasser V (2010) Paraglacial slope adjustment since the end of the Last Glacial Maximum and its long-lasting effects on secondary mass wasting processes: Hauser Kaibling Austria. Geomorphology. 120: 65-76.

Kellogg KS (2001) Tectonic controls on a large landslide complex: Williams Fork Mountains near Dillon Colorado. Geomorphology. 41: 355-368.

Lucente CC (2015) Il crollo del versante nord della rupe di San Leo del 27 febbraio 2014: studio e monitoraggio a un anno di distanza. Il Geologo dell'Emilia Romagna Anno XIV/2014. pp. 52.

Mantovani M, Devoto S, Forte E, Mocnik A, Pasuto A, Piacentini D, Soldati M (2013) A multidisciplinary approach for rock spreading and block sliding investigation in the north-western coast of Malta. Landslides. 10: 611-622.

Margielewski W (2006) Structural control and types of movements of rock mass in anisotropic rocks: Case studies in the Polish Flysch Carpathians. Geomorphology. 77: 47-78.

Margottini C, Di Buduo G (2017) The Geological and Landslides Museum of Civita di Bagnoregio (Central Italy). Landslide.s 14: 435-445.

Massironi M, Bistacchi A, Dal Piaz GV, Monopoli B, Schiavo A (2003) Structural control on mass-movement evolution: a case study from the Vizza Valley Italian Eastern Alps. Eclogae Geologicae Helvetiae. 96:85-98.

Pasuto A, Soldati M (2013) Lateral spreading. Treatise on Geomorphology, Elsevier. pp. 239–248.

Ribacchi R, Tommasi P (1988) Preservation and protection of the historical town of San Leo (Italy). In: IAEG International Symposium on Engineering Geology of Ancient Works Monuments and Historical Sites, 19-23 September 1988, Athens, Greece. pp. 55–64.

Spreafico MC, Cervi F, Marc V, Borgatti L (2015) Hydrogeological features of a highly fractured rock-slab. Rendiconti Online della Società Geologica Italiana. 35: 283-287.

Spreafico MC, Perotti L, Cervi F, Bacenetti M, Bitelli G, Girelli VA, Mandanici E, Tini MA, Borgatti L (2015) Terrestrial Remote Sensing techniques to complement conventional geomechanical surveys for the assessment of landslide hazard: The San Leo case study (Italy). European Journal of Remote Sensing. 48(1).

Spreafico MC, Francioni M, Cervi F, Stead D, Bitelli G, Ghirotti M, Girelli VA, Lucente CC ,Tini MA, Borgatti L (2016) Back Analysis of the 2014 San Leo Landslide Using Combined Terrestrial Laser Scanning and 3D Distinct Element Modelling. Rock Mechanics and Rock Engineering. 49(6): 2235-2251.

Spreafico MC, Cervi F, Francioni M, Stead D, Borgatti L (2017) An investigation into the development of toppling at the edge of fractured rock plateaux using a numerical modelling approach. Geomorphology. 288:83-98.

Vlcko J (2004) Extremely slow slope movements influencing the stability of Spis Castle UNESCO site. Landslides. 1: 67-71.

Viero A Teza G Massironi M Jaboyedoff M Galgaro A 2010 Laser scanning-based recognition of rotational movements on a deep seated gravitational instability: The Cinque Torri case (North-Eastern Italian Alps). Geomorphology. 122: 191-204.

Zerathe S Lebourg T (2012) Evolution stages of large deep-seated landslides at the front of a subalpine meridional chain (Maritime-Alps France). Geomorphology. 138:390-403.

Zischinsky U (1969) Über Sackungen. Rock Mechanics. 1: 30.

Zorzi L, Massironi M, Surian N, Genevois R, Floris M (2014) How multiple foliations may control large gravitational phenomena: a case study from the Cismon Valley Eastern Alps Italy. Geomorphology. 207: 149-160.

Stože landslide triggering simulation using LS-Rapid simulation model

Jošt Sodnik[1,2], Matej Maček[1], Matjaž Mikoš[1]

1) University of Ljubljana, Faculty of Civil and Geodetic Engineering, Jamova c. 2, 1000 Ljubljana, Slovenia
2) TEMPOS, environmental civil engineering, Ltd., Ljubljana, Slovenia, jost.sodnik@gmail.com

Abstract The LS-Rapid simulation model was applied to analyse the triggering of the 2000 Stože landslide that transformed into debris flow and damaged the village Log pod Mangartom. The modelling process and preparation of input data is described herein. Due to some limitations of the triggering model, additional tools were developed to overcome them. Limiting boundaries for key soil input parameters were proposed to help with preparation of the modelling data. The simulation revealed good agreement between the modelling results and the parameters of the surveyed landslide. We compared the triggering mechanism, the landslide volume, and its source and deposition areas. Since landslides are potential debris flow sources, estimating landslide volumes can be a key factor in estimating the magnitude of debris flow in the larger process of assessing debris flow hazards.

Keywords landslide, simulation, triggering, debris flow

Introduction

In November 2000, after over 40 days of intense rainfall, the Stože landslide (Fig. 1) was triggered (Mikoš et al. 2004). On November 15, in the first phase, a relatively dry debris landslide mass was halted in the channel of the Mangartski potok torrent. A debris landslide was triggered at an altitude between 1200 and 1600 m.a.s.l. In its second phase, on November 17, the deposited landslide mass was wetted by the inflowing water in the torrent (Mikoš et al. 2002), and turned into a wet debris flow that destroyed part of the village of Log pod Mangartom and caused 7 casualties (Mikoš 2011). The Stože landslide was one of the most devastating landslides in Slovenia of the past century.

The second phase of the wet debris flow was investigated by applying debris flow numerical modelling in order to assess debris flow hazards in the area, under the assumption that potential debris flows can be triggered on the Stože slope (Fazarinc 2002; Hojnik et al. 2001; Četina et al. 2006). The triggering phase was not investigated in detail, and the results of such a study that used landslide-triggering simulation would be useful for investigating potential landslides as debris flow sources. In this study, the LS-Rapid model was used to simulate triggering of the Stože landslide (the first phase of the 2000 event), and to compare simulation results with the field observations.

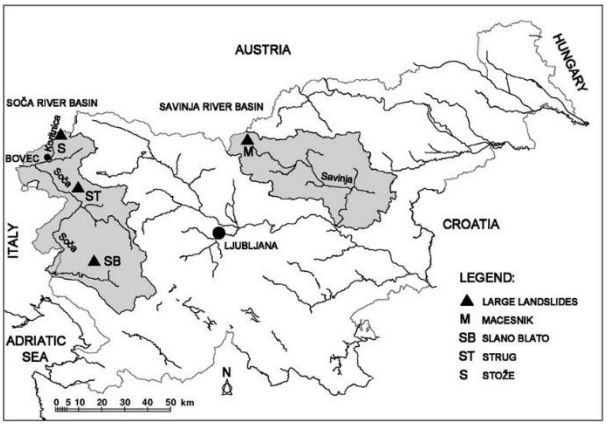

Figure 1 Location of the Stože landslide (Mikoš et al., 2004)

The LS-Rapid model was developed to assess the initiation and motion of landslides triggered by earthquakes, rainfalls or the combined effect of both. Models can simulate the entrainment of unstable deposits along the runout path, which serves to increase landslide volumes and hazard areas. The LS-Rapid model and the theoretical background behind it are described in detail in Sassa et al. (2010). A sensitivity analysis was carried out to determine the influence of estimated model parameters on the landslide volume.

The Stože landslide

On 15 November 2000, the Stože landslide was triggered as a relatively dry debris slide (1st phase), and then, on 17 November 2000, turned into a wet debris flow (2nd phase). The main cause of the Stože landslide was prolonged heavy rainfall. Rainfall at the village of Log pod Mangartom was measured at 1638 mm over the previous 48 days, which presents a recurrence interval of more than 100 years. In the first phase, a "dry" debris slide was triggered on the slope and the landslide mass stopped in the Mangartski potok torrent channel with a slope of 9°. Over the next 36 h, the landslide mass was additionally wetted by heavy rainfall and direct water inflow from the Mangartski potok. Early on 17 November 2000, a second event occurred: the previously deposited landslide mass turned into a wet debris flow that travelled approximately 5 km. On its way the debris flow destroyed 6 houses, severely damaged 23 houses and caused 7 casualties in the village of Log pod Mangartom. The simulated debris flow

velocities in the steepest part of the Mangartski potok channel of 45° reached as high as 60 km/h (Četina et al. 2006).

Immediately after the catastrophic event, the whole landslide area was mapped in the field, establishing an engineering geological map of the Stože landslide area with the main landslide features at a scale of 1:2500. The Stože slope inclined from 20° to 30° in the NS direction and consisted of permeable cracked dolomite covered in its lower and middle parts by unstable moraine sediments (low permeable silt with gravel that predominated in the debris flow) and in its upper part by highly permeable scree deposits. The area west and east of the landslide consists of a dolomite formation. The geological underground was further investigated using field geophysical methods such as ground seismometry, ground radar, and through the geological description of drilled cores from several structural boreholes in the landslide area and in the channel of the Mangartski potok torrent (Mikoš et al 2004).

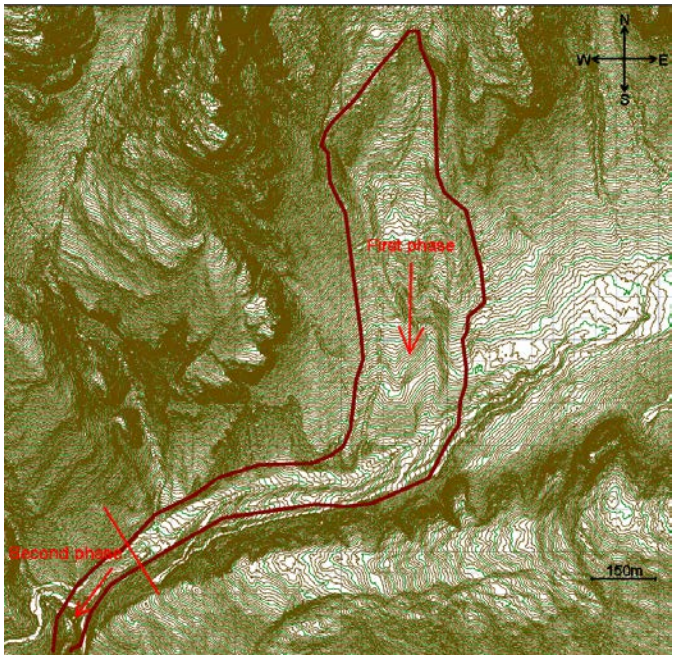

Figure 2 Pre-event topography of the case study area showing the contour of the Stože landslide.

The LS-Rapid simulation model and simulations of the Stože landslide triggering

Input data and parameters

A new LiDAR-based DTM with a resolution of 1 m was used to generate the topographic data for the Stože debris flow numerical model. The DTM was employed manually on-site using CAD tools corrected to the original state before the 2000 event based on topographic maps at scale 1:5000. Combining the data from both in CAD tools created a pre-event topography of the triggering area that could be used in the simulation model (Fig. 2).

The Basic Geological map of Slovenia at scale 1:100.000 was used to determine geological units and soil parameters for the LS-Rapid model (Fig. 3). Soil parameters and the depth of unstable mass for each geological unit on the Stože slope were assessed based on the geotechnical laboratory test results and expert judgement.

With the aid of additional topographical analysis we determined geological units where terrain slope exceeds the angle of internal friction of the soil. In reality, these areas consist in steep, bare weathered rock with no or only sporadic soil cover and are more prone to rock falling than sliding.

After this analysis, the two "potentially active" geological units were described as "scree material" and "moraine". Soil parameters for these two units were assessed (Tab. 1). To determine τ_{ss} (steady state shear resistance at the sliding surface) the model's authors suggested using an undrained ring-shear apparatus of this type, such as ICL-1 to ICL-3 (e.g. Oštrić et al. 2012).

No tests were performed in a ring shear apparatus, since it was not available at the time of the laboratory

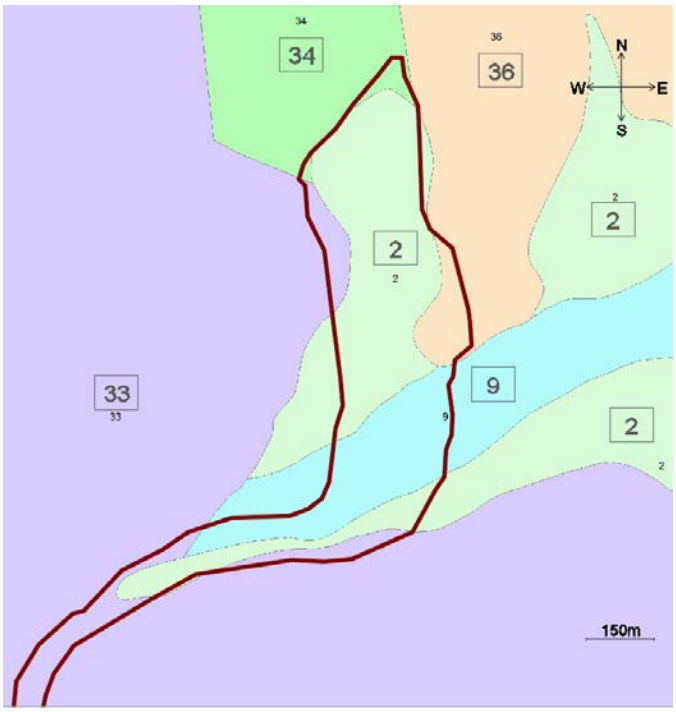

Figure 3 Geological map of the area: 33 – bedded dolomite; 34 – limestone, marlstone, dolomite; 36 – massive or bedded dolomite; 2 – Scree; 9 – moraine.

testing and has limitations in terms of the specimen's maximum grain size (2 mm). More than 60% of the landslide material has a grain sizeover 2 mm (Maček et al. 2017). Due to these limitations, the following relationship wasproposed (equation 1) between τ_{ss} and τ_p (peak shear resistance before failure) based on professional judgement:

Table 1 Soil parameters used in the triggering simulation with LS-Rapid

Parameter	Scree material	Moraine
K_0	0.50	0.5
φ_i (°)	40	36
φ_m (°)	40	36
τ_{ss} (kPa)	190	190
B_{ss}	1.0	1.0
φ_p (°)	42	37
c_p (kPa)	5.0	25
γ (kN/m^3)	22	23

where K_o is lateral pressure ratio, φ_i friction coefficient inside landslide mass, φ_m friction coefficient during motion at sliding surface, τ_{ss} steady state shear resistance at sliding surface, B_{ss} rate of excess pore-pressure generation, φ_p peak friction coefficient at sliding surface, c_p peak cohesion at sliding surface and γ unit weight of mass.

$$\tau_{SS} \approx 0{,}45\tau_p \xrightarrow{upto} 0{,}65\tau_p \qquad [1]$$

Based on the available borehole data, a soil depth (potentially unstable mass) of 30 m was used in the model for both geological units. For better representation of the real conditions, a "smoothing" function was applied to ensure a smooth increase at the landslide edges from 0 to 30 m in the middle of the debris slide area.

The LS-Rapid model includes two triggering factors: earthquakes and pore pressure. In the case of the Stože landslide, increased pore pressures triggered the landslide. The LS-Rapid model uses pore pressure ratio (r_u) to determine pore pressures in the landslide body.

$$r_u = \frac{h_w * \gamma_w}{h_m * \gamma_m} \qquad [2]$$

Therefore, r_u of 0.3, based on equation 2 presents approx. water table at 67%-layer height and r_u of 0.45 represents water table at ground surface. In our simulations, r_u of 0.3 was used as one of the possible realistic scenarios. On the other hand, r_u of 0.45 represents full saturation and the so-called "worst case scenario".

Triggering simulation

Fig. 4 shows model topography with unstable mass (scree and moraine). Other model parameters were set as follows: simulation time of 100 s with a time step of 0,005 s, shear displacement at the point of failure DL = 1 mm, and reduction at the end of shear strength of DU = 1000 mm.

The aim of the simulation was to analyse the triggering phase of the Stože landslide and to compare the modelling results with the contour of the surveyed landslide, traveling distance of the first phase e.g. "dry" debris slide and landslide volume. A sensitivity analysis of the τ_{ss} and r_u parameters was carried out to determine the influence of each parameter on the simulation results and to determine the soil parameters of the model that is closest to real landslide behaviour as given in Tab. 1.

Results

The user is given the opportunity to define the visualisation option of the simulation results. We chose to use coloured balls. On the images with the results, the blue colour represents a potentially unstable mass at the beginning of the simulation (no movement of the mass). Final simulation depths of the unstable mass are shown in various red colours. The orange / light-red colour is used for thin layer of the unstable mass, and dark red for the thick layer of the unstable mass. The exact values of the final simulated depths of the material can be found in the model's text output files. This data was used to calculate the landslide volume.

Contour of the Stože landslide

A comparison of the final simulated landslide area and the surveyed landslide contour after the 2000 event is presented in Fig. 5, and shows good agreement between the results and the surveyed contour.

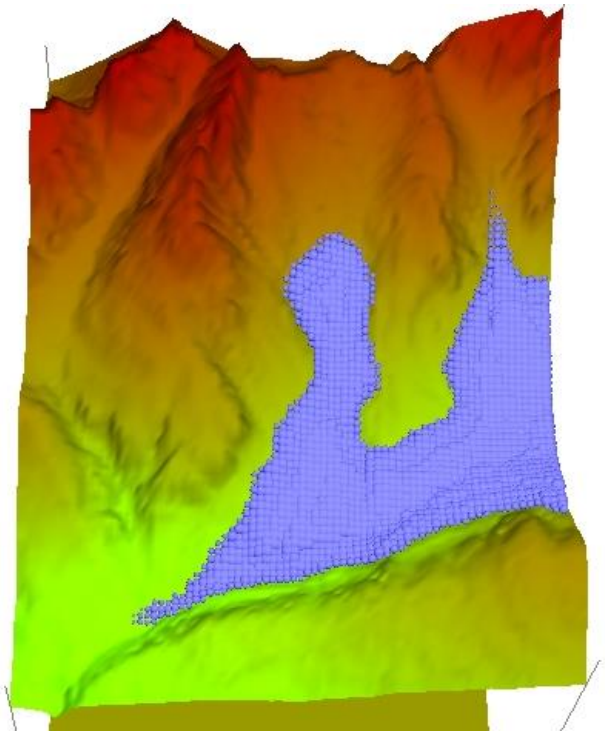

Figure 4 LS-Rapid model topography and unstable mass (view direction: N).

In the upper part of the Stože landslide, the simulated area is narrower than the real contour, most likely due to inaccuracy of the basic geological map and therefore lower accuracy of the position and surface of each geological unit. In the lower part of the Stože landslide, the simulated area is wider than the observed contour. The reason for this difference can be found in differences of the geological situation between the model and field situ-

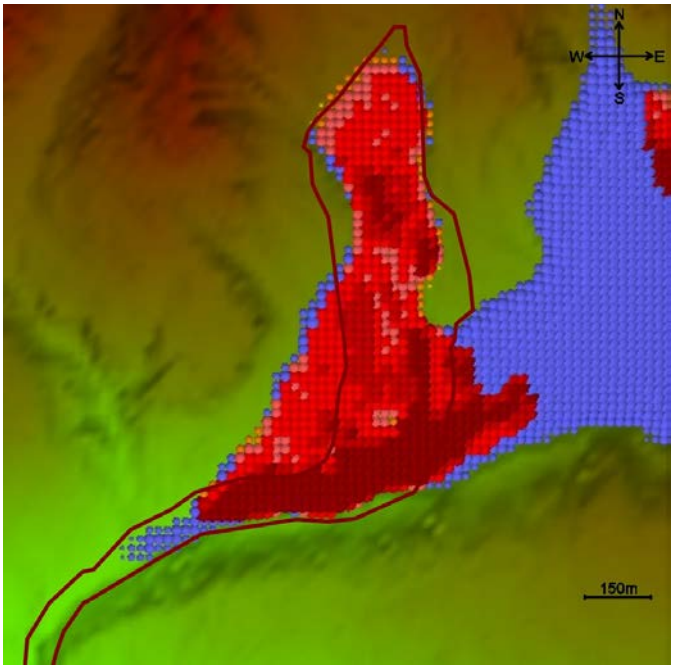

Figure 5 Results of the LS-Rapid model compared with the surveyed debris slide contour.

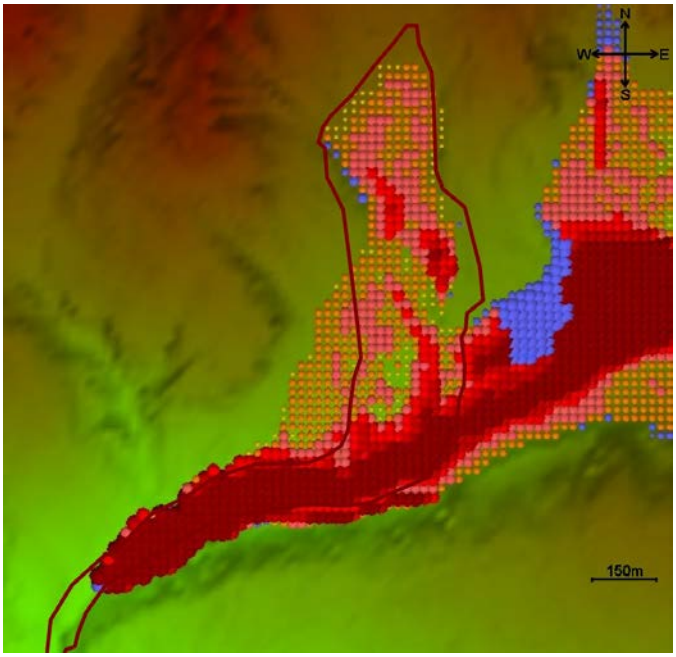

Figure 6 Model with the correct traveling distance (stopping point of the debris slide mass, model with lower τ_{ss} value) of the Stože landslide.

ation or also in the fact that some of the areas are very prone to sliding, but in the November 2000 event, they did not move. Some unstable areas outside of the landslide (the upper right part in Fig. 5) could be found, but can also be related to the fact that this small unstable area lies at the model border where are not fully regular simulation conditions.

Traveling distance of the Stože landslide

In the phase 1 the Stože debris slide travelled to the small bridge over the Mangartski potok (Mlinč). The final model results (Fig. 5) show stopping of the landslide mass upstream of the bridge, but the model with lower τ_{ss} (125 kPa) shows good agreement from that point of view (Fig. 6). The model with τ_{ss} = 125 kPa is however unsatisfactory in other comparisons (area, volume). It is possible that lower τ_{ss} values that are needed to stop the debris slide at the bridge and not upstream as in the modelling result, are caused by additional water inflow from the Mangartski potok, which lowers the τ_{ss} values on the field and cannot be modelled in the simulation.

Another specific characteristic of the first phase of the Stože landslide were the conditions on the left bank of the Mangartski potok, where the landslide travelled across the Mangartski potok channel and damaged the Mangartski potok, where the landslide travelled across the Mangartski potok channel and damaged the local road to the Mangart Mountain. Fig. 7 shows the final simulation conditions/results on the Mangartski potok left bank, where the flow super elevation is clearly seen. The red balls represent the thickness of the material. The dark red part is the thickest area and the light red the thinnest. The exact thickness of the material can be seen in the matrix output data of the model. The blue colour represents a potentially unstable mass that did not move during the simulation process. A computational grid 20m x 20m was selected.

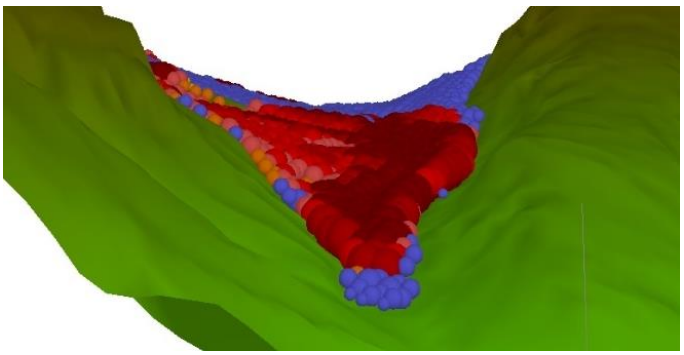

Figure 7 Mangartski potok, left bank final simulation conditions (view direction of ENE).

The Stože landslide volume

A reliable estimation of the landslide volume is very important in the process of debris flow hazard assessment, since the landslide mass presents an important source of material for the following debris flows. In the process of volume estimation, values for τ_{ss} and r_u were varied and the landslide volume for each combination was calculated (Tab. 2). All other parameters of the model remained the same as given in Tab. 1.

Landslide volume was calculated using matrices of the input topography and the final simulated topography, respectively. The estimated volumes of the Stože landslide

Table 2 τ_{ss} and r_u combinations with landslide volume calculations.

τ_{ss} (kPa)	r_u	Volume (m^3)
150	0.2	2,480,00
200	0.2	735,000
250	0.2	51,000
150	0.3	2,460,000
180	0.3	1,547,000
190	**0.3**	**1,195,000**
195	0.3	990,000
200	0.3	775,000
250	0.3	72,000
200	0.35	800,000
150	0.4	2,470,000
200	0.4	825,00
250	0.4	105,000

after the event were according to Rajar et al. (2001): mobilized volume: 1,580,000 m^3; material deficit volume: 1,200,000 m^3; material stopped inside debris slide triggering area: 380,000 m^3, and according to Četina et al. (2006): 1,200,000 m^3.

A comparison of the estimated volumes and the simulation results show that the best agreement is found with τ_{ss} of 190 kPa and r_u of 0.3 with a simulated volume of 1,195,000 m^3. With τ_{ss} of 190kPa we confirmed our proposed τ_{ss} = 0.45 and τ_p = 0.45 x 421kPa = 189kPa (Eq. 1). The best agreement with the real landslide volume is obtained using the lowest boundary of τ_{ss} proposed by Eq. 1, while the upper limit gives unrealistically low landslide volumes.

Simulation and model issues

The first issue with the LS-Rapid model is the matrix-based system with the matrix-based "user-unfriendly" data input. That problem becomes important when considering geologically heterogeneous areas where each geological unit has different parameters and the manual data input becomes very time consuming and inaccurate. To solve this problem, we developed an MS Excel-based application for the preparation of the matrix. Additional functions were implemented in the preparation of the matrix: as mentioned previously a "smoothing" function was employed to ensure a linear transition between two soil materials with different unstable mass depths.

The second important issue with the model is that only one pore pressure ratio value can be used as the triggering factor for the whole area covered in the model. Again, with geologically heterogeneous areas this becomes an important issue, since according to Eq. 2 not all units have the same specific weight (for instance scree and fine grain materials), therefore r_u factor is not comparable. To overcome this issue, we propose that the angle of internal friction of the fine-grained geological units be reduced in the model, as follows:

$$\mathrm{tg}\varphi_{\mathrm{model}} H\gamma\left(1 - r_{u,\mathrm{model}}\right) \approx \mathrm{tg}\varphi H\gamma\left(1 - r_u\right) \qquad [3]$$

where ϕ is friction angle, ϕ_{model} is the angle of internal friction used in the model, γ is the unit weight of the landslide mass, H is the depth of the slip surface, r_u is the pore pressure ratio, and $r_{u,model}$ is the pore pressure ratio used in the model.

Determination of τ_{ss} should be performed using a LS-Rapid linked ICL -1 to ICL-3 ring shear apparatus. The maximum grain-size limitation of this apparatus (D_{max}=2 mm) is an important issue when modelling landslides in the Alpine areas with prevailing gravel materials. This limitation in determining exact material parameters introduces a degree of uncertainty into the performed calculations – especially when modelling potential events where model validation is not possible.

Discussion

Debris flows represent a serious hazard in Alpine regions, including Slovenia, and debris flow hazard assessments should be properly implemented in spatial planning and land use management procedures. Since landslides often represent a source of debris flow and the landslide volume is the main factor in estimating the magnitude of debris flow, landslide-triggering simulations represent an important part in debris flow hazard assessment. The results of our study suggest that good estimations of key parameters and input data can result in good agreement between simulation results and field observations. However, large discrepancies between the modelled and observed landslide volumes were observed for different soil parameters. With this knowledge and experience, such an approach could also be used to simulate potential landslides and to estimate the magnitudes of potential debris flows, taking into account the possible range of volumes.

As regards input data, we found a lack of accuracy in the geological maps at scale 1: 100,000. These maps should be improved and prepared at smaller scale (e.g. 1:10,000/1:25,000) and should include data on depth of soil cover. Another, more expensive option is to carry out a detailed geological mapping of each potential debris flow hazard area.

On the other hand, the proposed approach to landslide-triggering simulation, where only pore pressure is considered as the triggering factor, suggests an opportunity for further development of the model and a link between the triggering model and the hydrological model. This way, triggering pore pressures could be linked with hydrological processes such as precipitation, infiltration, direct runoff, and evapotranspiration, and in the final phase of determining critical precipitation or precipitation triggering threshold.

Acknowledgments

The study was financially supported in part by the Slovenian Research Agency, grant P2-0180.

References

Četina M, Rajar R, Hojnik T, Zakrajšek M, Krzyk M, Mikoš M (2006) Case Study: Numerical Simulations of Debris Flow below Stože, Slovenia. Journal of Hydraulic Engineering. 132(2): 121-130.

Fazarinc R (2002) Mathematical modelling of a debris flow in Log pod Mangartom . Magistrsko delo, Univerza v Ljubljani, Fakulteta za gradbeništvo in geodezijo, Ljubljana, Slovenia. 169 p. (in Slovene)

Hojnik T, Četina M, Krzyk M, Rajar R (2001) A two-dimensional model of a debris flow in the area of Zgornji and Spodnji Log _In: 12. Mišičev vodarski dan, Maribor, 13.december 2001 : zbornik referatov. Vodnogospodarski biro, Maribor, Slovenia. pp. 84-91. (In Slovene)

Maček M, Smolar J, Petkovšek A (2017) Influences of rheometer size and the grain size on rheological parameters of debris flow. In: Mikoš, M., Tiwari, B., Yin, Y., Sassa, K. (eds.): Advancing Culture of Living with Landslides. Vol. 2, Advances in Landslide Science. Springer, Cham. (ISBN: 978-3-319-53497-8). pp. 399-406.

Mikoš M (2011) Public Perception and Stakeholder Involvement in the Crisis Management of Sediment-Related Disasters and their Mitigation: the Case of the Stože Debris Flow in NW Slovenia. Integrated environmental assessment and management. 7(2): 216-227.

Mikoš M, Vidmar A, Šraj M, Kobold M, Sušnik M, Uhan J, Pezdič J, Brilly M (2002) Hydrologic analyses of the Stože Landslide below Mt. Mangart . UJMA. 16: 326-334. (in Slovene)

Mikoš M, Četina M, Brilly M (2004) Hydrologic conditions responsible for triggering the Stože landslide, Slovenia. Engineering geology. 73(3/4): 193-213.

Oštrić M, Ljutić K, Krkač M, Setiawan H, He B, Sassa K (2012) Undrained ring shear tests performed on samples from Kostanjek and Grohovo landslide. In: Sassa K, Takara K, He B (eds.) Proceedings of the IPL symposium, 20-23 November 2012. Kyoto, Japan. pp. 47–52.

Rajar R, Hojnik T, Četina M, Zakrajšek M, Krzyk M (2001) A one-dimensional model of a debris flow in the area of Log pod Mangartom. In: 12. Mišičev vodarski dan, Maribor, 13.december 2001 : zbornik referatov. Vodnogospodarski biro, Maribor, Slovenia. pp. 92-101. (In Slovene)

Sassa K, Nagai O, Solidum R, Yamazaki Y, Ohta H (2010) An integrated model simulating the initiation and motion of earthquake and rain induced rapid landslides and its application to the 2006 Leyte landslide. Landslides. 7(3): 219-236.

Identification of potentially unstable rock blocks on the road cut in the Krka National park, Croatia

Marin Sečanj[(1)], Sanja Bernat Gazibara [(1)], Snježana Mihalić Arbanas [(1)], Martin Krkač[(1)], Mariana Martinko[(1)], Željko Arbanas[(2)]

1) University of Zagreb, Faculty of Mining, Geology and Petroleum Engineering, Pierottijeva 6, 10000 Zagreb, Croatia, marin.secanj@oblak.rgn.hr

2) University of Rijeka, Faculty of Civil Engineering, Radmile Matejčić 3, 51000 Rijeka, Croatia

Abstract In this paper, the visual and semi-automatic identification of potential rock fall source areas and unstable rock blocks on the cuts and slopes along 900 m section of the frequent trafficked Kistanje-Oklaj county road in the Krka Nation Park, Croatia is presented. The identification of discontinuities was conducted using conventional field mapping and by interpreting digital surface models derived from the high-resolution point cloud data obtained using the terrestrial laser scanning and unmanned aircraft system (TLS and UAS). Split-FX software was used to extract discontinuity surfaces semi-automatically from the point cloud data. Spatial kinematic analysis was performed for each triangle of TIN surface model of the investigated cuts and slopes in order to identify locations of possible instability mechanism. The aim of the paper is to identify the most critical parts on the cuts and slopes for the occurrence of plane, wedge, flexural and block toppling failures using the Kinematic Hazard Index (KI). Verification of identified rock fall areas is performed by visual inspection of hazardous blocks in the point cloud model. Identified rock fall prone areas, unstable blocks and probable instability mechanisms on the investigated road cut and slopes above provide the input data used to determine critical positions for further deterministic slope stability analysis. It is concluded that the KI is a useful tool for zonation purposes in the early phases of detailed investigations that are necessary for the design of rock slope protection measures.

Keywords Rock fall, Split-FX, Discontinuity extraction, Kinematic Hazard Index, Krka National park (Croatia)

Introduction

Rock falls are a common phenomenon on the steep slopes and road cuts in the Dinarides (Mihalić Arbanas et al. 2017). They are the result of unfavourable characteristics of the rock mass, weathering in combination with heavy rainfall and anthropogenic factor (Arbanas et al., 2012). One typical example is the Kistanje-Oklaj county road, which is frequently threatened by rock falls. To reduce the risk of injury or death and to prevent damage to infrastructure, it was necessary to design rock slope protection measures that included detailed geotechnical investigations and identification of potential rock fall source areas on the road cut and slopes above.

Traditional surveys require direct access to the rock face to collect all relevant discontinuity parameters necessary for the identification of areas on the cuts and slopes that are prone to rock falls, and to identify potentially unstable rock blocks. As the entire rock mass is not accessible it is necessary to employ remote sensing techniques to rapidly obtain information for the inaccessible areas. Over the past years many authors have been working on techniques by which to extract rock mass structural data from remotely acquired high resolution point clouds (Slob et al. 2005; Jaboyedoff et al. 2007; Gigli and Casagli 2011; Lato and Vöge 2011; Cacciari and Futai 2016), and some of them have been working on identification of rock fall source areas from surface models created from the point clouds (Günther et al. 2012; Gigli et al. 2012; Fanti et al. 2013). Using these approaches, rock mass structural data related to the investigated road cut and slopes can be quickly obtained, along with the relatively accurate identification of potentially unstable rock blocks.

Study area

The investigated road cut (Fig.1) is located in the Krka National park, Croatia, on the frequently trafficked county road, which is the only connection between the villages of Kistanje and Oklaj. Local residents and tourists are endangered by rock falls due to the location of the road, which cuts in to the old canyon bank of the Krka River.

The Investigated road cut, including the slope above it, are situated in the core of the anticline, which is built of the Eocene-Oligocene Conglomerates and Breccia i.e. the Promina Deposits (Grimani et al., 1972). The complexity of the geological-structural setting, which is the result of faulting and folding in the area, led to the formation of numerous discontinuities in rock mass as well as unstable, unfavourably oriented rock blocks with the potential to cause rock falls. Moreover, the investigated area is in the near proximity of the seismically active Knin area, which definitively increases the potential for rock falls in the area.

The endangered section of the road is around 900 m

Figure 1 View of the investigated road cut located on the bank of the Krka River in the National park Krka

long where the investigated road cuts and slopes cover the total area of around 4.2 ha. The height of the road cut varies from around 2-15 m, while the slope above it extends even further, from around 5 up to 40 m of height in some places.

Most of the slopes beside the road dip towards the SW, S and W (Fig. 2a). The average dip angle of the slopes above the road cut varies from about 5° in the NE part up to 45° in the SW part of the investigated area. The dip angle of the road cut face is commonly >60° (Fig. 2b). During the engineering geological mapping, numerous sets of discontinuities with unfavorable orientation and potentially unstable and detached rock blocks were detected using the probable instabilities mechanism commonly related to wedge failure as well as to plane failure and toppling.

Methodology

Detailed engineering geological mapping was carried out on limited parts of the rock mass of the road cut that were accessible. Because not all of the area is accessible, mapping of the entire rock mass with the extraction of relevant geometrical properties was carried out using remote sensing on a high-resolution point cloud.

In order to create high-resolution point cloud, field surveying and collection of spatial data was performed using the phase-shift terrestrial laser scanner (TLS) and the unmanned aircraft system (UAS). TLS was used to survey the road cut, while UAS photogrammetry method (Haala et al., 2011) was used to measure inaccessible parts of the slopes above the road cut as well as those on the road cut which could not be measured with TLS. A unique georeferenced point cloud was obtained based on registration and vegetation filtering. The point cloud was composed of about 150 million points with an average point resolution of 2 cm or 2,500 points per square meter. A triangulated irregular network (TIN) and digital elevation model (DEM), with 1x1 m resolution were generated from the point cloud. Point cloud processing and extraction of structural data, including discontinuity orientation and spacing, was performed using the Split-FX software (Split Engineering LCC 2007).

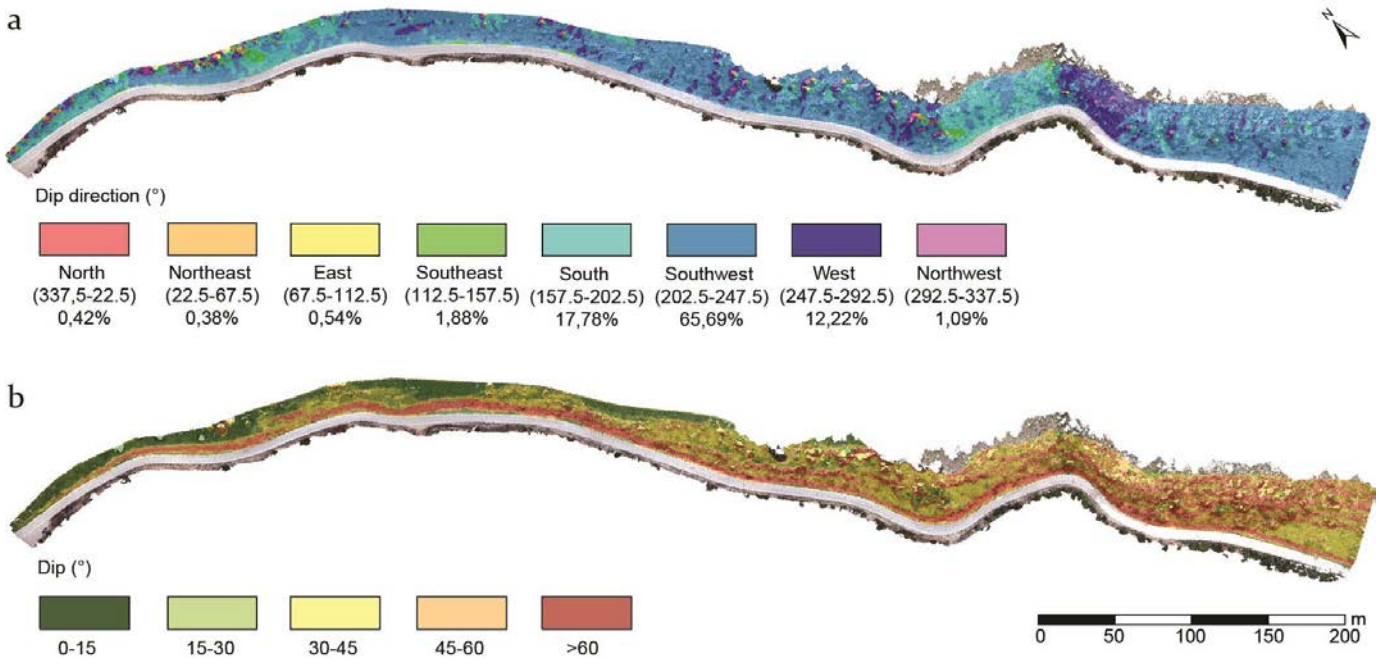

Figure 2 Distribution of investigated rock mass surface dip direction (a) and dip values (b) extracted from DEM with 1x1 m resolution.

From the point cloud a triangulated surface, i.e., mesh surface was created. In order to construct a high-quality mesh surface, it was necessary to adjust instrument view, i.e., scan line needed to run perpendicular to the rock face, because it was not set properly prior to the point cloud processing. Patches, which represent discontinuity planes (Fig. 3), were automatically generated by grouping neighbouring mesh triangles that fit the flatness criteria, and afterward by fitting a plane through the points bounded by the grouped triangles.

The best result from the automatically generated patches were obtained when the mesh surface was created from 10,000 triangles per meter and the minimum patch size was set to 10 mesh triangles with the maximum patch neighbour angle of 10°.

Figure 3 Automatically generated patches plotted on the point cloud in Split-FX software.

In order that the data represented would be valid noisy patches were excluded and all unrecognized discontinuities were inserted manually onto the mesh surface. For those discontinuities that only had their traces visible on the rock face, the best fitting plane were assigned to them and their orientation extracted. In the end, a total of 1,260 discontinuity planes were extracted. The orientations of discontinuities are presented as poles on the stereonet plot, and using the cluster analysis 7 discontinuity sets were determined (Fig. 4). The mean orientation values of discontinuities sets are listed in Tab 1. The areas prone to rock fall along the investigated road cut and slopes above it were identified using kinematic analysis, owing to its ability to determine whether a specific instability mechanism is kinematically possible, taking into consideration the geometry of the slope and related discontinuities.

Table 1 Discontinuity set mean orientation and standard deviation extracted from the semi-automatic analysis in Split-FX software.

Discontinuity set	α (°)	β (°)	σ (°)
Jn1	33	39	11.2
Jn2	203	88	14.7
Jn3	251	79	13.2
Jn4	281	75	11.2
Jn5	218	56	6.2
Jn6	310	81	6.7
Jn7	246	35	13.5

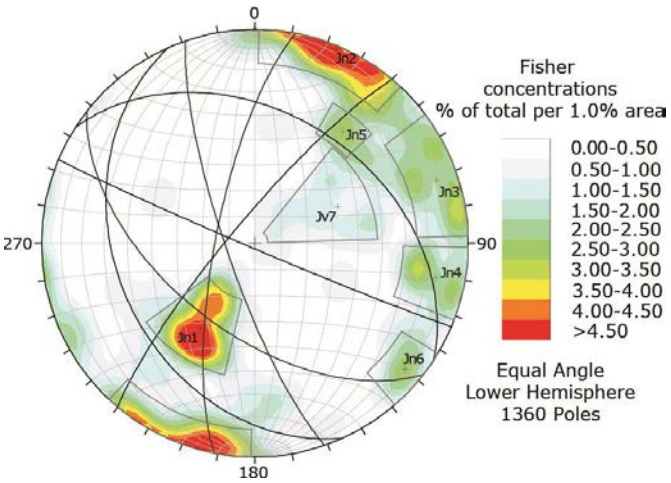

Figure 4 Stereographic projection of discontinuity poles and mean orientation of discontinuity sets extracted with the Split-FX software.

The instability mechanism investigated using this method were plane and wedge failure (Hoek and Bray 1981) and flexural and block toppling (Goodman and Bray 1976; Hudson and Harrison 1997).

For each instability mechanism, the Kinematic Hazard Index, KI (Casagli and Pini 1993) was calculated by counting poles, discontinuities and their intersections that fell into critical areas within the stereographic projection. KI is calculated using equations (1), (2), (3) and (4):

$Cpf = 100 \times (Npf / N)$ for plane failure, (1)
$Cwf = 100 \times (Iwf / I)$ for wedge failure, (2)
$Cbt = 100 \times (Nbt / N) \times (Ibt/I)$ for block toppling and (3)
$Cft = 100 \times (Nft / N)$ for flexural toppling, (4)

where *Npf*, *Nbt* and *Nft* are number of poles kinematically satisfying the conditions of plane failure, block toppling and flexural toppling. Iwf and Ibt are the number of intersections satisfying conditions for wedge failure and block toppling, while N and I are the total number of poles and intersections respectively.

The input parameters for the kinematic analysis are: the orientation of the slope (dip and dip direction obtained from the surface model), the discontinuity surface orientations (obtained from the point cloud in Split-FX software), and the average value of discontinuity friction angle accepted as 38°.

Spatial kinematic analysis is performed for each triangle or raster cell of the surface model. A similar approach has been used previously by several authors (Gigli et al. 2012; Fanti et al. 2013; Sdao et al. 2013). For these purposes, TIN surface was created using minimum thinning method from the point cloud model. This method was used to reduce the effect of vegetation leftovers after point cloud data filtration. For each triangle of the TIN surface model, geometrical properties of slope and discontinuities were assigned, and spatial kinematic analysis was performed. It is important to note that only discontinuities that were extracted from the point cloud were taken into account in this analysis. Minor or irregular fractures were not considered, which implies that the probability of instabilities in those areas is underestimated.

Results

The results of spatial kinematic analysis for each of the analysed instability mechanism are presented in the Fig. 5. The investigated slopes of the road cut demonstrate high probability for the occurrence of kinematic instability mechanisms with a maximal KI up to 33% for wedge failure (Fig. 5b). The areas with higher KI are generally located at the steepest parts of the slope facing W and SW. Natural slopes above the road cut show lower KI values because they dip at a gentler angle, with the exception of the far SE part of the investigated area, where the slopes are steeper, which is reflected in the higher KI values. The maximum KI related to plane failure is about 15% (Fig. 5a), while for flexural toppling its approx. 17% (Fig 5c). The kinematic analysis has shown that block toppling is the least likely mechanism to occur, with the maximum KI values of about 2%. Owing to the small KI values for the block toppling, changes in value could not be presented in the scale of the map in Fig 5.

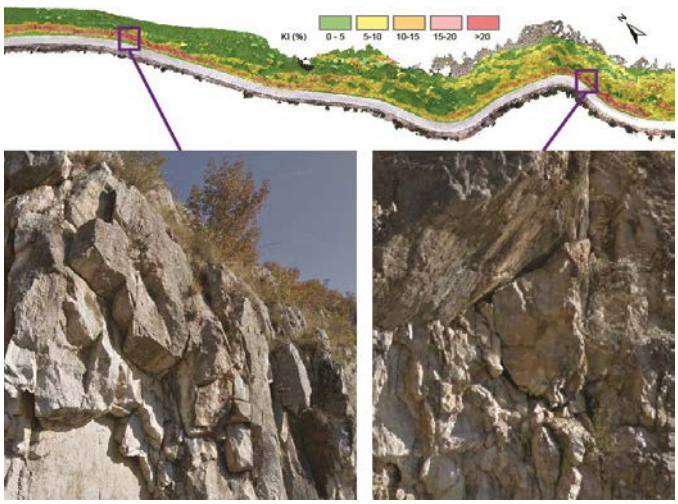

Figure 6 Example of identified potentially hazardous rock blocks from the grouped areas with higher kinematic index values.

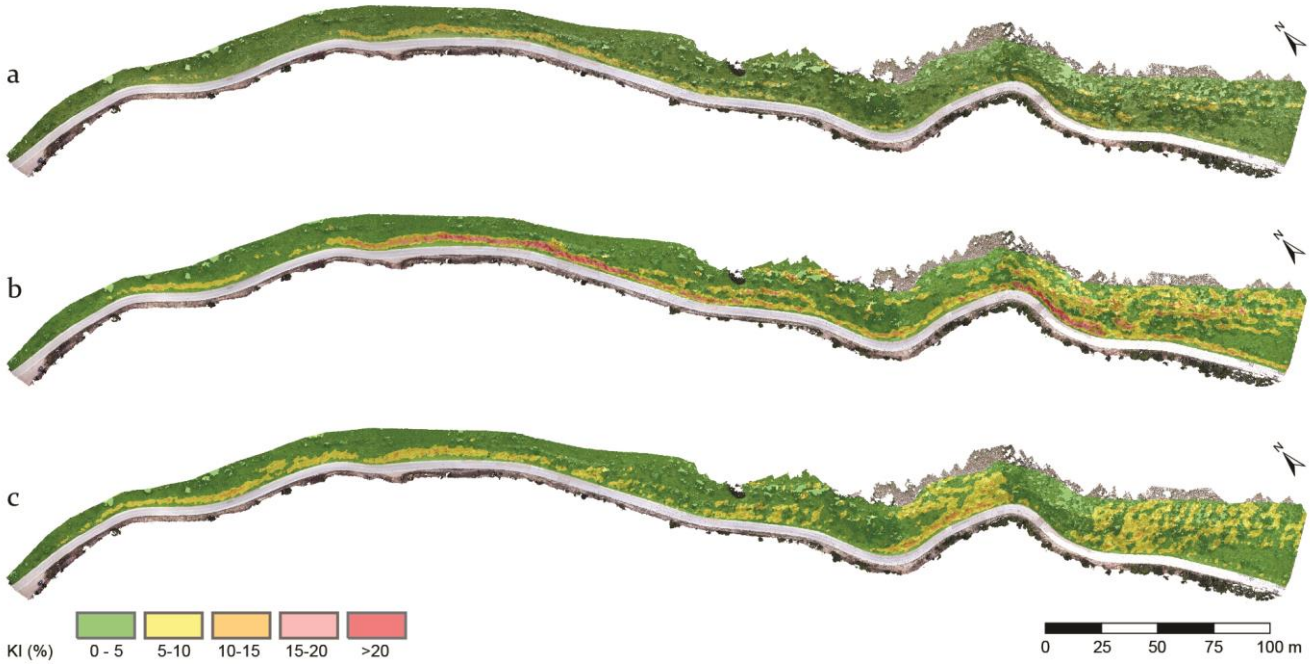

Figure 5 Results of the kinematic analysis. The higher the Kinematic Hazard indexes (KI), the higher the probability that the analysed instability mechanism will take place: (a) plane failure, (b) wedge failure and (c) flexural toppling.

The probability of instabilities is expressed by the colour scale, which varies from green to red as the KI increases. Areas with high KI were grouped as rock fall prone areas.

By comparing the location of identified rock fall prone areas with the corresponding areas on the point cloud, potentially hazardous rock blocks could be identified (Fig. 6). Block volumes vary from 0,1 up to 3,5 m^3; and with the future weathering or seismic shocks, these rock blocks could likely become detached.

Discussion and conclusion

The main advantages of the approach presented in this paper are rapid and objective analysis. The remote sensing technique allows for the quick retrieval of a high-resolution point cloud of the rock slope surfaces, and provides information for the inaccessible parts of the road cut and the slopes above it. Semi-automatic discontinuity surface extraction, along with spatial kinematic analysis
represent a fast and objective method for assessing rock fall prone areas and the potentially unstable rock blocks in them, including information whether a certain instability mechanism is probable. Field observation also confirmed the results of this analysis (Fig. 6).
On the other hand, there are some drawbacks in the presented approach. The accuracy of some parts of the created mesh surface is questionable, owing to the shadowed areas. For better, more accurate results the shadowed areas should be rescanned and the analysis reapplied. Also, in the spatial kinematic analysis all extracted discontinuities were used, whether they appear on some parts of the slope or not, thereby possibly underestimating or overestimating Kinematic Hazard Index values in certain parts.

For more reliable KI values, the slopes should be divided into quasi-homogeneous zones according to slope geometrical properties and structural-geological setting. Spatial kinematic analysis should then be applied for each quasi-homogeneous zone, with discontinuity sets that belong to that particular zone. Furthermore, it was not possible to determine all discontinuity friction angle values; as a result average values from existing data were used in the analysis. Because the discontinuity friction angle value can vary depending on the conditions related to the discontinuities, applying average values in the analysis may have led to overestimating or underestimating of the KI values in certain parts.

The approach using Kinematic Hazard Index is a useful tool in preliminary rock fall hazard assessment, with the following serious limitation related to the application of such. The results of spatial kinematic analysis present zones that exhibit varying degrees of rock slope instabilities, without an indication of rock slope factor of safety (Fs). Slope stability analysis in the zones with high KI values can result in Fs values higher than 1 (stable cuts and slopes), while analysis in zone with very low KI values (with only one possible mechanism of instability) can produce Fs values less than 1, which indicates relatively unstable cuts or slopes. As a result, the Kinematic Hazard Index should be used in combination with deterministic rock slope stability analyses. Consequently, identifying rock fall prone areas, localizing potentially hazardous rock blocks and probable instability mechanisms on the road cuts and slopes above it represent input data for further deterministic slope stability analysis. Zones with higher KI values enable a more objective selection of representative cross-sections for slope stability analysis. Deterministic rock slope stability analyses are of crucial importance in determining and implementing effective measures designed to reduce the risks associated with rock slope hazards and events.

Acknowledgments

Dissemination process is supported by the Development Fund of the Faculty of Mining, Geology and Petroleum Engineering, University of Zagreb

References

Arbanas Ž, Grošić M, Udovič D, Mihalić S (2012) Rockfall hazard analyses and rockfall protection along the Adriatic coast of Croatia. J Civ Eng Arch David Publishing Company 6(3):344–355

Cacciari PP, Futai MM (2016) Mapping and characterization of rock discontinuities in a tunnel using 3D terrestrial laser scanning. Bulletin of Engineering Geology and the Environment. 75: 223-227

Casagli N, Pini G (1993) Analisi cinematica della stabilità in versanti naturali e fronti di scavo in roccia. In; Proceedings 3° Convegno Nazionale dei Giovani Ricercatori in Geologia Applicata, Potenza (in Italian)

Fanti R, Gigli G, Lombardi L., Tapete D, and Canuti P (2013) Terrestrial laser scanning for rockfall stability analysis in the cultural heritage site of Pitigliano (Italy). Landslides. 10: 409-420

Gigli G, Casagli N (2011) Semi-automatic extraction of rock mass structural data from high resolution LIDAR point clouds. International Journal of Rock Mechanics and Mining Sciences. 48(2):187–198

Gigli G, Frodella W, Mugnai F, Tapete D, Cigna F, Fanti R, Intrieri E, Lombardi L (2012) Instability mechanisms affecting cultural heritage sites in the Maltese Archipelago. Nat Hazards Earth Syst Sci 12:1883-1903

Goodman RE, Bray JW (1976) Toppling of rock slopes. Proceedings of Special Conference on Rock Engineering for Foundations and Slopes. Boulder, Colorado, ASCE, 2: 201–234

Grimani I, Šikić K, Šimunić A (1972). Osnovna geološka karta SFRJ 1:100.000. List Knin L33–141.– Institut za geološka istraživanja Zagreb (1962–1966), Savezni geol. zavod, Beograd (in Croatian).

Günther A, Wienhofer J, Konietzky H (2012) Automated mapping of rock slope geometry, kinematics and stability with RSS-GIS. Nat Hazards. 61: 29-49

Haala N, Cramer M, Weimer F, Trittler M (2011) Performance test on UAV-based photogrammetric data collection. Proceedings of the International Conference on Unmanned Aerial Vehicle in Geomatics (UAV-g). 14-16 September 2011. Vol. XXXVIII-1/C22

Hoek E, Bray, JW (1981) Rock Slope Engineering. Revised Third Edition. Institution of Mining and Metallurgy, London. pp 257-250

Hudson JA, Harrison JP (1997) Engineering rock mechanics: an introduction to the principles and applications. Pergamon ed., Oxford

Jaboyedoff M, Metzger R, Oppikofer T, Couture R, Derron MH, Locat J, Turmel D (2007) New insight techniques to analyze rock-slope relief using DEM and 3D-imaging cloud points: COLTOP-3D software. In: Proceedings of 1st Canada – U.S. rock mechanics symposium, Vancouver, 27–31 May 2007, pp 61–68

Lato MJ, Vöge M (2012) Automated mapping of rock discontinuities in 3D lidar and photogrammetry models. International Journal of Rock Mechanics and Mining Sciences. 54: 150-158.

Mihalić Arbanas S, Sečanj M, Bernat Gazibara S, Krkač M, Begić H, Džindo A, Zekan S, Arbanas Ž (2017) Landslides in the Dinarides and Pannonian Basin – from the biggest historical and recent landslides in Croatia to catastrophic landslides caused by Cyclone Tamara (2014) in Bosnia and Herzegovina. Landslides (in prep)

Sdao F, Lioi DS, Pascale S, Caniani D, Mancini IM (2013) Landslide susceptibility assessment by using a neuro-fuzzy model: a case study in the Rupestrian heritage rich area of Matera. Nat. Hazards Earth Syst. Sci. 13: 397-407

Slob S, Hack R, Van Knapen B, Turner K, Kemeny J (2005) A method for automated discontinuity analysis of rock slopes with 3Dlaser scanning. Transport Res Rec 1913:187–208 Split Engineering, LCC. (2007) Split-FX V 2.4, Tucson, AZ

Recent developments in landslide research in Slovenia

Mateja Jemec Auflič[(1)], Matjaž Mikoš[(2)], Timotej Verbovšek[(3)], Miloš Bavec[(1)]

1) Geological Survey of Slovenia, Dimičeva ulica 14, 1000 Ljubljana, Slovenia, mateja.jemec@geo-zs.si

2) University of Ljubljana, Faculty of Civil and Geodetic Engineering, Ljubljana, Slovenia

3) University of Ljubljana, Faculty of Natural Sciences and Engineering, Ljubljana, Slovenia

Abstract This paper presents a brief overview of recent developments in landslide research in Slovenia, prepared by researchers from the University of Ljubljana (Faculty of Civil and Geodetic Engineering and Faculty of Natural Sciences and Engineering) and the Geological Survey of Slovenia. The first part of the paper focuses on causal factors and triggering factors that are largely responsible for movements of more than 10,000 landslides in Slovenia. The second part presents an overview of national legislation and strategies in the field of landslide risk. Despite inadequate legislation, research institutions continue to make determined steps toward reducing the risk of landslides. Broader landslide risk studies are generally performed in the frame of three types of funding schemes. The first consists of scientific research programs funded by the Slovenian Research Agency that are aimed at gathering new, fundamental knowledge. These studies further support and form the basis of the second type of studies - various applied research projects supported mainly by the relevant ministries and in some cases, by local communities. The application of knowledge and innovative techniques aimed at reducing landslide risk has also been developed through several EU projects. The primary objective of these projects is to identify landslide-prone areas and apply new monitoring technologies. Also, knowledge dissemination is particularly important, which also includes student education – two Slovenian ICL members are active in teaching, presenting the outcomes of the research projects and work of the ICL to students of civil engineering and geology.

Keywords landslides, research, projects, Slovenia

Introduction

The relevant preparatory and causal triggering factors for landslides can be divided after Popescu (2002) into four groups: (1) ground conditions; (2) geomorphological processes; (3) physical processes; and (4) man-made processes. The first group includes causal factors that are closely dependent on ground conditions or the material and mass characteristics of the ground. Mechanical characteristics can be determined by using drilling, trenching and adits, surface mapping of the landslide and the surrounding ground, and are explored in the subsurface. In the second group those factors prevail that are formed by geomorphological processes such as tectonic uplift, volcanic uplift, glacial rebound, fluvial erosion of the slope toe, wave erosion of the slope toe, glacial erosion of the slope toe, and vegetation removal (by erosion, forest fire, drought). The third group consists of factors that change over time and are related to the usual seasonal changes in temperature, distribution of rainfall, fluctuations in groundwater level, shrinking and swelling, snow melt and changes in the intensity of vegetation. The fourth group is represented by anthropogenic factors. In the 20th century, with the expansion of settlements and the development of different (manmade) activities, the pressure to build on less suitable and/or unfavourable areas in terms of slope stability has greatly increased, and such trends are also expected to prevail in the future. Many types of anthropogenic processes can influence the triggering process and interact with natural hazards, as recently presented by Gill and Malamud (2017). The use of new modern mechanical technology for maintaining agricultural land often requires extensive surface reconversion and the adaptation of slope terraces. One particularly common process is change of land use with the construction of agglomerations and infrastructural arrangements. All of these factors disturb the natural balance of soils and trigger complex processes that can lead to slope failures.

Precipitation and related phenomena represent, at the global level and in Slovenia, one of the most important triggering factors for the occurrence of landslides (Glade 2000, Jemec and Komac 2012, Peruccacci 2017). Over the past decade, extreme rainfall events in which a very high level of precipitation falls within a relatively short period have become increasingly important and more frequent, causing a number of undesirable consequences (Haque et al. 2016). Intense rainstorms cause flash floods and often trigger shallow landslides and soil slips. On the other hand, the damage of prolonged rainstorms depends on the region's adaptation and its capacity to store or infiltrate excessive rainwater. The amount and consequently the intensity of daily precipitation that increasingly causes floods in the eastern part of Slovenia is rather common for the north-western part of the country. Likewise, the effect of rainfall is very dependent on the prior wetting of the soil, on periods of full soil saturation, and on the fluctuation in groundwater levels due to the slow melting of snow, growing periods, underground

recharge etc. It must be emphasized that during extreme precipitation events the lack of implementation of preventive measures is reflected in the amount and cost of damage suffered, which is usually far greater than the amount invested in preventative actions. Therefore, a good knowledge of risk assessment for a certain region or municipality is essential for spatial planning and the protection of the environment.

Damage caused by landslides and snow avalanches in the period 1994–2008 amounted to 99 million euros in Slovenia (Statistical Office of Slovenia). Although landslides are very localized phenomena, the 15-year average landslide event damage represented 7.6 % of the total damage caused by disasters in Slovenia (and 0.03 % of GDP). In the last 15 years, landslide events such as those at Stože (Mikoš et al 2004), Slano Blato (Mikoš et al. 2009, Maček et al. 2016), Macesnik (Mikoš et al. 2005a), Strug (Mikoš et al. 2005b), Potoška Planina (Peternel et al. 2017) and other cases have again proven that these processes continue to pose a threat to human lives and property (Jemec Auflič et al. 2017).

Legislation

In the past decades, a number of strategies and countermeasures designed to deal with increased landslide risk have been developed, ranging from simple risk avoidance to large construction projects aimed at mitigating a few landslides whose volumes exceed one million cubic meters (Mikoš and Majes 2010). In the field of regulation, which oversees planning and construction in the landslide risk areas, Slovenian legislation remains insufficient – Slovenian legislation adopted the EU Flood Directive in 2007, but this only served to improve flood risk management, but not landslide risk management in Slovenia (Mikoš et al. 2014; 2018). Legislative acts such as the national act on natural and other disasters deal largely with warning, rescue, and remediation issues rather than with prevention measures; and are mainly divided into prevention, emergency protective measures, and permanent measures adopted in the process of remediation (Jemec Auflič and Komac 2011). The current protection strategy against landslides is part of The Waters Act (Official Gazette of RS 2002), which follows the Water Frame Directive of the European Parliament and Council 2000/60/EC, where developments in landslide-prone areas are specified primarily in terms of the adverse effects of water – meanwhile, spatial planning in areas that could be the source of or could increase the risk of landslide is overlooked entirely. The status was reviewed by Mihalić Arbanas et al. (2013), and as of early 2018 remains essentially the same. The new Construction Act was adopted in 2017 and will come into force in mid-2018. This act regulates various issues related to landslide risk reduction, such as the granting of construction permits, but does not regulate precautionary measures and landslide prevention issues. These issues are still part of the Water Act (2002), which does not tackle the geographically identified hazard and risk areas prone to land sliding and erosion processes in torrential catchments. Work is ongoing to prepare the Act on subsurface data (unofficial working title), which is intended to regulate the collection of geological data and certain activities related to geological exploration.

National and European projects and research

Despite inadequate legislation, researchers continue to make determined steps toward reducing the risk of landslides. In general, broader landslide risk studies are performed in the frame of three types of funding schemes. The first consists in scientific research programs funded by the Slovenian Research Agency that are aimed at gathering new, fundamental knowledge. These studies further support and form the basis of the second type of studies, which are various applied research projects supported mainly by the relevant ministries and in some cases, by local communities. European Commission financing mechanisms also offer opportunities to conduct quality research aimed at advancing landslide risk reduction through different projects, either scientific or applicative. Other ways of funding landslide research exist, but here we focus mainly on those that are most common and have particular impact in Slovenia.

Many studies have been undertaken during the last two decades related to landslide prevention on the regional and local level. One of the first steps towards an effective prevention strategy for tackling landslides was the initiation of a central landslide database. At the conclusion of the first phase of compiling the National Landslide Database (May 2005) there were more than 6,600 registered landslides (Komac and Ribičič 2006). Based on this landslide database a Landslide Susceptibility Map of Slovenia at a scale of 1:250,000 was created (Komac and Ribičič 2008). Likewise, a Debris-flow Susceptibility Map for Slovenia at a scale of 1:250,000 was also made available (Komac et al. 2010), as well as a Rockfall Susceptibility Map (1:250,000) (Čarman et al. 2011), which has not yet been conclusively validated (Fig. 1).

The results show that one-third of the population lives in landslide-prone areas, which is a clear indication that better spatial and urban planning is definitively required, both at the national as well as local level. Therefore, the next logical step was the development of a methodology model for landslide susceptibility at the municipal level. This effort was undertaken as a pilot project entitled “Elaboration of spatial database and web information system on geohazards (slope mass movements, erosion and snow avalanches)”, funded by the Ministry of the Environment and Spatial Planning. Within this project, susceptibility maps and web applications were elaborated at a scale of 1:25,000 for 14 (out of 212) Slovenian municipalities.

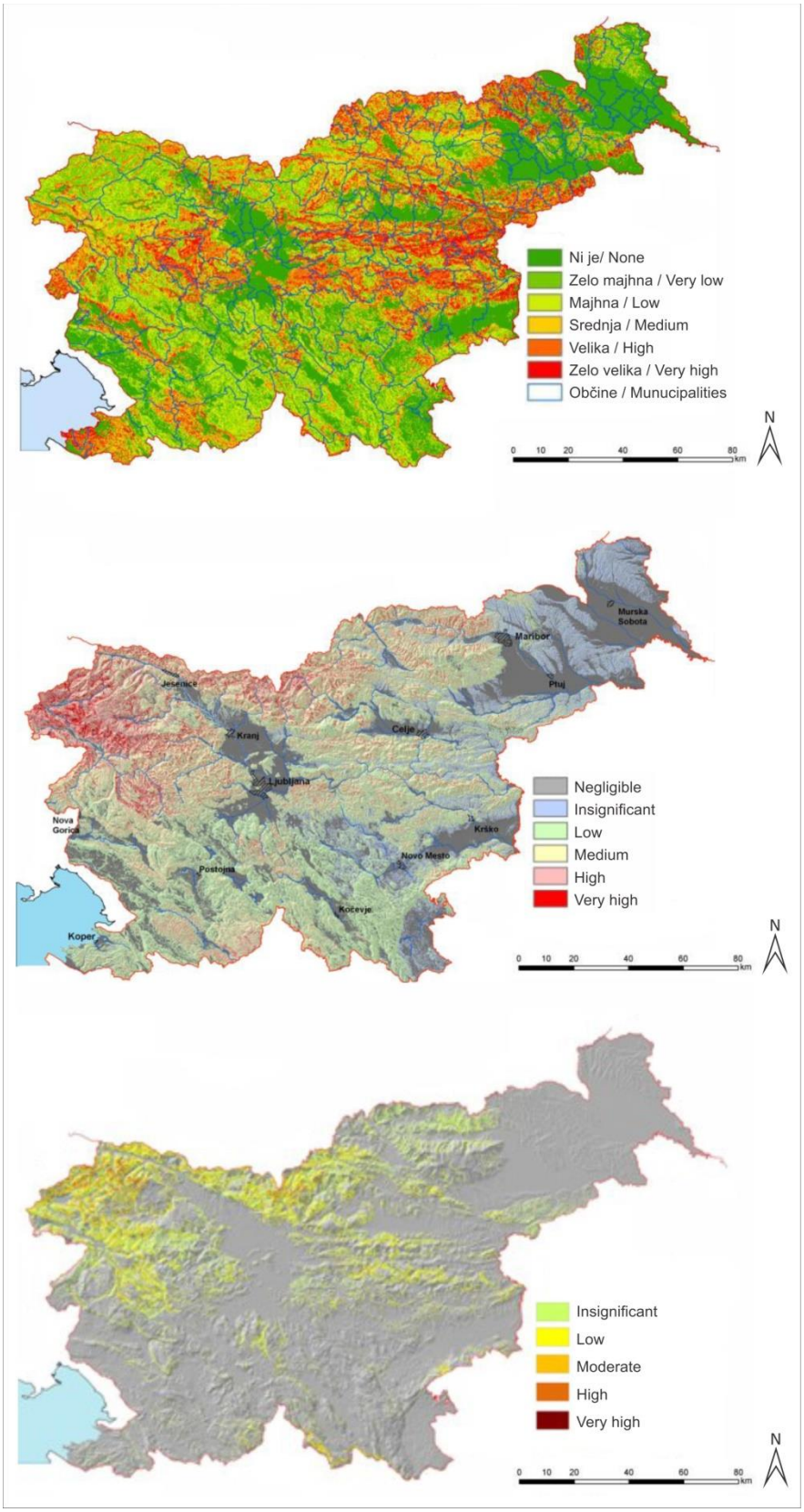

Figure 1 Susceptibility maps at a scale of 1:250,000: A–landslide susceptibility maps (Komac and Ribičič 2008), B–Debris-flow susceptibility map (Komac et al. 2010), C–Rockfall susceptibility map (Čarman et al. 2011).

Project products (maps, geodatabase, web application) serve as directly applicable warning maps and as a basis for spatial planning at the municipal and regional level.

The fact is that we cannot avoid landslides entirely – but we can minimise their impact on settlements, and on society as a whole and the environment. The ACPDR (Administration of the Republic of Slovenia for Civil Protection and Disaster Relief) is well aware of the issue, and initiated the development of a system designed to accurately assess and forecast landslide probability (MASPREM) in 2013. A near real-time system for forecasting landslide probability is currently operational and is in the validation phase (Jemec Auflič et al. 2016).

Through the implementation of several research programmes, our capacity to use remote sensing data (InSAR, PSInASR, UAV photogrammetry, and TLS) in the identification, observation and monitoring of unstable slopes has advanced significantly. The application of knowledge and innovative techniques aimed at reducing landslide risk has also been developed through several EU projects as shown in Tab. 1. The primary objective of these projects is to identify landslide-prone areas and apply new monitoring, and mitigation technologies. Knowledge dissemination is particularly important, which also includes student education. Two Slovenian ICL members are active in teaching, presenting the outcomes of the research projects and work of the ICL to students of civil engineering and geology.

Table 1 Past and ongoing European projects aimed at identifying landslide-prone areas and the application of new monitoring technologies

#	Acronym	Founding Scheme	Project description
1	PanGeo	FP7 (2011-2014)	Provides free access to geohazard information for many of the largest cities in Europe
2	SAFELAND	FP7 (2009-2012)	The project developed quantitative risk assessment and management strategies for landslides at local, regional, European and societal scales.
3	CapRadNet	IPA Adriatic Cross-Border Cooperation Programme (2016)	CapRadNet project aims at extending DSS hazard mitigation capability taking into account maritime, coastal, airport and metropolitan environments.
4	RECALL	DG ECHO (2015-2017)	Aims at designing and implementing smart, community based solutions supporting local authorities in their efforts to better plan and implement landslide and disaster prevention measures.
5	TERRAFIRMA	EU ESA GMES (2009-2012)	Terrafirma harnesses the unique power of satellite radar to detect and measure Earth-surface terrain motion.
6	SEDALP	Interreg Alpine Space (2013-2015)	SedAlp focuses on the integrated management of sediment transport in Alpine basins.
7	I2GPS	FP7 (2010-2011)	To develop a unique unit that combines radar interferometry and GPS and thus enables displacement monitoring in three dimensions.
8	InGeoClouds	ESRR (2012-2014)	Project aims at demonstrating the feasibility of employing a cloud-based infrastructure coupled with the necessary services to provide seamless access to geospatial public sector information, particularly geological, geophysical and other geoscientific information.
9	Start_it_up	Interreg Alpine Space (2013-2014)	The transfer of knowledge from the research and development to the "state-of the-art" in engineering, from innovation to application, requires transdisciplinary work methods.
10	AdaptAlp	Interreg Alpine Space (2008-2011)	AdaptAlp helped to gain important knowledge and data on climate change and natural hazards and to develop new methods and recommendations related to water regimes, hazard mapping and risk management.
11	ClimChAlp	Interreg Alpine Space (2006-2008)	Assessment of historical climate change and its impacts, as well as the effectiveness of using climate models, future scenarios and their effects on natural hazards, spatial development and key economic sectors were ascertained.
12	U-Geohaz	DG ECHO (2017-2019)	The project will propose a procedure to produce maps to continuously assess the potential and potential impact of geohazard activity using satellite data.
13	GIMS	EU, Horizon 2020, European GNSS Agency (2017-2020)	Aims to build and commercialize an advanced low-cost system based on EGNSS, Copernicus SAR and other in-situ sensors for the purpose of monitoring ground deformations with a focus on landslides and subsidence.

All Slovenian members of the ICL, comprising the Geological Survey of Slovenia (GeoZS), the Faculty of Civil and Geodetic Engineering (FGG), and the Faculty of Natural Sciences and Engineering (NTF), have been involved in the work of the ICL for several years now (FGG since 2008, GeoZS since 2011, and NTF since 2016), and in the Adriatic Balkan Network since 2012. In 2017, GeoZS and University of Ljubljana, Faculty of Civil and Geodetic Engineering, were both awarded World Centre of Excellence (WCoE) awards for Landslide Risk Reduction, and have joined the group of 20 World Centres of Excellence for the period 2017–2020. All three members have had active or have ongoing IPL projects (IPL 216; IPL 225; IPL 226; more detailed information about IPL can be found at http://iplhq.org/category/iplhq/ipl-ongoing-project/).
The overall objective of our research follows the Sendai Framework on Disaster Risk Reduction 2015–2030, which consists primarily in strengthening efforts to reduce losses related to landslide hazards by applying new, advanced technologies for landslide identification/ zonation and monitoring.

Discussion and conclusions

The Slovenian territory is, due to its complex geological structure and climatic regime, highly prone to landsliding, and more than 10,000 landslides have been recorded to date. Estimated damage in the period 1994–2008 amounted to 99 Mio € (7.6% of all damage in Slovenia or 0.03% of GDP). Precipitation is the main triggering factor; however, several different triggering factors and types of mass movements occur in the country. Several measures have already been taken to inform people and to obtain more knowledge about these processes, including the creation of a landslide database, participation in EU and national scientific and applied projects, and the creation of susceptibility maps for landslide, debris flow and rockfall processes. Participation in ICL activities levers our efforts.

However, much is still to be done in the field of legislation, which still lacks acts focused on landslide prevention and not only on their post-event remediation. The newly adopted Construction Act covers some aspects of landslide risk reduction, yet still does not adequately cover issues related to landslide prevention. Work is also ongoing on the preparation of the Act on Subsurface Data, which will regulate the collection of geological data and certain activities related to geological exploration.

References

Čarman, M, Kumelj Š, Komac M, Ribičič M (2011) Rockfall susceptibility map. Interdisciplinary Rockfall Workshop 2011 – Innsbruck – Igls.

Gill CJ, Malamud BD (2017) Anthropogenic processes, natural hazards, and interactions in a multi-hazard framework. Earth Sciences Review. 166:246-269.

Glade T, Crozier MJ, Smith P (2000) Applying probability determination to refine landslide-triggering rainfall thresholds using an empirical antecedent daily rainfall Model. Pure and Appl ied Geophysics. 157(6/8):1059–1079.

Haque U, Blum P, Da Silva P. F, Andersen P, Pilz J, Chalov Sergey R, Malet JP, Jemec Auflič M et al. Fatal landslides in Europe (2016) Landslides. 13/6:1545–1554.

Jemec Auflič M, Jež J, Popit T, Košir A, Maček M, Logar J, Petkovšek A, Mikoš M, Calligaris C, Boccali C, Zini L, Reitner J, Verbovšek T (2017) The variety of landslide forms in Slovenia and its immediate NW surroundings. Landslides. 14(4):1537-1546.

Jemec Auflič M, Šinigoj J, Krivic M, Podboj M, Peternel T, Komac M (2016) Landslide prediction system for rainfall induced landslides in Slovenia (Masprem) = Sistem opozarjanja na nevarnost proženja zemeljskih plazov v Sloveniji (Masprem). Geologija. 59(2): 259-271.

Jemec Auflič M, Komac M (2011) Standards und Methoden der Gefährdunsganalyse für schnelle Massenbewegungen in Slowenien = Standards and Methods for Hazard Assessment for Rapid Mass Movements in Slovenia. WLF Zeitung. 74(166):54-69.

Komac M, Kumelj Š, Ribičič M (2010) Debris-flow susceptibility map of Slovenia 1:250,000. Ljubljana: Geological Survey of Slovenia.

Komac M, Ribičič M (2006) Landslide susceptibility map of Slovenia at scale 1:250 000. Geologija. 49(2): 295-309.

Komac, M, Ribičič M (2008) Landslide susceptibility map of Slovenia 1:250.000. Geological Survey of Slovenia, Ljubljana.

Maček M, Majes B, Petkovšek A (2016) Lessons learned from 6 years of suction monitoring of the Slano blato landslide. Rivista Italiana di geotechnica. 1: 21–31.

Mihalić Arbanas S, Arbanas Ž, Abolmasov B, Mikoš M, Komac M (2013) The ICL Adriatic-Balkan Network: analysis of current state and planned activities. Landslides. 10(1): 103-109.

Mikoš M, Četina M, Brilly M (2004) Hydrologic conditions responsible for triggering the Stože landslide, Slovenia. Engineering Geology. 73(3-4): 193-213.

Mikoš M, Vidmar A, Brilly M (2005a) Using a laser measurement system for monitoring morphological changes on the Strug rock fall, Slovenia. Natural Hazards and Earth System Sciences. 5(1): 143-153.

Mikoš M, Fazarinc R, Pulko B, Petkovšek A, Majes B (2005b) Stepwise Mitigation of the Macesnik Landslide, N Slovenia. Natural Hazards and Earth System Sciences. 5(6):947–958.

Mikoš M, Petkovšek A, Majes B (2009) Mechanism of landslides in over-consolidated clays and flysch. Landslides. 6: 367–371.

Mikoš M, Majes B (2010) Mitigation of large landslides and debris flows in Slovenia. In: Werner ED, Friedman HP (Eds.) Landslides: Causes, Types and Effects. Nova Science Publishers, New York. pp. 105-131.

Mikoš M, Čarman M, Papež J, Janža M (2014) Legislation and procedures for the assessment of landslide, rockfall and debris flow hazards and risks in Slovenia. In: Stand der Technik - Innovationen der Ingenieurpraxis, Verein der Diplomingenieure der Wildbach- und Lawinenverbauung Österreichs. pp. 212-221.

Mikoš M, Čarman M, Papež J, Jež J (2018) TXT-tool 4.386-1.1: State-of-the-Art Overview on Landslide Disaster Risk Reduction in Slovenia. In: Sassa K, Tiwari B, Liu KF, McSaveney M, Strom A, Setiawan H (Eds) Landslide Dynamics: ISDR-ICL Landslide Interactive Teaching Tools. Springer, Cham. (DOI 10.1007/978-3-319-57777-7_43).

Peternel T, Kumelj Š, Oštir K, Komac M (2016) Monitoring the Potoška planina landslide (NW Slovenia) using UAV photogrammetry and tachymetric measurements. Landslides. 14(1): 395 – 406.

Peruccacci S, Brunetti M.T, Gariano SL, Melillo M, Rossi M, Guzzetti F (2017) Rainfall thresholds for possible landslide occurrence in Italy. Geomorphology. 290: 39–57.

Popescu ME (2002) Landslide causal factors and landslide remedial option. In: Keynote Lecture, Proceedings of the 3rd International Conference on Landslides, Slope Stability and Safety of Infra-Structures, Singapore. pp. 61-81.

Recent landslide risk assessment and remediation in the city of Karlovac

Katarina Ravnjak, Goran Grget, Goran Dašić, Mladen Sigurnjak, Marko Kaić

Geokon-Zagreb, Starotrnjanska 16a, Zagreb, 10000, Croatia, katarina.ravnjak@geokon.hr

Abstract Heavy rains were recorded in the Karlovac area in August, September and October 2014. Floods and rain activated 135 landslides, and it was important to register and classify the landslides according to their respective risk levels and to recommend actions aimed at urgent remediation works. This paper describes the course of emergency landslide remediation, from visual inspection through categorization of the landslides and forward to remediation. A total of 30 landslides were analysed and the process of landslide categorization was defined. The categorization process assesses the state of landslides simply and efficiently and classifies each landslide into three categories. The following terminology was chosen to present the landslide's condition and the need for remediation: Low Risk, Medium Risk and High Risk. Depending on the level of landslide risk remediation measures could be approached based on the technical solutions selected and defined by a geotechnical expert. Some solutions are shown in this paper.

Keywords landslide, landslide categorization, engineering geological landslide prospection, landslide remediation, Karlovac (Croatia)

Introduction

In August, September and October 2014, heavy rainfall was recorded for Karlovac, Croatia, including the greatest precipitation ever recorded for a single day. Such weather conditions activated 135 landslides and caused considerable damage. Roads, family houses and commercial facilities were all damaged.

Prospection was carried out on 30 landslides, and the categorization of landslides was defined. The inspections were carried out by a geotechnical and geological expert. As a part of the survey, an engineering geological form was completed separately for each site, thus the current engineering geological conditions were described with a drawing of the landslide along with corresponding photo documentation. After the prospection process was complete, the landslide categorization was determined. Each category defines further procedures in terms of remediation according to the type of solution, the implementation of temporary support structures, the implementation of investigations, designs for remediation and remediation works. This paper describes the course of landslide emergency remediation, from prospection through landslide categorization and on to remediation.

Landslide Prospection

The landslide prospection report contains descriptions of detailed visual inspections along with the registration of engineering geological conditions, landslide drawings and corresponding photo documentation. The forms for engineering geological prospecting were created and completed directly in the field. A table with basic location data and coordinates, slope characteristics and landslide characteristics was completed for each landslide. Under slope characteristics, the slope material, slope angle and slope direction, slope shape, position of landslides on the slope, and movement classification are all included. Landslide characteristics include landslide dimension, landslide expression, state of activity, movement mechanism and the possibility of future movement (progressive, retrogressive, extending), causes of sliding, structures on the landslide and nearby landslides. In addition to the landslide prospection, corresponding documentation in the form of photo documentation and landslide drawings for each landslide was included. Fig. 1 shows a landslide drawing as part of the engineering geological prospection for the Low Risk landslide.

Landslide categorization

Since the landslides were unexpected and sudden, there was a need to remediate all of the landslides at once. The problem then was to focus on determining the remediation priorities and to develop a remediation procedure. After a detailed prospection and the collection and preparation of data, the landslides were categorised (Geokon-Zagreb 2014a). The following terminology was chosen to describe the current risk state in the landslide categorization: Low Risk, Medium Risk and High Risk. Low risk implies more or less seasonal creeping of the landslide, without the threat of immediate endangerment to the permanently supporting structure, and without damage to dwellings, commercial buildings, public and industrial facilities, roads, railways, and above underground installations.

Recommended actions for the Low Risk category are as follows: regular maintenance, visual inspection by an ex-

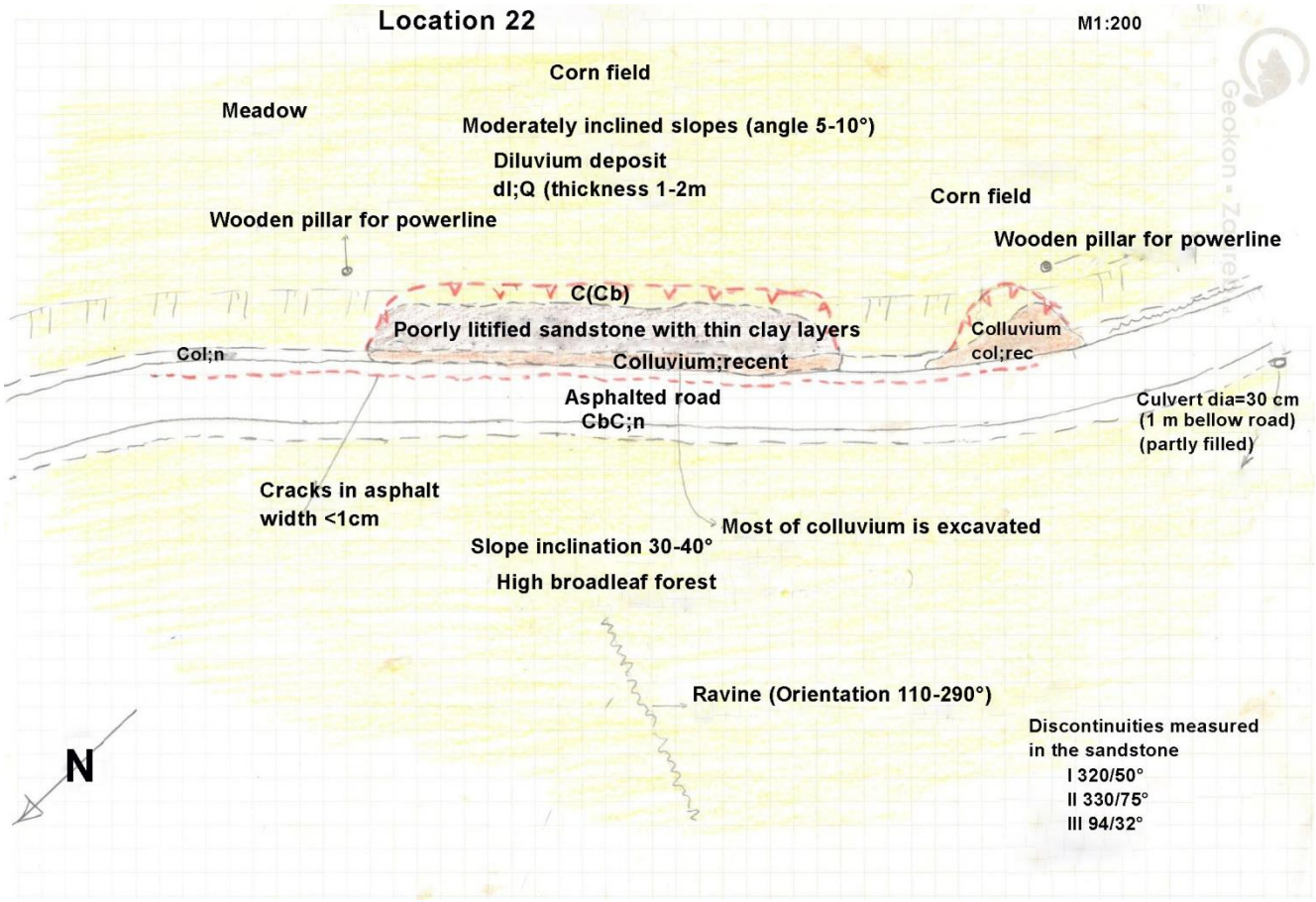

Figure 1 Landslide drawing, as part of the engineering geological prospection.

perienced geotechnical engineer, selection of the type of technical solution(s) for the remediation, in cooperation with a geotechnical expert and landslide remediation with a supervising engineer. Fig. 2 shows an example of a Low Risk landslide.

The Medium Risk category envisages a possible increase in the speed of the displacement or expansion of the landslide, where human life is not currently threatened, with temporary or permanent support structures that can be remediated, where there is no damage to dwellings, commercial buildings and/or public and industrial facilities, but roads, railways, above- and underground installations are endangered. Recommended actions for Medium Risk are as follows: enhanced monitoring of maintenance and condition, visual inspection by a geotechnical engineer, preliminary investigations, technical solution consisting of a temporary support structure by an expert, with monitoring after remediation. Fig. 3 shows an example of a Medium Risk landslide.

The High Risk category envisages the possible rapid expansion of the landslide or a constant increase in the speed of displacement, where human lives are endangered, permanent structures are damaged, as are dwellings, commercial buildings, public and industrial facilities, and with damage to roads, railways, and aboveandunderground installations. Recommended actions for High Risk landslides areas follows: implementation of geotechnical investigations, design of remediation measures and remediation with monitoring by an expert. Fig. 4 and Fig. 5 show an example of a High Risk landslide.

Depending on the risk of individual landslide sites or debris classified as Low Risk, remediation can be assessed based on a pre-designed technical solution. Locations defined as Medium Risk can also be remedied based on selected temporary remedial measures. Given the predesigned technical solution and the temporary remediation measures the landslide remediation scheme in both categories must be defined and monitored by an expert geotechnical design engineer.

After the remediation, it is prescribed that monitoring is carried out as part of regular maintenance. Monitoring must be carried out by a geotechnical engineer in order to promptly record changes or any undesired deformations and to modify technical solutions in that case.

It was important at all locations, regardless of the risk category, to start remediation as quickly as possible. Some landslides that appeared on the road cuts were estimated as Low Risk, but the damaged road prevented access to houses, schools etc., so immediate remediation was required. Fig. 6 shows an example of a road cut off. In Low Risk cases the subsoil should be inspected by the geotechnical engineering expert.

Figure 2 Example of a Low Risk landslide.

Figure 3 Example of a Medium Risk landslide.

Figure 4 Example of a High Risk landslide.

The solution should provide a description of the landslide with engineering geological conditions and a conclusion based on the prospection. The solution should include drawings of the current condition and drawings of the pre-designed technical solution. Typical technical solutions are subordinated to the planned remediation measures. For Medium Risk, it is necessary to create a technical solution for temporary landslide remediation with obligatory monitoring. In the technical solution of the temporary remediation a description of the landslide with engineering geological conditions and conclusions based on the prospection must be provided. A typical technical solution for temporary remediation should include drawings of the existing state of the site and temporary remediation measures with mandatory monitoring. In the case of High Risk, a geodetic survey, engineering geological investigations, geotechnical investigations and laboratory tests must all be conducted. After a geotechnical report has been prepared, a ge-otechnical design of the landslide remediation scheme is required, with mandatory geotechnical supervision and monitoring by a geotechnical expert.

Figure 5 Example High Risk landslide.

Figure 6 Road cut-off.

Pre-designed technical solutions and landslide remediation

Some pre-designed technical solutions are given for Low Risk category cases within the landslide categorization framework (Geokon-Zagreb 2014b).

Figure 7 Pre-designed technical solution.

Figure 8 Landslide remediation with stone retaining wall.

The geotechnical engineering expert should define the depth of the foundation of the supporting structure, make a prospection of the subsoil, define the height and width of the supporting structure, and make decisions on groundwater and/or surface water related to how it can be captured and drained. One type of pre-designed technical solution is a stone retaining wall, as seen in Fig. 7, which shows the resurfacing and protection using a stone material to prevent further erosion of the slope. The foundation preparation includes compaction of the ground material to be used for the foundation of the supporting structure, and use of an appropriate compactor with roller drum to the required compression modulus of 20 MPa. The stone to be installed should be solid and resistant to atmospheric impacts. Conditions and methods employed to test the quality of natural stone should be in accordance with the applicable EN 1341:2001. Everything must be done in accordance with EN 1997-1: 2012 Eurocode 7: Geotechnical design - Part 1: General rules and national supplement previous norm EN 1997-1: 2012 / NA: 2012 Eurocode 7: Geotechnical design – part 1: General rules – National annex, the decisions and guidelines of the expert, the geotechnical engineer, and the regulations and requirements of the supervising engineer. Several Low Risk landslides were remediated according to this pre-designed technical solution. Fig. 8 and Fig. 9 show an example of Low Risk landslide remediation.

Figure 9 Landslide remediation with stone retaining wall.

Both landslides see stone embedded in a 1:2 inclination (27˚ angle). First, a load-bearing geotextile was laid on the foundation soil, followed by crushed stone drainage material (16-64 mm). The stone was machine mounted with a manual trim thickness of 1.5 m or similar, depending on the depth of the sliding surface or escarpment. The material was compacted in 50 cm-layers to the required compression modulus of 40 MPa with vibratory plate compactors. A 10 cm-diameter PVC drainpipe was installed and connected to the drainage system. Fig. 10 shows an example of a Low Risk landslide remediated with prefabricated concrete elements. Fig. 11 shows a temporary slope protection scheme on a Low Risk landslide, and Fig. 12 shows remediation by arrangement in a stable slope on a Low Risk landslide.

The entire process, from visual detection of the unstable area through remediation of the landslide was performed for all examples of Low Risk landslide remediation. The steps involved in the examples are as follows: the site is identified as unstable and the risk level is determined; the eroded material is removed, the (boulder) stone structure is built, the slope above the stone area in earth-soil material is arranged in a stable slope, the drainage channels are cleared, and finally the slope is greened using hydro seeding.

Figure 10 Landslide remediation with prefabricated concrete elements.

Figure 11 Temporary slope protection on a Low Risk landslide.

Figure 12 Low Risk landslide remediation by arrangement in stable slope.

Conclusions

Strong and unexpectedly heavy rainfall caused many landslides in the Karlovac area. In order to address remediation schemes as quickly as possible and to define the priorities and scope of the work, the landslide categorization scheme must be defined.

Landslide categorization allows Low and Medium Risk landslides to be stabilized using pre-designed technical solutions; and the allocation of High Risk landslides for which serious action is required, from investigations to design documentation and urgent remediation.

The categorization scheme serves as a tool for determining remediation priorities, and each geotechnical engineering expert determines the categorization himself. The work involved in the categorization process serves as a tool for assessing the condition of the landslide and the urgency of any remediation schemes. The process of categorization is based on the research carried out, and along with additional tools, procedures and more knowledge can be improved in the future.

Such categorization and the results of it serve as a basis for decision-making and the timely remediation of landslides. In addition, it serves to provide a better understanding, management and lower risk of further instances of slope instability.

Acknowledgments

The authors gratefully acknowledge the support of our colleagues from Geokon-Zagreb, who though were not engaged in the preparation of this paper, participated in the development of the design documentation.

References

Geokon-Zagreb d.d. (2014) Technical report, Landslide Categorization Report, Zagreb.

Geokon-Zagreb d.d. (2014) Technical report, Pre-designed technical solutions, Zagreb.

HRN EN 1997-1:2012/A1:2013 (2013) Eurokod 7: Geotechnical design - Part 1: General rules.

HRN EN 1997-1:2012/NA:2012 (2012) Eurokod 7: Geotechnical design - Part 1: General rules – National annex.

EN 1341:2001 (2013) Slabs of natural stone for external paving - Requirements and test methods.

Estimation of possible economic losses of large water distribution systems due to landslides – Case studies from the Republic of Macedonia

Natasha Nedelkovska[(1)], Igor Peshevski[(2)], Milorad Jovanovski[(2)], Sead Abazi[(2)], Bojan Susinov[(2)]

1) Geohydroconsulting, Bagdadska 36A-1/2-10, 1000 Skopje, Republic of Macedonia, n_nedelkovska@hotmail.com

2) University "Ss. Cyril and Methodius", Faculty of civil engineering – Skopje, Skopje, Macedonia

Abstract Landslides represent a major risk in the Republic of Macedonia, where over the past ten years there have been over 150 landslides, with a significant economic impact on infrastructure. Most exposed to the risk of landslides are roads, water systems, parts of particular towns or municipalities and agricultural land. In this paper we present two case studies of landslides that endangered the operations of large hydro systems in the country. The landslide in the structural zone Vrutocki siphon, which is part of the Sharski vodi-Mavrovo hydro system that caries water to the hydroelectric power plants near the town Gostivar; and the landslide near the town of Bitola, which appeared in the area of the Strezevo hydro system, at the intake structure K-O that transfers water from the Strezevo artificial lake to REK Bitola, the largest hydroelectric power plant in the country. Basic information on the hydro systems is provided and their importance for the Macedonian economy are explained, as are the geological and geotechnical properties of the landslides at Vrutocki siphon and K-O. Annual landslide risk assessment is performed for both cases. The results show that if the landslides are not remediated, the economic losses due to damage and failure might be far greater than the total amount of funds spent on geotechnical investigations and remediation works. Further, design proposals for remediation of the landslides are briefly elaborated.

Keywords hydro systems, landslides, annual risk

Introduction

There are several large hydro systems in the Republic of Macedonia that are particularly important for the country's economy. These systems serve to supply water to the population and to industry, and are used for the irrigation of agricultural fields and for the production of electricity.

As Macedonia is a largely mountainous territory and is located within the very complex geological setting of the Balkan Peninsula, it is inevitable that some of these water systems are constructed in terrains that are highly susceptible to landslides. To illustrate, in the past 10 years alone over 35 landslides have been registered that endangered parts of such systems or interrupted their operation for some period of time. Geotechnical investigations were performed for some of these landslides and appropriate remediation measures were undertaken, while others have yet to be investigated or remediated.

In particular, there are two very specific cases of landslides that endanger water distribution systems that have great economic importance for the country. These are the landslides in the area of the Sharski vodi-Mavrovo Hydro System operated by HES Mavrovo in the northwestern part of Macedonia near Gostivar; and the landslides in the area of the Strezevo Hydro System operated by PE Strezevo in the south of the county (Fig. 1).

Figure 1 Overview map of the Republic of Macedonia. Blue mark – HES Mavrovo, red mark – HS Strezevo.

The HES Mavrovo system consists of 130 km of water channels and 170 km of access roads, all situated in the Shara, Bistra and Korab mountain ranges. The amount of electricity produced from the three electric power stations of Vrutok, Vrben and Raven that are supplied with water by these channels amounts to 379 GWh per year, or ~32% of all hydropower production in the entire country. Numerous landslides have been registered along these

channels and their access roads, with the landslide at the "Vrutocki siphon" structure the most significant in terms of size and importance.

HS Strezevo serves to irrigate the agricultural fields in Pelagonia (20.200 ha), supplies water for the town of Bitola (population ~ 60.000), supplies technical water to the largest thermo-electric power plant in R. Macedonia, REK Bitola, for cooling (via intake structure K-O), and supplies water for industry and electricity production at four smaller hydropower plants. The system consists of a 61 km collection channel that collects waters from the many sub-watersheds of the Baba mountain, the artificial dam and Lake Strezevo, and the main supply channel that is 44 km long. There are 8 landslides along this channel, with the landslide at the K-O intake the most important in terms of size and importance.

In order to present the possible economic losses due to the eventual activation of landslides along the hydro system water distribution channels, various risk scenarios for two major landslides are analysed in this paper: the one at the structure Vrutocki siphon of HES Mavrovo, and the other at the K-O structure of HS Strezevo.

Landslide in the area of the Vrutocki siphon

The Vrutocki siphon was constructed in the period 1962–1972 as part of the largest Hydro Energy System in the Republic of Macedonia – HES Mavrovo. The siphon (a metal pipe 2400 mm in diameter and 214,48 m long – fig. 2) carries water from one arm of the HES Mavrovo, which has a total length of 62 km. The position of the siphon is critical, lying only two kilometres from the hydroelectric plant.

This siphon transfers around 42% of the total water in the Mavrovo system. The average annual volume of water transferred through the siphon to the hydroelectric plant is around 3.383 m^3/sec, or ~ 6.28 million Euros worth of electrical power produced annually.

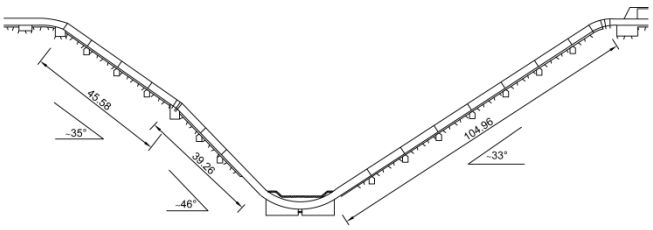

Figure 2 Vrutocki siphon structure – the landslide is in the zone of the right side of the structure. (Modified from Josifoski, Ilieski, Apostoloski, Tochi, Angelovski 2014).

Geotechnical profile of the landslide

The first landslides in zone of the Vrutocki siphon were detected in 1987. Appropriate monitoring activities were undertaken by the Operator HES Mavrovo, so it was established that the terrain was moving. A drainage system was constructed in 1994 above the access road in zone of the siphon. This measure was not enough as the deformation of the terrain continued. In 1999 there appeared very large deformations in the zone on the right side of the siphon and in the zone of the siphon saddle. Based on these observations the geotechnical investigations were performed consisting of engineering-geological mapping of the terrain, drilling of 5 boreholes, detailed logging of boreholes' core, sampling for laboratory testing, installation of piezometers and one inclinometer. According to the performed geotechnical investigations, the dimensions of the landslide which endangers the siphon were estimated: length 160m, width 85 m, depth from 20-29 m, affected area 13 600 m^2 and volume ~ 340 000 m^3.

The lithological composition of the terrain in the body of the landslide is represented by debris overlaying schists (graphitic and phyllitoides). Based on the site investigations, one of the factors for activation of the landslide is presence of high groundwater table as well as surface water infiltration, which affect the present materials by changing/lowering their physical-mechanical properties. The slip surface is estimated to be relatively deep, actually being at the contact between the graphitic schist and the phyllitoides (Crcarevski and Bagashov 2000).

The longitudinal profile of the landslide is shown on Fig. 3.

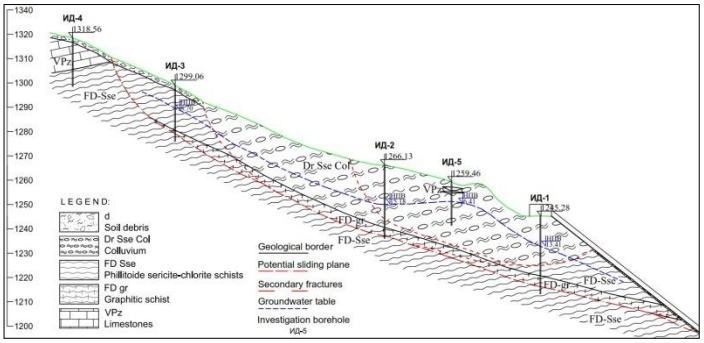

Figure 3 Geological profile of the landslide in the area of the Vrutocki siphon (modified from Crcarevski and Bagashov 2000).

Based on the site investigations and laboratory tests performed, the following parameters for material in the landslide body were adopted:

$\gamma = 21.8$ kN/m^3 $\varphi = 18.9°$ 40.0 kPa

Slope stability analyses were conducted using the slices method after Bishop, Janbu and Iterations. According to all of the methods the calculated safety factor is less than 1.0, which indicated and confirmed the monitoring data (Crcarevski and Bagashov 2000).

Landslide in the area of intake K-O

Intake K-O was constructed in 2005 along the main supply channel of the HS Strezevo, at chainage km. 13+239, for the distribution of water for the technical needs of REK Bitola (Fig. 4).

Operation of this intake is very important: the REK Bitola thermo-electric plant would not be able to operate without sufficient technological water for longer than 48 hours. REK Bitola is by far the largest producer of electricity in Macedonia, with production of some 4600 GWh per year i.e. ~ 50% of the total electrical production in Macedonia from all sources (annual report of the regulatory body for energy 2012). The position of the K-O intake along the channel is very specific. If, due to its critical position (ch. 13+239 out of the total 44 km of the channel) the K-O intake were to collapse under the influence of the landslide, the water supply for the town Bitola, together with related industry and irrigation, would be halted altogether.

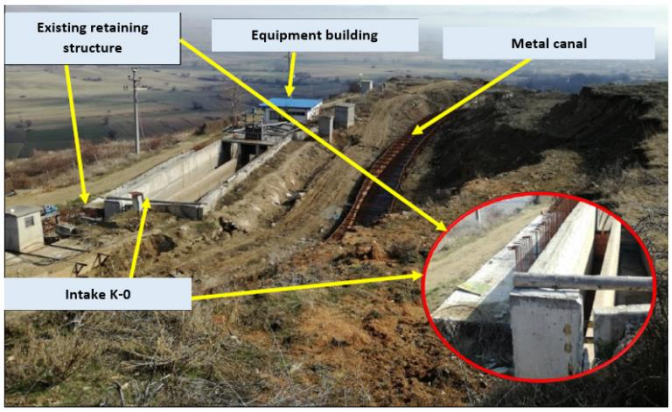

Figure 4 K-O structure – the landslide is in the entire zone of the structure (modified from Markovski 2017).

Geotechnical profile of the landslide

At the end of February 2015, after intensive rainfalls followed by fast snowmelts in the Bitola region, flooding and numerous slides occurred. One such landslide occurred in the area of the structure K-O.

Investigations were undertaken and the main design for remediation of the landslide was prepared. However, just but before its final operative realization, intensive rainfall occurred and the landslide was reactivated, causing visible deformations of the terrain at the intake K-O and damage to equipment and office/HQ buildings, electro-energetic systems, drainage systems and more.

Then, after intensive snowmelt in January 2017 at the cut above the intake K-O, a new landslide was activated in the soil debris zone. In order to prevent further deterioration of the state of the terrain and existing structures, as well as to prepare a durable solution for the stabilization of the terrain affected by landsliding, appropriate geotechnical investigations were performed (engineering-geological mapping of the terrain, drilling of 11 boreholes, SPT, detailed logging of borehole cores, sampling for laboratory testing, installation of piezometers). A geophysical survey was also performed that employed seismic refractive and reflective methods.

According to the performed geotechnical investigations, the geological profile of the terrain at the zone of the landslide was defined as composed of soil debris overlaying surface weathered and grussified granite.

The size of the landslide is estimated at 100 m in length and 80–110.5 m wide, with an affected area of 10,000 m^2 and a volume of around 120,000 m^3. The slip surface is estimated to be more than 5–8 m deep and up to 13 m deep in some places (Markovski 2017).

The longitudinal profile of the landslide is shown on Fig. 5.

Based on the site investigations and laboratory tests performed, the following parameters for the present materials were adopted:

d- soil debris:
$\gamma = 19.0$ kN/m^3; $\varphi = 23.0^0$; 3.0 kPa;
slip surface:
$\gamma = 19.0$ kN/m^3; $\varphi = 17.0^0$; 17.0 kPa;
weathered granite:
$\gamma = 24.0$ kN/m^3; $\varphi = 26.5^0$; 26.5 kPa;
regionally weakened granite:
$\gamma = 26.5$ kN/m^3; $\varphi = 30.0^0$; 30.0 kPa;
(Markovski, 2017)

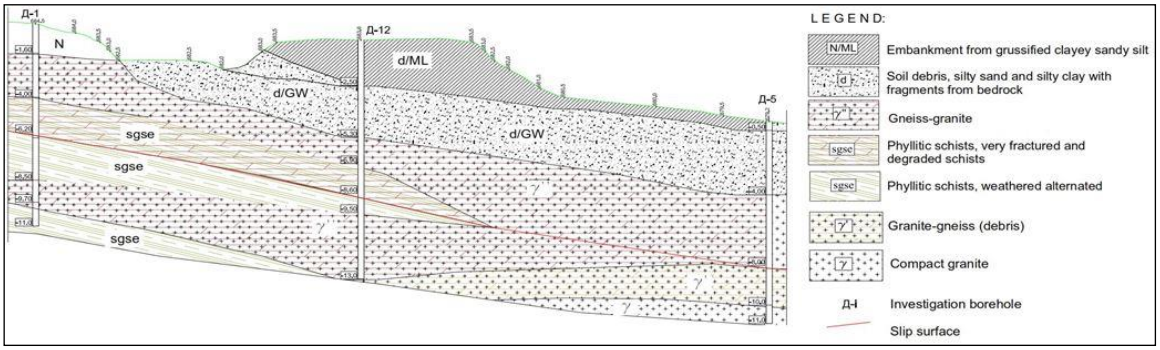

Figure 5 Geological profile of the landslide in the zone of intake K-O (modified from Markovski 2017).

Estimation of current annual risk

As suggested (Lee and Jones 2004) for the presentation of landslide risk, it is sufficient to provide an estimate of the landslide risk under the current conditions. This risk is expressed as an annual value.

Risk assessment for Vrutocki siphon landslide

The value of the structure Vrutocki siphon is estimated at ~ 1.5 million Euros, with an average total value of electricity produced each year of ~ 6.28 million Euros.

We have developed five different risk scenarios with different probabilities of occurrence and degree of damage due to landslide reactivation or total collapse (Tab.1).

Table 1 Landslide risk scenarios for the Vrutocki siphon.

Scenario	Probability of occurrence	Effects from landslides
Scenario 1	1 in 1 year (1)	Regular small repairs of the siphon without interrupting water distribution
Scenario 2	1 in 5 years (0,2)	Regular repairs of the siphon, duration 2 weeks
Scenario 3	1 in 10 years (0,1)	partial collapse of the siphon, 1/3 of total length, repair time 3 months
Scenario 4	1 in 25 years (0,04)	Partial collapse of the siphon, 2/3 of total length, repair time 5 months
Scenario 5	1 in 50 years (0,02)	Total collapse of the siphon, repair time 7 months

The risk calculations also take into account the following general conditions for all 5 scenarios: the landslide can occur at any time during the calendar year; losses to industry due to restricted or interrupted power are not taken into account; negative effects on the power distribution systems are not taken into account (defects, stoppages, etc.); negative effects of the general functioning of HES Mavrovo are not taken into account.

Tab. 2 presents the annual risk calculation, and Fig. 6 presents the landslide damage curve obtained for every possible combination of probability and associated losses.

Table 2 Annual risk calculation for the Vrutocki siphon landslide (all values expressed in Euros).

Scenario	Probability of landslide occurrence	Damage category			Total damage	Area (damage * frequency)
		Direct	Indirect			
		Vturocki siphon structure	Electricity production	Electricity distribution		
1	1	6.000			6.000	
2	0,2	60.000	240.8330	160.176	461.006	186.802
3	0,1	500.000	1.548.193	1.029.703	3.077.896	176.945
4	0,04	1.000.000	2.580.321	1.716.172	5.296.492	251.232
5	0,02	1.500.000	3.612.450	2.402.640	7.515.090	128.116
Average annual risk (area beneath curve) in Euros						743.095

Note: Area between 1 and 1 (Scenario 1) and 1 and 5 (scenario 2) annual events is calculated as: Area (damage * frequency) = (Probability 1 – Probability 2) * (Total Damage 2 + Total Damage 1) /2; Average annual risk = Σ area (damage * frequency)

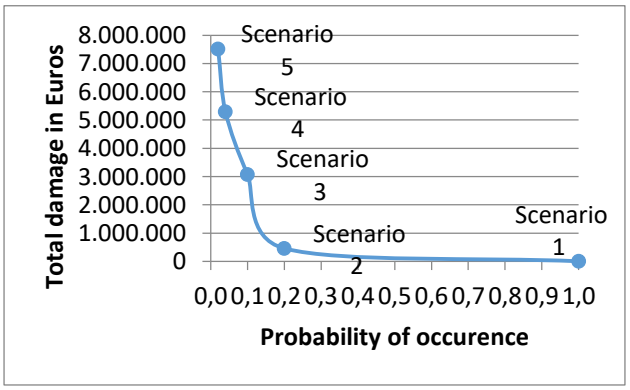

Figure 6 Landslide damage curve for the structure Vrutocki siphon

Risk assessment for K-O intake landslide

The value of the structure K-O is estimated at around 150,000 Euros. The average indirect economical value of the structure exceeds 300,000,000 Euros annually from electrical production alone. The value of other economic activities that are dependent on the operation of intake K-O are properly taken into account in the risk scenarios. As for the previous case, we have developed five different risk scenarios with different probabilities of occurrence and degree of damage as the result of landslide re-activation or total collapse (Tab. 3).

Table 3 Landslide risk scenarios for intake K-O.

Scenario	Probability of occurrence	Effects from landsliding
Scenario 1	1 in 1 year (1)	Regular small repairs of K-0 intake due to landslide, no interruption of water distribution
Scenario 2	1 in 5 years (0,2)	Repairs of the intake over 2 weeks, with 2 days interruption of water distribution
Scenario 3	1 in 10 years (0,1)	Partial collapse of the intake, 1/3 of the structure, still in working condition, repair time 1 month, whole channel stoppage 7 days
Scenario 4	1 in 25 years (0,04)	Partial collapse of the intake, 2/3 of the structure, working 50% of the time, repair time 2 months
Scenario 5	1 in 50 years (0,02)	Total collapse of structure, complete stoppage of water distribution, repair time 3 months

The risk calculations also take into account the following general conditions for all 5 scenarios: the landslide may occur during irrigation season (May–September); there is no alternative source water supply for the population, irrigation or for REK Bitola (one day of imported electricity from another country due to the switching-off of REK Bitola costs around 895,000 Euros); losses to agricultural and industrial production are not taken into account; expenses for supply of water to the population from other municipalities by tanks/cisterns is not taken into account; negative effects for the power distribution network (defects, stoppages, etc.); negative effects on the functioning of the fire department of Bitola; negative effects on human health in the case of longer periods without water distribution; negative effects on the power distribution systems are not taken into account (defects, stoppages, etc.); the above mentioned 4 small hydro power plants are not endangered (being located at the beginning of the supply channel); negative effects on the operation of PE Strezevo.

Tab. 4 presents the annual risk calculation, and Fig. 7 presents the obtained landslide damage curve for every possible combination of probability and loss.

Table 4 Annual risk calculation for K-O intake landslide (all values expressed in Euros).

Scenario	Probability of occurrence	Damage category						Total damage	Area (damage * frequency)
		Direct	Indirect						
		Intake structure K-0	Water supply to REK Bitola	Electricity production	Electricity distribution	Water supply Bitola & industry	Irrigation		
1	1	4.000						4.000	
2	0,2	10.000	9.000	1.788.000	1.189.198	1.300	6.500	3.003.998	1.203.199
3	0,1	50.000	31.500	6.260.000	4.163.526	4.500	23.000	10.532.526	676.826
4	0,04	100.000	135.000	26.830.000	17.844.633	19.500	98.000	45.027.133	1.666.789
5	0,02	150.000	405.000	80.490.000	53.533.899	58.000	293.000	134.929.899	1.799.570
Average annual risk (area beneath curve) in Euros									5.346.385

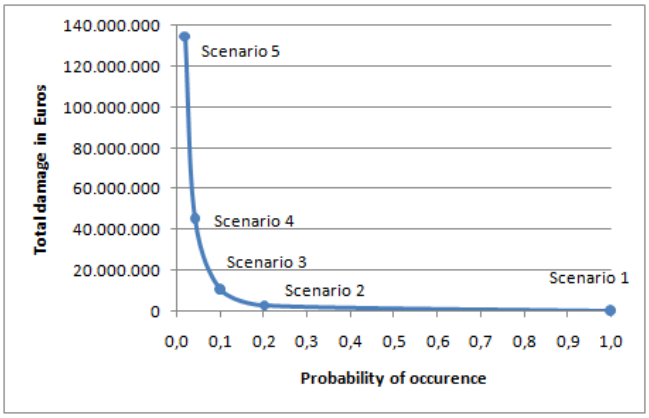

Figure 7 Landslide damage curve for structure K-O.

Basic designs for landside remediation

Vrutocki siphon landslide

Owing to the importance of the Vrutocki siphon for the HES Mavrovo, a basic design for remediation of the landslide was prepared. This design was divided into two phases: the first phase covers surface drainage and removal of material from the body of the landslide; the second phase covers the removal of a larger amount of material from the body of the landslide in combination with surface concrete channels for the removal of atmospheric waters and groundwater drainage.

During April 2008 the first phase of the basic design for remediation of the landslide began, and was concluded in May 2009.

Geotechnical monitoring (piezometers, inclinometers and geodetic osculation) showed a movement rate of 1–5 mm/year between 2009 and 2015. Therefore, the annual monitoring reports state that there is no urgent need for phase 2, which provides for more extensive remediation measures (Medarski and Chalchevski 2002).

The remediation solution, which includes sums for investigations and design, would cost some 500,000 Euros.

K-O landslide

Based on the results obtained from the geotechnical investigations and documented damage to existing structures (intake, temporal metal canal, equipment building, steel pipe etc.), a basic design for the remediation of the landslide was prepared. The following measures were proposed: global stabilization of the terrain with the construction of a reinforced-concrete retaining wall built on piles, stabilization of the landslide crown with removal of material and the formation of stable slopes with inclinations of 1.5:1 to 1:2, depending on the geological composition of the terrain. Drainage of the terrain and protection of atmospheric water should be provided by the construction of vertical drainages and open lateral canals. Following the repair (or replacement) of the steel pipe that carries water to REK Bitola, stabilization with anchor blocks built on micropiles is proposed (Markovski 2017).

The remediation solution, which includes the cost of investigations and design, would cost some 630,000 Euros.

Conclusions

The presented landslide risk assessment showed that in the case of large water distribution systems, depending on their intended use and interconnection with other economic activities, the cost of indirect damage due to eventual landslide activation could be many times greater than costs related to direct damage or the loss of a particular structure along the system. In economic terms, for both of the analysed landslides, it was found that the estimated annual risk is far greater than the cost of remediation measures taken together with appropriate geotechnical investigations and the preparation of basic designs.

Based on the experience gained during this exercise, it is recommended that this approach be adopted and a landslide risk assessment be systematically performed for all known landslides in the area of (all) hydro systems across the Republic of Macedonia. This in turn would enable the planning of funds and the prioritisation of landslide risk reduction activities for the operators of such systems.

References

Crcarevski J, Bagashov U (2000) Report from performed geotechnical investigations of the terrain in the zone of structure's entrance: Siphon for river Vrutocka. Mavrovo EE GeoMavrovo, Skopje, Macedonia. (In Macedonian)

Josifoski Z, Ilieski S, Apostoloski D, Tochi M, Angelovski G (2014) Synthesis report for the state of the siphon "Vrutocka river" and the undertaken sanitation works. Skopje, Macedonia. (In Macedonian)

Lee E M, Jones D K C (2004) Landslide risk assessment. ICE Publishing, London, UK. (ISBN: 0727731718). 454p.

Markovski V (2017) Basic Design for landslide sanation at chainage 13.300 of main intake canal of hydrosystem Strezevo, structure K-O and pipeline for distribution of technological water to REK Bitola from the accumulation Strezevo. Geotehnika-Nova Ltd, Skopje, Macedonia. (In Macedonian)

Markovski V (2017) Report for geotechnical investigations and laboratory testing for landslide at chainage 13.300 of main intake canal of hydrosystem Strezevo, structure K-O and pipeline for distribution of technological water to REK Bitola from the accumulation Strezevo. Geotehnika-Nova Ltd, Skopje, Macedonia. (In Macedonian)

Medarski N, Chalchevski M (2002) Basic Design for sanation of the slope in the zone of entrance of siphon for river Vrutocka. CEI "Makedonija", Skopje, Macedonia. (In Macedonian)

Regulatory commission for energy of the Republic of Macedonia. Yearly report 2012. Skopje, Macedonia. (In Macedonian)

A web service for landslide mapping based on Earth Observation data

Daniel Hölbling[(1)], Elisabeth Weinke[(1)], Florian Albrecht[(1)], Clemens Eisank[(2)], Filippo Vecchiotti[(3)], Barbara Friedl[(1)], Antonia Osberger[(1)], Arben Kociu[(3)]

1) Department of Geoinformatics - Z_GIS, University of Salzburg, Schillerstraße 30, 5020 Salzburg, Austria, daniel.hoelbling@sbg.ac.at

2) GRID-IT - Gesellschaft für angewandte Geoinformatik mbH, Innsbruck, Austria

3) Geological Survey of Austria (GBA), Vienna, Austria

Abstract Information about the location, extent and distribution of landslides is most often collected using a combination of ground surveys and image interpretation following landslide triggering events. New technologies and effective services for landslide information retrieval that use more Earth Observation (EO) data at high spatial and temporal resolutions can support these efforts while reducing costs and time involved. Here we introduce a user-oriented EO-based web service for landslide mapping that can assist practitioners in collecting landslide information. The pre-operational service is developed in close collaboration with potential users from national and regional authorities. Semi-automated and easy-to-use mapping workflows as well as functionalities for validating the landslide mapping results and for identifying landslide-affected infrastructure are implemented in the web mapping application.

Keywords landslides, web service, Earth Observation (EO), user requirements, object-based image analysis (OBIA), web mapping application, validation

Introduction

Landslides are a recurrent natural hazard in almost all mountainous regions of the Earth, claiming lives and destroying manmade infrastructures. Therefore, regional authorities, infrastructure maintainenace people and emergency services require information on both past and new occurrences of landslides in order to protect infrastructures at risk and to minimise damage. Information on landslides is often collected using time-consuming and expensive ground surveying and manual image interpretation schemes after landslide triggering events. The high workload involved in data acquisition and the subjectivity associated with time- and labour- intensive manual visual image interpretation lead to a trade-off between completeness, accuracy and detail (Galli et al. 2008; Guzzetti et al. 2012; Hölbling et al. 2015). The increased availability and quality of Earth Observation (EO) data from different satellite sensors in combination with new computational methods help further attempts to automate the preparation of landslide maps while reducing the time and costs invloved. Casagli et al. (2016) describe several landslide-related services based on optical satellite data and synthetic aperture radar (SAR) data to support disaster management. However, there is still a lack of interaction between science and policy, and a lack in the provision of innovative tools that can easily be used by stakeholders to support their efforts in the rapid mapping, documentating and monitoring of landslides. Taking up this issue, we introduce a pre-operational web-based service for efficient and user-oriented landslide mapping based on EO data, which was developed within the *Land@Slide* research project (EO-based landslide mapping: from methodological developments to automated web-based information delivery, www.landslide.sbg.ac.at) (Hölbling et al. 2016).

Web services have become the state-of-the-art standard for fast and straightforward provision of analysis results (e.g. Granica et al. 2007). A service-oriented architecture (SOA) that uses representational state transfer (REST) technology to implement the web service (Thies and Vossen 2008; Fu and Sun 2011) is able to present geospatial data that complies with the relevant standards, i.e. standards from the Open Geospatial Consortium (OGC). A standard-conform implementation enables easy access to the web service, not only for a single user but for a variety of stakeholders (Albrecht et al. 2016). Geospatial web services can be categorized into map services, data services, analytical services and metadata catalog services according to the functions and services they provide. Whereas map services provide maps in an image format, data services allow us to query, edit and synchronize data over the Web. Analytical geospatial services perform a variety of GIS analysis functions, and metadata catalog services enable the publishing and searching of metadata (Fu and Sun 2011). The conceptual architecture of the web-based platform, which provides the web service, is essentially a client/server architecture that is usually comprised of three tiers (Fu and Sun 2011).

Development of the *Land@Slide* service relies on three main pillars: (1) gathering and defining user needs and requirements for an EO-based landslide information service, (2) developing semi-automated object-based im-

age analysis (OBIA) methods and establishing a suitable landslide mapping workflow for integration into the web service, and (3) implementing the web mapping application with its responsive user interface. Currently, the web service for landslide mapping includes examples from landslide-affected areas in Austria (federal states of Salzburg and Vorarlberg) and from the Gader Valley in South Tyrol, northern Italy. The most common trigger in these areas, and thus for the landslide examples included, is heavy rainfall (Fig. 1).

Figure 1 Rainfall-triggered landslides in the Bregenzerwald, federal state of Vorarlberg, Austria. Photo: GBA.

Materials and Methods

Assessment of user requirements

The process of collecting user requirements followed a user-centred design approach that enables us to fashion the service after user demands (Saffer 2007; Wealands et al. 2007). Such approaches have, for example, been used in designing geoinformation services for the communication of near-realtime information for disaster management (Atzl 2013) and for EO-based geoinformation for aviation (Albrecht et al. 2014). Semi-structured interviews with regional authorities and stakeholders from Austria, Italy and Germany provided information used to compile the user requirements. The potential users were asked about their need for landslide information and about the value they see in using EO data for landslide investigation. They also expressed their expectations for a landslide web mapping service regarding reliability and usability. The interviews revealed the value of the service within the application scenarios for landslide documentation and mapping, for monitoring specific sites that are prone to landslides, for updating and complementing existing landslide inventory maps, as well as for landslide rapid mapping (Albrecht et al. 2016). Based on an anlyisis of user requirements and the tasks and aims specified in the *Land@Slide* project, the service concept was refined (Fig. 2). Steps in the technical and user-centric implementation toward development of the web-based landslide mapping service were defined accordingly (Weinke et al. 2016).

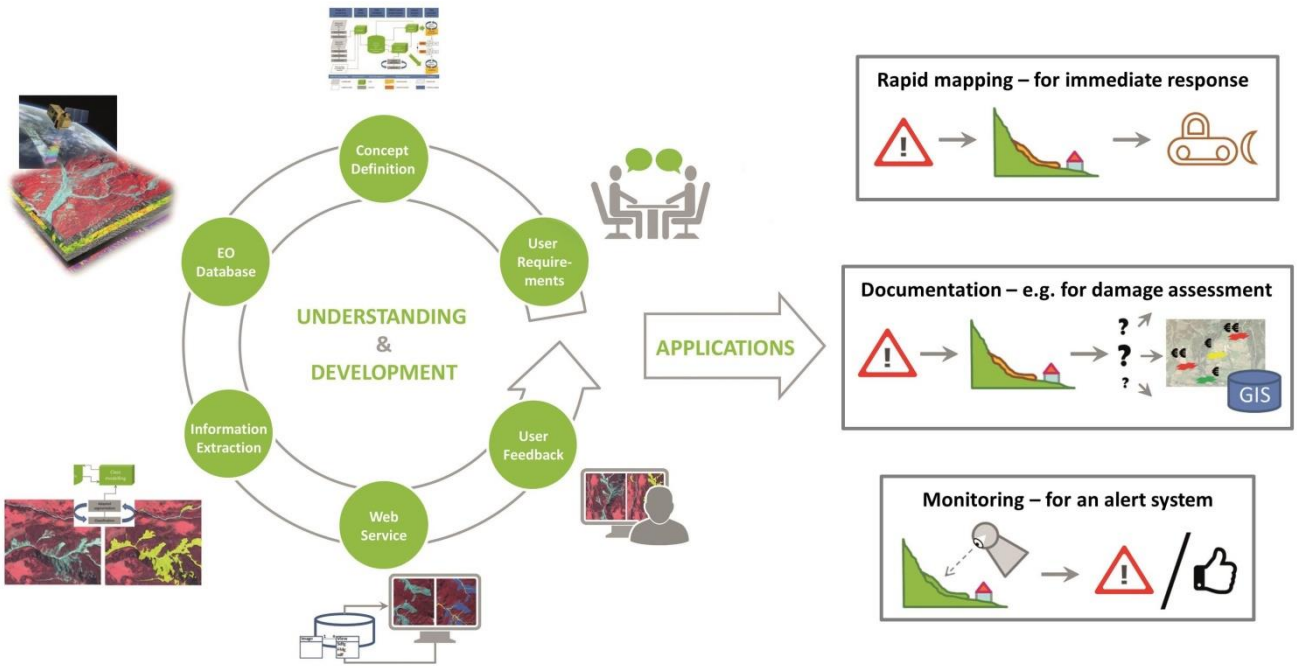

Figure 2 Overall *Land@Slide* service concept and potential applications.

User-oriented and semi-automated landslide mapping workflow

Optical satellite imagery from different high resolution (HR) and very high resolution (VHR) sensors (e.g. Landsat 7, Sentinel-2, SPOT-5, WorldView-2/3) was acquired for selected study areas in the Austrian and Italian Alps. Image pre-processing steps that were necessary prior to the implementation of the data into the web platform included pansharpening, orthorectification and reprojection to WGS 84 Web Mercator (EPSG:3857).

OBIA methods were developed and tested for the semi-automated mapping of landslides. Finally, a mapping workflow was defined and implemented in the web service. So far, only very few web applications include OBIA approaches (e.g. Tiede et al. 2012). First, image objects are created by applying an image segmentation algorithm. At present, the multi-resolution segmentation (Baatz and Schäpe 2000) available within the eCognition software (Trimble Geospatial) is used in the web service. Both knowledge-based and statistical classification methods were tested prior to the web-based implementation. In order to improve the practical suitability for users only selected statistical classification algorithms (Naive Bayes, Random Forest, J48) from the Waikato Environment for Knowledge Analysis (Weka) machine learning software are currently included in the web service. The user needs to select landslide training samples, and based on their spectral characteristics the segmentation-derived image objects are classified. Moreover, the slope values derived from available digital elevation models (DEMs) that are implemented in the web platform are considered for classification. After execution of the selected classification algorithm the (preliminary) landslide mapping results are displayed and made available for download. This procedure allows also users not entirely familiar with sophisticated image analysis methods to produce mapping results quickly and easily. In the final step, the results can be manually edited, i.e. false positives can be removed, unclassified image objects can be assigned to the class landslide and the boundaries can be refined by making use of basic geoprocessing functions.

In order to evaluate the accuracy of the classification the semi-automated classification results can be compared against manual reference classifications, which are available for selected test sites, or against uploaded reference data using the implemented tools. Therefore, basic accuracy assessment measures are implemented.

Next to the mapping workflow, which allows the users to perform their own analysis, some demonstration examples were prepared using eCognition and more sophisticated, knowledge-based classification techniques. The OBIA results were thoroughly evaluated by comparing them to results from manual mapping (see Hölbling et al. 2017). These examples are shown within a subsection of the web service platform to demonstrate and explain the general concepts and functionality of OBIA to users.

Web-based platform and service development

The *Land@Slide* platform has largely been developed based on a range of free and open source technologies and on widely used open standards (e.g. from the Open Geospatial Consortium). The conceptual architecture of the web-based platform comprises three tiers: (1) the data tier, (2) the logic tier and (3) the presentation tier. One advantage of this architecture is the straightforward maintenance and actualization of the platform. The data tier consists of a file storage system and the spatial data catalogue is based on the relational database management system PostgreSQL and the spatial extension PostGIS. The data tier is used to manage multi-temporal EO data, DEMs, other geospatial data (e.g. roads, railways, river network), as well as descriptions and protocols for data processing and analysis. The logic tier is the interface between the data and the presentation tier, and consists of a GIS server (GeoServer) as well as the geoprocessing workflow modules. For the geoprocessing workflows, application programming interfaces of GDAL, eCognition, Weka and the spatial functions of the spatial database extension PostGIS are used. Further on, the Open Source Java Framework Spring was used to provide flexible database access. Based on the Spring RESTful (Representational State Transfer) web service the API data of the database (e.g. workflow descriptions, results and data inputs) is provided as REST-Services. In combination with the JavaScript library AngularJS, HTML5 and CSS3 an interactive user interface is generated in the presentation tier. The five geoprocessing workflow modules (see Fig. 3) of the logic tier are published as map, data and analytical services.

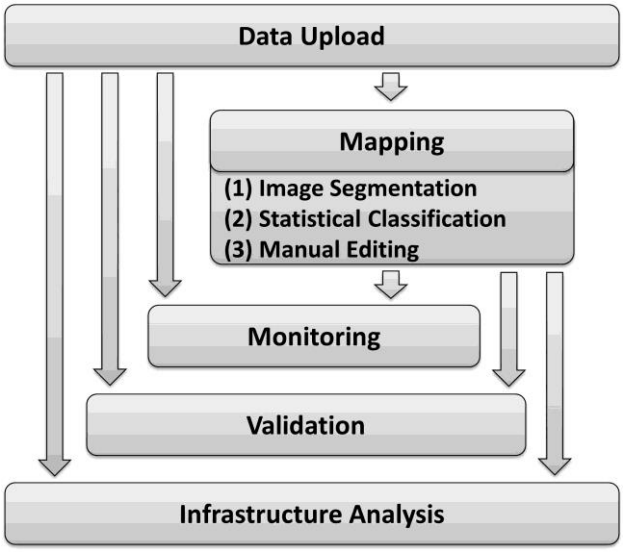

Figure 3 Main modules of the *Land@Slide* web service (modified after Weinke et al. 2017).

Service validation

Evaluation of the *Land@Slide* platform followed a validation protocol that consists of a set of quality criteria for checking whether the web service was able to fulfil the user requirements. This developed validation protocol is based on principles laid out in the Quality Assurance Framework for Earth Observation (QA4EO; http://QA4EO.org), which has been initiated by the Committee on Earth Observation Satellites (CEOS; http://ceos.org). These principles have been implemented by Broglia et al. (2010) for a validation protocol for emergency response geoinformation products. Fig. 4 presents the validation criteria categories.

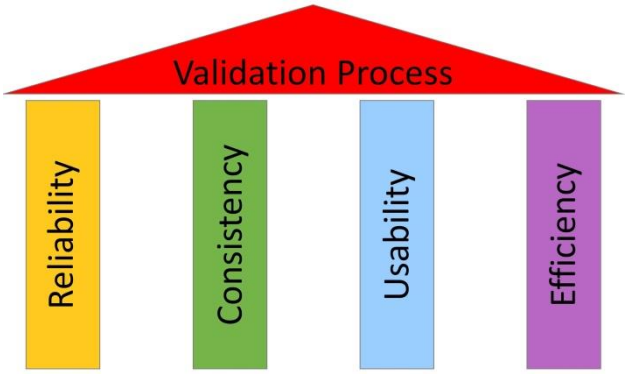

Figure 4 The four pillars of validation.

A user/validation workshop enabled us to collect feedback according to the validation criteria. Apart from evaluating the achievable accuracy of landslide mapping, the validation workshop specifically focused on the usability, efficiency and user friendliness of the web service. The implemented landslide mapping workflow met the user expectations in terms of consistency and reproducibility of the results, and in terms of the overall efficiency as regards elaboration time and response performance. Furthermore, we received positive feedback during the workshop on the user friendliness of the platform and the reliability and consistency of EO data for landslide mapping and its integration in a web mapping service. The user feedback included, among other issues, requests to improve some of the functionalities of the web service user interface. Additional functions were, for example, requested for an easier object splitting procedure and for the merging of classified image segments in order to quickly improve the results of landslide delineation and classification.

Results

Fig. 5 shows the *Land@Slide* web service interface. The pre-operational web service platform consists of several sections. First, it includes an overview of the components of the service and a short description of the service modules. Second, the potential of OBIA for landslide mapping and monitoring is shown using selected demonstration examples from the study areas in Austria and Italy (Hölbling et al. 2017). This section includes background information on the project, the needs for such a web service and a step-by-step description of the methodology. With that, the user is able to gain insights into the service idea, the potential of semi-automated object-based mapping methods, and the applicability of various satellite data for landslide mapping before performing own analysis.

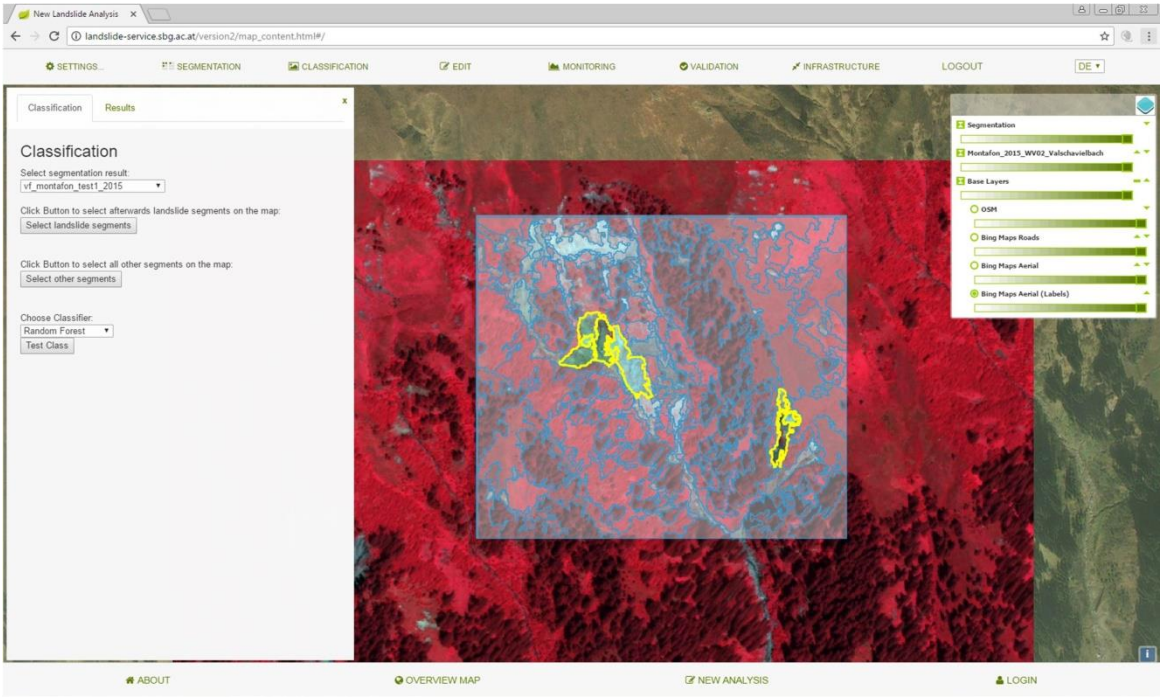

Figure 5 The *Land@Slide* web service interface.

The third and most important component enables the user to perform own analysis by following an easy-to-apply guided workflow, including (1) mapping of landslides (segmentation, classification, editing), (2) monitoring of landslides (comparing mapping results from different points in time and thus monitoring the evolution of landslides), (3) validation (comparison of semi-automated mapping results to manual mapping results or other reference data) and (4) infrastructure analysis. The infrastructure analysis allows the user to compare the classification results to freely available data, such as OpenStreetMap, in order to identify landslide-affected infrastructure (e.g. buildings, roads, mountain trails).

Discussion and Conclusion

The platform and web service for landslide mapping has been conceived through strong consideration of user needs and requirements, and has been validated in collaboration with stakeholders, decision-makers and experts, which is essential in efforts to produce landslide information products that can assist the targeted management of natural hazards.

Potential use cases of the proposed web service consist in (1) the creation of digital landslide inventories at regional or national scale, (2) the updating of existing landslide inventories, (3) the provision of post-event landslide information (e.g. landslide-affected infrastructure) for disaster management (rapid mapping) and documentation. The platform has largely been developed based on a range of free and open source technologies and on widely used open standards. The only commercial software currently employed is eCognition, which is used for image segmentation. It is planned to develop the final platform solution using open source technologies exclusively to ensure interoperability among and between components and to reduce costs. Therefore, the next steps taken toward improving and extending functionality will comprise the incorporation of various image segmentation algorithms and an extended set of statistical classification algorithms from Open Source libraries.

Completion of the data upload module will allow the integration of external EO data, aerial photography and Unmanned Aerial Vehicle (UAV) imagery in predefined formats by the user. Furthermore, the possibilities of automated inclusion of the most recent Sentinel-2 data need to be evaluated. This would be an important step towards the development of an operational Copernicus downstream service. The web-based information extraction chain and platform of the first prototype focuses on landslides in Austria and Italy. The platform and its services can be extended to other regions as well, in order to assess different types of geohazards or environmental changes such as soil and river erosion. Prospectively, the existing platform could be further developed toward a comprehensive multi-geohazard spatial data infrastructure (SDI) solution.

Acknowledgments

This research has been supported by the Austrian Research Promotion Agency FFG in the Austrian Space Applications Program (ASAP 11) through the project *Land@Slide* (contract n° 847970).

References

Albrecht F, Hölbling D, Weinke E, Eisank C (2016) User requirements for an Earth Observation (EO)-based landslide information web service. In: Aversa S, Cascini L, Picarelli L, Scavia, C (eds) Landslides and Engineered Slopes. Experience, Theory and Practice, Vol. 2. CRC Press: Boca Raton, London, New York, Leiden. pp. 301-308.

Albrecht F, Lipok F, Dittrich J, Logemann V (2014) Geo-Information in the Cockpit: Safe Emergency Landing in Alpine Terrain. Proceedings of CERGAL 2014: International Symposium on Certification of GNSS Systems & Services, 08-09 July 2014. Dresden, Germany. pp. 148-152.

Atzl C (2013) Nutzerzentrierte Präsentation mobiler Multimediainhalte in Raum und Zeit - Local C&C View. In: Strobl J, Blaschke T, Griesebner G, Zagel B (eds) Angewandte Geoinformatik 2013. Wichmann: Heidelberg, Germany. pp. 300-309.

Baatz M, Schäpe A (2000) Multiresolution Segmentation - an optimization approach for high quality multi-scale image segmentation. In: Strobl J, Blaschke T, Griesebner G (eds) Angewandte Geographische Informationsverarbeitung. Wichmann: Heidelberg, Germany. pp. 12-23.

Broglia M, Corbane C, Carrion D, Lemoine G, Pesaresi M (2010) Validation Protocol for Emergency Response Geo-information Products. JRC Scientific and Technical Reports. Publications Office of the European Union: Luxembourg. 52p.

Casagli N, Cigna F, Bianchini S, Hölbling D, Füreder P, Righini G, Del Conte S, Friedl B, Schneiderbauer S, Iasio C, Vlcko J, Greif V, Proske H, Granica K, Falco S, Lozzi S, Mora O, Arnaud A, Novali F, Bianchi M (2016) Landslide mapping and monitoring by using radar and optical remote sensing: Examples from the EC-FP7 project SAFER. Remote Sensing Applications: Society and Environment. 4:92-108.

Fu P, Sun J (2011) Web GIS -Principles and Applications. Esri Press: Redlands, California, USA. 296p.

Galli M, Ardizzone F, Cardinali M, Guzzetti F, Reichenbach P (2008) Comparing landslide inventory maps. Geomorphology. 94(3-4): 268-289.

Granica K, Almer A, Hirschmugl M, Proske H, Wurm M, Schnabel T, Kenyi L W, Schardt M (2007) Generation and webgis representation of landslide susceptibility maps using VHR satellite data. IEEE International Geoscience and Remote Sensing Symposium (IGARSS), 23-28 July 2007. Barcelona, Spain. pp. 2455-2458.

Guzzetti F, Mondini A C, Cardinali M, Fiorucci F, Santangelo M, Chang K-T (2012) Landslide inventory maps: New tools for an old problem. Earth-Science Reviews. 112(1-2):42-66.

Hölbling D, Eisank C, Albrecht F, Vecchiotti F, Friedl B, Weinke E, Kociu A (2017) Comparing Manual and Semi-Automated Landslide Mapping Based on Optical Satellite Images from Different Sensors. Geosciences. 7(2):37.

Hölbling D, Eisank C, Friedl B, Weinke E, Kleindienst H, Kociu A, Vecchiotti F, Albrecht F (2016) EO-based landslide mapping: from methodological developments to automated web-based information delivery. 13th Congress Interpraevent 2016 – Extended Abstracts, May 30 - June 02, 2016. Lucerne, Switzerland. pp. 102-103.

Hölbling D, Friedl B, Eisank C (2015) An object-based approach for semi-automated landslide change detection and attribution of changes to landslide classes in northern Taiwan. Earth Science Informatics. 8(2): 327-335.

Saffer D (2007) Designing for Interaction: Creating Smart Applications and Clever Devices. New Riders: Berkeley, California, USA. 231p.

Thies G, Vossen G (2008) Web-oriented Architectures: On the Impact of Web 2.0 on Service-oriented Architectures. IEEE Asia-Pacific Services Computing Conference, 2008, 09-12 December. Yilan, Taiwan. pp. 1075-1082.

Tiede D, Huber J, Kienberger S (2012) Implementation of an interactive WebGIS-based OBIA geoprocessing service. International Conference on Geographic Object-Based Image Analysis (GEOBIA), 7-9 May 2012. Rio de Janeiro, Brazil. pp. 402-406.

Wealands K, Benda P, Miller S, Cartwright W E (2007) User Assessment as Input for Useful Geospatial Representations within Mobile Location-Based Services. Transactions in GIS. 11(2): 283-309.

Weinke E, Albrecht F, Hölbling D, Eisank C, Vecchiotti F (2016) Verfahren zur Implementierung eines Kartierungsdienstes für Rutschungen auf Basis von Fernerkundungsdaten und Nutzereinbindung. AGIT – Journal für Angewandte Geoinformatik. 2-2016: 46-55.

Weinke E, Hölbling D, Albrecht F, Friedl B (2017) Land@Slide Hangrutschungsservice: Potentiale für einen Copernicus Downstream Service. AGIT – Journal für Angewandte Geoinformatik. 3-2017: pages pending.

MyDewetra CapRadNet: the evolution of the DewetraNet platform for hydrometeorological risk management and marine ecosystems monitoring

Miranda Deda[(1)], Luca Molini[(1)], Paolo Campanella[(1)], Paola Tepsich[(1)], Antonio Libroia[(1)], Marco Massabo[(1)], Mateja Jemec Auflič[(2)]

1) CIMA Research Foundation, Via Magliotto 2, 17100 Savona, Italy, miranda.deda@cimafoundation.org

2) Geological survey of Slovenia, Ljubljana, Slovenia

Abstract MyDewetra CapRadNet represents the evolution of the Dewetra platform, a fully operational platform since 2008 used by the Italian Civil Protection Department and designed by the CIMA Research Foundation to support operational activities of national or international scale. In 2012, the platform was officially endorsed by the World Meteorological Organization. Originally designed as a single-application web-GIS platform designed for multi-risk mapping, forecasting and monitoring, the system has evolved into a portal for several applications designed also for marine ecosystem monitoring and to help foster a community of expert users through the capabilities provided by the standards of web 2.0, like social networks. The CapRadNet project has enabled deployment of the updated system at the national and international level in Albania, Bosnia and Herzegovina, Croatia and Slovenia.

Keywords web-GIS, emergency management, real-time data, hydro-meteorology, geology, marine ecosystems

Introduction

Establishing a viable forecasting and warning system for communities at risk requires a combination of data, forecasting models, real-time observations and trained teams. These components should exist and be organized in a network to exchange information, procedures and expertise in all operational civil protection centres.

Developed since 2008, Dewetra (Pagliara et al. 2011; Italian Civil Protection Department and CIMA Foundation 2014) is a web-GIS integrated system for the real-time monitoring of hydro-meteorological events, for the management of hydro-meteorological risks, and for environmental monitoring and disaster risk mitigation. It is a fully operational platform used by the Italian Prime Minister's Office – Italian Civil Protection Department (ICPD) – "Centro Funzionale Centrale". This decision support system (DSS) has been designed by the CIMA Research Foundation on behalf of the ICPD with the aim of developing a flexible and robust tool to support both operational activities of Civil Protection in Italy and International Cooperation initiatives abroad.

In 2012, Dewetra was endorsed by the World Meteorological Organization (WMO 2011), since the platform is perfectly in line with the strategic plan 2012–2015 that emphasizes the importance of improving the delivering of services and the complete and flexible use of information inside an environment compliant with international standards (INSPIRE and ISO categories). Today, Dewetra is operational in Albania, Lebanon, Serbia, Bolivia, and in the Organization of Eastern Caribbean States (OECS).

When, during the ADRIARadNet project (http://cetemps.aquila.infn.it/adriaradnet/) the platform was extended to partners and beneficiaries from different institutions and countries, developers faced the most challenging barrier to effective data sharing policy, i.e., institutions and governments are far more inclined to allow access to data rather than forms of physical transfer. To this end, the CIMA Foundation modified the formerly centralized system into a distributed architecture of connected and federated databases, namely the DewetraNet. In this configuration, DewetraNet was delivered to the project partners, thus enabling data owners and/or producers to store, update and ensure access to data.

Designed as a capitalization project of AdriaRadNet, the CapRadNet project (http://cetemps.aquila.infn.it/capradnet/) aimed to exploit the experiences and results of other completed IPA projects, such as CAPS2, RoofOfRock and AIR.NET, in order to address EUSAIR objectives by implementing actions within Pillar 3 (Environmental quality) and Pillar 2 (Connecting the region). These tasks have largely been addressed by upgrading the DSS to the current standards of web 2.0: The newly developed system has taken advantage of the most up-to-date technologies in order to optimize response times and user experience.

For these reasons, the original DSS single application has evolved into a portal for applications (MyDewetra CapRadNet) tailored to different purposes: Dewetra 2.0 for the forecasting and monitoring of hydro-meteorological and hydro-geological risks, SeaWetra for marine ecosystems monitoring, and the Kumalè dedicated blog to foster the development of an expert-user community. In the following sections the architecture of the updated system is presented comprehensively.

IMyDewetra, the evolution of a distributed ICT infrastructure

Deployed during the AdriaRadNet Project, DewetraNet is a DSS based on a distributed ICT architecture, i.e., it is composed of several nodes (Dewetra Data Servers -DDS) installed in each partner institution[1]. Each node – which is basically a server able to host standard-based applications like GeoServer, GeoNode, etc. – publishes the data on DewetraNet as a common sharing standard (e.g., OGC's WXSs). Thus, the partners are in charge of publishing data, sharing, storage, and operational efficiency, and the system allows the end-user to visualize and process the data on a single platform. The DewetraNet website is hosted on the Amazon cloud service. The following figure offers an overview of the IT architecture of the system (Fig. 1).

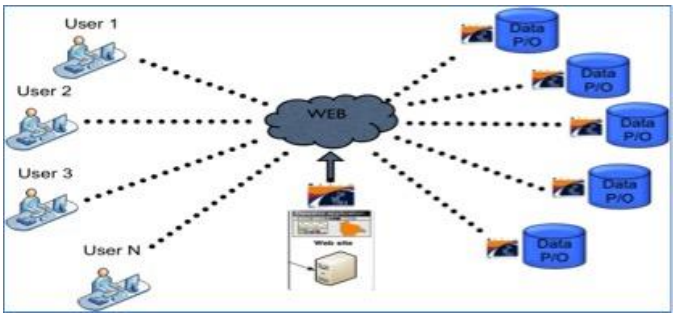

Figure 1 Data distribution infrastructure of the DewetraNet system.

The DewetraNet platform has been improved in two ways: the first part of the process has been devoted to updating the already existing nodes of the system. The CIMA Foundation's ICT experts have worked remotely on the client servers to install the latest version of the platform. DewetraNet, deployed during the AdriaRadNet Project, has been replaced by the recently developed MyDewetra CapRadNet web portal (http://adriatic-ionian.mydewetra.org/), which takes advantage of the most up-to-date technologies, like HTML5.0, AngularJS, Geonode, and Python in order to optimize response times and the end-user experience.

All of the already-operational components have been integrated into the new platform. The updated version of DewetraNet (hereinafter: MyDewetra) draws on the same criteria for data sharing and visualization. MyDewetra includes:

- an updated version of the tool designed for hydro-meteorological and geological data analysis and visualization of geo-spatialized information (Dewetra2.0)
- a real-time integrated system for Mediterranean marine ecosystem monitoring (SeaWetra)
- an expert-dedicated blog (Kumalè)
- an on-line User Guide (DeWiki)
- a public dashboard to provide free access to real-time observational data (e.g., weather radars and raingauges) to the general public.

Dewetra 2.0

Following the experience gained with DewetraNet, the spatial data is organized into four macro categories according to the classification of elements suggested by the EU Floods Directive: environmental data, human health and social data, cultural and heritage data, and economic data. The interface has been specifically designed to allow the user to view layers and information and to easily navigate and search through the data. The data is collected and organized in order to provide information about flood hazards and risks over the territory, the elements exposed, as populations and infrastructure that may be affected by an adverse event, and the resources and measures required to mitigate the risk. The restyling of the application has been specifically designed, implemented and optimized so as to be accessible from mobile devices.

The user interface is organized as follows:

- Control Map, managed by the open source Java Script Library Leaflet. Control is instantiated as the system is started using the Google Hybrid map provided by Google-Maps services as the background layer
- Toolbar, contains many action buttons to access the data shared on the platform (observational data, forecast models, static layers) and other functionalities (e.g. Search, Export Data, etc.)
- Display, allows users to modify, respectively, the start- and end-date of the time range for any time window into the past in order to analyse the data available
- Layer List, containing the layer name and the available options that apply are displayed in the top left corner.

The data available through the platform and the data providers are listed in the Tab 1 below. Fig 2 shows the landslide forecasting model by GeoZS as one of the layers available on MyDewetra CapRadNet.

SeaWetra 2.0

The SeaWetra platform is a near real-time integrated system for Mediterranean Marine Ecosystem Monitoring and Conservation (Fig 3). The system is based on providing different data that can help in decision making with special regard to marine environments.

[1] CETEMPS University of L'Aquila, Italy
CIMA Research Foundation, Italy
CFD_ABR functional centre of Abruzzo civil protection, Italy
DNZ Dubrovnik and Neretva Region, Croatia
IZSAM Zooprophylactic Institute of Abruzzo and Molise Regions 'G. Caporale', Italy
GeoZS Geological Survey of Slovenia
BHNC Office of the Prime Minister of Herzegovina-Neretva Canton Government, Bosnia
PC MARCHE Marche Region - Security and Civil Protection Integrated Policies Department (SCPD), Italy
CNR-IMAA National Research Council of Italy- Institute of Methodologies for the Environmental Monitoring, Italy
IGEWE Energy, Water and Environment Department, Albania
DPEC General Directorate of Civil Emergency, Ministry of Internal Affairs, Albania

Table 1 Data available through the platform and the data providers

Data	Type	Coverage	Frequency of update	Provider
Italian observational network	observation	Italy	15 minutes	CIMA
Cingoli radar	observation	Central Italy	10 minutes	CP Marche
Tortoreto radar	observation	Central Italy	10 minutes	CP Abruzzo
Durres radar	observation	Central Albania	10 minutes	IGEWE
Dubrovnik radar	observation	Southern Croatia	10 minutes	DNZ
Italian radar network	observation	Italy	10 minutes	CIMA
MSG	observation	Western Hemisphere	15 minutes	CP Marche
MICRAdria	observation	Italy	10 minutes	CETEMPS
IMERG	observation	Global	3 hours	CIMA
GSMaP	observation	Global	1 hour	CIMA
SSM/I	observation	Global	Twice daily	CIMA
HSAF SM products	observation	Italy	daily	CIMA
HSAF Precipitation products	observation	Western Hemisphere	3-hourly	CIMA
FloodPROOFs output maps	observation	Italy	daily	CIMA
GFS 0.5°	forecast	Global	daily (10-day forecast)	CIMA
COSMO-I7	forecast	Southern-Central Europe	twice daily (3-day forecast)	CIMA
WRF 3km	forecast	Southern-Central Europe	daily (2-day forecast)	CETEMPS
WRF 12km	forecast	Europe	daily (4-day forecast)	CETEMPS
FloodPROOFs	forecast	Drini-Buna (Albania), Marche (Italy)	daily	CIMA
CHyM	forecast	Central Italy, Drini-Buna (Albania), Neretva (Croatia)	daily (4-day forecast)	CETEMPS
Aladin	forecast	Southern-Central Europe	daily	DNZ
Landslide prediction model	forecast	Slovenia/Croatia	daily	GeoZS

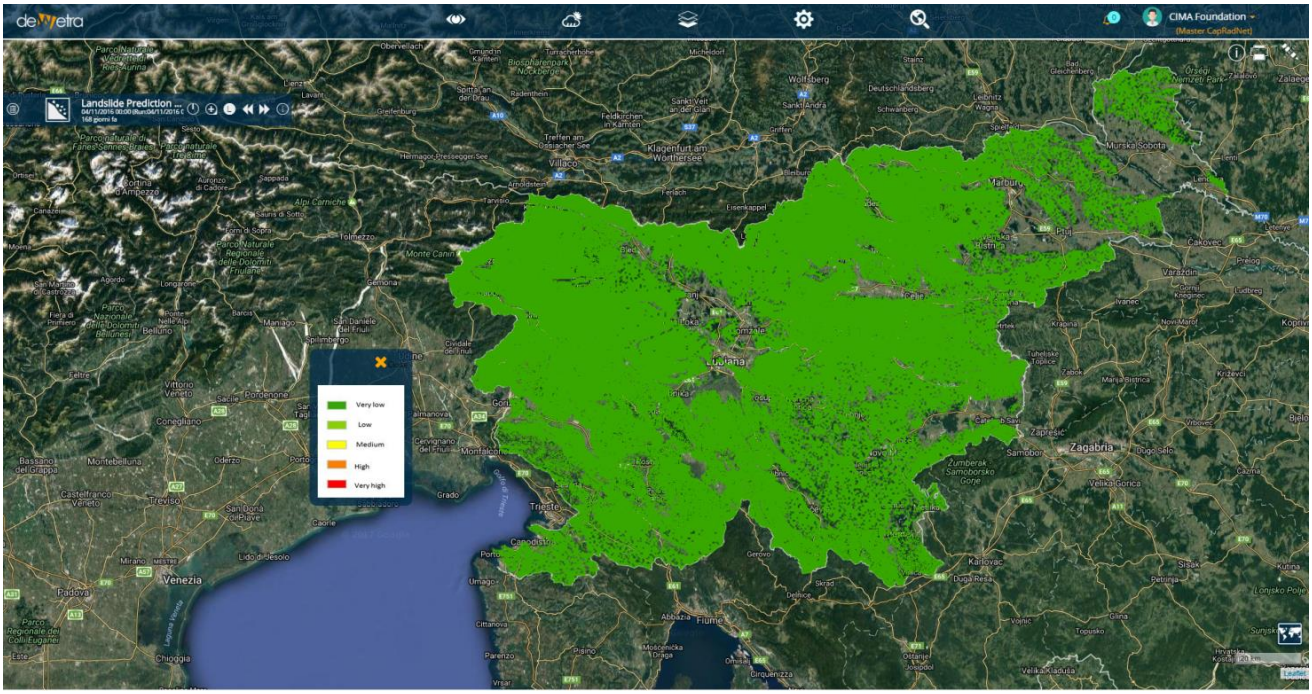

Figure 2 The GeoZS landslide forecasting model is one of the layers available on MyDewetra CapRadNet.

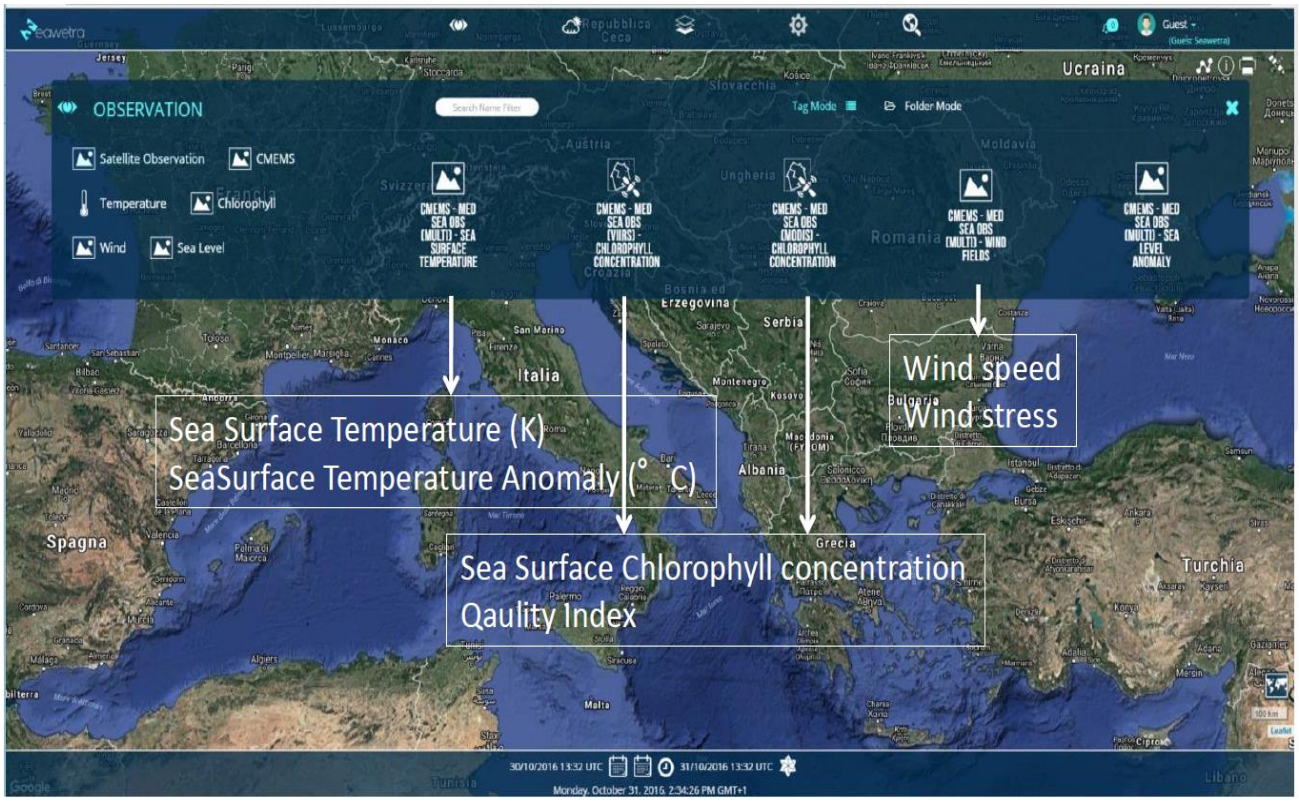

Figure 3 SeaWetra user interface. In the example, the CMEMS' product layer list.

SeaWetra is organized on the basis of two main objectives: 1) to collect, archive, visualize and share geographical information from multiple sources over a large spectrum in an interoperable format and according to international standards, 2) to provide stakeholders and governing institutions in protected marine areas with dedicated tools. Data sources are inserted and managed within the platform, taking into account their diverse space-time scales and degrees of uncertainty and reliability. The SeaWetra platform system architecture is based on open-source software and open-data, and complies with OGC (WXS) standards and the INSPIRE Directive (2007/2/EC).

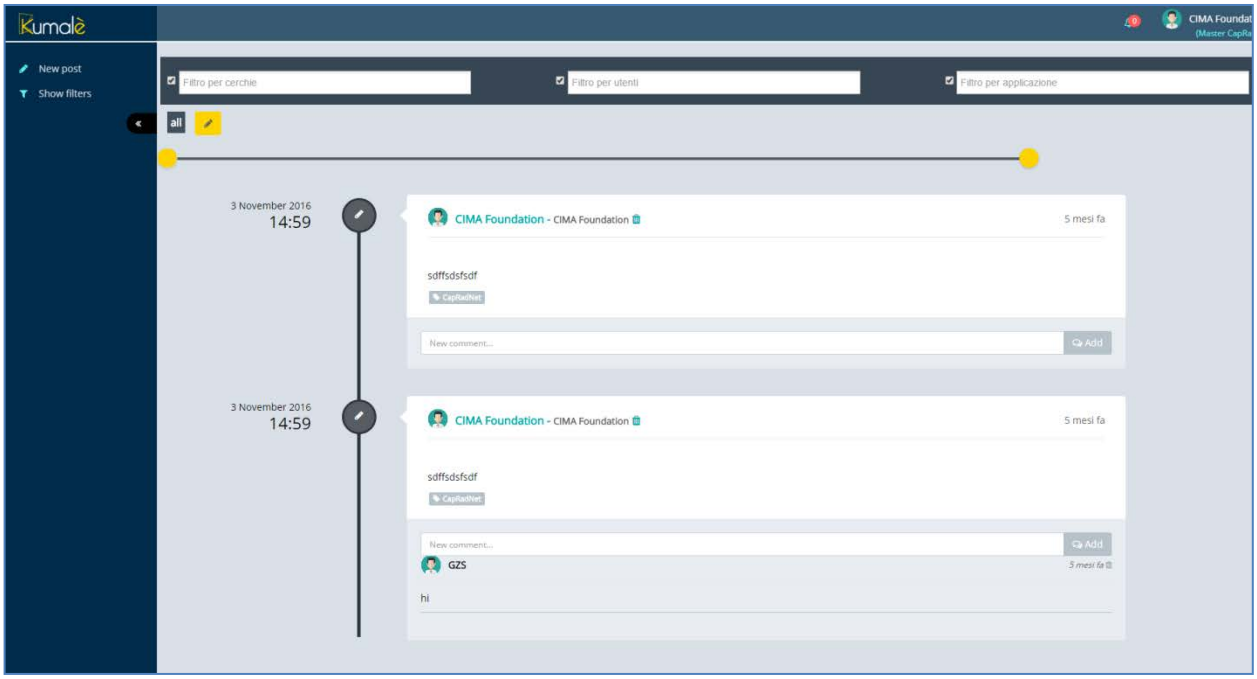

Figure 4 Kumalè, main dashboard.

As part of its further development, SeaWetra has integrated physical as well as biological oceanographic data, such as sea temperature, salinity, currents, sea level, winds, chlorophyll, nutrients (phosphate and nitrate) and dissolved oxygen concentrations, net primary production and phytoplankton biomass as provided by the Copernicus Marine Environment Monitoring Service (hereinafter CMEMS, http://marine.copernicus.eu/). Copernicus, previously known as GMES (Global Monitoring for Environment and Security), is the EU programme for the establishment of a European capacity for earth observation and monitoring. Copernicus services address six main thematic areas that have reached different degrees of maturity. Some are already operational (land monitoring and emergency management), while others are still in pre-operational mode (atmosphere monitoring and marine monitoring); or in the development phase (climate change monitoring and services for security applications). As regards marine monitoring services, the European Commission and Mercator Ocean have signed an agreement to implement and manage the CMEMS. The latter has been operational since early May 2015.

CMEMS delivers a 140-product catalogue (28 with full Mediterranean coverage, 22 gridded products, 13 near-real-time products, 2 forecast products), covering the globe's oceans as well as regional areas and encompassing satellite observations, oceanographic models and in situ observations. Each available product contains several datasets, and each dataset can contain more than one variable. Among all of the available products, 28 include Mediterranean coverage. Six products out of the total have been chosen, ensuring gridded products of near-real-time (satellite observations) and forecast data (oceanographic models) for the main oceanographic variables usually employed in marine environmental monitoring, namely:

- Mediterranean Sea physics analysis and forecast
- Mediterranean Sea biogeochemistry analysis and forecast
- Mediterranean Sea l4 gridded maps nrt sla
- Mediterranean Sea surface chlorophyll concentration from satellite observations
- Mediterranean Sea high resolution and ultra-high resolution sea surface temperature analysis
- Global ocean wind L4 near-real-time 6-hourly observations

Kumalè

Kumale is a social micro blog developed to ensure a useful and traceable exchange of messages in real-time between the users of the platform, both during emergencies and in peacetime (Fig. 4). Users are able to apply filtering options to the messages (sender, object, topic, date, etc.). The main section of the dashboard is dedicated to the timeline, where the user can visualize all of the posts sent and received as displayed chronologically, starting from the most recent onward. All of the institutions that are party to the project, regardless of whether they are partners or associates, have been provided the opportunity to write posts, open new threads and upload and download any type of attachment.

DeWiki

DeWiki is the online handbook for the applications hosted on the MyDewetra Web-portal (Fig. 5). Users can access the manual directly from the dashboard of the portal (Fig. 6) by clicking on the multi-coloured star on the left toolbar. DeWiki is written exclusively using the Me-

diawiki paradigm (https://www.mediawiki.org), a completely free software package. Only registered members of the portal can add or delete pages, sentences, figures or tables to the handbook.
The handbook is structured in separate sections for each application (Dewetra 2.0 and SeaWetra 2.0 so far). The handbook is structured as follows:

- Access to the platform: the section that provides information on how to enter the system once the user has been granted an account
- User Interface
- specific sections dedicated to Observations, Forecast Models and Static Layers.

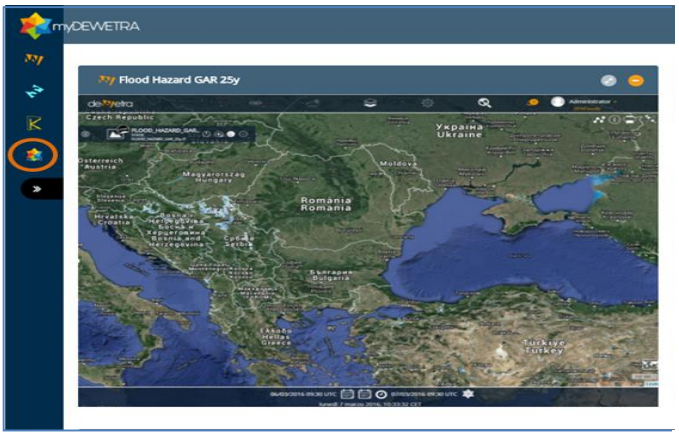

Figure 5 The orange circle highlights the access button to the DeWiki online handbook.

Figure 6 Homepage of the DeWiki online handbook.

Conclusion

MyDewetra CapRadNet has been fully operational since November 2016 for all of the partner institutions of the CapRadNet project, and allows end-users to upload and visualize all of the data required to design a hydro-meteorological/hydro-geological risk scenario or monitor Mediterranean marine ecosystems. The MyDewetra CapRadNet platform represents the evolution of the Dewetra and DewetraNet platforms that have already proven to be effective throughout the full cycle of emergency management:

- in the preparedness phase, supplying the end user with all the available information needed to assess a complete risk scenario, from the characterization of an incoming hazard to its possible impacts on people and infrastructures;
- in the response phase, with the most-recently updated data provided by the real-time or near-real-time monitoring tools
- in the recovery phase, displaying data on shelters, infrastructures, etc.
- in the mitigation phase, updating the risk/hazard maps, enabling overlay impacts, human activities, historic data on climate change assessment, etc.

Due to its ICT-distributed architecture, MyDewetra CapRadNet is able to deal with restrictive data policies, as data is not physically transferred from the owners/producers but shared through standard WXSs. This way the providers are in charge of data publishing, sharing, storage and operational efficiency, and end-users are provided the possibility of visualizing all information required.

As Dewetra and DewetraNet, MyDewetra CapRadNet represents a customised open-source application developed to observe common ISO/WMO standards; interested stakeholders, research and public institutions may make requests directly to the developer or through a WMO cooperation agreement.

References

Directive 2007/2/EC of the European Parliament and of the Council of 14 March 2007 establishing an Infrastructure for Spatial Information in the European Community (INSPIRE) 14.03.2007

Italian Civil Protection Department, CIMA Research Foundation (2014) The Dewetra Platform: A Multi-perspective Architecture for Risk Management during Emergencies. In: Hanachi C., Bénaben F., Charoy F. (eds) Information Systems for Crisis Response and Management in Mediterranean Countries. ISCRAM-med 2014. Lecture Notes in Business Information Processing, vol 196. Springer, Cham.

Pagliara P., Corina A., Burastero, A., Campanella P., Ferraris L., Morando M., Rebora N., Versace C. (2011) Dewetra, Coping with Emergencies. In: Santos MA, Sousa L, Portela E (eds) Proceedings of the 8th International ISCRAM Conference, 8-11 May 2011, Lisbon Portugal.

WMO Strategic Plan 2012-2015, WMO-No. 1069, 2011. (ISBN 978-92-63-11069-5). 21p.

Landslide Risk Reduction and the Slovenian National Platform on Disaster Risk Reduction

Matjaž Mikoš

University of Ljubljana, Faculty of Civil and Geodetic Engineering, Jamova c. 2, 1000 Ljubljana, Slovenia, Matjaz.Mikos@fgg.uni-lj.si

Abstract The field of landslide risk reduction (LRR) is part of broader global efforts toward disaster risk reduction (DRR). In 2015, the United Nations (UN) adopted the Sendai Framework for DRR 2015–2030, which together with the 2030 Agenda for Sustainable Development, provides us with a framework and defines the aims of joint LRR efforts. The paper provides an overview of selected UN documents related to the Sendai Framework that are important for LRR. Especially important are those indicators that have been adopted by the UN aimed at monitoring the implementation of the Sendai Framework. Furthermore, the role of national platforms (NP) in DRR is discussed, and thereafter the Slovenian NP is presented briefly. Its role and structure are then compared to other selected NPs elsewhere. The paper closes with an overview of relevant LRR legislation in Slovenia, and defines the important challenges for LRR in the implementation of the Sendai Framework. International cooperation within the framework of the activities of the International Consortium on Landslides (ICL) provides an excellent framework for these efforts.

Keywords disaster risk reduction, landslide risk reduction, national platforms, Sendai Framework, Sustainable Development Agenda

Introduction

The official statement of the Republic of Slovenia during the Global Platform for Disaster Risk Reduction in Cancun, Mexico (Bizjak 2017): "As a central European country with a diverse landscape, Slovenia can be affected by many disasters and has therefore developed a comprehensive system of protection against natural and other disasters. Since gaining independence 25 years ago we've put a lot of emphasis on prevention and later, on comprehensive disaster risk reduction measures that are included in all phases of the disaster management cycle. As an EU Member State Slovenia shares the clear vision that is presented in the EU statement for Global Platform for Disaster Risk Reduction "*From Commitment to Action*". Slovenian legislation follows the guidelines of EU civil protection legislation, which has a strong focus on prevention and preparedness policy and action. However, the challenges we are facing today are becoming more and more complex and inter-related, and require greater awareness that disaster risk reduction is our collective responsibility."

UN strategic documents on Disaster Risk Reduction

Sendai Framework on Disaster Risk Reduction 2015–2030

UN Member States adopted the Sendai Framework for Disaster Risk Reduction 2015–2030 (Sendai Framework 2015) on 18 March 2015 at the Third UN World Conference on Disaster Risk Reduction in Sendai City, Miyagi Prefecture, Japan. The Sendai Framework is the first major agreement of the post–2015 development agenda, with seven targets and four priorities for action.

The Sendai Framework will apply to the risk of small- and large-scale, frequent and infrequent, sudden and slow-onset disasters caused by natural or manmade hazards, as well as related environmental, technological and biological hazards and risks. It aims to guide the multi-hazard management of disaster risk in development at all levels as well as within and across all sectors.

The expected outcome of the Sendai Framework is a substantial reduction of disaster risk and loss of life, livelihoods and health and in the economic, physical, social, cultural and environmental assets of persons, businesses, communities and countries.

The goal of the Sendai Framework Prevent is to prevent new and reduce existing disaster risks through the implementation of integrated and inclusive economic, structural, legal, social, health, cultural, educational, environmental, technological, political and institutional measures that prevent and reduce exposure to hazards and vulnerability to disasters, increase preparedness for response and recovery, and thus strengthen resilience. There are seven global targets of the Sendai Framework for DRR 2015–2030 (Tab. 1).

To meet the seven SF targets, there is a need for focused action within and across sectors by States at the local, national, regional and global levels in the following 4 priority areas:

1 - Understanding disaster risk.
2 - Strengthening disaster risk governance to manage disaster risk.
3 - Investing in disaster risk reduction for resilience.
4 - Enhancing disaster preparedness for effective response and to "*Build Back Better*" in recovery, rehabilitation and reconstruction.

A set of 38 global indicators was identified to measure global progress in the implementation of the Sendai Framework for Disaster Risk Reduction in reaching its seven targets.

Table 1 Seven targets of the Sendai Framework for DRR 2015–2030.

Targets of the Sendai Framework on DRR 2015–2030
Target A: Substantially reduce global disaster *mortality* by 2030, aiming to lower average per 100,000 global mortality over 2020–2030 compared to 2005–2015
Target B: Substantially reduce the number of *affected people* globally by 2030, aiming to lower the average global figure per 100,000 over 2020–2030 compared to 2005–2015
Target C: Reduce *direct disaster economic loss* in relation to global gross domestic product (GDP) by 2030
Target D: Substantially reduce *disaster damage to critical infrastructure and disruption of basic services*, among them health and educational facilities, including through developing their resilience by 2030
Target E: Substantially increase the number of countries with *national and local disaster risk reduction strategies* by 2020
Target F: Substantially enhance *international cooperation* to developing countries through adequate and sustainable support to complement their national actions for implementation of this framework by 2030
Target G: Substantially increase the availability of and access to *multi-hazard early warning systems* and *disaster risk information and assessments* to the people by 2030

Monitoring implementation of the Sendai Framework

The indicators were developed by the *Open-ended intergovernmental expert working group on indicators and terminology relating to disaster risk reduction* (see http://www.preventionweb.net/drr-framework/sendai-framework-monitor/ or OIEWG's Report (2017), established by the UN General Assembly. They will generate the information base for the development of Sendai Framework implementation strategies, facilitate the development of risk-informed policies and decision-making processes, and guide the allocation of appropriate resources.

UN ISDR Terminology

The UNISDR Terminology aims to promote a common understanding and usage of disaster risk reduction concepts and to assist the disaster risk reduction efforts of authorities, practitioners and the public (http://www.preventionweb.net/english/professional/terminology/).

Governmental Official Statements during 3rd UN WCDRR

An Official Statement of the Republic of Slovenia was made by Mr Miloš Bizjak (2015), State Secretary at the Ministry of Defence, stating: "As an EU Member State, Slovenia strongly supports the determination of the EU to continue playing an active role in the implementation of the new framework, and its readiness to engage in an open and constructive dialogue with all partners and stakeholders. In 2015, a new seven-year "post–2015" Resolution on the National Programme on Protection against Natural and Other Disasters will be adopted in Slovenia, with a strong focus on cooperation among all stakeholders at different levels within risk assessment and disaster risk management. Let me give an example for these activities in the field of landslide risk reduction. In 2017, Slovenia will host the 4th World Landslide Forum, an activity of the International Consortium on Landslides and a part the ICL-IPL Sendai Partnership 2015–2024 entitled "Landslide Disaster Reduction for a Safer Geoenvironment".

Government Announcements and Voluntary Commitments to the Sendai Framework

The Government of Republic of Slovenia supported the Sendai Framework Goal No. 1 – "Risk prevention: the adoption of risk-informed development pathways that minimize the generation of new disaster risks" on the national level by stating: "Slovenia commits to developing a new seven years *Resolution on the National Programme on Protection against Natural and Other Disasters* to be adopted in 2015. Slovenia will focus on cooperation among all stakeholders at different levels within risk assessment and management." – note: the Resolution was adopted by the Slovenian Parliament in November 2016 (Resolution 2016).

The Government of the Republic of Croatia supported the Sendai Framework Goal No. 2 – "Risk reduction: actions to address and reduce pre-existing disaster risk" by stating: "Croatia will work towards the integration of disaster risk reduction into national development and strategic documents, as well as in practice by developing DRR projects to be co-financed by EU Structural and other funds. Croatia will strengthen its National Platform by emphasizing stronger involvement of local governments, the academic community and the private sector. Also, it is one of our priorities to include disaster risk reduction in school curricula and strengthen teachers' knowledge so as to teach children to acquire critical thinking and life-saving skills".

The Government of the Republic of Serbia supported the Sendai Framework Goal No. 2 – "Risk reduction: actions to address and reduce pre-existing disaster risk" by stating: "Serbia commits to the integration of disaster risk reduction into development policies and plans. In this regard, Serbia commits to develop policy, legislative and institutional frameworks for disaster risk reduction that are capable of monitoring progress based on specific and measurable indicators. We will ensure adequate identification of risks, more effective action to reduce consequences of disasters as well as emergency response".

The Sendai Framework Goal No. 2 - "Risk reduction: actions to address and reduce pre-existing disaster risk" was supported by a voluntary commitment of the International Consortium on Landslides (ICL) on the global level by stating: "The ISDR-ICL Sendai Partnerships 2015–2025 for the Global Promotion of Understanding and Reducing Landslide Disaster Risk is a sound global platform that will be mobilized in the period 2015–2025 to pursue prevention, to provide practical solutions, education, communication, and public outreach to reduce landslide disaster risk. These Partnerships will engage all signifi-

cant stakeholders concerned with the challenge of understanding and reducing disaster risk, including relevant international, national, local, governmental, and non-governmental institutions, programmes and initiatives. The Partnerships will focus on delivering tangible and practical results that are directly related to the implementation of the goals and targets of the post-2015 Framework for Disaster Risk Reduction."

DRR and Sustainable Development

The Sendai Framework indicators recommended by the OIEWG will be used also to measure specific global targets of SDGs, namely the following:

- No. 1 - End poverty in all its forms everywhere,
- No. 11 - Make cities and human settlements inclusive, safe, resilient and sustainable, and
- No. 13 - Take urgent action to combat climate change and its impacts within the global indicator framework for the Goals and targets of the 2030 Agenda for Sustainable Development.

Sendai Framework Data Readiness Review 2017

A list of global indicators was prepared to meet SDG targets (Tab. 1). By mid-2017, 87 countries had responded to the 2017 Sendai Framework Data Readiness Review and submitted to UNISDR their national (country) data readiness report, among them the following countries from the Adriatic-Balkan region: Albania, Croatia, Montenegro, and Slovenia (Tab. 2).

The Slovenian report reviews the availability of data in Slovenia, reports on the indicators recommended for measuring the global targets of the Sendai Framework 2015–2030, and identifies current gaps (Slovenia Report 2017).

Albania and Slovenia have reported national disaster loss databases operated by the government (at present and for the period 2005–2015); Croatia and Montenegro reported having no such database (Tab. 2).

Over 90% of the 87 countries currently collect data disaggregated by hydrological and meteorological hazard types, and over 80% of countries collect data on geophysical hazards; these are the three most commonly available categories.

Table 2 Overview of selected questions and answers for selected indicators from five countries' reports in the Sendai Framework Data Readiness Review 2017 (from UNISDR 2017; and country reports).

Indicator	Questions and Answers	AUT	AL	CRO	MN	SLO
generic	Do you have a national database for collecting disaster losses? (If no, when do you plan to start collecting data attributed to disasters?)	No (2018)	Yes	No (2018 – should develop DRR strategy)	No (?)	Yes
generic	What resources do you need to collect data on disasters?	C, F	-	C, F, TT	C, F	-
generic	Which tool or methodology are you using to collect and store your loss data?	-	UN DesInventar	-	-	National strategy
A-2	Do you record/collect the number of deaths attributed to disasters? (if no, when you plan?)	No (2018)	Yes	No (2018)	No (after adoption of NRA)	Yes
B-2	Do you collect the number of injured or ill attributed to disasters?	No (2018)	Yes	No (2018)	No (after adoption of NRA)	Yes
C-5	Do you collect data on direct economic loss resulting from damaged or destroyed critical infrastructure (CI) attributed to disasters?	No (2018)	No (2019)	No (first identifying critical infrastructure)	No (after adoption of NRA)	Yes
D-4	Do you collect the number of kilometres of roads destroyed or damaged by disasters?	No (2019)	Yes	No (first identifying critical infrastructure)	No (after adoption of NRA)	Yes
E-1	Do you have a national DRR strategy? (If no, when do you plan to develop one?)	No (2018)	No (2019)	No (2017/18)	No (end of 2017)	No (until 2020)
E-2	Do you have local DRR strategies led by local government? (If no, when do you plan to develop such?)	Yes (20%)	No (2020)	No (should be recommended in DRR strategy)	No (after adoption of NRA)	No (do not know)
G-2	Do you have a multi-hazard monitoring and forecasting systems? (If no, when you plan to have it operational?)	No (2020)	Yes	Yes	Yes	Yes
G-6	Do you collect data on the percentage of population exposed to or at risk from disasters, protected through pre-emptive evacuation following early warning?	Yes	No	No	No	Yes

Legend: irrelevant questions are indicated by a sign minus (-); C – Capacity, F – Financial, TT – Technology Transfer; UN DesInventar - a conceptual and methodological tool for the construction of databases tracking loss, damage, or effects caused by emergencies or disasters (www.desinvestar.org); NRA – National Risk Assessment

National Platforms on Disaster Risk Reduction (NP DRR)

In general on national platforms

The United Nations Office for Disaster Risk Reduction (UN ISDR; http://www.unisdr.org/) encourages the establishment of multi-stakeholder coordination mechanisms for disaster risk reduction, including National Platforms for Disaster Risk Reduction (NP DRR), in order to highlight the relevance, benefit and cost-benefit of a coordinated and consistent approach to disaster risk reduction at the national level.

Countries and national platforms are therefore key partners to implementing disaster risk reduction strategies at the national level to help build resilient communities; a list of countries with their national platforms and national focal points to support the Sendai Framework for Disaster Risk Reduction adopted by UN in 2015 is given here: http://www.unisdr.org/partners/countries.

The official UN ISDR terminology defines National Platform for DRR as: "A generic term for national mechanisms for coordination and policy guidance on disaster risk reduction that are multi-sectoral and interdisciplinary in nature, with public, private and civil society participation involving all concerned entities within a country."

As of late-September 2017, there were a total of 68 National Platforms established worldwide (http://www.unisdr.org/partners/countries), and 27 in the Europe Region. In the Adriatic-Balkan region, the following countries have national platforms (listed alphabetically): Bosnia and Hercegovina, Bulgaria, Croatia, Greece, Hungary, Italy, Macedonia, Montenegro, Serbia, and Slovenia - only Albania and Romania (and Kosovo) are still without a national platform, but they have national focal points for the Sendai Framework.

Guidelines for National Platforms on DRR

When establishing a new national platform for DRR or strengthening an existing NP, we may follow the guidelines as prepared by UNISDR. The guidelines on the composition of NP for DRR (UNISDR 2007) are as follows:

- National Platforms for DRR should build on any existing systems relevant to DRR. They should facilitate the participation of key players from line ministries, disaster management authorities, scientific and academic institutions, NGOs, the National Society of the Red Cross or Red Crescent, the private sector, opinion shapers and other sectors closely related to the DRR purpose. Whenever possible, National Platforms for DRR may invite the participation of donor agencies and country-based UN organizations.
- The Office or Ministry leading the National Platform for DRR should be a permanent structure that is in a sufficiently high position to coordinate the participation of all relevant partners with a national coordination mandate in disaster risk reduction, disaster management, national planning or environment. The leading Office or Ministry should have a capacity for strong leadership and the capacity to coordinate other sectors and leverage political commitment and mobilize resources for and knowledge on DRR.

Slovenian National Platform on DRR

The Slovenian National Platform was established in July 2014 as the Council of the Government of the Republic of Slovenia for Protection against Natural and other Disasters. It is a kind of an advisory body to the Slovenian national government, acting as a National Platform for Disaster Risk Reduction (NP DRR). The structure of the Slovenian National Platform follows the UNISDR guidelines and is as follows:

a) Governmental bodies:
- Ministries: the Environment and Spatial Planning; Interior; Infrastructure; Health; Foreign Affairs; Education, Science and Sports; Culture; Defence
- Office of the Prime Minister of the Republic of Slovenia
- National Civil Protection Commander

b) Non-governmental organisations:
- Fire Fighting Association of Slovenia
- Slovenian Red Cross
- CIPRA Slovenia – Association for the Protection of the Alps
- Slovenian Electronic Communication Society SIKOM

c) Academic and research institutions: Slovenian Rectors Conference & Research Centre of the Slovenian Academy of Sciences and Arts.

d) Local level administration bodies: Associations of Municipalities of Slovenia.

e) Private sector entities: Chamber of Commerce and Industry of Slovenia.

f) Media: RTV Slovenija (The Radio and Television Corporation of Slovenia).

The main aim of the platform is to facilitate dialogue between the Government of the Republic of Slovenia and civil society, as well as non-governmental, scientific and research and other organizations and associations on disaster risk reduction, building disaster resilience and sustainable development in line with the objectives of the Sendai Framework for Disaster Risk Reduction.

The Administration of the Republic of Slovenia for Civil Protection and Disaster Relief (ACDPR; www.sos112.si) administratively and financially supports the regular activities of the platform. The ACPDR is a constituent body of the Ministry of Defence. It performs administrative and professional protection, rescue and relief tasks as well as other tasks related to protection against natural and other disasters, including landslide disasters. The ACPDR is divided into six internal organizational units (four sectors and two services) based in Ljubljana as well as 13 other ACPDR branches operating throughout Slovenia. Each branch has a regional notification centre that is on duty 24 hours daily. A total of some

300 people are employed at ACPDR branches and regional notification centres.

The main duties and activities of the Slovenian National Platform for DRR are as follows, namely to:

- take an active part in the development and implementation of the Slovenian National Programme on Protection Against Natural and Other Disasters;
- facilitate cooperation of stakeholders in all phases of the disaster management cycle – prevention, preparedness, response to disasters, and recovery;
- participate in the legislative process;
- contribute to awareness-raising on the importance of prevention activities and promote resilience to disasters;
- cooperate with other relevant bodies from related fields and strive towards synergy;
- organize public consultations on disaster management, and to
- participate in the relevant international activities and cooperate with platforms of other countries.

Slovenian national legislation and procedures in the field of hazard and risk assessment

We can summarise the main conclusions of a recent Slovenian state-of-the-art review of the present status of the Slovenian national legislation and procedures for the hazard and risk assessment of landslides, including rock falls and debris flows (Mikoš et al. 2014).

The relevant governing act in Slovenia is the 2002 Waters Act, which foresees several legislation documents accepted by the ministry in charge for waters in Slovenia (at present: Ministry of the Environment and Spatial Planning). Thanks to the European Flood Directive, these procedures are already regulated in the field of flood protection, but still need to be regulated as they apply to other water-related natural disasters and geo-hazards, such as mass movements (landslides, including rock falls and debris flows).

Over the past decade, several methodologies and different hazard maps have been prepared, but no legal acts (such as decrees, regulations, recommendations or similar acts, let alone standards) have been accepted on the basis of such. Generally, state legislations overseeing spatial planning and water management in the form of acts are up-to-date in Slovenia, but much more should be done for the direct implementation of such.

Conclusions and a look into the future

We should use the ICL-ABN regional network to enhance our joint efforts for the implementation of the Sendai Framework for DRR 2015–2030, in particular by enhancing cooperation between the existing National Platforms for DRR (and focal points for DRR in countries without a NP) in the region. We could also support the establishment of national platforms in those countries where no such national body exists (e.g. Albania).

Furthermore, we should strengthen our efforts in the Adriatic-Balkan region to incorporate the goals of the 2017 Ljubljana Declaration on Landslide Risk Reduction and of the concept of the 2020 Kyoto Commitment for Global Promotion of Understanding and Reducing Landslide Disaster Risk (Sassa 2017b) into the activities of the national platforms for DRR in the region.

An important step forward in the region would be to develop a system by which the indicators of the Sendai Framework implementation would be followed; there is still a large gap in a considerable number of countries (Tab. 2).

Building on the success of the WLF4 (Alcántara-Ayala et al. 2017; Mikoš et al. 2017), we should report extensively on our activities in the Adriatic-Balkan region over the course of the Fifth World Landslide Forum 2020 in Kyoto, Japan, 2–6 November 2020 (Sassa 2017a; Sassa 2017d), entitled "Implementing and Monitoring for ISDR-ICL Sendai Partnerships 2015–2025" (http://wlf5.iplhq.org/).

The regional symposia on landslides in the Adriatic-Balkan region (ReSyLAB) should become a regular biannual event (2013 – Zagreb, 2015 – Belgrade, 2017 – Ljubljana, 2019 – Tirana, 2021 - ...), attracting more and more stakeholders from the region. We should expand the ICL members' regional network (ICL-ABN) to new full ICL members in other countries of the region, and work to gain new ICL associate members in the regions from among national and/or regional authorities and professional engineering firms, as proposed by ICL (Sassa, 2017c).

As the core activity of the Sendai Partnerships 2015–2025, the International Consortium of Landslides has created a two-volume work called Landslide Interactive Teaching Tools (LITT), which will be updated regularly and improved over the coming years, based on the responses from users and lessons learned during its application.

The two volumes of LITT include numerous teaching tools from a variety of international organizations and institutes; include guidelines for monitoring, modelling, and risk mitigation; and cover mathematical and physical analysis and monitoring related to landslides (Sassa et al. 2017a; 2017b). The ICL members from the ICL-ABN regional network have made a noteworthy contribution to this interactive work, and we should continue to update our work, and possibly expand it to include new knowledge. We may invite new ICL Associates to support the project with their knowledge and expertise when updating the LITT to a new version.

Further, we should support the existing ICL World Report on Landslides (WRL; http://iplhq.org/ls-world-report-on-landslide/), which is a web application that aims to create platform for cooperation on sharing landslide case studies in the global landslide community, with new case studies from the Adriatic-Balkan region to

broaden the WRL content and improve both its visibility and use.

The 3rd ReSyLAB in Ljubljana ended on the International Day for Disaster Reduction (13 October 2017; the first was celebrated in 1989). In 2017 the motto was: "Home Safe Home: Reducing Exposure, Reducing Displacement"; the focus this year is on Target B of the Sendai Framework for DRR, with the aim of reducing the number of people affected by disasters by 2030.

Acknowledgments

The author, as the President of the Slovenian National Platform for DRR for the period 2014–2018, wishes to thank the Administration of the Republic of Slovenia for Civil Protection and Disaster Relief for their institutional support to the Slovenian National Platform for DRR. The author of this paper also served as a member of the Slovenian delegation to the 3rd UN WCDRR (report in Mikoš 2016).

References

Alcántara-Ayala I, Sassa K, Mikoš M, Han Q, Rhyner J, Takara K, Nishikawa S, Rouhban B, Briceño S (2017) The 4th World Landslide Forum: Landslide Research and Risk Reduction for Advancing the Culture of Living with Natural Hazards. International Journal of Disaster Risk Science. 8(4):498-502.

Bizjak M (2015) Slovenia: Statement made at the Third UN World Conference on Disaster Risk Reduction (WCDRR). URL: http://www.preventionweb.net/files/globalplatform/sloveniafinal[1].pdf [last accessed: 19.09.2015].

Bizjak M (2017) Slovenia: Statement made at the Global Platform for Disaster Risk Reduction (2017). URL: http://www.preventionweb.net/english/professional/policies/v.php?id=53860 [last accessed: 18.4.20017].

Framework (2015). Sendai Framework for Disaster Risk Reduction 2015-2030. United Nations. URL: https://www.preventionweb.net/files/43291_sendaiframeworkfordrren.pdf [last accessed: 13.03.2017]

Mikoš M (2016) Slovenija in 3. svetovna konferenca Združenih narodov o zmanjšanju tveganja nesreč, Sendai, Japonska, 2015 = Slovenia and the 3rd United Nations World Conference on Disaster Risk Reduction, Sendai, Japan, 2015. Ujma. 30:309-316. (in Slovenian with English abstract)

Mikoš M, Čarman M, Papež J, Janža M (2014) Legislation and procedures for the assessment of landslide, rockfall and debris flow hazards and risks in Slovenia. Wildbach- und Lawinenverbau. 78(174): 212-221.

Mikoš M, Yin Y, Sassa K (2017) The Fourth World Landslide Forum, Ljubljana, 2017. Landslides. 14(5): 1843-1854.

OIEWG (2017) Report of the open-ended intergovernmental expert working group on indicators and terminology relating to disaster risk reduction. United Nations General Assembly. URL: http://www.preventionweb.net/files/50683_oiewgreportenglish.pdf [last accessed: 13.03.2017]

Resolution (2016) Resolucija o nacionalnem programu varstva pred naravnimi in drugimi nesrečami v letih od 2016 do 2022 = Resolution on the National Programme for Protection against Natural and Other Disasters 2016-2022. Official Gazette of the Republic of Slovenia. 75:10506-10523. (in Slovenian)

Sassa K (2017a) The Fifth World Landslide Forum—Implementing and Monitoring the ISDR-ICL Sendai Partnerships 2015–2025. Landslides. 14(3): 1283-1288.

Sassa K (2017b) The 2017 Ljubljana Declaration on landslide risk reduction and the Kyoto 2020 Commitment for global promotion of understanding and reducing landslide disaster risk. Landslides. 14(4): 1289-1296.

Sassa K (2017c) Participants in the Fourth World Landslide Forum and call for ICL members, supporters, and associates. Landslides. 14(5): 1839-1842.

Sassa K (2017d) The Fifth World Landslide Forum - Implementing and monitoring the ISDR-ICL Sendai Partnerships 2015–2025 - Timeline of the WLF5 organization process and call for session proposals. Landslides. 14(5): 1857-1859.

Sassa K, Guzzetti F, Yamagishi H, Arbanas Ž, Casagli N, McSaveney M, Dang K (eds) (2017a) Landslide Dynamics: ISDR-ICL Landslide Interactive Teaching Tools, Vol. 1: Fundamentals, Mapping and Monitoring. Springer International Publishing. (ISBN 978-3-319-57774-6). 605p.

Sassa K, Tiwari B, Liu KF, McSaveney M, Strom A, Setiawan H (eds) (2017b) Landslide Dynamics: ISDR-ICL Landslide Interactive Teaching Tools, Volume 2: Testing, Risk Management and Country Practices. Springer International Publishing. (ISBN ISBN 978-3-319-57777-7). 862p.

Sendai Framework (2015). Sendai Framework for Disaster Risk Reduction 2015-2030. UNISDR, Geneva. 35p. URL: http://www.unisdr.org/files/43291_sendaiframeworkfordrren.pdf [last accessed: 13.03.2017]

Slovenia Report (2017). Sendai Framework Data Readiness Review – Report. The Government of the Republic of Slovenia. 62 p. URL: http://preventionweb.net/go/53202 [last accessed: 13.03.2017]

UNISDR (2007). Guidelines – National platforms for disaster risk reduction. UNISDR, Geneva. 17p. URL: http://www.preventionweb.net/files/601_engguidelinesnpdrr.pdf [last accessed: 13.03.2017]

UNISDR (2017). Sendai Framework data readiness review 2017 – Global summary report. UNISDR, Geneva. 77p. URL: http://www.preventionweb.net/publications/view/53080 [last accessed: 13.03.2017]

Author index

Symposium sponzors

Portal eGeologija

The eGeologija web portal of the Geological Survey of Slovenia enables quick access to all sorts of quality geological data at the single entry point at www.egeologija.si.

Geological data, standardized and interpreted, in the form of datasets, services and maps are now available to the widest range of users. Users, individuals also, can search the data and download them to their environment for future use.

eGeologija allows the user to easily search and browse by categories, types of resources, fields of research and web services. In the metadata catalog there are two search methods, textual search and search by location. The user can also access individual web browsers which are established and maintained by the Geological Survey of Slovenia. They offer detailed insight into the variety of geological data.

An important feature of the eGeologija portal is an interactive map viewer that displays the requested datasets or web services on the map. This viewer allows displaying and viewing of geological data and their content with the basic functionalities such as zooming, panning, transparency, identifying, printing, searching by location, and adding other data sources using web mapping services.

http://egeologija.si/geonetwork/srv/eng/catalog.search#/home


GeoZS
Geološki zavod
Slovenije


University of Ljubljana
Faculty of Civil and Geodetic Engineering

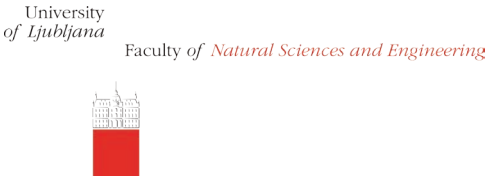
University
of Ljubljana
Faculty of Natural Sciences and Engineering


ReSyLAB 2017
3rd Regional Symposium on Landslides
in the Adriatic-Balkan Region

The main objective of the 3rd ReSyLAB symposium was to provide a stimulating forum for geoscientists, engineers, professionals, and decision-makers concerned with landslide hazards and risks as well as their impact on society-in the Adriatic-Balkan Region as well as worldwide. Following the ISDR-ICL Sendai Partnerships 2015–2025 for the Global Promotion of Understanding and Reducing Landslide Disaster Risk and the 2017 Ljubljana Declaration on Landslide Risk Reduction, the 3rd ReSyLAB symposium explored possible ways of enhancing cooperation between the landslide science community and the diverse range of stakeholders both in the Adriatic-Balkan Region and around the world.

This book "Advances in Landslide Research" is a collection of twenty five peer-reviewed papers prepared by authors from seven countries (Austria, Croatia, Italy, Macedonia, Serbia, Slovenia, and Spain) in the context of the 3rd ReSyLAB topics: mapping, investigating, monitoring, analysis, and mitigation of landslides, as well as case studies on innovative landslide analysis techniques and landslide risk mitigation solutions. Recent developments in landslide research and new-advanced technologies for landslide monitoring are presented.

We would like to thank all of the authors of the submitted research papers and the numerous reviewers that peer reviewed the papers. We appreciate all the help we have received from the members of the International Scientific Committee and all of those individuals that expressed their support throughout the organization process. Finally, we would like to thank all of the sponsors who made the organization of this symposium possible.

ReSyLAB 2017

3rd Regional Symposium on Landslides in the Adriatic-Balkan Region, Ljubljana

ISBN 978-961-6498-58-6

9 789616 498586